**Evaluation of the AIMS-II and Micro-Deval for Friction Characteristics of Aggregates**

by

Mary Greer

A thesis submitted to the Graduate Faculty of
Auburn University
in partial fulfillment of the
requirements for the Degree of
Master of Science

Auburn, Alabama
May 10, 2015

Key Words: AIMS, Micro-Deval, Skid Resistance, Surface Texture, Pavement Friction, Hot-Mix Asphalt



Approved by

Richard Willis, Chair, Associate Research Professor for Civil Engineering
Michael Heitzman, Co-chair, Assistant Director of the National Center for Asphalt Technology
David Timm, Brasfield & Gorrie Professor for Civil Engineering
Mary Robbins, Assistant Research Professor for Civil Engineering

## ABSTRACT

There is a need for a rapid quantitative way to evaluate the quality of aggregate friction properties for use in an asphalt surface (wearing) course. Aggregates that are resistant to polishing and capable of retaining their shape characteristics are desirable in the asphalt wearing course. The wearing course should be capable of maintaining an adequate amount of friction when subjected to polishing due to heavy traffic in order to ensure the safety of the roadway. Current laboratory procedures used to evaluate the friction properties of aggregates are said to be time consuming and subjective. The purpose of this research study was to evaluate the correlation between aggregate performance in a laboratory test consisting of the second generation Aggregate Imaging Measurement System (AIMS-II) and Micro-Deval to field friction performance.

The AIMS-II device was used to quantify aggregate shape characteristics (angularity, texture, and form) before conditioning (polishing) and after conditioning in the Micro-Deval at different increments of time. The aggregates used for testing were selected based on their friction performance in surface courses at the National Center for Asphalt Technology (NCAT) Pavement Test Track. Field friction performance data for the selected test sections was obtained using the locked-wheel skid trailer. Aggregate shape indexes, more specifically, angularity and texture, were compared with the results obtained from the skid trailer in the field to see if a correlation could be established.

The results showed the AIMS-II device was capable of detecting changes in aggregate shape characteristics when subjected to conditioning in the Micro-Deval. However, the analysis showed a good correlation between the AIMS-II indexes and the field friction data could not be established with the procedure that was used in this research study. This research study was a useful step in working towards developing a test method that may use the AIMS-II in conjunction with the Micro-Deval to predict the skid resistance of an asphalt wearing course mixture in the field. Future research is needed to enhance the test method used in this research study and take other factors into consideration that affect field friction performance.

## ACKNOWLEDGEMENTS

The author would like to thank Dr. Richard Willis and Dr. Michael Heitzman for all of their guidance and support throughout writing this thesis. Their dedication and patience throughout the process were greatly appreciated, and this research would not have been possible without their assistance. The author would also like to thank all of the committee members, including Dr. David Timm and Dr. Mary Robbins, for their feedback with this thesis as well as their valued guidance throughout graduate school and Dr. Saeed Maghsoodloo for his help with the statistical analysis. Also, the author greatly appreciates the National Center for Asphalt Technology laboratory personnel for completing any work asked of them that was needed to complete this research study. Lastly, a special thanks to Dr. Randy West for giving the author the opportunity to work at NCAT and complete a Master's Degree with their program.

## TABLE OF CONTENTS

## LIST OF TABLES

## LIST OF FIGURES

## LIST OF ABBREVIATIONS

| | |
|---|---|
| AASHTO | American Association of State Highway Transportation Officials |
| AIMS | Aggregate Imaging Measurement System |
| ASTM | American Society for Testing and Materials |
| BMD | Before Micro-Deval |
| BPN | British Pendulum Number |
| BPT | British Pendulum Tester |
| CA | Coarse aggregate |
| CAA | Coarse aggregate angularity |
| COV | Coefficient of variation |
| CTM | Circular Texture Meter |
| DFT | Dynamic Friction Tester |
| ESALs | Equivalent Single Axle Loads |
| E-UIAIA | Enhanced University of Illinois Aggregate Image Analyzer |
| FA | Fine aggregate |

| | |
|---|---|
| FAA | Fine aggregate angularity |
| FDG | Fine-Dense Graded |
| FHWA | Federal Highway Administration |
| GLS | Generalized Least Squares |
| Grn | Granite |
| Gsa | Apparent specific gravity |
| Gsb | Bulk specific gravity |
| Gssd | Specific gravity at saturated surface dry condition |
| HFST | High Friction Surface Treatment |
| IQR | Interquartile range |
| K-S | Kolmogorov-Smirnov test |
| Lms | Limestone |
| LTPP | Long Term Pavement Performance |
| LTS | Laser Texture Scanner |
| MPD | Mead Profile Depth |
| MTD | Mean Texture Depth |

| | |
|---|---|
| NCAT | National Center for Asphalt Technology |
| OGFC | Open Graded Friction Course |
| RMS | Root Means Square |
| SHRP | Strategic Highway Research Program |
| SMA | Stone Matrix Asphalt |
| SN40R | Locked-Wheel Skid Trailer Skid Number at a slip speed of 40 mph with a ribbed tire |
| SP | Sand patch |
| TLA | Trinidad Lake Asphalt |
| TWPD | Three Wheel Polishing Device |

# CHAPTER 1: INTRODUCTION

## 1.1 Background

Transportation agencies have made safety a high priority regarding pavement infrastructure. To optimize roadway safety, pavement friction, also referred to as skid resistance, is an essential component to take into consideration when evaluating an asphalt pavement surface. The skid resistance of an asphalt pavement decreases when subjected to polishing from heavy traffic. State agencies monitor pavement friction to ensure the pavement surface is maintaining an adequate amount of skid resistance. It is important to prevent the pavement surface friction from dropping below the minimum thresholds applied by state agencies. This reduces the risk of potential crashes caused by inadequate friction on the roadway, especially in wet weather conditions. However, it should be noted that state agencies do not report their thresholds due to liability.

Several methods and devices are capable of measuring pavement friction in the field. The most common device used is the locked-wheel skid trailer, equipped with either a ribbed or smooth testing tire (Hall et al. 2009). If the locked-wheel skid trailer indicates a pavement surface is characterized by a friction number lower than the minimum threshold, corrective measures, such as applying a surface treatment or resurfacing the pavement, should be taken to prevent the increased risk of accidents. However, such maintenance and treatment methods can be costly and time consuming. Therefore, there is a need for laboratory test protocols to evaluate a surface mixture's ability to retain a sufficient amount of friction prior to placing it in the field.

Aggregates make up a majority of the materials used in an asphalt pavement mixture. Therefore, it is important that good quality aggregates are used in the surface mix design. The quality of an aggregate may be determined by evaluating its shape characteristics. Aggregate shape characteristics, more specifically aggregate texture and angularity, are key components that

influence a mixture's ability to provide a sufficient amount of friction between the pavement surface and vehicle tire (Hall et al. 2009). Understanding these parameters and the role they play in pavement friction is essential to the safety of the roadway. There are several methods used to evaluate aggregate shape characteristics in the laboratory before and after the aggregates are subjected to conditioning. Some of these tests are said to be subjective and time consuming (Hall et al. 2009). Therefore, researchers continue to examine the use of aggregate imaging systems to quantify aggregate shape characteristics. This research study focuses on the use of such a device, known as the second generation Aggregate Imaging System, Model AFA2A (AIMS-II). The AIMS-II device quantifies aggregate shape characteristics before and after conditioning. For the purpose of this research, aggregates were conditioned using the Micro-Deval aggregate conditioning test. This allowed the user to evaluate the AIMS-II device's capability of detecting changes in aggregate shape characteristics when aggregates were subjected to conditioning.

### 1.2 Project Objectives

The objective of this study was to evaluate the feasibility of using the AIMS-II device in conjunction with the Micro-Deval as an aggregate testing protocol in the laboratory for evaluating pavement friction in the field. The second objective was to determine if a correlation could be established with the AIMS-II lab results and field friction performance data using the locked-wheel skid trailer.

### 1.3 Scope of Work

As part of this research study, five different aggregate sources were collected for testing: two limestone, two granite, and a high friction aggregate, bauxite. The aggregate sources were selected based on their availability and use in surface mixtures of different test sections at the

NCAT Pavement Test Track. Aggregate particles of the #4 sieve size (passing the 3/8 inch sieve and retained on the #4 sieve) and the #16 sieve size (passing the #8 sieve and retained on the #16 sieve) were obtained for each aggregate source. However, only aggregate passing the #8 and retained on the #16 sieve were collected for the bauxite. The high friction surface treatment composed of bauxite in the field only contained fine particles. The shape characteristics of each aggregate sample were quantified using the AIMS-II device prior to any conditioning. The aggregates were then subjected to conditioning in the Micro-Deval at intervals of 20, 40, 60, 80, and 100 minutes for coarse aggregates and 10, 20, and 30 minutes for the fine aggregates that were tested. The AIMS-II device was then used to track changes in aggregate shape characteristics after each Micro-Deval conditioning interval. Field friction performance data was obtained from the selected NCAT Test Track sections using the locked-wheel skid trailer at 40 miles per hour, equipped with a ribbed testing tire. The AIMS-II lab results at the preconditioned values and at different intervals of Micro-Deval was compared with the field friction data to see if the two could be correlated. The different intervals that were used for comparison after conditioning were selected based on terminal conditioning. Terminal conditioning refers to the point at which friction values (or AIMS-II indexes) tend to level off at a steady rate. The friction numbers may still be decreasing, but they essentially remain the same with increased conditioning (Kowalski et al. 2010). Terminal conditioning values were used because state agencies are concerned with the friction data that continues at a steady decline after subjected to conditioning as opposed to preconditioned values.

# CHAPTER 2: LITERATURE REVIEW

## 2.1 Pavement Friction Overview

Pavement friction is defined as "the force that resists the relative motion between a vehicle tire and a pavement surface" (Hall et al. 2009). This resistive frictional force (F) is generated when a tire rotates or slides over a pavement surface (Figure 2.1).

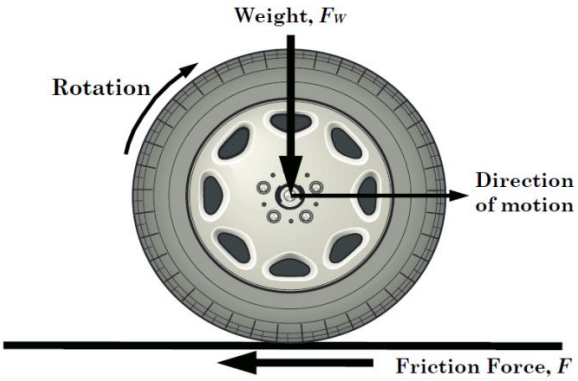


**Figure 2.1: Simplified diagram of forces acting on a vehicle tire (Hall et al. 2009)**

While friction is a force vector, it is commonly quantified using a friction coefficient, $\mu$. This term is a function of the frictional force, $F$, and the vertical load due to the vehicle load supported by the tire, $F_w$, and is calculated using Equation 2.1 (Hall et al. 2009).

$$\mu = \frac{F}{F_w} \qquad Equation\ 2.1$$

Where:

$\mu$: Friction coefficient

$F$: Frictional force

$F_w$: Vertical load due to the vehicle load

The greater the frictional force between the vehicle tire and pavement surface, the higher the friction coefficient. This results in what is commonly referred to as a skid resistant pavement. Thus, throughout this thesis, pavement friction and skid resistance will be used interchangeably.

Pavement friction is an essential component to highway safety. It is a result of the combined effects of adhesion and hysteresis force components (Figure 2.2). Adhesion is the frictional force component generated from the tire-pavement interaction as they come into contact with one another, and its magnitude heavily relies on the pavement micro-texture. Hysteresis is the frictional force component that results from the energy loss as the vehicle tire deforms over the surface with its magnitude depending more on the pavement macro-texture as well as the tire material and tire pressure (Hall et al. 2009). An increase in pavement micro-texture and macro-texture results in an increase in adhesion and hysteresis, respectively, which together, yield a larger frictional force generated between the vehicle tire and pavement.

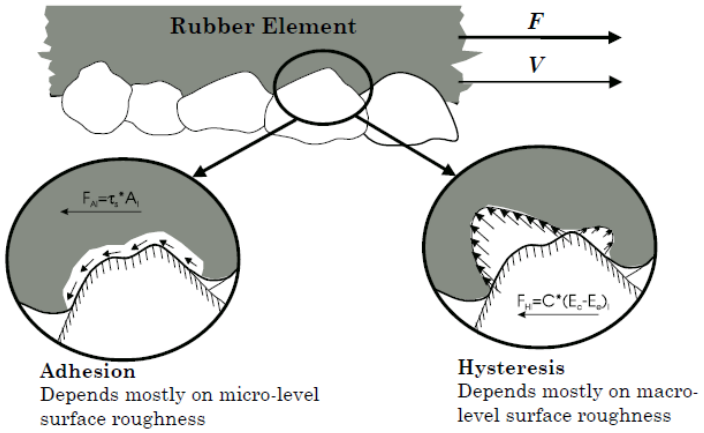


**Figure 2.2: Adhesion and hysteresis frictional force components (Hall et al. 2009)**

## 2.2 Factors Affecting Pavement Friction

Pavement friction is affected by a number of factors which can be grouped into four categories (Hall et al. 2009):

- Pavement Surface Characteristics: micro-texture, macro-texture, mega-texture, material properties, and temperature
- Vehicle Factors: vehicle speed, braking, and driving maneuver
- Tire Properties: tire tread, rubber composition, inflation pressure, load, and temperature
- Environmental Effects: climate and contaminants on the roadway

While all of these factors play an important role in the resulting pavement friction, pavement surface characteristics, more specifically the influence of material properties on micro-texture and macro-texture, will be the primary focus for the purpose of this research; therefore, these two key properties will be discussed in more detail.

## 2.3 Pavement Texture

It has been well established that pavement friction is a function of the pavement's texture. Texture consists of two primary components that affect pavement friction, macro-texture and micro-texture. Macro-texture focuses on the mixture properties as a whole within wavelengths of 0.5 mm to 50 mm, such as aggregate gradation or compaction method, whereas micro-texture is influenced by individual aggregate shape and surface properties within the mix characterized by wavelengths less than 0.5 mm (Hall et al. 2009). Figure 2.3 provides a better representation of the differences in magnitude of each of the texture components.

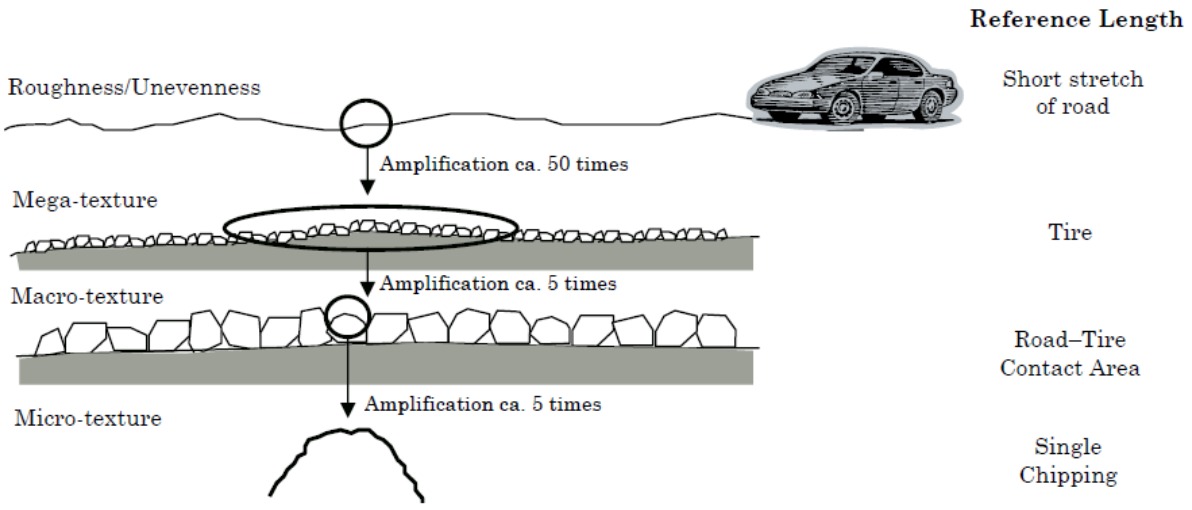


**Figure 2.3: Texture ranges that exist for a given pavement surface (Hall et al. 2009)**

The magnitude of pavement friction is controlled by micro-texture at lower speeds, whereas macro-texture primarily contributes to pavement friction between the roadway surface and vehicle tire at high speeds. A pavement mixture capable of maintaining adequate micro-texture under the polishing action of traffic is desired in order to keep a strong interaction between the tire and pavement surface. Similarly, a sufficient amount of macro-texture is favorable on a pavement surface to ensure that water does not build up on the surface and is adequately dispersed to prevent vehicles from hydroplaning (Hall et al. 2009).

## 2.4 Measuring Friction

The importance of understanding pavement friction in regards to roadway safety has been well established. However, determining the best approach for measuring a pavement's surface friction can be complicated as a number of different methods exist and are currently used.

### *2.4.1 British Pendulum Tester (BPT)*

The BPT is one tool used to quantify friction at low speeds for either aggregates or pavement mixtures, following ASTM E303 standard testing procedure. Figure 2.4 shows a picture of the BPT setup along with a magnified view of the BPT's scale (right), which is discussed in more detail later.

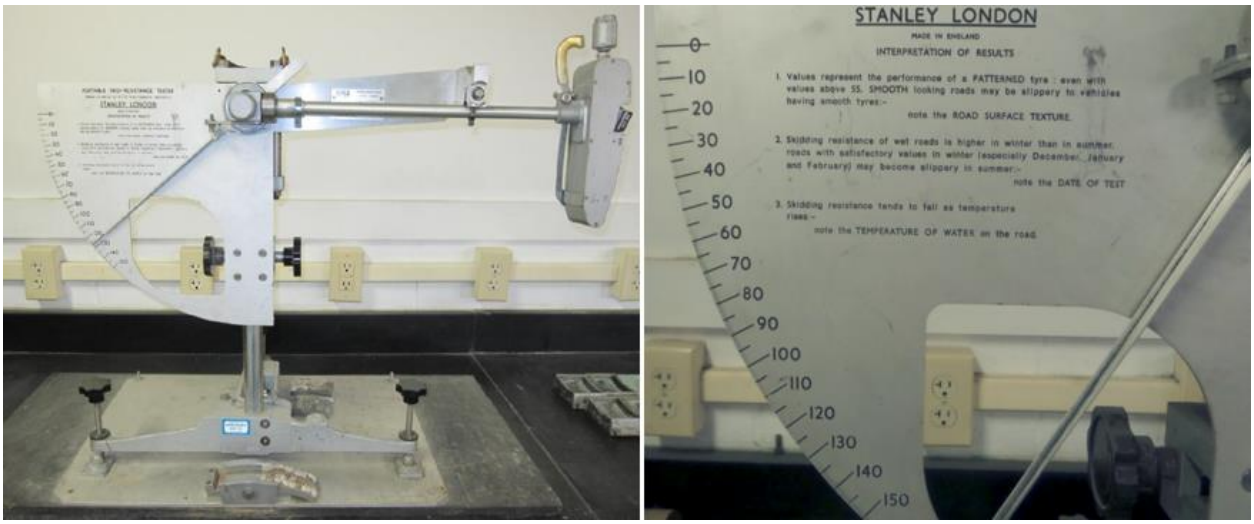


**Figure 2.4: BPT setup (left) and magnified view of the scale (right) (Erukulla 2011)**

A sufficient amount of water is sprayed to cover the testing area prior to any testing. Then, a swinging pendulum with a rubber pad attached to the bottom is released and slides across the pavement surface or aggregate sample contained in a mold. The test is executed a total of five times with water being sprayed every time prior to releasing the swinging pendulum. The results from the first swing are not recorded, but the results from the subsequent four swings are. A British Pendulum Number (BPN) is recorded for each swing from a scale of 0 to 150, which can be seen in the right photograph of Figure 2.4. The BPN is recorded as the maximum height reached after contacting the testing surface. A higher BPN indicates that the surface is

characterized by a greater amount of friction, whereas a lower BPN reveals the surface is characterized by less friction. Serigos et al. (2013) used the device to provide spot measurements of the low-speed skid resistance of pavement sections in the field. The researchers' results were then compared with pavement texture results obtained from the laser texture scanner (LTS), discussed in a later section within this chapter. Although this testing methodology is not new, it is still commonly used today. However, testing field data with updated, automatic technology, such as the dynamic friction tester (DFT) or locked-wheel skid trailer, seems more practical. The BPT can be subjective to the user, as the drop height of the swinging pendulum is controlled by the operator and could affect results. Additionally, when using the BPT for aggregate testing, the aggregates must be strategically placed in a special mold specific to the device and held together by epoxy. This task can prove to be tedious and time-consuming, and it could introduce additional variability to the testing procedure.

### *2.4.2 Dynamic Friction Tester (DFT)*

The DFT is another device used to measure pavement friction of mixtures in the field or laboratory following ASTM E1911. Figure 2.5 shows a top view (left) as well as a side view (right) of the DFT.

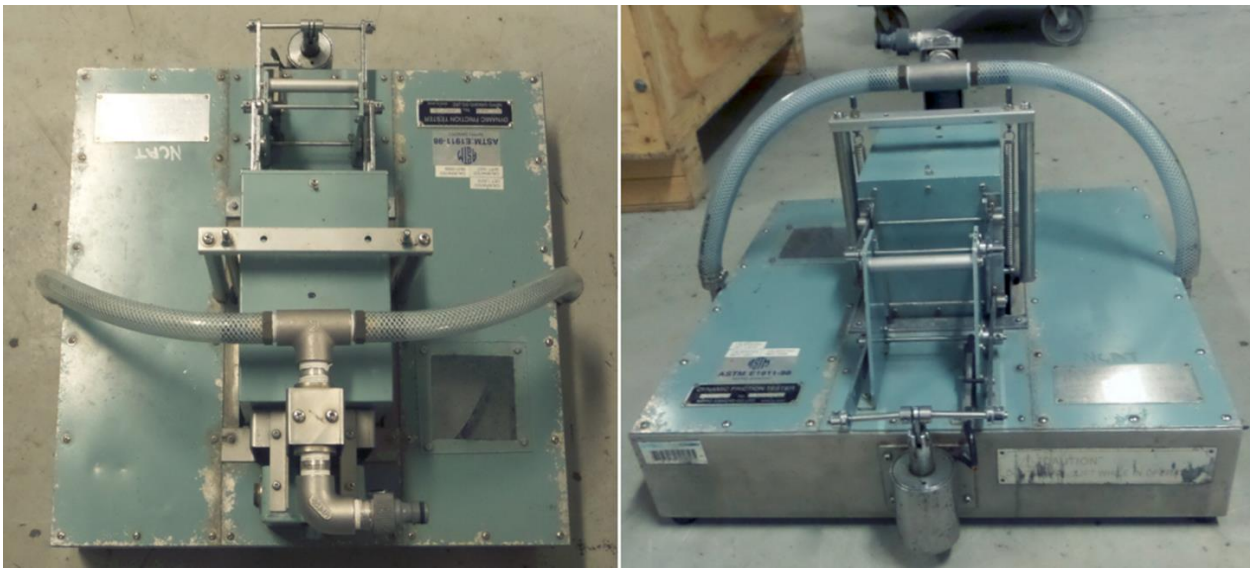

**Figure 2.5: Top view (left) and side view (right) of the DFT**

Equipped with three spring loaded rubber sliders that come in contact with the pavement surface, a spinning horizontal disk is lowered on to the pavement with water spraying in front of the sliders to simulate wet weather. Figure 2.6 shows a view of the DFT from the bottom illustrating the rotating disk as well as the three rubber sliders. A magnified view of the rubber slider is shown in the top right corner of the picture.

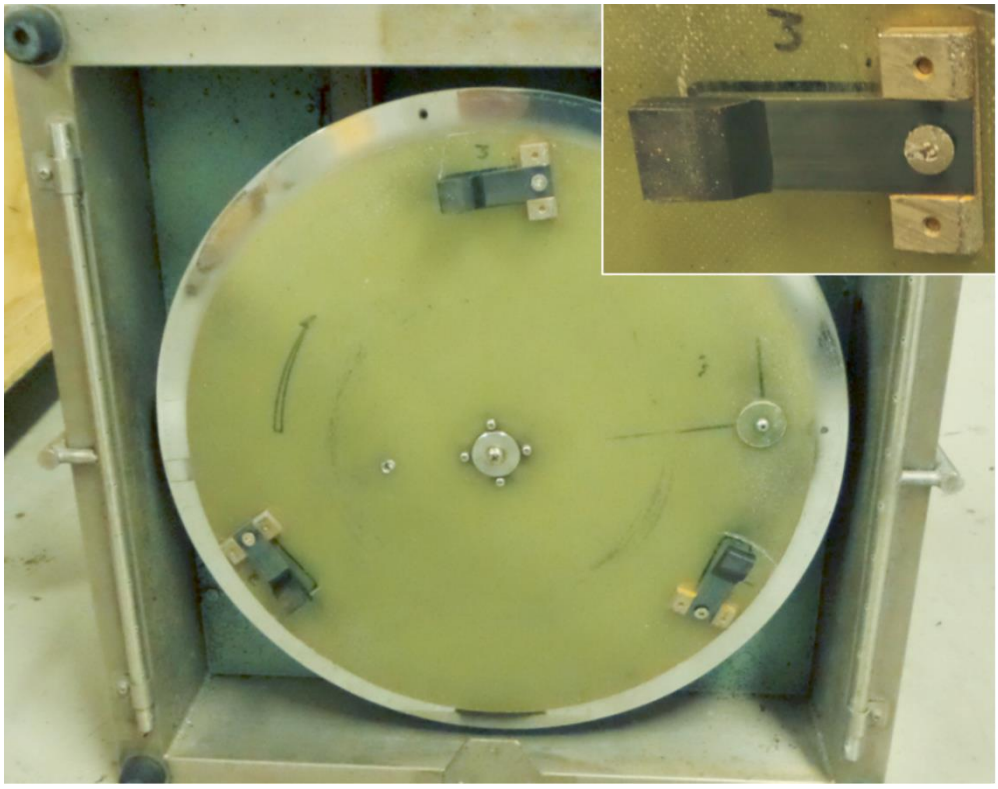

**Figure 2.6: Photographic illustration of the DFT's horizontal disk and three rubber sliders**

The friction coefficient generated between the rubber pads and pavement surface is recorded at varying speeds of 80, 60, 40, and 20 km/h as the disc decreases in speed and comes to a complete stop. The friction coefficient is calculated by converting the torque generated by the rotating disc to the force induced on the rubber sliders and dividing that force by the weight of the disk and motor assembly (ASTM E1911). A positive correlation has been established between the DFT and the locked-wheel skid trailer, which is discussed in more detail in the next section of this chapter.

### *2.4.3 Locked-Wheel Skid Trailer*

The locked-wheel skid trailer (ASTM E274) is one of the most commonly used devices to obtain field friction data. The test involves using a vehicle or trailer with at least one test wheel to

measure the skid resistance of the pavement. Once the vehicle is brought to the desired speed, water is sprayed in front of the test wheel before initiating the braking system to lock the test wheel. The resulting torque from the interaction between the tire and pavement surface is recorded along with the test speed to calculate the skid resistance. This is then reported as a skid number (SN).

The test wheel can either be ribbed (ASTM E501) or smooth (ASTM E524); however, the ribbed tire is currently the most common method of the skid trailer used in the United States (Hall et al. 2009). Figure 2.7 shows an example of the ribbed test tire (left) compared to a smooth test tire (right).

**Figure 2.7: Photographic illustration of a ribbed (ASTM E501) versus smooth test tire (ASTM E524) (Choubane et al. 2006)**

Each tire has been shown to delineate differences in different textural wavelengths. It has been noted that the ribbed tire is sensitive to pavement micro-texture and tends to generate higher skid

numbers, whereas the smooth tire was found to be more sensitive to pavement macro-texture (Yut et al. 2013). As part of the FHWA's Long Term Pavement Performance (LTPP) study, six LTPP sections in Connecticut were tested with the skid trailer using the smooth tire and ribbed tire at 40 mph. When the SNs using the smooth tire (SN40S) were compared with the SNs using the ribbed tire (SN40R), the results yielded a very low correlation coefficient ($R^2$) of 0.024 (Figure 2.8). This further indicated the two tires were sensitive to different aspects of pavement texture (Yut et al. 2013). Therefore, it is important to understand the implications of tire type on lab to field comparisons.

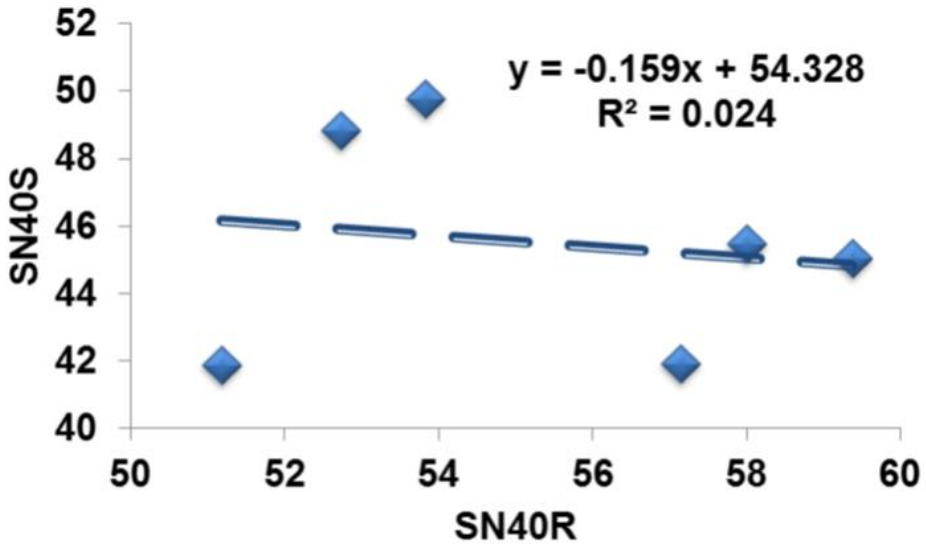


**Figure 2.8: Smooth tire SNs versus ribbed tire SNs correlation plot (Yut et al. 2013)**

### *2.4.4 Lab Test Correlations with Locked-Wheel Skid Trailer*

Correlations have been made between DFT laboratory testing of slabs and skid trailer field results using a ribbed tire on pavement test sections at the NCAT Test Track (Erukulla 2011). Four different mixtures which were part of the 2003 Test Track research cycle were made into slabs. These slabs were then tested using the DFT after being subjected to incremental polishing cycles using the Three Wheel Polishing Device (TWPD). The TWPD was developed by NCAT to polish slabs, so the decrease in surface texture and friction could be tested, as discussed later. The Test Track sections were tested using the skid trailer at 40 mph to obtain the corresponding skid number (SN40R). To clarify, Erukulla (2011) refers to the SN40R as SN64R, which are synonymous, as 40 mph is equivalent to 64 km/h. The "64" in SN64R indicates the speed at which the skid trailer was tested, whereas the "R" denotes the type of test tire used, which was ribbed in this case. If a smooth tire had been used to test the pavement skid resistance with the skid trailer traveling at 64 km/h, the appropriate notation would be SN64S. This testing was completed at different trafficking intervals, measured using Equivalent Single Axle Loads (ESALs). As expected, the friction coefficients obtained from the DFT at varying speeds and the SN64Rs obtained from the skid trailer appeared to be decreasing with increased polishing and trafficking, respectively. The laboratory DFT values at 60 km/h ($DFT_{60}$) were used to draw comparisons with skid trailer field data (SN64R). $DFT_{60}$ results were used as these values correlated best with SN64R data out of all the speeds (80, 60, 40, and 20 km/h) at which the DFT collects friction data (Erukulla 2011). The DFT ranked the laboratory made slabs (Figure 2.9) the same as the test sections that were tested using the skid trailer (Figure 2.10). The ranking is shown in red next to the mix designation at the top of the graphs.

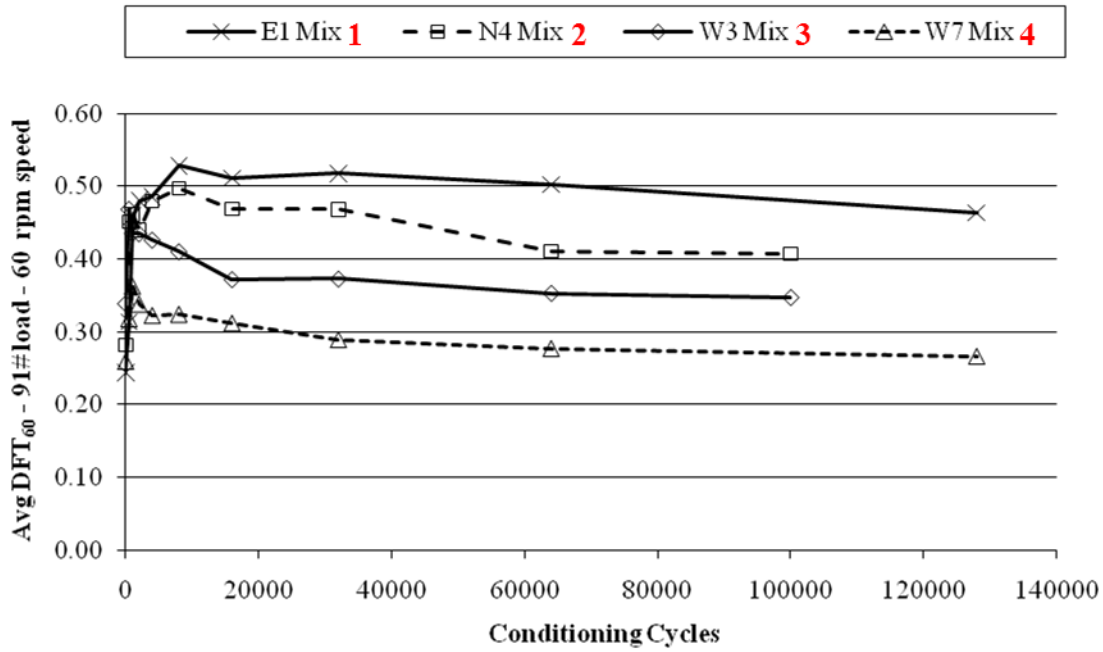


**Figure 2.9: Laboratory $DFT_{60}$ values versus TWPD conditioning cycles for the four slabs (Erukulla 2011)**

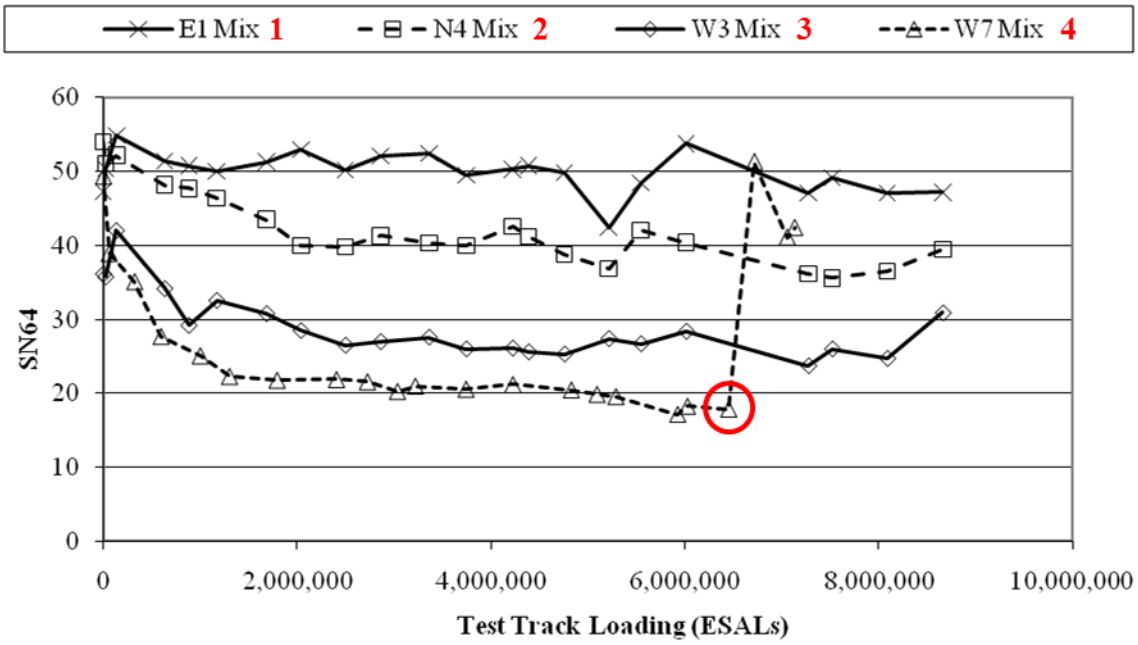


**Figure 2.10: Field SN64R versus ESALs for the four test sections (Erukulla 2011)**

It should be noted that the field mixture used on section W7 was replaced with a different mixture shortly after 6 million ESALs due to its poor friction performance. Therefore, the terminal SN64R that was used in the research analysis is circled in red in Figure 2.10. The higher SNs in the figure for that section portray the friction performance of the new mixture that was used as the replacement and were excluded from analysis.

A positive correlation was developed between the skid trailer field results (SN64R) and laboratory results when using the DFT values at 60 km/h multiplied by 100, as shown for the x-axis in Figure 2.11.

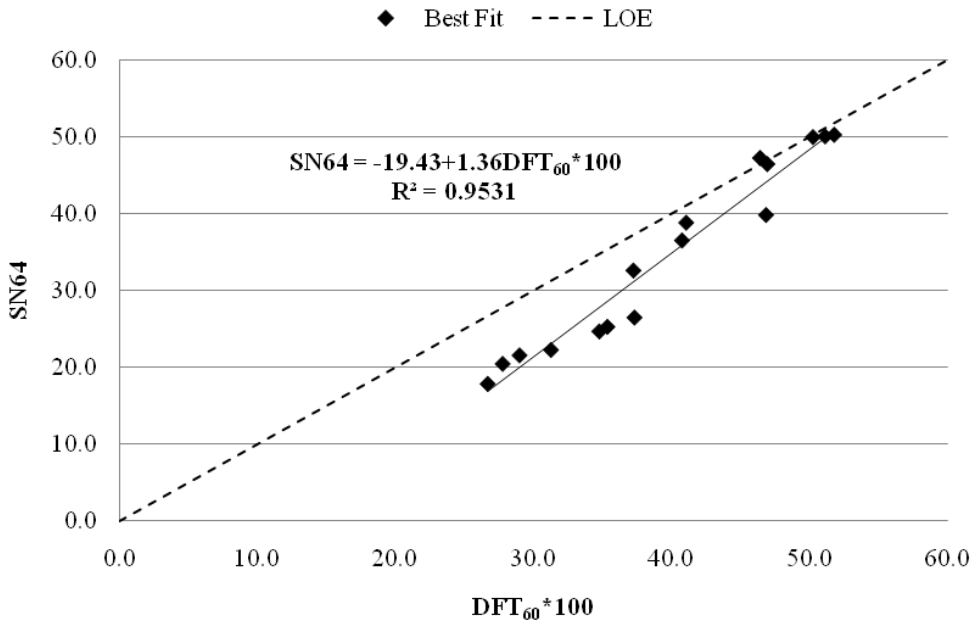


**Figure 2.11: Laboratory (DFT60*100) versus NCAT Test Track (SN64R) correlation (Erukulla 2011)**

While comparing laboratory mixtures to field mixtures is important and useful, there is still a need for improving the correlation between a single aggregate source micro-texture properties and field mixture friction data to relate the aggregate source's ability to resist polishing with the

overall mixture's ability to resist polishing under traffic. It is important for agencies to be able to identify aggregates that would be suitable for use in a surface mixture that are capable of providing good skid resistance when subjected to heavy traffic.

## 2.5 Measuring Mixture Surface Texture

The texture of aggregates and pavement mixtures, on both a macro and micro level, is a key component that influences a mixture's ability to provide an adequate amount of friction between the pavement surface and vehicle tire. Therefore, identifying aggregates and pavement mixtures characterized by high texture values is important to roadway safety. Several tests and equipment are currently used to quantify a pavement's surface macro-texture and micro-texture.

### *2.5.1 Volumetric Sand Patch Test*

The volumetric sand patch test (ASTM E965) is used to determine the average depth of the pavement's surface macro-texture. A known volume of dry Ottawa natural silica sand is spread over the cleaned pavement surface being evaluated. Once the sand is spread into a circular patch, the diameter is measured and recorded a minimum of four times at different locations. The average diameter is then used to find the area of the sand patch. The resulting Mean Texture Depth (MTD) is calculated by dividing the known volume of sand used by the area of the circular sand patch.

Other versions of the test use other materials such as glass spheres or a known volume of grease that is applied to the surface between two strips of masking tape. This is referred to as the grease patch method. With advancements in technology, the use of this test seems outdated and impractical due to operator subjectivity. Therefore, researchers should consider using automated equipment if it is available to them.

### *2.5.2 Circular Texture Meter (CTM)*

The use of laser technology is a more advanced approach to measuring the surface texture of a pavement. Several devices are currently available to measure pavement texture. The Circular Texture Meter (CTM) is a static device that uses laser technology to quantify the macro-texture of a pavement surface (ASTM E2157). The CTM provides texture measurements using a laser displacement sensor mounted on a 142 mm arm that rotates clockwise measuring pavement texture at a sampling rate of approximately 0.9 mm. The surface profile is recorded and divided into eight, 100 mm (4 in.) long segments, and the resulting Mean Profile Depth (MPD) and Root Mean Square (RMS) statistics are reported for each segment. Figure 2.12 provides an illustration of how the MPD is calculated for each segment.

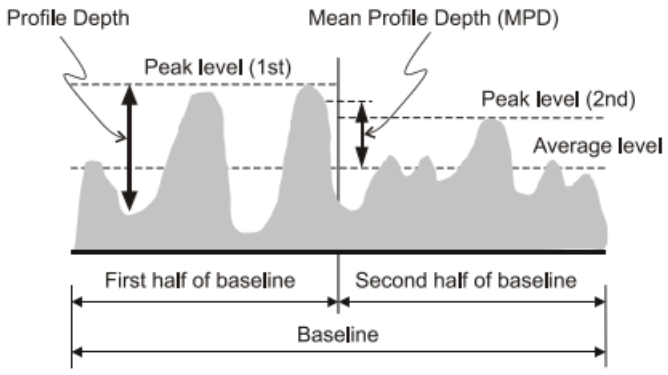


**Figure 2.12: Graphical representation of calculating the MPD from the CTM (McGhee et al. 2003)**

The slope of each segment is converted to a zero mean profile reference height, noted as "Average level" in Figure 2.12, by subtracting a linear regression of the segment. This reference height is characterized as having an area above it equal to the area below it. Each segment is then further divided into two equal halves, noted as first and second half of baseline in the figure. The

highest peak is determined in each half segment (Peak level), and the average of these two peak heights is the mean segment depth (McGhee et al. 2003). Therefore, the overall MPD is the average of the mean segment depths for all eight segments that make up the tested circumference of the CTM. The RMS is a "…statistical value offering one measure of how much the actual data (measured profile) deviates from a best fit (modeled data) of the data" (McGhee et al. 2003). Together, the MPD and RMS provide information on whether the surface texture is positive (surface projections) or negative (depressions) (Applied Pavement Technology 2015).

Previous research (Henry et al. 2000, McGhee et al. 2003) has shown a good correlation between the MTD provided by the sand patch test and the MPD provided by the CTM. Mcghee et al. (2003) confirmed the use of the CTM as a potential replacement tool for the sand patch test. Researchers compiled sand patch test and CTM data from 26 surfaces at the Wallops Flight Facility in Virginia and 55 surfaces at Virginia's Smart Road test bed. The texture values provided by the Wallops facility were reported as an average value of three replicates of each test type for each surface. Virginia's Smart Road data was reported as a single value for each test, where the sand patch test was conducted at the same location as the center of the CTM's circular track. The data compilation between the two facilities showed a strong correlation between the sand patch test's MTD and the CTM's MPD (Figure 2.13).

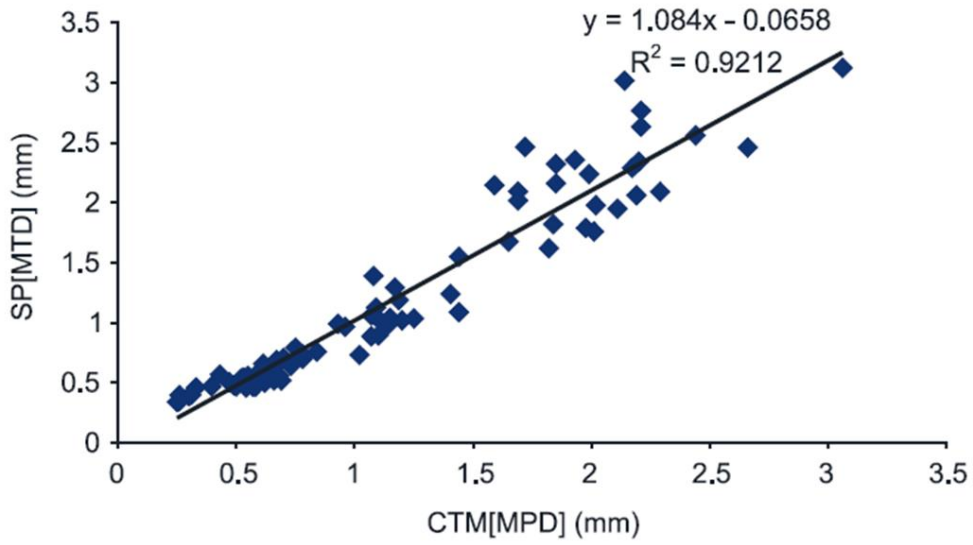


**Figure 2.13: Correlation between CTM MPD and sand patch MTD (McGhee et al. 2000)**

Figure 2.13 shows that the comparison between the MTD and MPD yielded approximately a one-to-one relationship, having a small y-intercept. Additionally, an $R^2$ value of 0.92 for this particular research agreed with previous research conducted by Abe et al. (2000) who found the correlation between the sand patch MTD and CTM's MPD to yield an $R^2$ value of 0.97. Therefore, the use of the CTM as a texture measuring device is practical and eliminates the operator subjectivity introduced by the volumetric sand patch test.

One disadvantage of the CTM is that it focuses on macro-texture measurements only and is not used to evaluate the micro-texture of the pavement. Because pavement micro-texture plays a key role in pavement friction, it would be useful to have a device that measures both macro and micro-texture using laser technology.

### *2.5.3 Laser Texture Scanner (LTS)*

Serigos et al. (2013) evaluated the Laser Texture Scanner's (LTS) ability to quantify pavement micro-texture by using it to test the same locations as the CTM and BPT (mentioned previously) for twenty-eight test sections in the field. The LTS is a device similar to that of the CTM; however, because the device uses a higher sampling rate than that of the CTM, it is also capable of defining pavement micro-texture by separating the texture components within a surface profile. Components within the surface profile that were characterized by a wavelength between 0.05 mm and 0.50 mm were considered micro-texture, whereas macro-texture is defined as wavelengths between 0.50 mm and 50.0 mm (Serigos et al. 2013). The method of filtering these surface profiles from the LTS was found to be successful for all twenty-eight pavement test sections that were evaluated. This showed micro-texture could be included in the analysis.

As mentioned previously, Serigos et al. (2013) compared texture data with BPT data taken at the same locations in the field to demonstrate that the prediction of the BPN could improve when accounting for both macro and micro-texture, rather than only taking macro-texture into account. Macro-texture measurements were taken using the CTM, whereas the pavement surface micro-texture was collected using the LTS. The researchers analyzed the effects of CTM macro-texture and LTS micro-texture on the BPN separately (Figure 2.14).

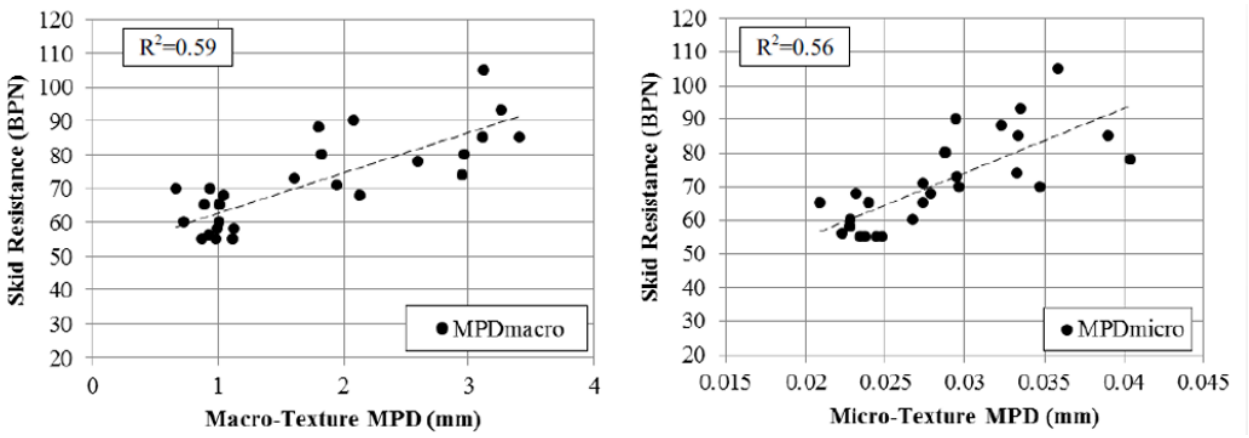


**Figure 2.14: Relationship between macro-texture MPD and BPN (left) and micro-texture MPD and BPN (right) (Serigos et al. 2013)**

It is apparent that a relationship between the CTM measured macro-texture and BPN as well as LTS measured micro-texture and BPN exists; in each cases, the BPN increased as the macro and micro-texture increased. The researchers came up with a linear regression reference model to explain the prediction of BPN, initially accounting for macro-texture only (Equation 2.2).

BPN Linear Regression (Serigos et al. 2013):

$$BPN = \alpha + \beta_{MACRO_{MPD}} * MACRO_{MPD} + \beta_{TREAT} * Treat \quad Equation\ 2.2$$

Where:

$\alpha$, $\beta_{MACRO\ MPD}$, $\beta_{TREAT}$: Regression coefficients

$MACRO_{MPD}$: MPD of the surface macro-texture as measured by the CTM

Treat: Value of 1 if test section consisted of light texturing treatment; otherwise 0

Using Generalized Least Squares (GLS) statistics, the regression parameters were estimated. It should be noted that a light texturing treatment was applied to some of the test sections at the time of testing. T-statistics obtained from using the GLS showed that the application of the

treatment was statistically significant in explaining the BPN, and therefore, was included in the regression model to obtain an $R^2$ of 0.670.

The micro-texture parameters, as measured by the LTS, were then incorporated into the reference model (Equation 2.2). This was also calculated using GLS. The regression model that incorporated the LTS measured micro-texture data with the CTM macro-texture measurements increased the adjusted $R^2$ value from 0.670 to 0.775. This supports the accepted theory that micro-texture greatly influences the performance of a pavement in terms of friction and should be accounted for when correlating texture data with field friction data. Although both the CTM and LTS were successful in quantifying pavement texture, the two devices are used to test pavement surfaces. This still leaves a need for a simpler laboratory protocol to quantify aggregate textural characteristics.

### 2.6 Existing Laboratory Conditioning Devices

Because asphalt mixtures are composed primarily of aggregates, it is important to use aggregates which resist polishing to ensure the mixtures maintain their friction properties. An aggregate might be characterized by a high level of initial angularity or texture, which is indicative of its field performance. However, if the aggregate cannot maintain a sufficient level of friction under traffic loadings, the aggregate may not be applicable for a pavement surface course. Therefore, laboratory polishing equipment may be used to assess an aggregate's or a pavement surface's resistance to polishing. For the purpose of this research, the primary focus will be on equipment used to polish aggregates.

### *2.6.1 Los Angeles (L.A.) Abrasion Test*

The L.A. Abrasion (ASTM C535) is a device that has been used to assess coarse aggregate resistance to degradation (Figure 2.15). An aggregate sample containing material retained on the #12 (1.70 mm) sieve of known gradation is placed inside a steel drum with a specified number (six to twelve) of 450 gram steel charges. The drum is equipped with shelves inside that pick up the aggregate sample and steel charges and drop them the height of the drum as it rotates. After the drum rotates 1,000 revolutions at 30 to 33 rpm, the material is removed and washed over a #12 sieve. The material is oven dried, and the percent loss of the aggregate sample is determined as aggregate passing the #12 sieve.


**Figure 2.15: L.A. Abrasion testing equipment (Pavement Interactive 2012)**

Previous research has concluded that the L.A. Abrasion test does not correlate well with field pavement performance (Wu et al. 1998) and acts more as an impact test rather than simulating

the polishing action from heavy traffic in the field (Lane et al. 2000). Wu et al. (1998) tested sixteen aggregate sources that varied in performance levels in asphalt concrete using a variety of impact tests, such as the Los Angeles Abrasion test, Micro-Deval (discussed within the next section), Aggregate Impact Value, Aggregate Crushing Value, and degradation in the Strategic Highway Research Program (SHRP) Gyratory Compactor. Table 2.1 shows what Wu et al. (1998) characterized as a good, fair, and poor historical pavement performance rating. For the purpose of this research and literature review, the focus will be on the Los Angeles Abrasion and Micro-Deval aggregate conditioning tests, as these are the tests commonly used in the United States.

**Table 2.1: Pavement performance evaluation criteria (Wu et al. 1998)**

| Pavement Performance Rating | Description |
|---|---|
| Good | Used for many years with no significant degradation problem during construction and no significant popouts, raveling, or potholes during service life |
| Fair | Used at least once where some degradation occurred during construction and/or some popouts, raveling, and potholes developed, but pavement life extended for over 8 years |
| Poor | Used at least once where raveling, popouts, or combinations developed during the first two years, severely restricting pavement |

The L.A. Abrasion results of the sixteen aggregate sources were compared with the historical pavement performance rating (Figure 2.16). As a result, they demonstrated that the L.A. Abrasion was not capable of delineating between aggregates as related to good, fair, and poor

performance. In some cases, aggregate sources characterized as poor resulted in an L.A. Abrasion mass loss close to those aggregate sources that were characterized as good.

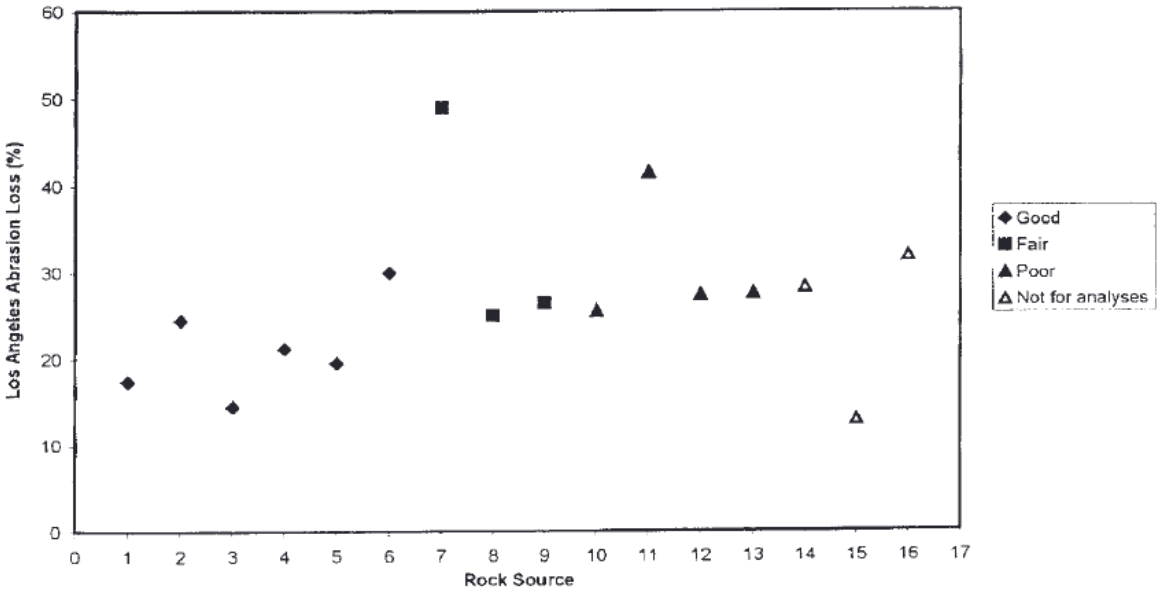


**Figure 2.16: Pavement performance ratings with L.A. Abrasion results (Wu et al. 1998)**

### *2.6.2 Micro-Deval Aggregate Conditioning Test*

The Micro-Deval (Figure 2.17) is a device used to condition an aggregate sample. The aggregate's resistance to polishing, abrasion, and breakage can then be tested. An aggregate sample with a specified gradation (ASTM D6928 for coarse aggregates or ASTM D7428 for fine aggregates) is soaked in a specified volume of water for a minimum of one hour prior to testing. The aggregate sample and volume of water are then placed inside a steel drum with a specified mass of steel balls. The interaction of the steel charges and aggregates degrades the aggregate sample as the container rotates for a specified time or number of revolutions. The percent of material that passed the 1.18 mm (#16) sieve for coarse aggregates and 75 um (#200) for fine aggregates, is then measured to detect the aggregate sample's abrasion resistance and durability.

**Figure 2.17: Micro-Deval apparatus**

Previous research has shown the Micro-Deval test to be a good tool in evaluating coarse aggregate quality in the presence of water. An aggregate's quality and abrasion resistance may be categorized into three different performance levels as good, fair, or poor depending on the percent loss upon conducting the Micro-Deval test. As mentioned previously, Wu et al. (1998) tested sixteen aggregate sources varying in asphalt concrete field performance levels using the Micro-Deval. Researchers compared the Micro-Deval performance rating (good, fair, or poor) based on mass loss with the subjective ratings of the asphalt concrete mixtures from different state transportation agencies, using the same criteria provided in Table 2.1. They found the Micro-Deval to yield the same ratings for most of the aggregate sources (Figure 2.18).

The solid horizontal lines show the average of the Micro-Deval mass loss for each of the different groups rated by the state agencies. Wu et al. (1998) determined that 18% mass loss delineated aggregates of poor quality from the fair and good quality aggregate, which is depicted by the dashed line in the figure. It should be noted that the Micro-Deval test was the only impact test of the five (mentioned previously) that showed clear delineations among the aggregate groups (Wu et al. 1998)

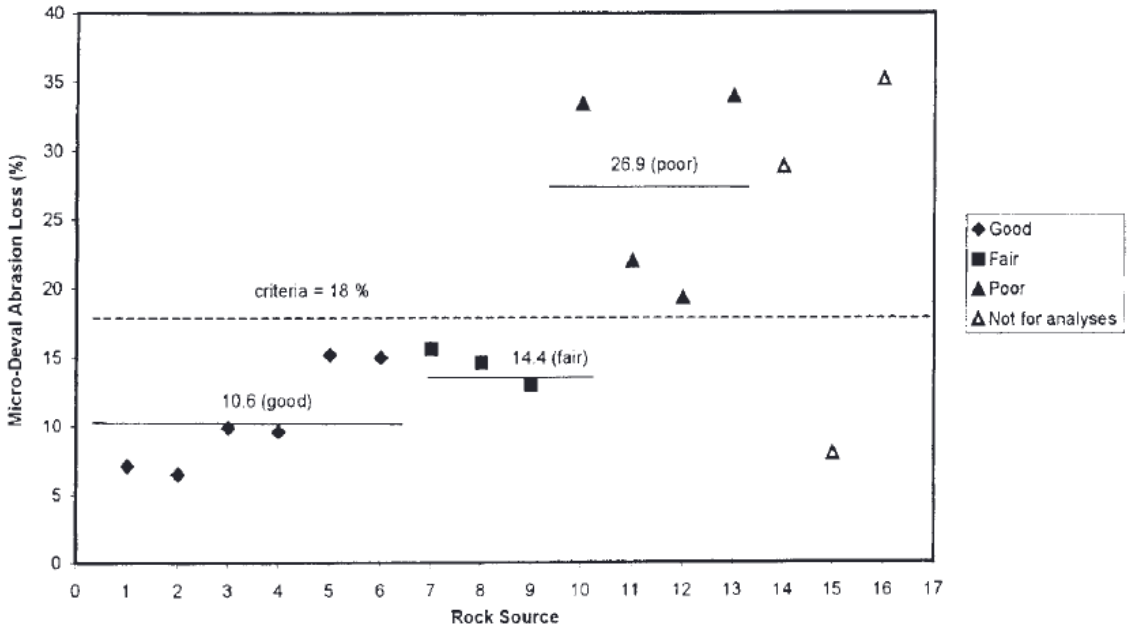


**Figure 2.18: Pavement performance ratings with Micro-Deval abrasion (Wu et al. 1998)**

Similarly, Cooley et al. (2002) selected 72 different aggregate sources from eight different states (AL, GA, FL, KY, MS, NC, SC, and TN) varying in historical asphalt pavement performance and evaluated their quality using the L.A. Abrasion and Micro-Deval tests. They found mixed results among the Micro-Deval data for each state. For example, of the five states that selected aggregate sources with at least two different performance histories, only Micro-Deval results for

AL and GA agreed with the historical performance rankings. The Micro-Deval results for the remaining three states did not distinguish between the three categories of aggregates (good, fair, and poor) that were ranked based on historical performance. The researchers concluded that the mineralogical type resulted in the wide range of Micro-Deval results and suggested that specifications for the Micro-Deval test method be dependent on parent aggregate type. Despite the mixed results, the Micro-Deval is still considered to be a useful tool in evaluating the quality and abrasion resistance of aggregates ranging from poor to good historical asphalt pavement performance.

### *2.6.3 L.A. Abrasion and Micro-Deval Test Differences*

In the progression of test development, the Micro-Deval test procedure was compared to the industry standard L.A. Abrasion. Research showed the two yielded significantly different results which is to be expected as they simulate different types of impacts and abrasion on the aggregate sample. The impact from the L.A. Abrasion simulates the impact aggregates experience during handling and construction, whereas the Micro-Deval abrasion relates closer to what aggregates would experience in the field when subjected to traffic.

As mentioned previously, Cooley et al. (2002) tested 72 aggregate sources using the L.A. Abrasion and Micro-Deval and found that the L.A. Abrasion resulted in a higher percent loss than that of the Micro-Deval, sometimes more than double the percent loss. This can be attributed to the L.A. Abrasion test using fewer but significantly larger steel charges (46.8 mm diameter) as opposed to the several smaller ones used in the Micro-Deval test protocol (9.5 mm diameter). The L.A. Abrasion drum is also equipped with baffles inside which pick up the aggregates and large steel charges and drops them the height of the drum. This increases the possibility for damage compared to the Micro-Deval test. The harsher impact tends to yield

higher mass loss values for some high quality aggregates that have otherwise performed well in the field (Rogers et al. 2003).

Additionally, the L.A. Abrasion test is run on oven dry aggregates as opposed to the Micro-Deval protocol, which tests aggregates in the presence of water. Aggregates are rarely dry in the field and experience more polishing and abrasion than the type of impact simulated by the L.A. Abrasion (Rogers et al. 2003). Therefore, the Micro-Deval appears to be more appropriate than the L.A. Abrasion in evaluating an aggregate's resistance to traffic wear while the L.A. Abrasion test is more appropriate in assessing aggregate breakdown during handling, mixing, and placement.

### *2.6.4 British Polishing Wheel*

The British Polishing Wheel (ASTM D3319) is a device used to polish coarse aggregates. The polishing resistance of the coarse aggregates are then tested using the BPT described previously. The British Polishing Wheel is equipped with a cylindrical wheel and a pneumatic rubber tire (Figure 2.19). Coarse aggregates are placed in the same mold as described for BPT testing. The cylindrical wheel is characterized by a flat-surface periphery capable of holding fourteen test specimens. Test specimens are clamped to the wheel so as to create a continuous surface of coarse particles for polishing. As the wheel rotates at 320 +/- 5 rpm, the rubber tire comes in contact with the coarse aggregates subjecting them to polishing. During testing, water and a silicon carbide grit (No. 150) are continuously fed onto the specimens prior to coming in contact with the rubber tire. The water should be fed at a rate of 50 to 75 mL/minute, and the grit is fed at a rate of 6 +/- 2 g/minute (ASTM D3319). After the coarse aggregates have been subjected to polishing for the desired time, the specimens are removed, washed, and tested using the BPT in accordance with ASTM E303.

**Figure 2.19: British Polishing Wheel apparatus**

### *2.6.5 NCAT Three Wheel Polishing Device (TWPD)*

The TWPD is a device developed by NCAT that is used to condition laboratory compacted HMA slabs (Figure 2.20). The friction and texture loss of the HMA wearing course may then be evaluated using the DFT and CTM, respectively. The device is equipped with three pneumatic rubber tires, inflated at 50 psi, that come in contact with the slab surface. The wheels are attached to a turntable allowing them to rotate in a circle that is characterized by the same diameter as that of the DFT and CTM (11.2 inches). A variable load may be applied to the wheels by adding steel plates on the turntable. During conditioning, water is continuously circulated from the water tank through PVC pipes that are attached to the wire mesh enclosure. Once the counter reaches the

desired number of revolutions, the device shuts off and the slabs are measured for texture and friction using the CTM and DFT, respectively..

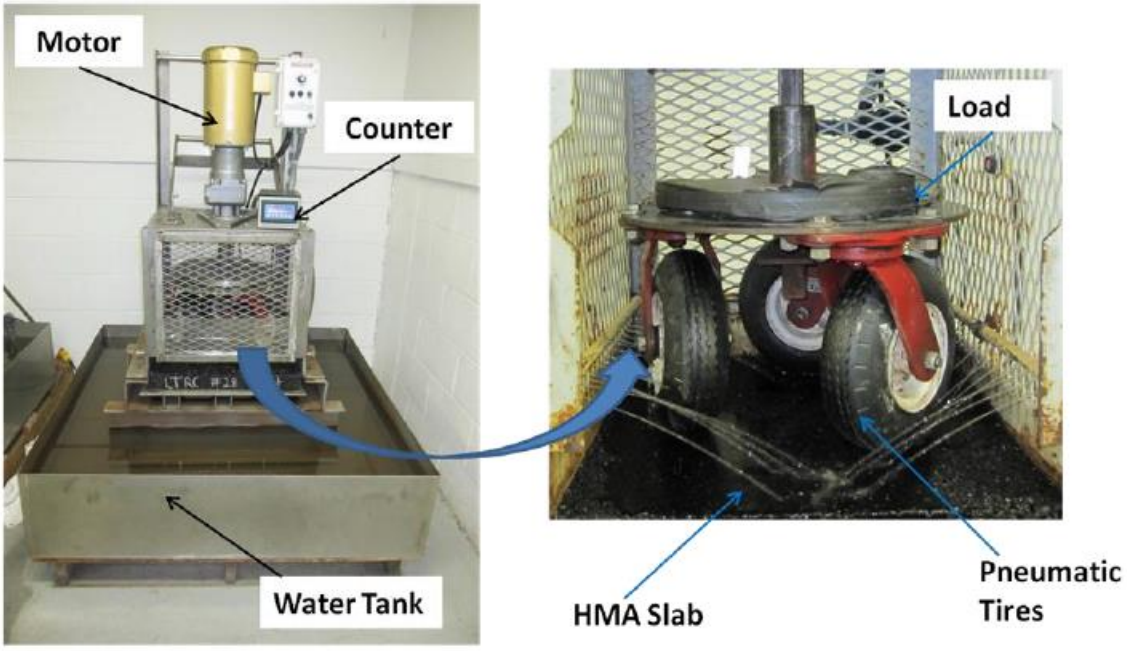


**Figure 2.20: NCAT Three Wheel Polishing Device (Erukulla 2011)**

## 2.7 Aggregate Imaging Systems

Aggregate imaging analysis is an automated way of quantifying aggregate shape properties while eliminating the subjectivity introduced by Superpave consensus property tests, such as *Uncompacted Void Content of Fine Aggregates (AASHTO T304), Flat and Elongated Particles in Coarse Aggregates (ASTM D4271), and Percent of Fractured Particles in Coarse Aggregates (ASTM D5821).* Several different imaging systems have been developed and evaluated within the last decade to assess their ability to appropriately characterize aggregate shape properties. The focus of this work is on the recently developed second generation Aggregate Imaging Measurement System (AIMS-II) and the second generation of the Enhanced University of

Illinois Aggregate Image Analyzer (E-UIAIA). Although a recent NCHRP study recommended the AIMS-II device to quantify aggregate shape characteristics, both imaging devices were deemed capable of producing validated indexes for aggregate shape properties that may be correlated with field performance data (Masad et al. 2007).

### *2.7.1 The Second Generation Aggregate Imaging Measurement System (AIMS-II)*

The AIMS-II device (Figure 2.21), developed by Pine Instruments, is a computer automated system that captures aggregate images. The device then uses these images to analyze and quantify both coarse and fine aggregate shape characteristics through a series of algorithms. AIMS-II is equipped with two lighting configurations (back lighting and top lighting) and a microscope-camera system enclosed in a case to protect it from outside light sources (Pine Instrument Company 2011).

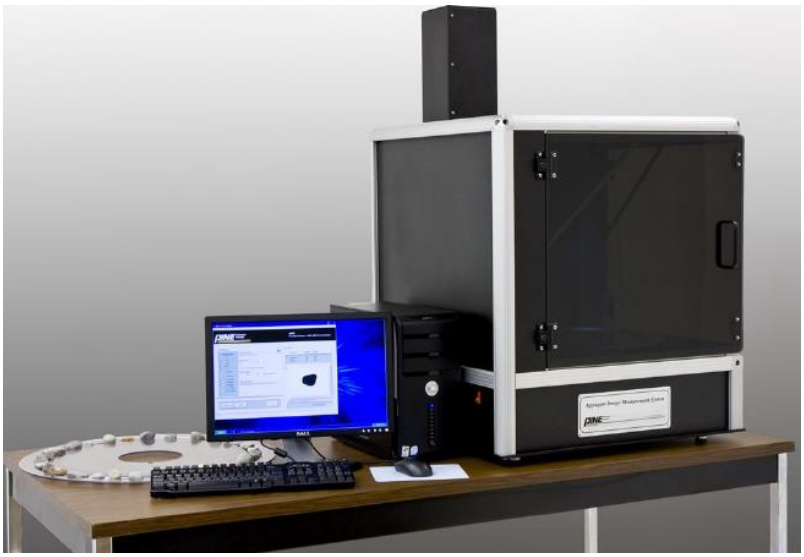

**Figure 2.21: The second generation Aggregate Imaging Measurement System (Pine Instrument Company 2011)**

The aggregates set in a rotating tray are individually scanned such that the camera captures images of each particle. Coarse aggregates require three separate scans, while fine aggregates only use a single scan for analysis. For coarse aggregates, the first scan uses the back lighting to capture a black and white silhouette of each aggregate. This scan is used to quantify the aggregate's angularity using the gradient method, as discussed within the next chapter. Additionally, the first scan is used to record the centroid of the particle so the system may recognize the particle location for additional scans. Top lighting is used during the second scan to determine particle height measurements. The third scan captures grey scale images used to analyze each particle's surface texture from wavelet analysis (Pine Instrument Company 2011). These three scans are critical in quantifying coarse aggregate angularity, particle surface texture, sphericity, and flatness and elongation ratios. For fine aggregates, a single scan is used to quantify fine aggregate angularity and two-dimensional form. The AIMS-II software program exports all the data into a spreadsheet consisting of the relevant shape characteristics for each particle and corresponding statistics for the sample group, such as mean, standard deviation, and cumulative distribution.

### *2.7.2 Enhanced University of Illinois Aggregate Image Analyzer (E-UIAIA)*

Similar to the AIMS-II, the E-UIAIA (Figure 2.22) is a second generation device originally developed by Dr. Erol Tutumluer which was designed to quantify shape properties for coarse aggregates only.

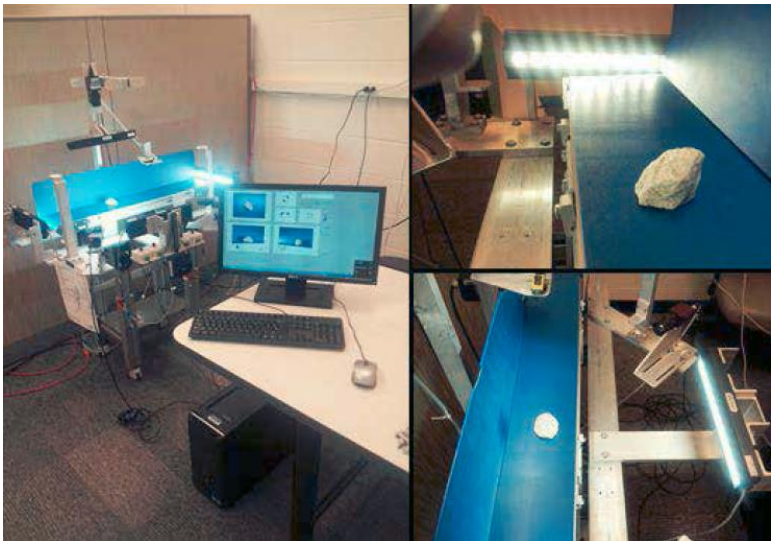

**Figure 2.22: The Enhanced University of Illinois Aggregate Image Analyzer (Mahmoud et al. 2014)**

The E-UIAIA uses a different type of high resolution camera system than that of the AIMS-II to capture three projections of the particles as they move along a conveyor belt to determine gradation, form, angularity, texture, surface area, and volume (Mahmoud et al. 2014). The device is equipped with dimmer controls that allow the operator to adjust the lighting to obtain the best quality aggregate images (Moaveni et al 2013). Similar to the AIMS-II, the E-UIAIA also uses a software program to export the calculated shape characteristics to a spreadsheet for further analysis.

## 2.8 Relevant Research on AIMS

As previously mentioned, the Superpave consensus property tests are commonly used as part of material acceptance for several state agencies. One major disadvantage of these tests is that they can be laborious, time consuming, and subjective. Therefore, researchers are hopeful in replacing

the Superpave consensus property tests with an automated aggregate imaging system as part of material acceptance protocol in the future.

Gudimettla et al. (2008) compared results obtained from Superpave consensus property tests with the first generation AIMS test results for a variety of aggregates. The following comparisons were made as part of the research study:

- Uncompacted Void Content of Fine Aggregates (AASHTO T304) and AIMS Fine Aggregate Angularity (FAA)
- Uncompacted Void Content of Fine Aggregates (AASHTO T304) and AIMS Fine Aggregate Two Dimension Form
- Flat and Elongated Particles in Coarse Aggregates (ASTM D4271) and AIMS Flat and Elongation
- Percentage of Fractured Particles in Coarse Aggregates (ASTM D5821) and AIMS Coarse Aggregate Angularity (CAA)

The first generation AIMS fine aggregate angularity and two dimensional form results ranked the aggregates the same when compared with AASHTO T304 results. Fine aggregate angularity is an important parameter for ensuring adequate internal friction within the aggregate structure that is developed to prevent rutting (Prowell et al. 2005). The results obtained from comparing AASHTO T304 with AIMS FAA and AIMS two-dimensional form for three different sizes of three aggregate sources that were tested are shown in Table 2.2 with the numerical ranking represented as a letter in parenthesis. It should be noted that the table reflects the results from one of the several projects that were part of the research study. The rankings for all the projects' aggregates that were used in this research were the same for AASHTO T304, AIMS FAA, and

AIMS two-dimensional form except for one, ME-0359 (Table 2.3). The aggregates are listed in the corresponding order of their ranking in the table.

**Table 2.2: Example of results obtained from AASHTO T304, AIMS FAA, and two-dimensional form (Gudimettla et al. 2008)**

| | AASHTO T304 FAA (Method A) | AIMS FAA | | | AIMS Two-Dimensional Form | | |
|---|---|---|---|---|---|---|---|
| | | 2.36 mm | 1.18 mm | 0.600 mm | 2.36 mm | 1.18 mm | 0.600 mm |
| 1/4" Washed | 44 (A) | 4,081 (A) | 4,729 (A) | 4,422 (A) | 8.5 (A) | 9.0 (A) | 8.8 (A) |
| 2A Gravel | 42 (C) | 3,271 (C) | 3,205 (C) | 3,381 (C) | 6.8 (C) | 6.5 (C) | 7.3 (C) |
| C Gravel | 42.8 (B) | 3,342 (B) | 3,677 (B) | 3,902 (B) | 6.9 (B) | 7.4 (B) | 8.3 (B) |

**Table 2.3: Rankings obtained from AASHTO T304, AIMS FAA, and AIMS two-dimensional form (Gudimettla et al. 2008)**

| Project ID | Fine Aggregates | AASHTO T304 FAA | AIMS FAA | AIMS Two-Dimensional Form |
|---|---|---|---|---|
| NJ 0671 | #8, #10, RAP | A,B,C | A,B,C | A,B,C |
| ME 0570 | Crusher Dust, Crusher Sand | A,B | A,B | A,B |
| NE 0569 | 1/4" Washed, C Gravel, 2A Gravel | A,B,C | A,B,C | A,B,C |
| KS 0568 | Crushed Sand 2, Natural Gravel | A,B | A,B | A,B |
| NY 0466 | Washed Screenings, Screenings, RAP, Natural Sand | A,B,C,D | A,B,C,D | A,B,C,D |
| MN 0465 | ST Cloud Sand, Kraemer Sand, RAP, West Lakeland Sand | A,B,C,D | A,B,C,D | A,B,C,D |
| KS 0464 | CH-1A, Crushed Sand 2A, Crushed Gravel 1, Crushed Sand 2, Natural Sand | A,B,C,D,E | A,B,C,D,E | A,B,C,D,E |
| LA 0462 | Crushed Gravel, RAP, Concrete Sand | A,B,C | A,B,C | A,B,C |
| NC 0360 | Screenings, RAP, Natural Sand | A,B,C | A,B,C | A,B,C |
| ME 0359 | Washed Ledge Sand, -3/8 Ledge Sand, RAP, Hancock Sand | A,B,C,D | B,A,C,D | B,A,C,D |

Additionally, the AIMS flat and elongated (F&E) results and the F&E values obtained from ASTM D4271 ranked similarly in most cases for both ratios, 1:3 and 1:5. Deviations between the two test results can be attributed to user subjectivity introduced in the ASTM D4271 procedure. Flatness and elongation ratios have not been tied directly to pavement friction but rather to influencing the mixture's volumetric properties (Prowell et al. 2005).

Results from ASTM D5821 and AIMS coarse aggregate angularity comparison appeared to be inconclusive because they do not measure similar properties. ASTM measures fractured faces while the AIMS measures aggregate angularity. A majority of the aggregates were said to have 100 percent fractured faces when following ASTM D5821 procedure, while the AIMS provided different angularity values for those aggregates. The ASTM procedure does not measure angularity and the AIMS does not detect fractured faces (Gudimettla et al. 2008). Table 2.4 shows a few examples of the project results obtained from ASTM D5821 and AIMS CAA.

**Table 2.4: Example of CAA results obtained from ASTM D5821 and AIMS (Gudimettla et al. 2008)**

| Project ID | Coarse Aggregates | ASTM D5821 CAA 1 Fractured Face (%) | ASTM D5821 CAA 2 Fractured Faces (%) | AIMS CAA |
|---|---|---|---|---|
| NJ 0671 | 8's | 100 | 100 | 2,748 |
| | 57's | 100 | 100 | 2,995 |
| | RAP | 99 | 1 | 2,714 |
| ME0570 | 1/2's | 99 | 98 | 3,509 |
| NE 0569 | 1/4 Washed | 100 | 100 | 2,585 |
| | 2A Gravel | 32 | 21 | 2,248 |
| | C Gravel | 60 | 43 | 2,314 |

This introduces a potential limitation with the ASTM procedure in that an aggregate source may be characterized by higher angularity when compared to another aggregate source as defined by

AIMS, but the two could have the same percentage of fractured faces. The ASTM procedure would show no indication of any differences between the two aggregate sources when considering angularity. Coarse aggregate angularity is said to be the second most important property behind gradation for HMA pavement performance (Prowell et al. 2005). There is a need to be able to sufficiently quantify this parameter, and inspecting fractured faces may not adequately accomplish this.

This research study (Gudimettla et al. 2008) provided useful insight towards the advancement of using an automated aggregate imaging system as an alternative to Superpave consensus property tests in the future. Superpave consensus property tests are not intended to evaluate an aggregate's capability of providing adequate friction to a surface mixture. For example, the Superpave consensus property tests do not adequately provide coarse aggregate surface micro-texture measurements, but the AIMS is capable of measuring micro-texture, an important aggregate property that influences pavement friction (Hall et al. 2009).

Although the first generation AIMS device was used in the Superpave and AIMS comparison study, it can be assumed that with the advancements in the AIMS-II device, the results would yield similar rankings to that of the first generation. As part of the AIMS-II implementation study (Gates et al. 2011), results generated by the first generation AIMS device were compared with those of the second generation for a variety of aggregate sources, including 32 coarse aggregate samples and 21 fine aggregate samples. Both systems ranked the aggregate sources the same among each of the shape parameters and provided comparable results. For example, Figure 2.23 shows the comparison between the first generation AIMS (AIMS 1 in the figure) and the second generation AIMS (AIMS 2 in the figure) of the angularity indexes for all the aggregate sources tested. Therefore, they concluded that any research studies that used the first generation

AIMS were applicable to characterizations obtained from the second generation device, AIMS-II (Gates et al. 2011).

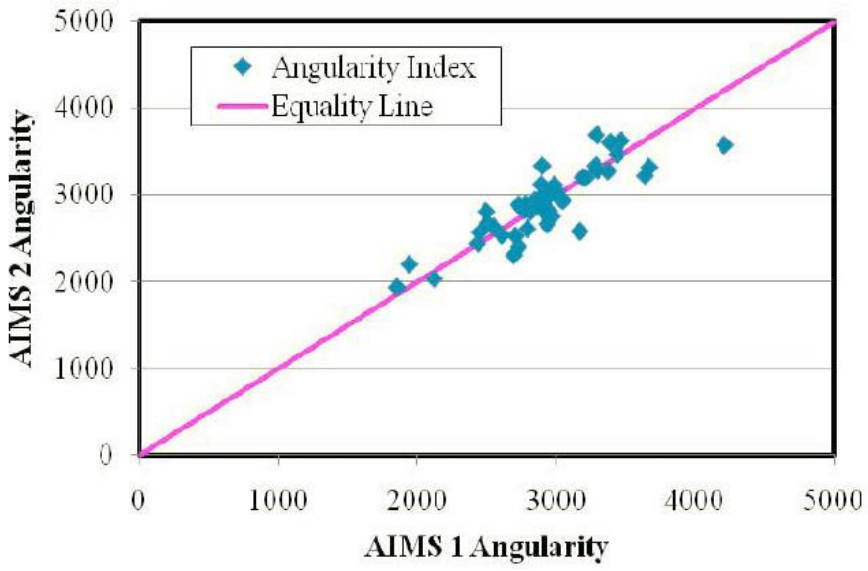


**Figure 2.23: Angularity index comparison between the AIMS-I and AIMS-II devices (Gates et al. 2011)**

Another research study conducted at the University of Illinois at Urbana-Champaign focused on evaluating the feasibility of using two aggregate imaging devices, AIMS-II and the E-UIAIA, in conjunction with the Micro-Deval to track an aggregate's resistance to polishing, abrasion, and breakage (Moaveni et al. 2013). It should be noted that this particular research study was one of many research tasks conducted for an ongoing project in cooperation with the Illinois Department of Transportation (IDOT) (Mahmoud et al. 2014). Researchers retained the material captured on the 9.5 mm sieve for eleven aggregate sources before subjecting them to conditioning in the Micro-Deval for 15, 30, 45, 60, 75, 90, 105, 180, and 210 minutes. As part of a separate research task, Mahmoud et al. (2014) determined that 210 minutes was sufficient polishing time in the Micro-Deval for the aggregates to reach terminal texture and angularity.

However, for both devices, the rate of texture loss reduced significantly after 105 minutes of conditioning in the Micro-Deval, indicating the initial point at which the aggregates began approaching terminal values. The aggregate samples were analyzed using the AIMS-II and E-UIAIA prior to conditioning and after each conditioning cycle. Researchers found that both imaging devices were capable of detecting aggregate degradation in the Micro-Deval. Additionally, the researchers developed regression equations using statistical analysis to predict angularity and surface texture as a function of Micro-Deval conditioning time for each aggregate type and device in the form of Equation 2.3 (Moaveni et al. 2013). Each aggregate source was characterized by a different equation with different fitting parameters to show the rate of texture or angularity loss. Table 2.5 shows an example of the fitting parameters used to model the AIMS-II texture results, and Table 2.6 shows an example of the fitting parameters used to model the AIMS-II texture results.

Surface Texture Index (Moaveni et al. 2013):

$$Shape\ Property\ (t) = a + b * exp^{-ct} \qquad Equation\ 2.3$$

Where:

*a*, *b*, and *c*: Fitting parameters based on statistical analysis relating to initial, final, and rate of change in texture

*t*: Micro-Deval conditioning time (minutes)

**Table 2.5: Example of AIMS-II fitting parameters for predicting angularity loss from Micro-Deval conditioning (Moaveni et al. 2013)**

| Aggregate | Fitting parameters | | | Goodness of fit | | |
|---|---|---|---|---|---|---|
| | a | b | c | SSE | $R^2$ | RMSE |
| FP1 | 1492 | 1185 | 0.0174 | 42313.4 | 0.968 | 77.7 |
| FP2 | 1433 | 1232 | 0.014 | 59492.5 | 0.957 | 92.2 |
| FP3 | 1384 | 1189 | 0.0155 | 62591.8 | 0.953 | 94.6 |
| FP4 | 1877 | 1053 | 0.0185 | 41115.8 | 0.962 | 76.6 |
| FP5 | 1443 | 1331 | 0.0186 | 71236.7 | 0.958 | 100.9 |
| FP6 | 1924 | 560.6 | 0.0529 | 48740.8 | 0.856 | 83.4 |
| FP7 | 2618 | 274.4 | 0.0239 | 9983.13 | 0.878 | 37.8 |
| FP8 | 2112 | 1144 | 0.0114 | 84878.4 | 0.924 | 110.1 |
| FP9 | 1590 | 1635 | 0.0248 | 30378.7 | 0.985 | 100.6 |
| FP10 | 2098 | 730 | 0.019 | 22076.9 | 0.957 | 56.2 |
| FP11 | 1130 | 1323 | 0.0209 | 105951 | 0.94 | 123 |

**Table 2.6: Example of AIMS-II fitting parameters for predicting surface texture loss from Micro-Deval conditioning (Moaveni et al. 2013)**

| Aggregate | Fitting parameters | | | Goodness of fit | | |
|---|---|---|---|---|---|---|
| | a | b | c | SSE | $R^2$ | RMSE |
| FP1 | 120.8 | 137.6 | 0.0266 | 547.7 | 0.97 | 8.8 |
| FP2 | 151.1 | 162.1 | 0.0256 | 500.5 | 0.98 | 8.5 |
| FP3 | 93.27 | 92.7 | 0.0304 | 190.5 | 0.98 | 5.2 |
| FP4 | 97.16 | 65.95 | 0.0095 | 102.4 | 0.97 | 3.8 |
| FP5 | 53.34 | 14.83 | 0.0341 | 43.2 | 0.83 | 2.5 |
| FP6 | 164.7 | 64.5 | 0.0256 | 531.2 | 0.88 | 8.7 |
| FP7 | 204.1 | -49.39 | 0.0866 | 366.8 | 0.86 | 7.2 |
| FP8 | 437.7 | -16.49 | -0.003 | 3287.2 | 0.06 | 21.7 |
| FP9 | 659.1 | 29.18 | 0.9935 | 6603.2 | 0.1 | 46.9 |
| FP10 | 436.8 | 161.8 | 0.0176 | 1489.8 | 0.94 | 14.6 |
| FP11 | 353.8 | -16.31 | 2.413 | 1805.8 | 0.12 | 16.1 |

While both devices were successful in detecting aggregate degradation from Micro-Deval conditioning, the two devices showed some significant differences in the texture and angularity results for the particles analyzed. For example, the E-UIAIA recorded one of the limestone sources to have one of the highest terminal angularity values, whereas the AIMS-II showed the same aggregate to have one of the lowest terminal angularity values when compared with the other aggregates. Although each device uses a different scale for angularity index and surface texture index, they should be able to rank the aggregates similarly. This could be attributed to the two different algorithms and methods used within the devices to calculate surface texture and angularity indexes. Additionally, the results obtained from the E-UIAIA showed more fluctuation, especially in the surface texture indexes, than that of the AIMS-II. This was noted by the E-UIAIA having a higher coefficient of variation (COV) within laboratory measurements than seen by the AIMS-II. Because this indicates the AIMS-II to have higher repeatability, it may be a more desired test. Moaveni et al. (2013) also specified that the AIMS-II results showed a better correlation with historical friction data obtained from IDOT. However, no evidence was presented within the report and was assumed to be part of the ongoing research project for the state.

Mahmoud et al. (2014) and Moaveni et al. (2013) concluded that the use of the Micro-Deval for aggregate polishing in conjunction with the AIMS-II for aggregate shape analysis proved to be feasible for coarse aggregates. With the success of this study, research should be taken a step further to show correlations of the polishing curves with field friction data. Additionally, the feasibility of using Micro-Deval with AIMS-II to detect changes in fine aggregate shape properties should be explored as they are an important part of the mix design as well. Correlating these texture and angularity indexes obtained from the imaging devices with field friction data

should be further studied as these aggregate properties influence pavement performance, especially friction, and could be used as part of material acceptance tests and contribute to enhancing roadway safety.

### 2.9 Summary of Literature Review

Pavement texture, on both a macro and micro level, is essential to providing adequate pavement friction to ensure the safety of the roadway system. Aggregate imaging systems have been proven to be successful in quantifying aggregate shape properties. They provide advantages over Superpave consensus properties in that these devices reduce operator subjectivity and are not labor intensive. Additionally, aggregate imaging systems provide information on the micro-texture of the coarse aggregates, a key component in pavement friction that is not currently assessed by Superpave consensus properties.

Aggregate imaging systems, more specifically the AIMS-II device, in conjunction with the Micro-Deval has proven to be successful in measuring degradation of aggregate angularity and texture. There is still a research need to come up with a laboratory test protocol that is capable of analyzing aggregate degradation due to polishing and correlates with field friction performance.

## CHAPTER 3: AIMS-II TEST DESCRIPTION

The AIMS-II is used to automatically quantify aggregate shape characteristics. As a tray of aggregates rotates around, a microscope-camera system is used to capture images of the aggregates using top lighting or back lighting. A photo of this camera system is shown in Figure 3.1.

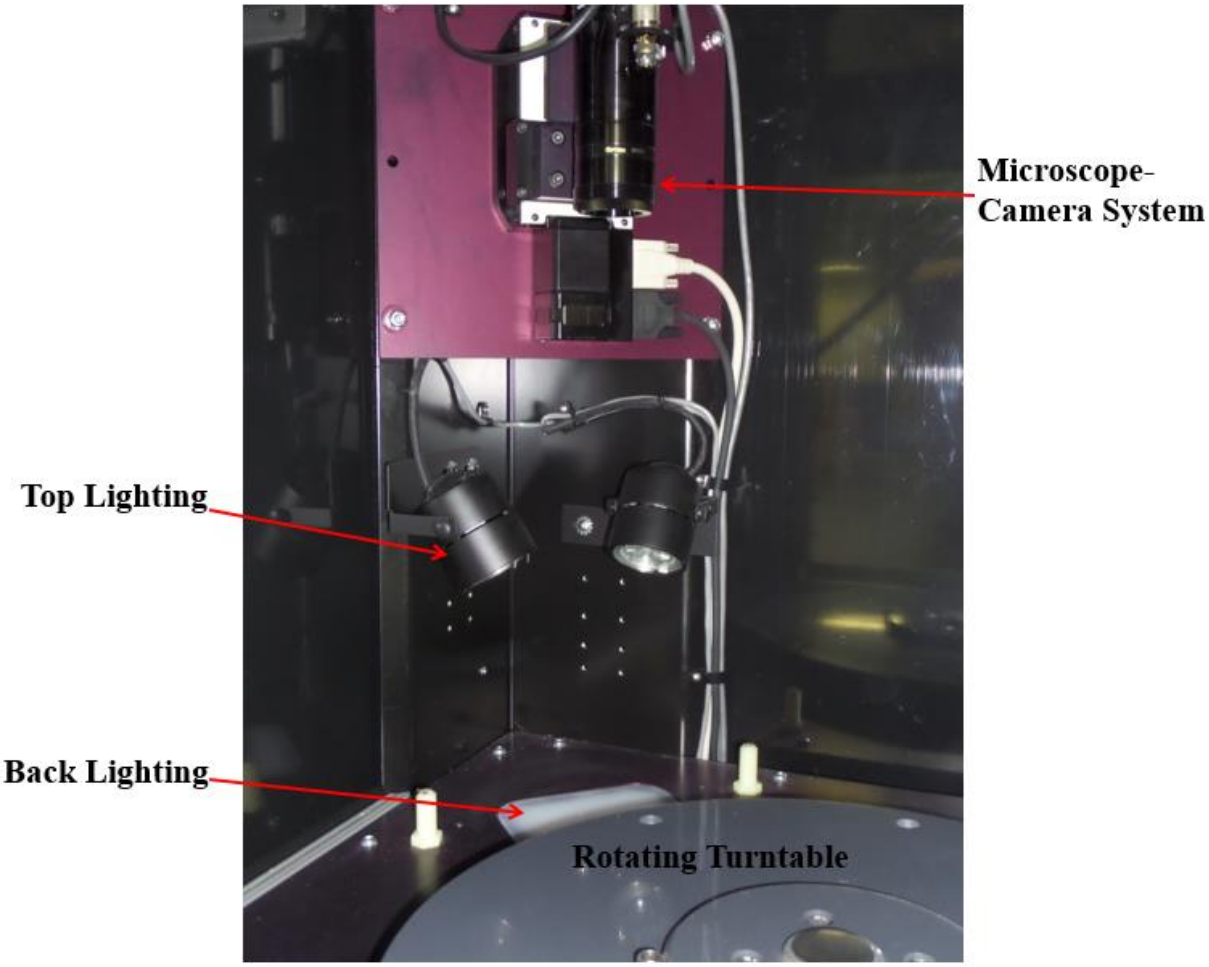


**Figure 3.1: AIMS-II camera system setup**

The AIMS-II software program then uses the images of each particle to calculate aggregate angularity, surface texture, three-dimensional form (sphericity), and flatness and elongation ratios for coarse aggregates (particles retained on the #4 sieve). Fine aggregate angularity and

two-dimensional form are calculated for the fine aggregates (particles passing the #4 and retained on the #200 sieve). The AIMS-II device does not measure the surface texture of fine aggregate. Though the reason is not explicitly stated, it is likely the AIMS-II is not capable of measuring a property at that small of a scale. The software interface allows the operator to select the coarse or fine aggregate size that is being analyzed. For coarse aggregates, the options to choose from are standard sieve sizes of the 1" (25 mm), 3/4" (19 mm), 1/2" (12.5 mm), 3/8" (9.5 mm), 1/4" (6.35 mm), and the #4 (4.75 mm). The fine aggregate selections include standard sieve sizes of the #8 (2.36 mm), #16 (1.18 mm), #30 (0.60 mm), #50 (0.30 mm), #100 (0.51 mm), and the #200 (0.075 mm) sieve. These sieve sizes indicate material that is retained on those sieves.

The system also allows the operator to select the particle count they wish to achieve, so the image acquisition will terminate once the specified particle count is reached. For the purpose of this research, the AIMS-II was run to scan all particles that were placed on the tray, resulting in a range of approximately 60-90 scanned particles for coarse aggregates and 160-300 scanned particles for fine aggregates for each replicate as discussed later. This was done to ensure that after all outliers were removed, the particle count remained above the AIMS-II specified minimum of 50 and 150 particles for coarse and fine aggregates, respectively.

### 3.1 AIMS-II Coarse Aggregate Testing

A tray was selected based on the aggregate size described previously. This establishes the trough size in which the aggregate is going to be placed. Each coarse aggregate particle was placed in the trough. Particle orientation depended on how the aggregate randomly came to rest in the trough (Figure 3.2). The number of particles placed in the trough depended on the size of the aggregate and the size of the trough. The design of the tray and trough allows the system to align

each aggregate directly under the camera to ensure each aggregate would be in full view for image acquisition. It was important to ensure the particles were spaced far enough apart to ensure the device did not misrepresent two aggregate particles as a larger aggregate particle.

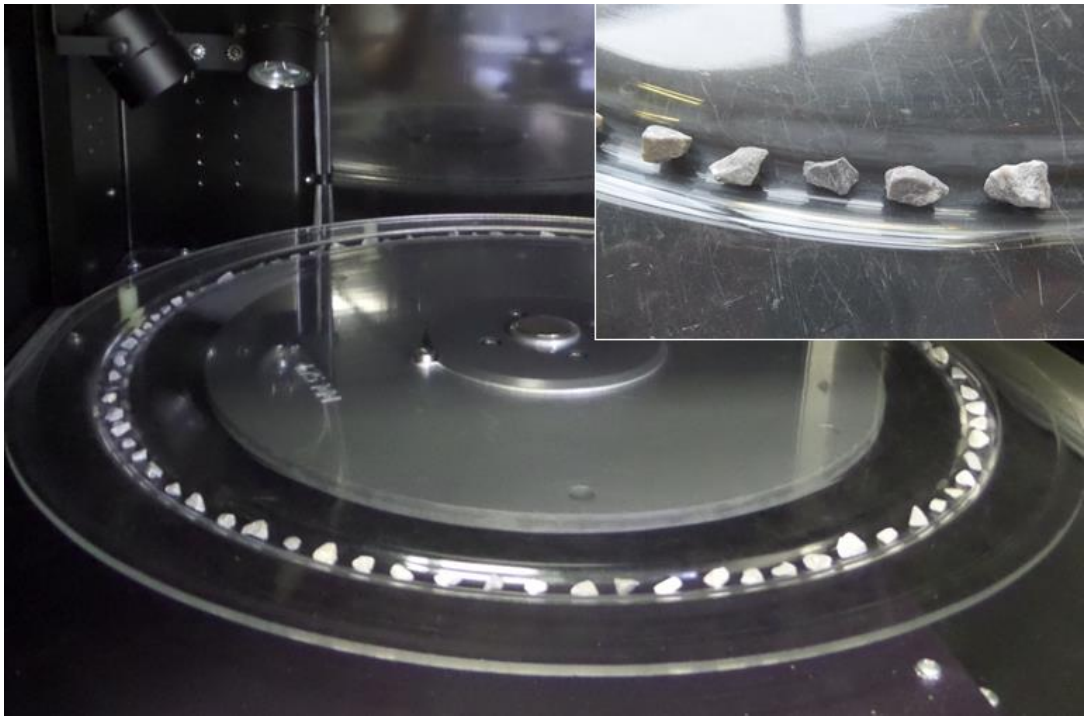

**Figure 3.2: Coarse aggregates spread on tray trough**

Image acquisition was initiated when the doors were closed, and the tray returned to its initial position. As the aggregate tray completed its first pass, each aggregate was scanned under the camera unit using back lighting. This created a black and white silhouette of each particle to determine the centroid and quantify angularity. If the entire particle was not in camera view, the particle was rejected from the analysis, and the tray would rotate to the next particle. Figures 3.3 and 3.4 show an example of the black and white silhouette generated by the first scan for an accepted particle as well as a rejected particle, respectively. The camera view of the rotating aggregates is shown in the left picture, whereas the angularity image that is produced is shown in

the right picture of the figures. To clarify, the particle that was being scanned is circled in green (accepted particle) and red (rejected particle) in the left picture.

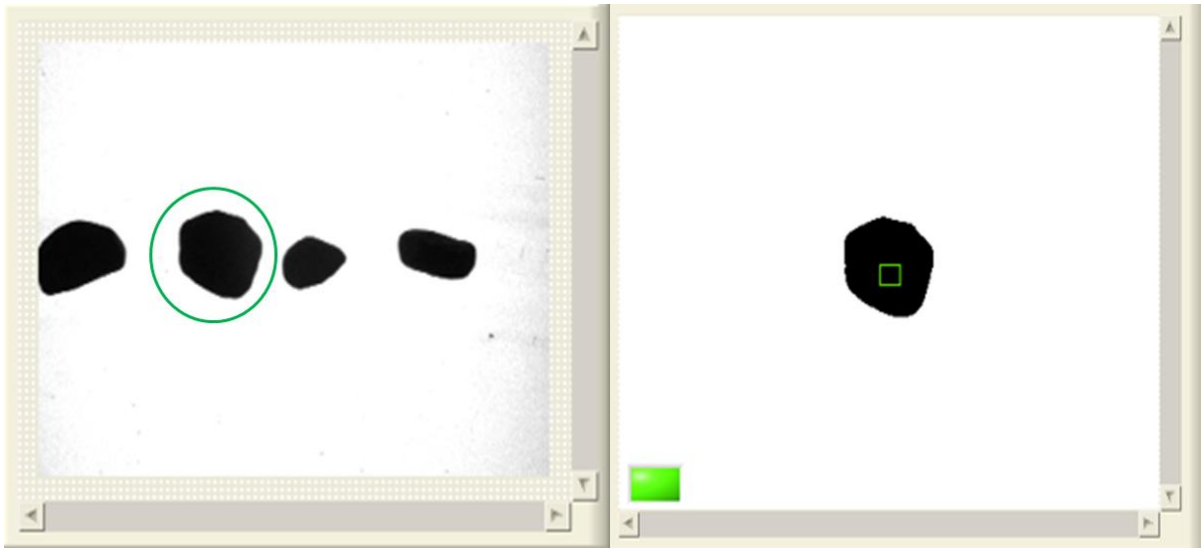

**Figure 3.3: Example of accepted particle in the AIMS-II coarse aggregate analysis**

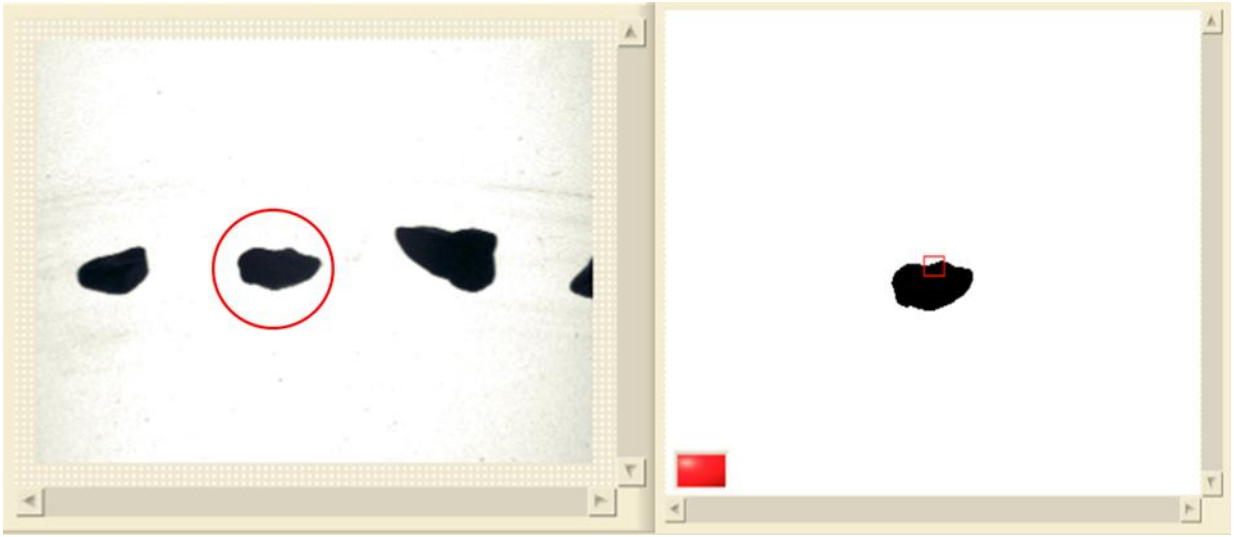

**Figure 3.4: Example of rejected particle in the AIMS-II coarse aggregate analysis**

The small box seen in the right picture of the figures indicates whether the aggregate was entirely in camera view (green box) or if any part of the aggregate was outside camera view (red box). If a particle was too small or was not properly placed in the trough, the AIMS-II recognized its existence, but the particle was not used in the analysis and was skipped during subsequent scans. This feature of the imaging system permits this study to cycle the aggregate sample through multiple conditioning cycles without re-sieving the aggregate to a specific particle size.

During the second scan, top lighting was used to measure the particle height at the previously determined centroid. The camera unit magnified the particle on the third scan to generate gray scale images that captured aggregate surface texture, as shown in Figure 3.5.

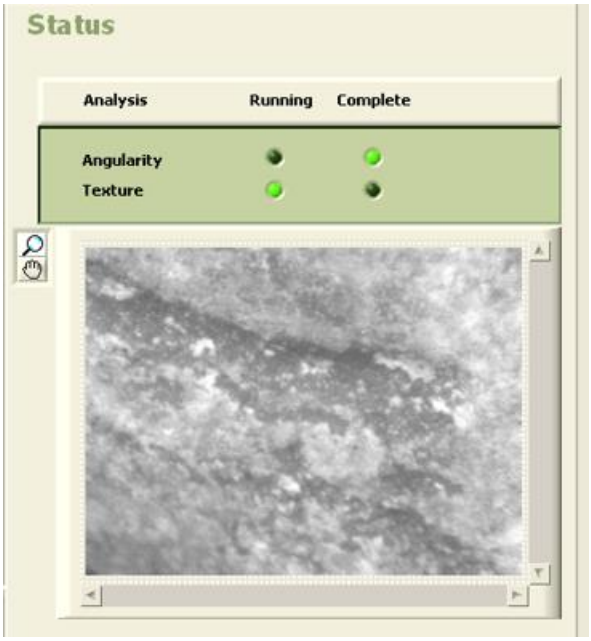


**Figure 3.5: Gray scale image used to capture coarse aggregate texture**

The software program used the three scans in a series of algorithms to calculate coarse aggregate angularity, texture, sphericity, and flatness and elongation ratios. This process is discussed in detail later in this chapter.

### 3.2 AIMS-II Fine Aggregate Testing

Fine aggregate image acquisition only requires one scan to obtain the particle shape properties. Additionally, there are only two trays to select from for fine aggregate analysis. The first is a transparent tray similar to those used for the coarse aggregates, whereas the second tray is an opaque tray designed for smaller fine aggregates that are retained on or passing the #50 sieve. The opaque tray may also be used to analyze more translucent particles which could present challenges to imaging on the transparent tray. The transparent tray uses backlighting to capture aggregate images, whereas the opaque tray uses top lighting for image scans. The transparent tray was used throughout the AIMS-II fine aggregate analysis of this research as the aggregates used were #16 and dark enough for imaging purposes.

Fine aggregate particles were sprinkled into the rotating tray's trough until the tray was full (Figure 3.6). Similar to the coarse particles, fine particle orientation was based on how the particle randomly came to rest in the trough.

**Figure 3.6: Fine aggregates spread on tray trough**

Upon initiating the imaging process of the AIMS-II, the tray returned to its initial position. The camera system used back lighting to capture images as the tray rotated which were used to quantify fine aggregate angularity and two-dimensional form. While it was important to spread out the fine particles, it is more difficult for the operator to control the placement of the fine particles than that of the coarse. Therefore, the AIMS-II was capable of rejecting particles that appear to be touching each other. For example, Figure 3.7 shows which aggregates are being scanned inside the device on the left image, while the right image shows which particles were actually accepted as part of the analysis. The picture on the left shows a red circle around particles that were touching each other and consequently, were eliminated them from the analysis. Additionally, the figure shows other fine particles that appeared within camera view in the left picture but were not included in the scan because the entire particle was not in camera view.

**Figure 3.7: Example of rejected fine particles from being too close together**

## 3.3 AIMS-II Shape Properties

The AIMS-II software uses scanned images to calculate the necessary aggregate properties through a series of algorithms. The results are then exported into a Microsoft Excel file that may be used for further analysis. The Excel file is organized by shape parameter and includes all the raw data, corresponding basic statistics, and a graph that reflects the cumulative distribution of the particles for each parameter.

### *3.3.1 Aggregate Angularity*

Aggregate angularity is captured from the two-dimensional images of the first scan for both coarse and fine aggregates using the gradient method. This method quantifies the variations at the particle boundary using a scale of 0 to 10,000. A particle characterized as a perfect circle would have an angularity index approaching a value of 0. The sharper the corners of the particle are, or the greater the change in inclination of the gradient vectors on the outer edge points, the higher the angularity index is (Pine Instrument Company 2011). The AIMS-II considers an

angularity index of 3,300 or less a low angularity aggregate, 3,300 to 6,600 as medium angularity, and angularity indexes greater than 6,600 are characterized as high angularity. Figure 3.8 provides a representation of how gradient vectors would appear for a smooth particle versus an angular particle. Additionally, Equation 3.1 is used to calculate the angularity of the particle from the gradient method.

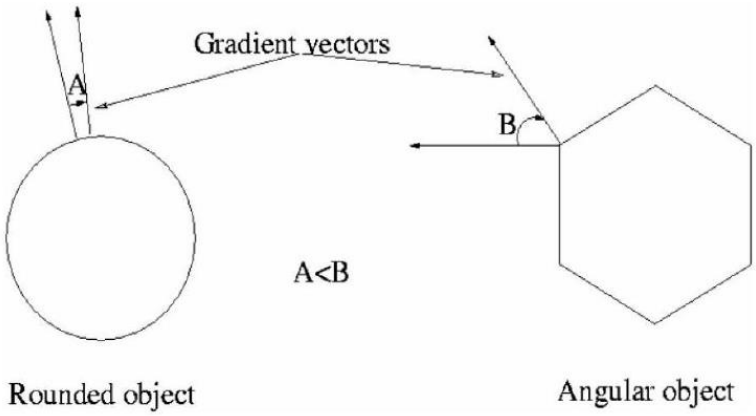


**Figure 3.8: Gradient vector for smooth versus angular particle (Pine Instrument Company 2011)**

Aggregate Angularity (AASHTO TP81):

$$Angularity = \frac{1}{\frac{n}{3} - 1} \sum_{i=1}^{n=3} |\theta_i - \theta_{i+3}| \qquad Equation\ 3.1$$

Where:

$\theta$: Angle of orientation on particle boundary point i

$n$: Total number of boundary points

$i$: The $i^{th}$ point on the particle boundary

Equation 3.1 uses a step size of three for calculating the gradients to reduce any noise effects created during image acquisition which may affect the results (Masad et al. 2003). Any bias towards particle size is significantly reduced by using the average as opposed to the summation in calculating angularity (Moaveni et al. 2013). This allows the angularity index to put more of an emphasis on the particle edges rather than particle size. This further justifies why it was acceptable to use the entire Micro-Deval sample as opposed to using only those retained on the #4 or #16 sieve as mentioned in Step 7a of the laboratory research procedure.

### *3.3.2 Surface Micro-texture*

The surface micro-texture is a coarse aggregate property measured using wavelet analysis, which provides texture information in the horizontal, vertical, and diagonal directions. Particle texture refers to the smoothness or roughness of a particle surface and is dependent on particle surface irregularities at wavelength less than 0.5 mm. According to the AIMS-II, the surface texture index ranges from 0 to 1,000 and is calculated "at a given decomposition level [as] the arithmetic mean of the squared values of the wavelet coefficients for all three directions" (Pine Instrument Company 2011) using Equation 3.2. A surface texture index approaching 0 indicates a smooth, polished aggregate surface. Additionally, the AIMS-II denotes a texture index of 260 or lower as low, 260 to 550 as a medium texture level, and texture indexes above 550 as high.

Surface Micro-texture (AASHTO TP81):

$$Texture\ Index = \frac{1}{3N}\sum_{i=1}^{3}\sum_{j=1}^{N}\left(D_{i,j}(x,y)\right)^2 \qquad Equation\ 3.2$$

Where:

$N$: Total number of coefficients in an image

$i$: 1, 2, or 3 for horizontal, vertical, or diagonal direction of texture

$j$: Wavelet index

$D$: Decomposition function

$x, y$: Location of the coefficients in transformed domain

### *3.3.3 Aggregate Form*

Aggregate form is characterized for both coarse and fine aggregates by the AIMS-II using the images captured during the aggregate scans. Figure 3.9 shows a representation of what is referred to as form according to the AIMS-II device.

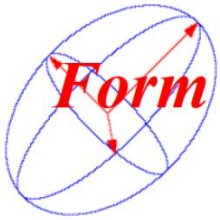


**Figure 3.9: Representation of AIMS-II aggregate form (Pine Instrument Company 2011)**

Coarse aggregate form is referred to as sphericity and is used to describe the overall three-dimensional shape of the particle. Sphericity is calculated using Equation 3.3 and ranges on a scale of 0 to 1, where a particle that is characterized by equal dimensions (cubical) has a sphericity value of 1. Therefore, a value that is characterized as a perfect circle would have a sphericity index approaching 0 (Pine Instrument Company 2011). According to the AIMS-II

software, a sphericity index of 0.3 or less is considered a low sphericity index, 0.3 to 0.7 is considered a medium sphericity index, whereas an index greater than 0.7 is considered to have a high sphericity index.

Sphericity (AASHTO TP81):

$$Sphericity = \sqrt[3]{\frac{d_s d_I}{d_L^2}} \qquad Equation\ 3.3$$

Where:

$d_s$: Shortest dimension of the particle

$d_I$: Intermediate dimension

$d_L$: Longest dimension

Fine aggregate form is referred to as two-dimensional form and is indicative of the changes in the particle radius in all directions of a two-dimensional image. The particle radius is defined as the distance between the particle center and the outer edge at a given point (Pine Instrument Company 2011). Two-dimensional form (*Form2D*) is calculated using Equation 3.4 with values ranging from 0 to 20, where a particle characterized as a perfect circle would have a value approaching 0. The AIMS-II software indicates that a two-dimensional form value of 6 or less is considered low, 6 to 12 is considered a medium level of two-dimensional form, and a value greater than 12 is considered high.

Two-Dimensional Form (AASHTO TP81):

$$Form2D = \sum_{\theta=0}^{\theta=360-\Delta\theta} \left[\frac{R_{\theta+\Delta\theta} - R_\theta}{R_\theta}\right] \qquad Equation\ 3.4$$

Where:

$R_\theta$: Radius of the particle at an angle of θ

$\Delta\theta$: Incremental difference in the angle

### *3.3.4 Flat and Elongated Properties*

The flatness and elongation properties for coarse aggregates is represented using a variety of ratios based on the measured particle dimensions from the three scans.

Flatness Ratio (AASHTO TP81):

$$Flatness = \frac{d_s}{d_I} \qquad Equation\ 3.5$$

Elongation Ratio (AASHTO TP81):

$$Elongation = \frac{d_I}{d_L} \qquad Equation\ 3.6$$

Flat and Elongated Ratio (AASHTO TP81):

$$FE = \frac{d_L}{d_s} \qquad Equation\ 3.7$$

Flat or Elongated Value (AASHTO TP81):

$$ForE: \frac{d_I}{d_s}\ or\ \frac{d_L}{d_I} > Ratio\ (ie: 1, 2, 3 \ldots) \qquad Equation\ 3.8$$

The variables used in the flatness and elongated ratios are defined the same as they were for calculating sphericity from Equation 3.3. For each of the above ratios, the AIMS-II software records the cumulative percentage of particles that were characterized by a ratio greater than 1:1,

2:1, 3:1, 4:1, or 5:1. Due to the large amount of data, only the flat and elongated ratios (Equation 3.7) were analyzed for the coarse particles for the purpose of this research.

The range of values as well as the values the AIMS-II considers to be low, medium, and high for each AIMS-II index are summarized in Table 3.1. To clarify, coarse aggregate is denoted as CA in the table, whereas fine aggregate is denoted as FA.

**Table 3.1: Summary of AIMS-II index ranges**

| AIMS-II Index | Aggregate Sizes Measured | Range | Low | Medium | High |
|---|---|---|---|---|---|
| Angularity | CA, FA | 0 - 10,000 | < 3,300 | 3,300-6,600 | > 6,600 |
| Texture | CA | 0 - 1,000 | < 260 | 260-550 | > 550 |
| Sphericity | CA | 0 - 1.0 | < 0.3 | 0.3-0.7 | > 0.7 |
| Form 2D | FA | 0 - 20 | < 6 | 6-12 | > 12 |

# CHAPTER 4: EXPERIMENTAL PLAN

## 4.1 Research Plan

The purpose of this research was to analyze the use of the Micro-Deval apparatus in conjunction with the AIMS-II device comparing the laboratory polishing resistance of aggregates to field friction performance data. Currently, the use of these devices is not standardized for measuring friction characteristics. This study applied portions of existing test standards, including ASTM D7428, ASTM D6928, and AASHTO TP81. Micro-Deval and AIMS-II testing were conducted on five aggregate sources at NCAT's laboratory. Each aggregate source and size was tested individually. Particle shape properties were analyzed using the AIMS-II prior to any conditioning as well as after incremental Micro-Deval polishing.

## 4.2 Material Selection

Five aggregate sources characterized by different geology and field friction performance properties were selected as part of this research. Three of the chosen aggregates were part of NCAT's 2009 Test Track friction study. These aggregates included the following: a Columbus granite, a LaGrange granite, and a Calcined bauxite that was used in a high friction surface course constructed in 2006. A Calera limestone was selected as part of this research because of its use in NCAT's 2000 Test Track friction study. Though it was only used as screenings in NCAT's 2009 cycle, an Opelika limestone was also used as a comparison to the limestone source from Calera due to the Calera limestone's poor friction performance.

Two sizes of each aggregate (coarse and fine) were used in this project. The coarse aggregate was defined as material passing the 3/8 inch sieve and retained on the #4 sieve based on the gradations used in the surface mixtures from the 2009 Test Track cycle. The largest percentage of aggregates used in the surface mixtures were retained on the #4 sieve. Aggregates passing the

#8 sieve and retained on the #16 sieve were selected for fine aggregate testing. Testing a fine aggregate two sieve sizes below the selected #4 provided some delineation between the coarse and fine aggregate sizes while maintaining a large enough particle size in hopes that a sufficient amount of degradation could still be observed. Therefore, aggregates retained on the #4 (4.75 mm) and #16 (1.16 mm) sieve sizes were used for AIMS-II testing as part of the research. Table 4.1 shows a summary of the aggregate sources' properties and their designated stockpile at NCAT's Test Track. The aggregate volumetric properties were obtained from the laboratory database, including apparent specific gravity (Gsa), bulk specific gravity (Gsb), and the specific gravity at the saturated surface dry state (Gssd). It should be noted that only Bauxite retained on the #16 sieve was used, as this material was used for a high friction surface study, and all material used in the study passed the #4 sieve.

**Table 4.1: Summary of laboratory tested aggregate properties**

| Aggregate Type | Sieve Size | NCAT Stockpile | Gsa | Gsb | Gssd | Absorption (%) |
|---|---|---|---|---|---|---|
| Opelika Lms | #4 | Opelika LMS 78 | 2.863 | 2.769 | 2.802 | 1.2 |
| | #16 | Opelika LMS 8910 | 2.812 | 2.784 | 2.794 | 0.4 |
| Columbus Grn | #4 | Columbus Grn 89 | 2.713 | 2.61 | 2.648 | 1.5 |
| | #16 | Columbus Grn M10 | 2.739 | 2.735 | 2.736 | 0.1 |
| LaGrange Grn | #4 | LaGrange 78 | 2.666 | 2.617 | 2.635 | 0.7 |
| | #16 | LaGrange M10 | 2.725 | 2.707 | 2.714 | 0.3 |
| Calera LMS | #4 | Calera LMS 78 | 2.871 | 2.836 | 2.848 | 0.4 |
| | #16 | Calera LMS 820 | 2.779 | 2.645 | 2.693 | 1.8 |

### *4.2.1 Field Data*

Pavement sections from the 2000 and 2009 research cycles were selected for the purpose of this research. These sections varied in mixture properties and field friction performance. Historical field friction data were obtained from NCAT's database for each selected pavement section to serve as ground truth field performance measures. These sections were used to select the aggregates for laboratory testing. Aggregate laboratory test results using the AIMS-II device and Micro-Deval were compared to the field friction performance data.

#### *4.2.1.1 Selection of NCAT Test Track Pavement Sections*

The NCAT Pavement Test Track is a full-scale accelerated pavement testing (APT) facility. The Test Track is a 1.7 mile (2.8 km) oval divided into 46 different research sections, each 200 feet in length. Each test section is funded by an external sponsor for research purposes. Several field performance parameters, such as rutting, cracking, roughness, texture, friction, and noise are measured regularly to monitor pavement mixture performance under controlled, accelerated traffic loads, quantified as ESALs.

Pavement surface mixtures that contained a high percentage of recycled material were avoided to ensure that the friction performance was mostly influenced by the virgin aggregates in the mixture and not the recycled aggregate. Additionally, sections were selected based on aggregate availability.

The first selected surface mix was a high friction surface treatment (HFST) composed of bauxite ranging from #5 to #12 sized particles. The second mix type was an open graded friction course (OGFC) composed primarily of LaGrange granite. The third and fourth surface mixes, characterized as a stone matrix asphalt (SMA) mix and a fine-dense graded (FDG) mix, were composed primarily of Columbus granite. The fifth mix type was an SMA mix from the 2000 NCAT Test Track research cycle made of primarily Calera limestone. Table 4.2 shows the mixture identification that will be used throughout the thesis, the construction year, the Test Track sections, and the materials used as part of the aggregate skeleton. Some of the test sections characterized as a FDG Columbus granite surface mixture contained binder replacement. The binder was replaced at 25% of the weight of total binder used in the original mix design. The original mix design was used in the control section, S9 (Brown et al. 2002, Willis et al. 2009, and West et al. 2012). However, these differences showed no effect on friction field performance. It

should be noted that the Calera limestone Test Track section was replaced with a different surface mixture due to poor friction performance. The data used in this research study for the Calera limestone section reflects the data shown in Brown et al. (2002).

**Table 4.2: NCAT Pavement Test Track sections mix identification**

| Mixture ID | Year Constructed | Sections | NMAS | Materials |
|---|---|---|---|---|
| HFST Bauxite | 2006 | E2, E3 | N/A | Bauxite |
| OGFC Columbus Granite | 2009 | N12 | 1/2 inch | 7 Columbus Granite |
| | | | | 89 Columbus Granite |
| | | | | Other: Flyash, Hydrated lime, Cellulose |
| Fine-Dense Graded Columbus Granite | 2009 | N5, N6, N7, S9, S10, S11, S12 | 3/8 inch | 89 Columbus Granite |
| | | | | 8910 Opelika Limestone Screenings |
| | | | | M10 Columbus Granite |
| | | | | Shorter Coarse Sand |
| OGFC LaGrange Granite | 2009 | N1, N2, S8 | 1/2 inch | 78 LaGrange Granite |
| | | | | Coarse Fraction Local RAP (15% by weight of mix) |
| SMA Calera Limestone | 2000 | W7 | 3/8 inch | 7 Calera Limestone |
| | | | | 821 Calera Limestone |
| | | | | Other: Fly Ash |

*4.2.1.2 Locked-Wheel Skid Trailer Measurements*

Test track friction data were collected using the locked wheel skid trailer equipped with the ribbed tire to obtain skid numbers at 40 mph (SN40R) for each pavement section on a monthly basis, following the testing protocol set forth in ASTM E501. All testing was conducted in the middle 150 feet, leaving 25 feet at the beginning and end of each section as transition zones between sections. The friction data of the test sections in consideration were obtained from NCAT historic data records.

## 4.3 Test Procedure

The test procedure carried out for the coarse aggregates slightly from that of the fine aggregates. Therefore, the procedures are described separately within this chapter. The Micro-Deval testing procedures for coarse and fine aggregates (ASTM D6928 and ASTM D7428) were used as the basis for conditioning the aggregates. However, modifications were made to the ASTM test procedures for the purpose of this research study. For example, only a single sized aggregate was tested as opposed to one of the specified gradations. The total conditioning times were also modified based on aggregate size and were divided into incremental conditioning times to track changes in aggregate shape parameters using the AIMS-II.

### *4.3.1 Coarse Aggregate Micro-Deval/ AIMS-II Testing Procedure*

The testing procedure for the AIMS-II and Micro-Deval for all aggregate sources of the #4 sieve size was as follows:

1) The aggregate sources were sampled from their corresponding stockpiles according to AASHTO T2: *Standard Practice for Sampling Aggregates*, washed, oven dried, and sieved to obtain particles passing the 3/8 inch sieve yet retained on the #4 sieve.
2) Approximately 1,500 grams of each processed sample were obtained using proper aggregate splitting procedures for testing purposes according to AASHTO T248: *Standard Practice for Reducing Samples of Aggregate to Testing Size*. The sample size was determined from ASTM D6928: *Standard Test Method for Resistance of Coarse Aggregate Degradation by Abrasion in the Micro-Deval Apparatus*.
3) The Micro-Deval sample was split to obtain 90 gram replicate AIMS-II samples. The 1,500-gram Micro-Deval sample was significantly larger than the sample required by the

AIMS-II. The AIMS-II procedure required 50 coarse particle count minimum, which was approximately 90 grams. Therefore, the 1500 gram sample was split in accordance with AASHTO T248 into 16 smaller 90-gram samples for AIMS-II analysis. Using Excel's random number generator, three replicates of the 16 samples (approximately 90 grams each) were selected for analysis in the AIMS-II. To clarify, each of the three smaller samples that were randomly selected to run through the AIMS-II will be referred to as replicates throughout the thesis. Splitting the samples into 16 smaller samples was found to be suitable for AIMS-II repeatability purposes, which is discussed later within this section.

4) The three replicates for each aggregate source were measured in the AIMS-II device for angularity, texture, sphericity, and flat and elongated ratios. The data were evaluated for outliers and repeatability using the Minitab statistical software as discussed later.
5) Once measurements in the AIMS-II were complete and data checked for repeatability, the smaller samples were recombined to make up the 1,500 gram Micro-Deval sample. The 1,500 gram sample was then conditioned in the Micro-Deval following ASTM 6928. However, instead of using a specific gradation provided by the testing standard, the procedure was used to condition the single sized aggregate sample. The 1,500 gram sample was soaked in the Micro-Deval container for an hour in two liters of water, and 5,000 grams of steel charges were added to the container for conditioning. Because the #4 sieve size was selected for testing, the total conditioning time of 95 minutes was selected based on the gradation from the standard Micro-Deval procedure that contained the greatest mass of the #4 material. For simplicity, the total conditioning time in the Micro-Deval was rounded up to 100 minutes, and the sample was conditioned in increments of

20 minutes. Moaveni et al. (2013) found that 210 minutes was necessary conditioning time for coarse aggregates to ensure terminal angularity and texture indexes were reached. However, they noted that the rate of angularity and texture losses appeared to slow down significantly after 105 minutes of Micro-Deval conditioning, indicating 100 minutes of conditioning was approaching terminal conditioning.

6) After 20 minutes of Micro-Deval conditioning, the steel charges were removed using a magnet. The conditioned sample was washed over the #16 sieve, dried, and weighed. The material passing the #16 sieve was recorded as mass loss. Throughout the thesis, a cycle includes an increment of 20 minutes of polishing in the Micro-Deval followed by AIMS-II testing. The first cycle consists of AIMS-II testing prior to any conditioning.
7) Steps 3 through 6 were repeated until the sample completed five conditioning/testing cycles using 20 minute incremental polishing times. This resulted in an overall conditioning time of 100 minutes in the Micro-Deval.
    a. The Micro-Deval samples were not sieved to obtain particles only passing the 3/8 inch sieve and retained on the #4 sieve after conditioning when they were analyzed in the AIMS-II during Step 4. This was done to ensure the sample remained together throughout the entire experiment. The AIMS-II is capable of rejecting particles that are too small and do not fit entirely within camera view. Therefore, keeping the entire sample together was considered appropriate.

### *4.3.2 Fine Aggregate Micro-Deval/ AIMS-II Testing Procedure*

The testing procedure for the AIMS-II and Micro-Deval for all aggregate sources of the #16 sieve (passing the #8 and retained on the #16) was as follows:

1) The aggregate sources were sampled from their corresponding stockpiles, washed, oven dried, and sieved to obtain particles passing the #8 sieve yet retained on the #16 sieve.
2) Approximately 500 grams was weighed out for each processed sample. This sample size was specified in ASTM D7428: *Standard Test Method for Resistance of Fine Aggregate to Degradation by Abrasion in the Micro-Deval Apparatus*.
3) The Micro-Deval sample was split to obtain 30-gram replicate AIMS-II samples. The 500-gram Micro-Deval sample was significantly larger than the sample required by the AIMS-II. The AIMS-II procedure required a 150 fine particle count minimum, which was approximately 30 grams. Three replicates of the 16 AIMS-II samples were selected using Excel's random number generator.
4) The AIMS-II measured the angularity and two-dimensional form of the three replicates for each of the fine aggregate sources. The AIMS-II fine aggregate data was evaluated for outliers and repeatability as discussed later.
5) The 16 smaller samples were combined again to make up the 500 gram Micro-Deval sample. The sample was then conditioned in the Micro-Deval following ASTM D7428. The procedure was used to condition the single sized aggregate sample, as opposed to a gradation that is provided by the testing standard. The 500 gram sample was soaked in 0.75 liters of water in the Micro-Deval container for an hour. Approximately 1,250 grams of steel charges were added to the Micro-Deval container for conditioning. ASTM D7428 specified a total conditioning time of 15 minutes for the gradation that contained the greatest mass of the #16 sized particles. This study elected to have a minimum of three testing cycles with a minimum of 10 minutes of conditioning for each cycle. Based on

these parameters, the total conditioning time was modified from 15 minutes to 30 minutes.

6) After 10 minutes of Micro-Deval conditioning, the steel charges were removed using a magnet. The conditioned sample was washed over the #50 sieve, dried, and weighed. The mass loss was recorded as the material passing the #50 sieve. ASTM D7428 specifies material passing the #200 sieve is considered lost material for the provided gradations. It was determined that using material passing the #200 sieve as lost material was too small of a sieve size when testing only #16 aggregate particles. The coarse aggregate Micro-Deval procedure (ASTM D7428) specified that coarse aggregates passing the #16 sieve were considered lost material, which is two standard sieve sizes smaller than the #4, the particle size that was tested. Therefore, lost material for the #16 fine particles was characterized as material passing the #50 sieve, two standard sieve sizes below the #16 sieve.
7) Steps 3 through 6 were repeated until the sample experienced a total conditioning time of 30 minutes.
    a. The Micro-Deval samples were not sieved to obtain particles only passing the #8 sieve and retained on the #16 sieve after conditioning when they were analyzed in the AIMS-II during Step 4. This was done to ensure the sample remained together throughout the entire experiment.

### *4.3.3 AIMS-II Selection of Sample Size*

As mentioned previously, the Micro-Deval procedure requires a significantly larger aggregate sample than the AIMS-II. The AIMS-II procedure requires a minimum of 50 coarse particles and 150 fine particles to be scanned, whereas the Micro-Deval requires 1,500 grams and 500 grams

of coarse and fine aggregates, respectively. Therefore, a brief repeatability study was carried out on the #4 coarse aggregate without any conditioning in order to determine the appropriate sample size that would yield at least 50 readings within the AIMS-II for each replicate. The repeatability analysis was only conducted on the Opelika limestone coarse aggregate angularity. Aggregate surface texture tends to be more variable within a sample, so using the angularity data to test repeatability deemed more appropriate.

Initially, the 1,500 gram Micro-Deval sample of the #4 aggregate size was split into eight, approximately equal, samples using a splitter. Each sample was numbered one through eight in the order they were split and collected, and the random number generator in Microsoft Excel was used to select which three samples were to be tested in the AIMS-II. Upon completion of testing, it was determined that the sample could be split further into sixteenths while maintaining an adequate amount of particles to be read within the imaging system. The precision between the replicates improved when the particles were further split into 16 smaller samples.

To test the repeatability of the results, the Kolmogorov-Smirnov (K-S) test was used to compare the three runs with one another, two data sets at a time (Tools for Science 2015). The K-S test assesses the differences among two datasets. The test results in a measurement of the maximum difference (D) between the two datasets (Figure 4.1) and a p-value that indicates the statistical difference between the two datasets. Figure 4.1 shows a theoretical example on the left, whereas the right image shows an example of two datasets provided by this research study. Table 4.3 shows the maximum difference between two cumulative distributions at a given angularity index and the corresponding p-value when comparing two data sets for the samples split in eighths as well as sixteenths.

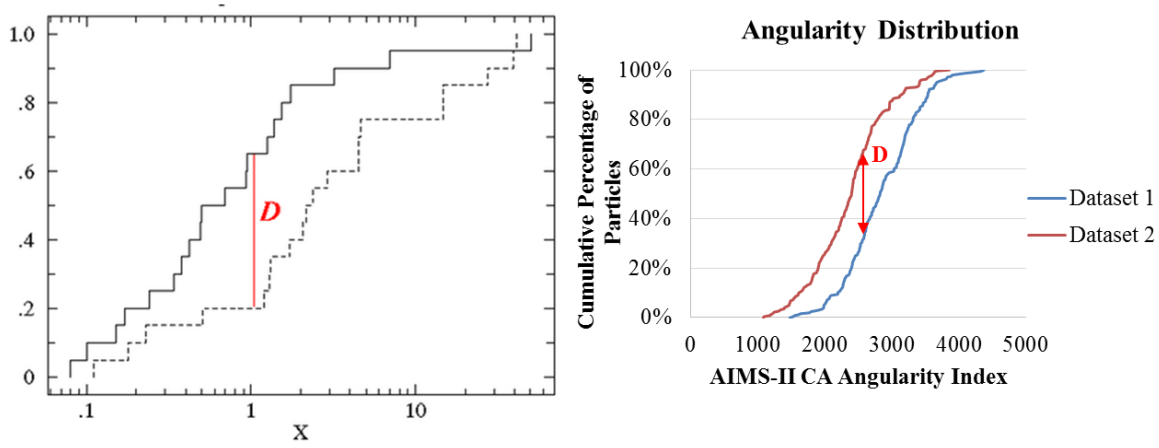


**Figure 4.1: Maximum difference, D, in Kolmogorov-Smirnov test as theoretical example (left) (Tools for Science 2015) and example for this research study (right)**

**Table 4.3: Kolmogorov-Smirnov test results for the repeatability analysis**

| Angularity K-S Test Results for Repeatability Analysis | | | | |
|---|---|---|---|---|
| K-S Comparisons | Split in 8ths | | Split in 16ths | |
| | Max Difference | P-value | Max Difference | P-value |
| Run 1 vs 2 | 0.2344 | 0.014 | 0.0903 | 0.897 |
| Run 2 vs 3 | 0.1293 | 0.442 | 0.0838 | 0.927 |
| Run 1 vs 3 | 0.1634 | 0.175 | 0.0901 | 0.863 |

A lower p-value denotes that the difference between the two data sets are more significant. Technically, a p-value less than 0.05 indicates the difference between the two runs are statistically significant with a confidence level of 95%. While only the first two runs of the sample split in eighths are considered to be statistically different, the p-values of the data set comparisons from the sample split in sixteenths are substantially higher further justifying that splitting the sample into sixteenths deemed more appropriate.

Figures 4.2 and 4.3 show an example of the aggregate angularity cumulative distributions of the three replicates scanned when the samples were split into eighths and sixteenths, respectively.

Table 4.4 shows the averages of each replicate and the standard deviation of the three replicates for a sample split in eighths and sixteenths. When the sample was split into sixteenths, the standard deviation was reduced. This further justifies splitting the sample into sixteenths as opposed to eighths. The process for removing any outliers, discussed later within the chapter, was carried out during the repeatability investigation for consistency.

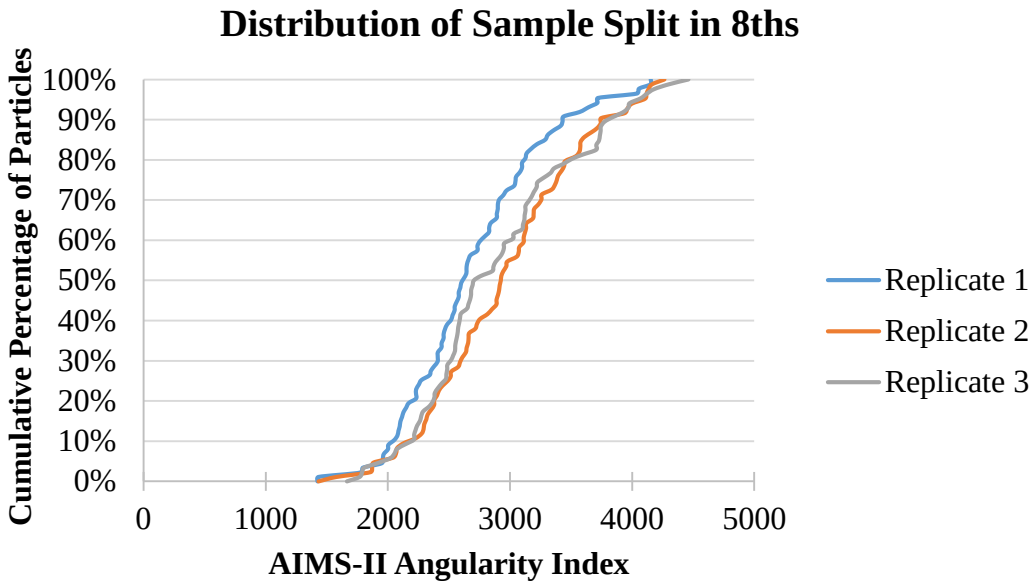


**Figure 4.2: Angularity cumulative distribution of the Micro-Deval sample split in 8ths**

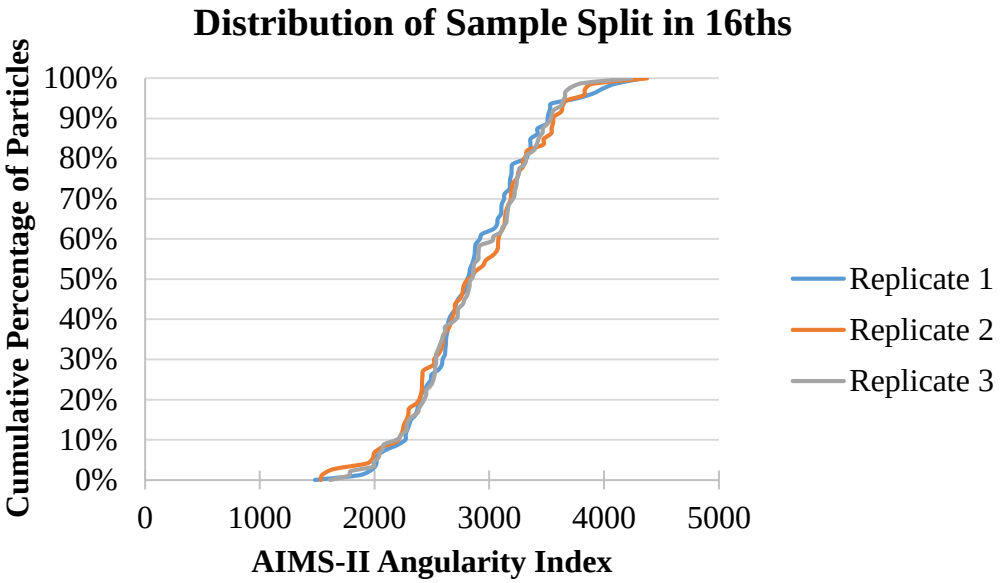


**Figure 4.3: Angularity cumulative distribution of the Micro-Deval sample split in 16ths**

**Table 4.4: Standard deviations for sample split in eighths versus split in sixteenths**

| Parameter | Split in 8ths | Split in 16ths |
|---|---|---|
| Replicate 1 Average | 2690.96 | 2847.91 |
| Replicate 2 Average | 2942.37 | 2852.37 |
| Replicate 3 Average | 2891.45 | 2854.43 |
| SD | 132.92 | 3.34 |

From the graphs, it is apparent that when the sample was properly split into 16 smaller samples, the results produced by the AIMS-II yielded higher repeatability. Additionally, splitting the sample into sixteenths yielded the smallest possible sample to have the required minimum particle count to run through the AIMS-II device.

The results of this repeatability study of the Micro-Deval sample for the coarse aggregate showed that splitting the sample in sixteenths was an appropriate test procedure. This analysis

was the basis for splitting the fine aggregate sample into sixteenths. No additional repeatability study was done for the fine aggregate sample.

## 4.4 Data Quality Control

Data quality control analysis was run on AIMS-II test results to detect outliers among the datasets. The results were also checked with the AIMS-II precision statement to ensure repeatable results were achieved. These activities are described in the following subsections.

### *4.4.1 Defining Outliers*

Some of the replicates appeared to have significantly lower or higher data points for each shape property which would misrepresent the true sample properties. Therefore, Minitab statistical software was used to analyze the data and identify any outliers within the sample. This analysis was executed for the combined three replicates after each time the aggregates were measured in the AIMS-II for each aggregate source.

After measurement in the AIMS-II, the data from the three replicates were combined into one dataset for further analysis. The combined three replicates for statistical analysis will be referred to as a dataset throughout the thesis. Minitab provided a graphical summary using a boxplot to represent variability of the data (Figure 4.4). The left edge of the rectangular box represents the $25^{th}$ percentile (25% of the data is less than or equal to this value), whereas the right edge of the rectangular box represents the $75^{th}$ percentile (75% of the data is less than or equal to this value). The middle line shown in the rectangular box represents the median. The interquartile range (IQR) is computed by subtracting the $25^{th}$ percentile from the $75^{th}$ percentile. The stems of the boxplot extend 1.5*IQR below the $25^{th}$ percentile (to the left) and 1.5*IQR above the $75^{th}$ percentile (to the right) (Devore 2012). Any data point outside these stems are represented by an

asterisk (*). When the graphical summary was carried out for the data, all data points that were outside of the stems were considered “first order outliers” and were removed from the data. These are circled in red in Figure 4.4. The example shown in Figure 4.4 reflects a similar graphical summary of what was shown for the remaining datasets that were analyzed for outliers. There would only be a few measurements that reflected very high or very low AIMS-II indexes. Therefore, it was determined that these isolated individual measurements did not reflect the true distribution of the population and were removed as first order outliers. Removing these data points from the dataset was acceptable, as a typical dataset for the coarse aggregates contained approximately 180-270 data points and 480-900 data points for the fine aggregates. Recalling the AIMS-II requires 50 particles for coarse aggregates and 150 for fine aggregates, these particle counts remained well above the minimum.

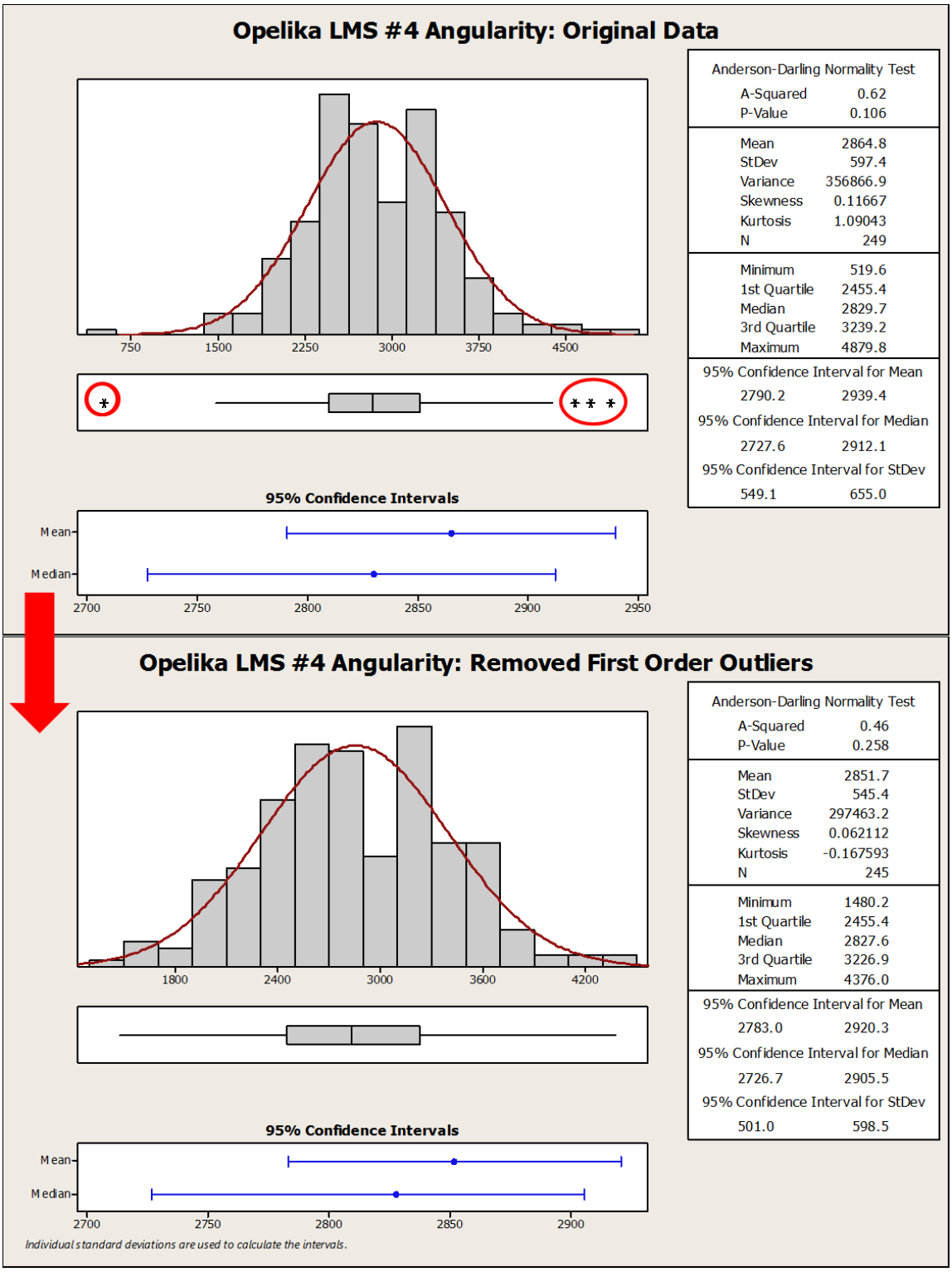


**Figure 4.4: Example of removing first order outliers from a data set**

A second level graphical summary of the statistics on the updated data set (data excluding first order outliers) was run to determine if any additional outliers outside the adjusted stems of the boxplot remained (i.e., second order outliers). The second order outliers were essentially treated as a group; either all of the second order outliers were to be removed or all remained part of the analysis. The AIMS-II precision statement was checked prior to removing any second order outliers. If the average of each of the three replicates fell within the precision statement, the second order outliers were automatically included as part of the analysis. However, if the average of any of the three replicates fell outside of the limits specified within the precision statement, a third level graphical summary was performed to assess how much the overall mean was affected if the second order outliers were removed. There were no instances in which the overall mean changed by more than 5% when removing the second order outliers. Therefore, all second order outliers remained part of the analysis for all data sets. Minitab graphical summaries showing only the distributions for coarse aggregate angularity, fine aggregate angularity, and coarse aggregate texture can be found within Appendix A.

### *4.4.2 Test Repeatability*

The results for angularity and texture only were checked against the precision statement in AASHTO TP81: *Determining Aggregate Shape Properties by Means of Digital Image Analysis* as these were the properties used to find correlations with field data. The precision statement specifies acceptable upper and lower limits with a COV as a percent of the overall average (boundary +/- average*COV) for each of the shape parameters. The COV corresponding to AIMS-II angularity indexes is 2.9%, whereas the COV corresponding to AIMS-II texture indexes is 4.5%. Tables showing the overall mean, lower and upper limits, as well as the means of each replicate are shown in Appendix B. It should be noted that while some of the replicates'

means fell outside the precision statement, which are shown in red within the tables, these values were reasonably close and were accepted for use in data analysis.

# CHAPTER 5: LABORATORY RESULTS AND DISCUSSION

This chapter focuses on the laboratory results obtained from the AIMS-II device before and after aggregates were subjected to incremental conditioning times in the Micro-Deval apparatus. The change in mass loss and aggregate property indexes provided by the AIMS-II device as result of Micro-Deval conditioning were tracked. These AIMS-II indexes for coarse aggregates included angularity, texture, sphericity, and flat and elongated ratios. The AIMS-II indexes provided for fine aggregates were angularity and two-dimensional form.

The Micro-Deval test procedures set forth in ASTM D7428 and ASTM D6928 were the basis of selecting 100 minutes and 30 minutes of total conditioning time for coarse and fine aggregates, respectively. As shown in the following results, the test protocol was not able to achieve terminal conditioning, thus the AIMS-II indexes did not achieve terminal values as shown in the following results. As mentioned previously, terminal values indicate that AIMS-II index is decreasing at a much slower and steady rate and essentially remaining the same with increased conditioning.

## 5.1 Micro-Deval Aggregate Mass Loss

As described in Step 6 of the test protocol in Chapter 3 for both coarse and fine aggregates, the Micro-Deval mass loss was recorded. Material passing the #16 sieve was considered lost material for coarse aggregates, and material passing the #50 sieve was considered lost material for fine aggregates. The amount of mass loss due to conditioning in the Micro-Deval is an indication of aggregate durability. The change in coarse aggregate (CA) and fine aggregate (FA) mass was recorded at each Micro-Deval polishing time as a cumulative percent loss (Figures 5.1 and 5.2, respectively).

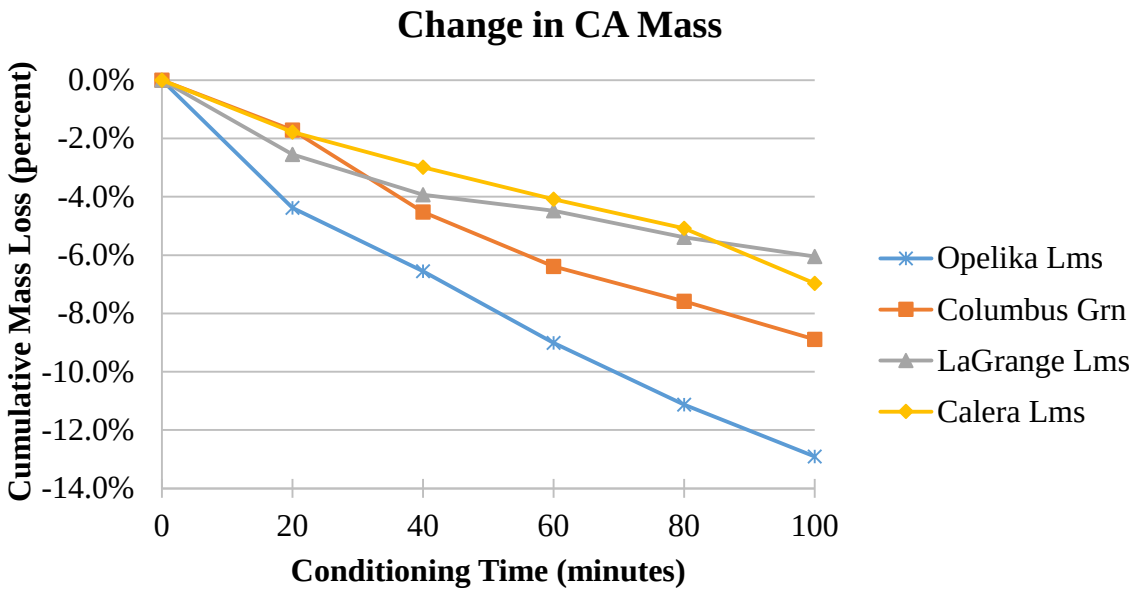


**Figure 5.1: Change in coarse aggregate mass loss from Micro-Deval conditioning**

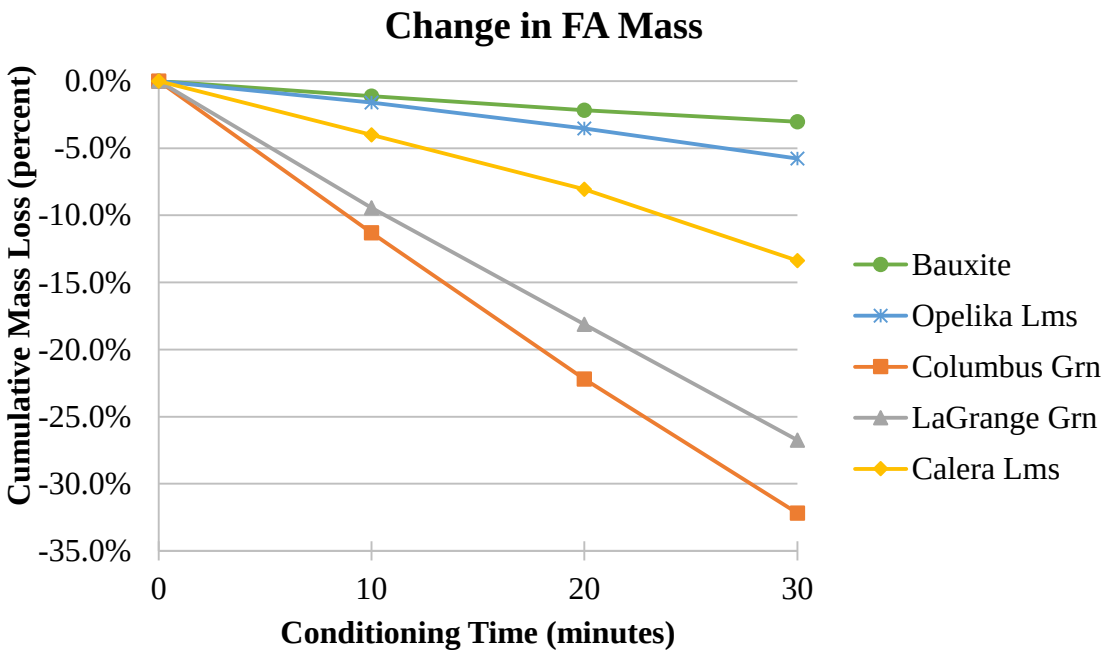


**Figure 5.2: Change in fine aggregate mass loss from Micro-Deval conditioning**

As expected, all aggregate sources experienced some mass loss due to conditioning in the Micro-Deval. A steeper slope in the figure indicates a higher rate of mass loss for the aggregate. With the exception of the Opelika limestone source, the fine aggregates experienced a greater percentage of average mass loss after 30 minutes of conditioning than the coarse aggregates after 100 minutes of conditioning. This may be attributed to the sample of fine particles having a higher surface area exposure to abrasion than coarse aggregates based on an equal mass of sample. There are more pieces broken off of multiple fine particles compared to the fewer coarse particles.

The bauxite was characterized by the least percent mass loss among all the #16 particles that were tested indicating the bauxite to be the most durable. This was expected, as the bauxite is considered to be a good aggregate source for use in high friction surface courses and is capable of maintaining its durability under heavy traffic loads (Federal Highway Administration 2012).

Additionally, the ranking among the aggregates differs from coarse and fine aggregates of the same sources (Table 5.1). The ranking is based on the cumulative percent loss at the end of the total conditioning time (100 minutes for coarse aggregates and 30 minutes for fine aggregates) with the aggregate that was characterized by the greatest mass loss ranked last. Bauxite was excluded from the table because only the #16 size was tested, and the test results clearly show bauxite experienced the least amount of mass loss,. The table shows that aggregate durability varies among different sizes of the same aggregate source; thus, aggregate size should be considered when evaluating an aggregate for use in a surface course.

**Table 5.1: Percent mass loss ranking among CA and FA at total conditioning**

| Aggregate Source | CA Ranking | FA Ranking |
|---|---|---|
| Opelika LMS | 4 | 1 |
| Columbus GRN | 3 | 4 |
| LaGrange GRN | 1 | 3 |
| Calera LMS | 2 | 2 |

*1 = lowest mass loss, 4 = highest mass loss

## 5.2 AIMS-II Aggregate Angularity

As described in Chapter 3, the AIMS-II aggregate angularity was recorded for coarse and fine aggregates. Coarse aggregate angularity is an indication of macro-texture, whereas fine aggregate angularity relates to the internal friction of the aggregate structure. The average coarse aggregate and fine aggregate angularity index was recorded at each conditioning time interval (Figure 5.3 and Figure 5.4, respectively).

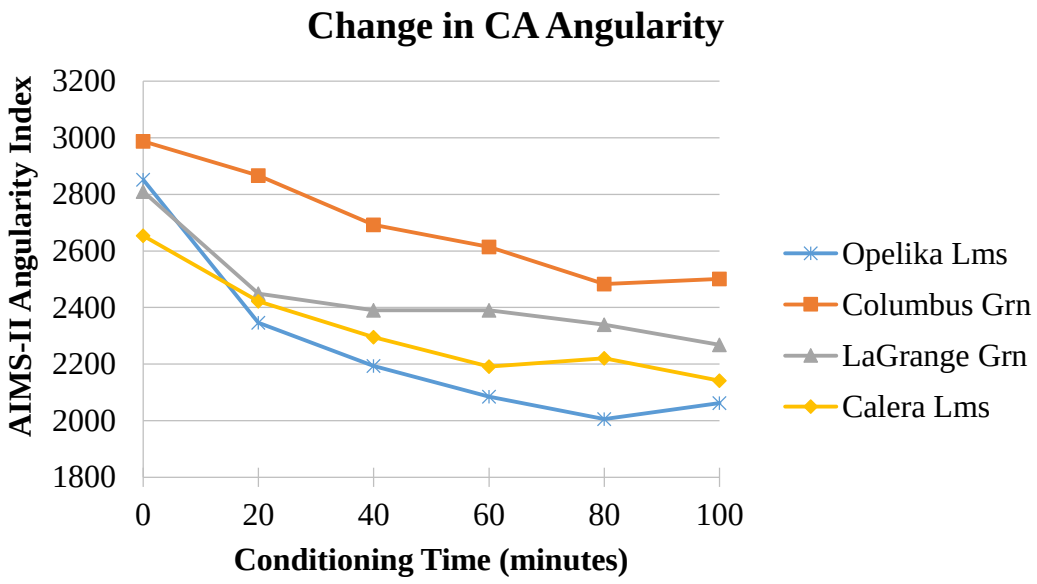


**Figure 5.3: Change in AIMS-II coarse aggregate angularity from Micro-Deval conditioning**

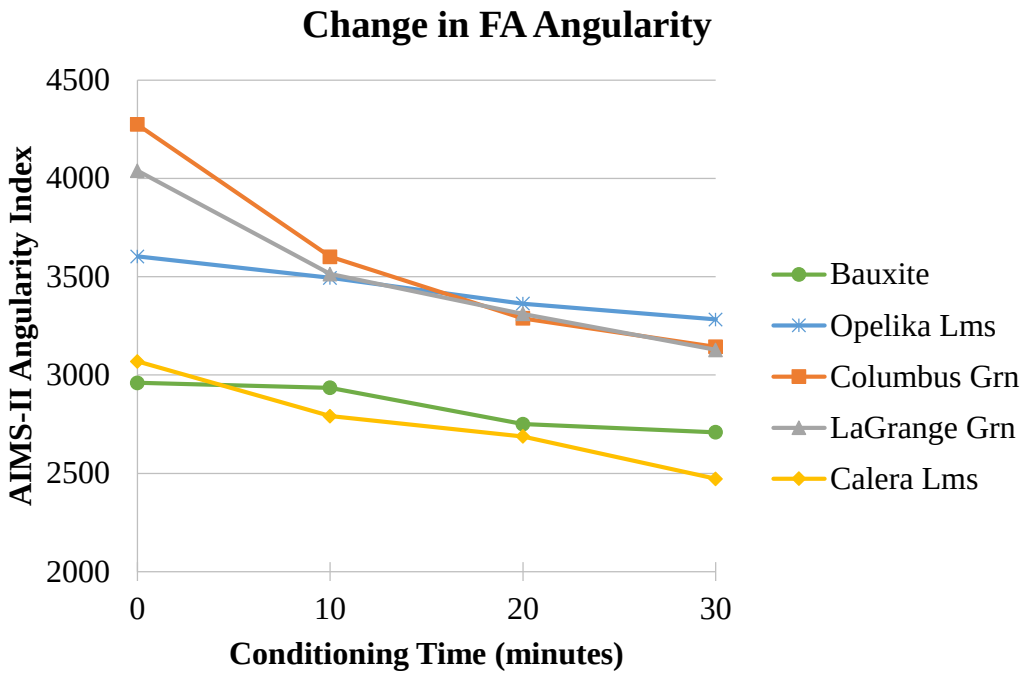


**Figure 5.4 Change in AIMS-II fine aggregate angularity from Micro-Deval conditioning**

Overall, the figures show the aggregate angularity indexes decrease with increased polishing time in the Micro-Deval. This indicates that the aggregate edges are abrading from the impact of the steel charges and surrounding aggregates within the Micro-Deval container. As the rate of angularity is decreasing, the aggregate surfaces are becoming more resistant to the abrasion. Moaveni et al. (2010) observed that the rate of change in angularity significantly decreased at approximately 105 minutes of Micro-Deval conditioning time for coarse aggregates. This is close to the total conditioning time selected for the coarse aggregates as part of this research study. However, the rate of coarse aggregate angularity loss appears to reduce after approximately 80 minutes of conditioning for all aggregate sources that were selected as part of this research study. The fine aggregates did not have an obvious point at which the rate of angularity loss reduced significantly. Therefore, future research studies should consider taking

fine particles beyond 30 minutes of conditioning time in order to see a noticeable decrease in the rate of angularity loss despite 30 minutes being double the conditioning time specified in ASTM D7428.

Similar to the mass loss results, there were differences between the angularity indexes of the coarse and fine aggregates of the same source. The fine aggregates were characterized by a higher initial angularity when compared to the coarse aggregates of the same source. An aggregate may initially be characterized by a high angularity index, but it is important for the aggregate to be able to maintain an adequate level of angularity when subjected to polishing. Therefore, the percent reduction in angularity (reduction in angularity/initial) was recorded to evaluate the aggregates' ability to retain its initial angularity (Table 5.2).

**Table 5.2: Percent loss in AIMS-II angularity for coarse and fine aggregates**

| Aggregate Source | CA | FA |
|---|---|---|
| Opelika Lms | 27.7% | 8.9% |
| Columbus Grn | 16.7% | 26.5% |
| LaGrange Grn | 19.3% | 22.6% |
| Calera Lms | 19.3% | 19.5% |
| Bauxite | N/A | 8.5% |

It has been established that coarse aggregate angularity is the second most important property behind gradation for overall HMA pavement performance (Prowell et al. 2005). Table 5.2 shows the Opelika limestone to have the largest percent loss in angularity for coarse aggregates. Under heavy traffic volumes at the NCAT Test Track, the surface courses typically do not consist of only a limestone source. Limestone sources tend to polish easily under heavy traffic loads, resulting in a decrease in pavement friction performance. To improve friction performance, another aggregate more resistant to polishing is blended with the limestone. Fine aggregates

characterized by higher angularity are more desirable because they provide internal friction within the aggregate structure to prevent rutting but do not directly relate to pavement surface friction.

The cumulative distribution of angularity indexes was tracked before Micro-Deval conditioning (BMD) and at each conditioning time (20, 40, 60, 80, and 100 minutes or 10, 20, and 30 minutes) for each aggregate source and size. Figure 5.5 provides an example of this for the #4 Opelika limestone. The AIMS-II delineation between low, medium, and high angularity indexes are labeled and separated by vertical black lines within the graph. The cumulative distributions for all of the aggregate sources may be found in Appendix C.

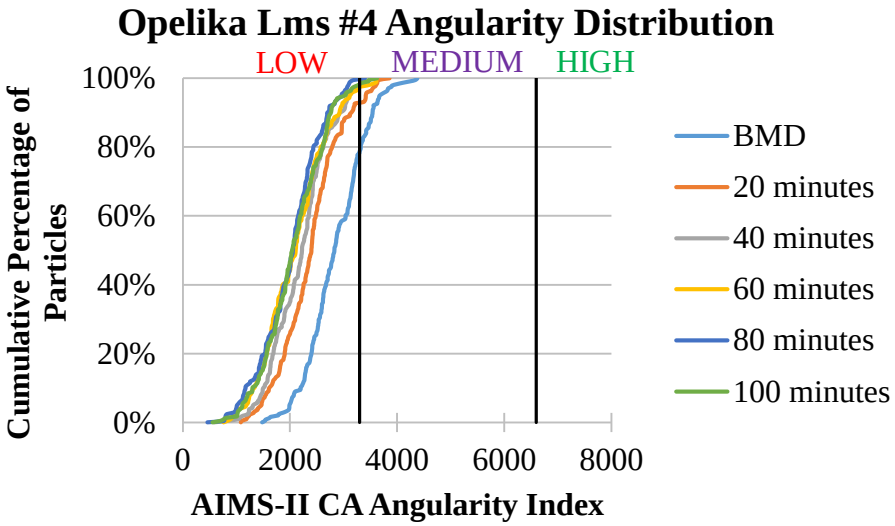


**Figure 5.5: Example of AIMS-II angularity distribution trend for Opelika limestone #4**

A similar trend in the shift of the angularity distribution was observed for all aggregate sources. The distribution shifted left as the aggregates were conditioned in the Micro-Deval indicating that a larger percentage of particles became more rounded when subjected to conditioning. Additionally, the differences in angularity between successive distributions decreased with

increased polishing time. This is demonstrated using the K-S test. Table 5.3 shows the K-S test results that correspond to Figure 5.5. The maximum difference between two successive distributions decreases as the distribution curves get closer. The K-S test results for all aggregate distributions are located in Appendix D.

**Table 5.3: Example of K-S test results for Opelika limestone #4 AIMS-II angularity**

| Opelika Lms #4 Angularity | | |
|---|---|---|
| Comparisons | Max Difference | P-value |
| BMD vs 20 | 0.38 | 0.00 |
| 20 vs 40 | 0.16 | 0.01 |
| 40 vs 60 | 0.13 | 0.06 |
| 60 vs 80 | 0.09 | 0.34 |
| 80 vs 100 | 0.07 | 0.65 |
| BMD vs 100 | 0.53 | 0.00 |

The K-S test results shown in Table 5.3 provide the maximum difference between the two distributions as well as the corresponding p-value at a 95% confidence interval. A low p-value means the distributions are significantly different at a 5 percent level; these values are shown in red. The initial distribution prior to any conditioning and at the total conditioning time were compared in order to confirm that the K-S test recognized a significant change in distribution caused by Micro-Deval conditioning. It should be noted that the K-S test results from the fine aggregates' angularity showed several cases in which the distribution at 20 minute conditioning significantly differed from the distribution at 30 minutes. This further indicated fine aggregate conditioning should be carried out beyond 30 minutes conditioning time to reach terminal angularity values.

Figures 5.6 and 5.7 show the cumulative distribution of particles for each of the coarse and fine aggregate sources, respectively, after total conditioning time. It was noted that the distribution

curves had similar shape. Therefore, the location of the distribution curves ranks similarly to the mean value of each curve. Distribution curves further to the left also had a lower mean value.

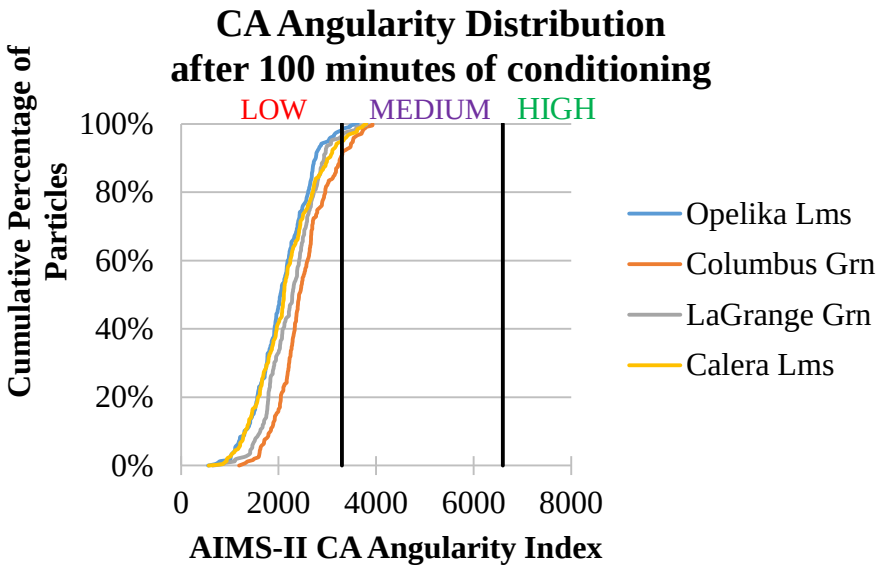


**Figure 5.6: AIMS-II coarse aggregate angularity cumulative distribution after 100 minutes of Micro-Deval conditioning**

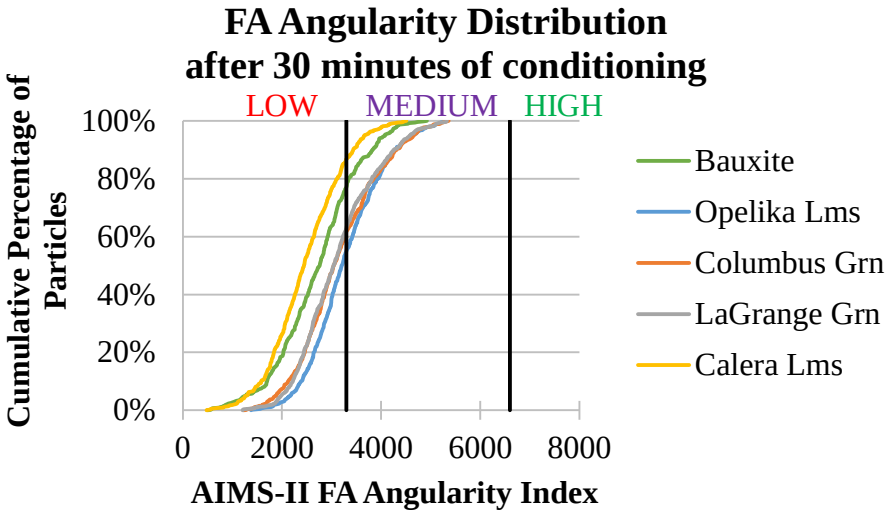


**Figure 5.7: AIMS-II fine aggregate angularity cumulative distribution after 30 minutes of Micro-Deval conditioning**

### 5.3 AIMS-II Coarse Aggregate Texture

The AIMS-II texture index was recorded after each Micro-Deval conditioning cycle for each coarse aggregate source (Figure 5.8). As mentioned in Chapter 3, the AIMS-II does not evaluate surface texture of fine aggregates. Coarse aggregate texture relates to the surface micro-texture of the individual particles, a parameter that influences the overall pavement friction.

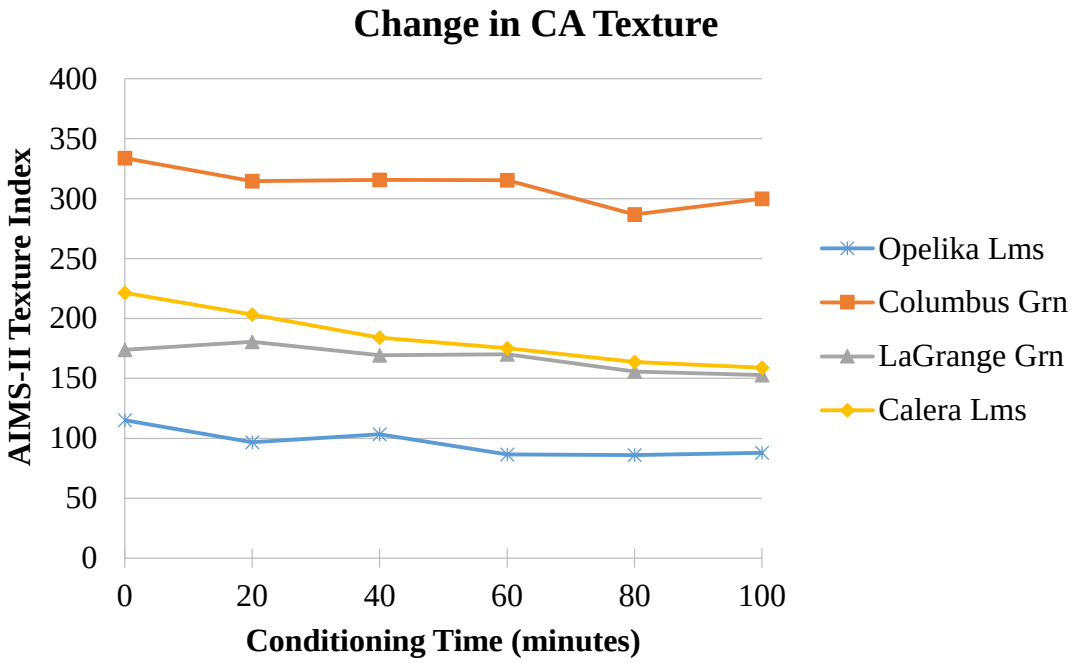


**Figure 5.8: Change in AIMS-II coarse aggregate texture from Micro-Deval conditioning**

As expected, coarse aggregate surface texture decreased with increased Micro-Deval conditioning time. The figure shows apparent distinctions among the different aggregate texture values. The Columbus granite was characterized by the roughest surface texture at terminal conditioning, whereas the Opelika limestone was characterized by the smoothest surface texture after the 100 minutes of conditioning. Because it is important for an aggregate source to be able

to maintain adequate surface texture when subjected to polishing, the loss of texture as a percent of initial surface texture was computed for each aggregate source after 100 minutes of conditioning (Table 5.4).

Figure 5.8 shows Calera limestone has a higher terminal texture index than both the LaGrange granite and Opelika limestone. However, Table 5.4 shows the Calera limestone also has the highest rate of texture loss after 100 minutes of conditioning which is further portrayed by the steeper slope in Figure 5.8. If the Micro-Deval conditioning time were increased, it is possible that the Calera limestone could reach a terminal surface texture value less than that of the LaGrange granite. This is an important consideration as an aggregate might appear to have a higher initial surface texture but under polishing conditions could not retain its micro-texture. This could result in a mixture's inability to maintain an adequate amount of pavement friction.

**Table 5.4: Percent loss in AIMS-II coarse aggregate texture**

| Aggregate Source | Percent Texture Loss |
|---|---|
| Opelika Lms | 23.8% |
| Columbus Grn | 10.2% |
| LaGrange Grn | 14.6% |
| Calera Lms | 28.2% |

Similar to aggregate angularity, the cumulative distribution of coarse aggregate texture indexes was tracked before conditioning in the Micro-Deval (BMD) and after 20, 40, 60, 80, and 100 minutes of conditioning. Figure 5.9 shows an example of the #4 Opelika limestone with the corresponding K-S test results in Table 5.5. The cumulative distributions and corresponding K-S test results of all the aggregate sources may be found in the appendices.

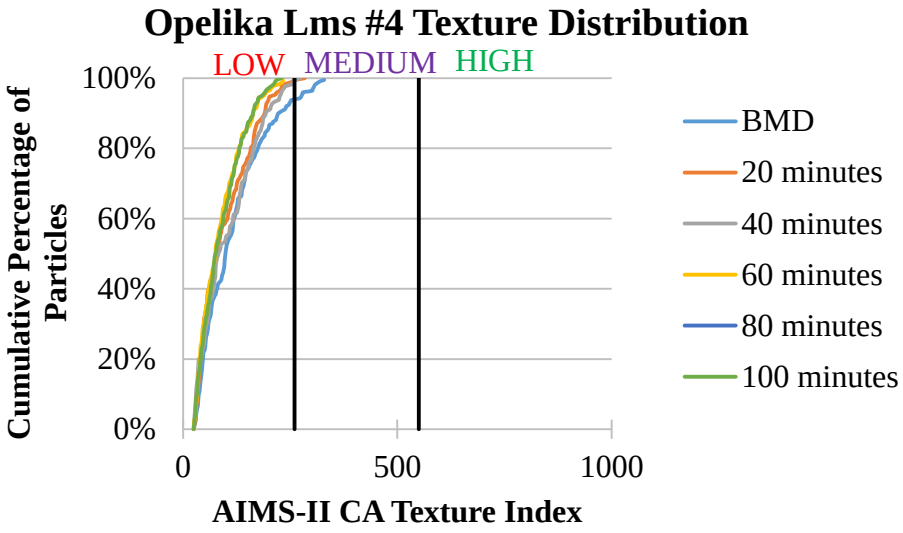


**Figure 5.9: Example of AIMS-II texture distribution trends for Opelika limestone #4**

**Table 5.5: Example of K-S test results for Opelika limestone #4 AIMS-II texture**

| Opelika Lms #4 Texture | | |
|---|---|---|
| Comparisons | Max Difference | P-value |
| BMD vs 20 | 0.14 | 0.03 |
| 20 vs 40 | 0.09 | 0.45 |
| 40 vs 60 | 0.17 | 0.01 |
| 60 vs 80 | 0.05 | 0.99 |
| 80 vs 100 | 0.06 | 0.92 |
| BMD vs 100 | 0.16 | 0.01 |

Similar to the trends observed from the angularity results, the distribution of texture indexes shift left with increased conditioning time demonstrating that the surface texture becomes smoother when subjected to conditioning in the Micro-Deval. Additionally, the differences between successive distributions decreases with increased polishing time. This is further demonstrated in Table 5.5. The maximum difference decreases by approximately half when looking at the BMD versus 20 minute and the 80 minute versus 100 minute comparisons. There was no statistical

difference between the samples beginning at 60 minutes. This statistical analysis agrees with Figure 5.8 that suggests the Opelika limestone reaches a terminal AIMS-II surface texture at 60 minutes of conditioning, indicating the average AIMS-II texture index is leveling off and essentially remaining constant at this point in conditioning.

Figure 5.10 shows the cumulative distribution of each aggregate source's surface texture after 100 minutes of Micro-Deval conditioning. The further right the distribution is shifted indicates rougher texture distribution at terminal conditioning. After 100 minutes of conditioning, the Columbus granite consisted of the largest percentage of particles characterized by rougher texture compared to the other aggregate sources. Therefore, the Columbus granite would provide the most micro-texture to a pavement mixture compared to other sources in this study. This suggests that the Columbus granite should provide more pavement surface friction.

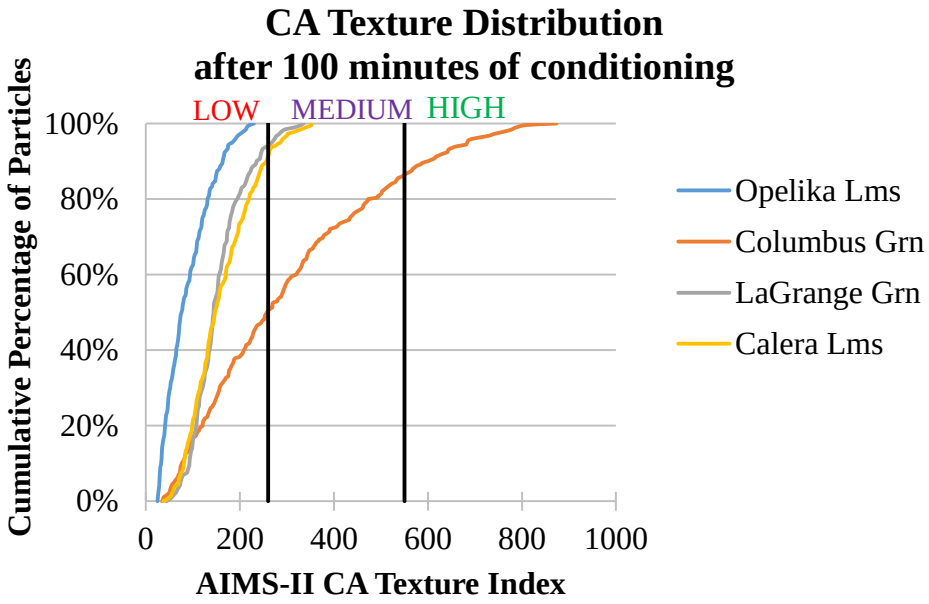


**Figure 5.10: AIMS-II coarse aggregate texture cumulative distribution trends after 100 minutes of Micro-Deval conditioning**

## 5.4 AIMS-II Aggregate Form

### *5.4.1 AIMS-II Coarse Aggregate Sphericity*

Figure 5.11 shows the change in the average AIMS-II sphericity index for each coarse aggregate at each incremental polishing time. The figure reveals that there was no change in sphericity with increased Micro-Deval conditioning time. According to the AIMS-II, all aggregate sources were consistently characterized as having a medium level of sphericity (value of 0.3- 0.7) when considering the overall average. The Opelika limestone consistently had the lowest sphericity index, indicating that these particles tended to be slightly more spherical than the other aggregate sources. This was further demonstrated in Figure 5.12 by showing that the cumulative distribution of the sphericity indexes for the Opelika limestone was shifted farthest left of the aggregate sources after 100 minutes of conditioning.

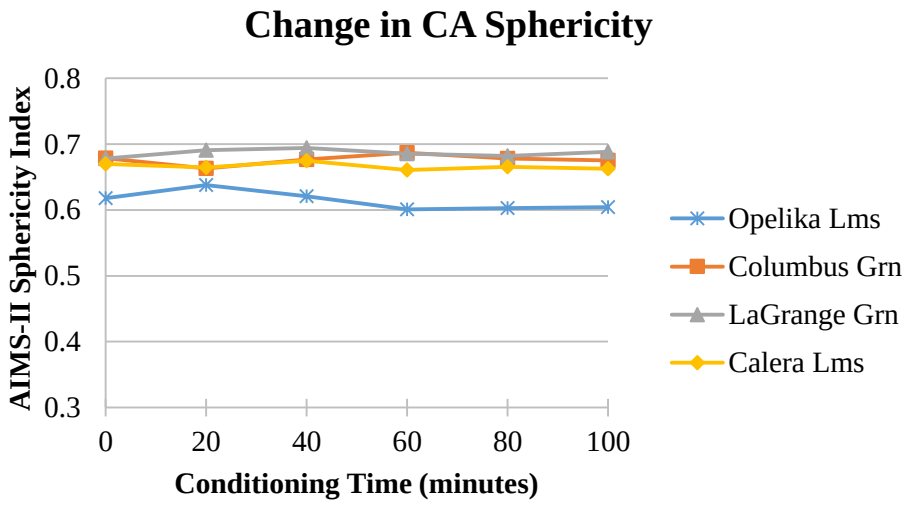


**Figure 5.11: Change in AIMS-II coarse aggregate sphericity from Micro-Deval conditioning**

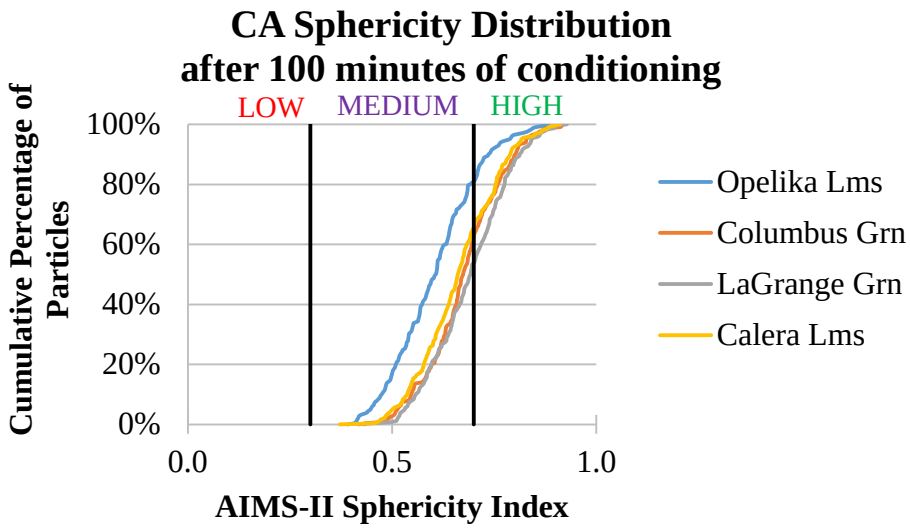


**Figure 5.12: AIMS-II coarse aggregate sphericity cumulative distribution trends after 100 minutes of Micro-Deval conditioning**

### *5.4.2 AIMS-II Coarse Aggregate Flatness and Elongated (F&E) Ratio*

Although flatness and elongation properties are not tied to pavement friction, the average AIMS-II F&E ratios for each coarse aggregate were tracked at each conditioning time to see if there were any trends (Figure 5.13). The graph reveals that there was no change in the average F&E ratios with increased Micro-Deval conditioning time. These results also agree with the results shown for sphericity.

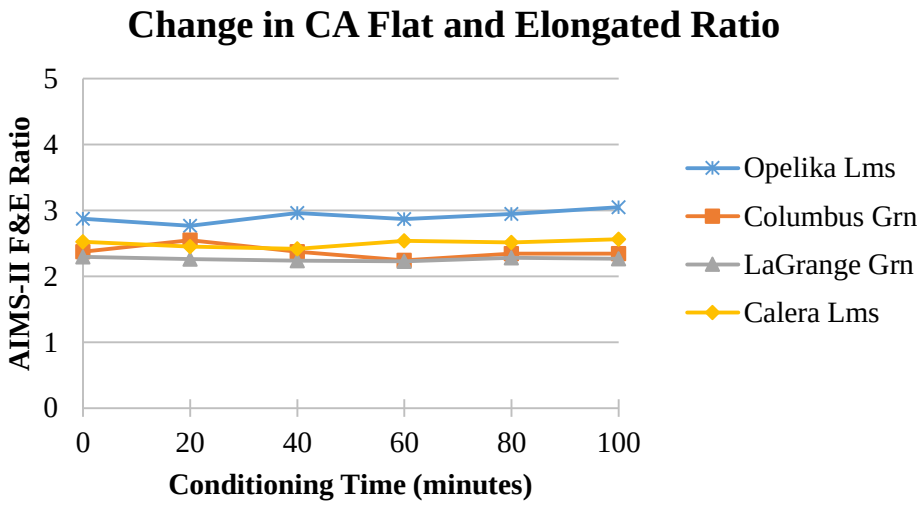


**Figure 5.13: Change in AIMS-II coarse aggregate F&E ratios from Micro-Deval conditioning**

### *5.4.3 AIMS-II Fine Aggregate Two-Dimensional Form (Form2D)*

The change in fine aggregate two-dimensional form was tracked with Micro-Deval conditioning time (Figure 5.14). The figure reveals that the AIMS-II form2D value decreased with increased polishing time in the Micro-Deval. This indicates that as the aggregates were polished, they were becoming increasingly circular. According to the AIMS-II procedure, all AIMS-II form2D averages were characterized as medium values, as they fell within the range of 6 to 12. The Opelika limestone was characterized by the highest average form2D value indicating it portrayed a more elongated oval shape than seen by the other aggregate sources. Bauxite portrayed a fairly consistent shaped throughout conditioning which was also demonstrated by its small change in angularity values shown previously (Figure 5.4, Table 5.2).

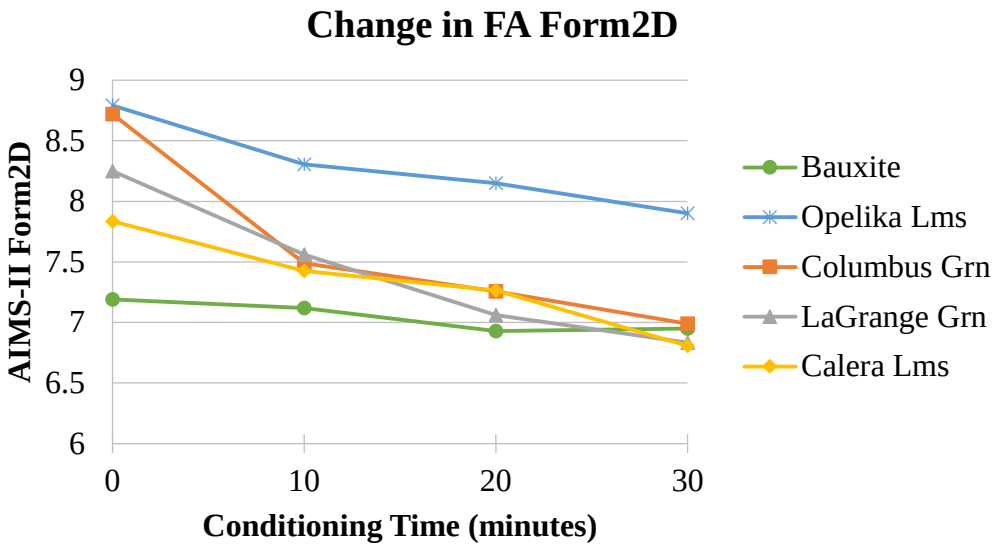


**Figure 5.14: Change in AIMS-II fine aggregate form2D from Micro-Deval conditioning**

Although the fine aggregate form2D values were not expected to provide any correlations with field friction data, the cumulative distribution was tracked at each conditioning time. The primary purpose of this was to show how the bauxite, an aggregate used in high friction surface treatments, compared to the other aggregate sources. Figure 5.15 shows an example of the AIMS-II form2D distribution of the bauxite before Micro-Deval conditioning and after each conditioning time interval. For comparison, Figure 5.16 shows an example of the form2D cumulative distribution of the Columbus granite before and after incremental Micro-Deval conditioning. The corresponding K-S test results are shown in Table 5.6. The distributions of the form2D value with the corresponding K-S test results for all aggregate sources may be found in the appendices. It should be noted that the other aggregate sources' distributions reflected more closely to what was observed with the #16 Columbus granite form2D distribution with a noticeable shift in distribution to the left after being subjected to conditioning. As expected, the

bauxite reflected minimal changes in distribution after increased conditioning, further indicating the durability of bauxite and its resistance to change in shape.

Additionally, Figure 5.17 shows the distributions of form2D values for each aggregate source after 30 minutes of conditioning. Apart from the Opelika limestone, there are barely any differences between the form2D distributions among the aggregate sources. This indicates that there is little variation in the overall two-dimensional shape among the fine aggregates tested.

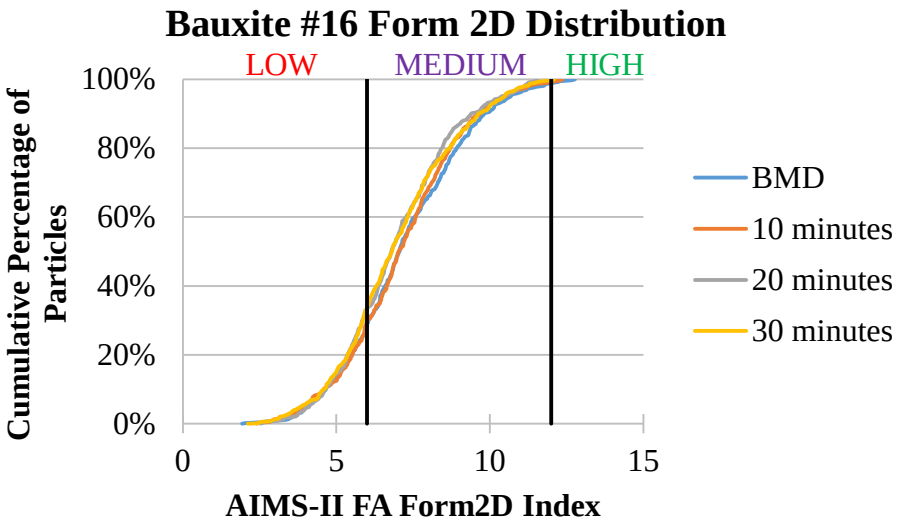


**Figure 5.15: Example of AIMS-II fine aggregate form2D distribution trends for bauxite**

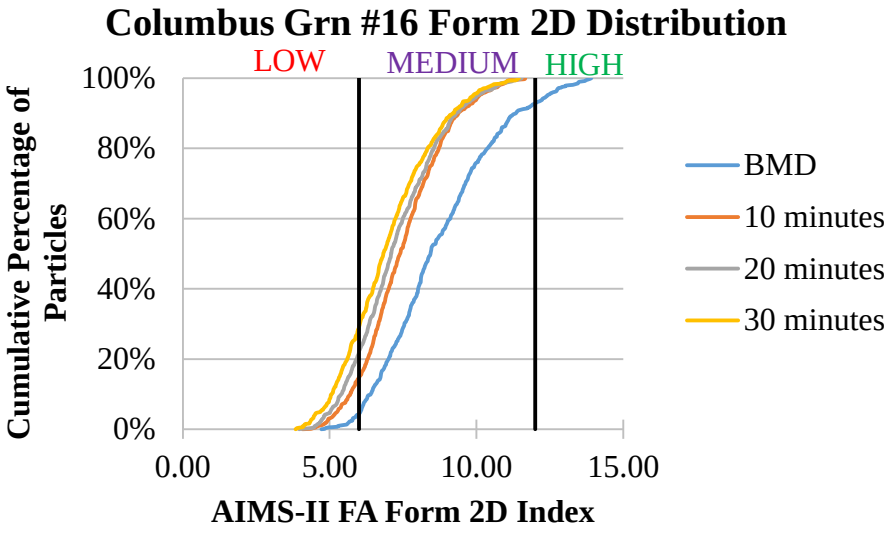


**Figure 5.16: Example of AIMS-II FA formd2D distribution trends for Columbus granite**

**Table 5.6: Example of K-S test results of AIMS-II form2D distributions for bauxite and Columbus granite**

| Comparisons | Bauxite | | Columbus Granite | |
|---|---|---|---|---|
| | Max Difference | P-value | Max Difference | P-value |
| BMD vs 10 | 0.04 | 0.78 | 0.28 | 0.00 |
| 10 vs 20 | 0.08 | 0.12 | 0.10 | 0.00 |
| 20 vs 30 | 0.04 | 0.76 | 0.09 | 0.02 |
| BMD vs 30 | 0.07 | 0.15 | 0.37 | 0.00 |

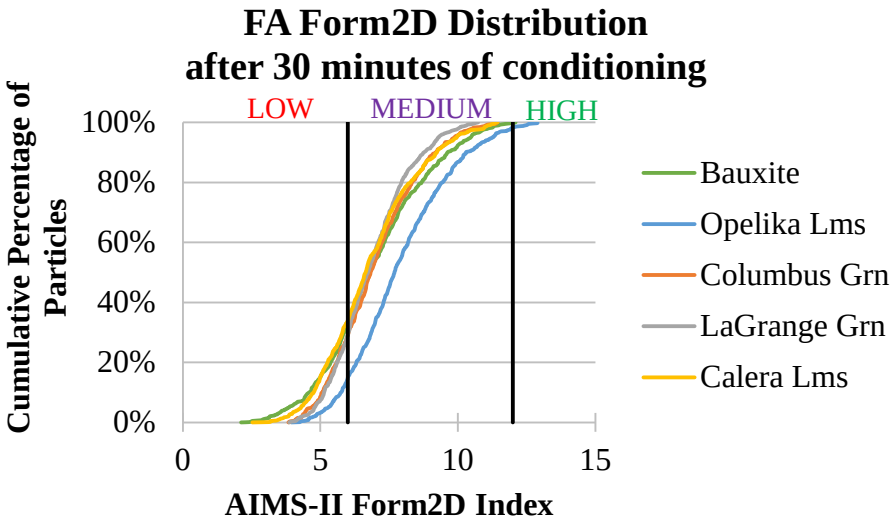


**Figure 5.17: AIMS-II fine aggregate form2D distribution trends after 30 minutes of Micro-Deval conditioning**

### 5.5 Summary of Lab Results

All aggregate sources were measured for mass loss after conditioning in the Micro-Deval. As expected, the bauxite experienced the least percentage of mass loss, indicating it to be more durable than other aggregate sources that were tested. The AIMS-II device was capable of detecting changes in aggregate shape properties among both coarse and fine aggregates. Both coarse and fine aggregate angularity indexes decreased with increased Micro-Deval conditioning time, indicating that the aggregates became increasingly more rounded at the particle edges. As expected, the bauxite experienced the least amount of loss in angularity. Coarse aggregate texture decreased with increased polishing within the Micro-Deval. When comparing the aggregate sources in this study, the Columbus granite was characterized by a rougher surface texture before and after conditioning indicating it to be a better aggregate source for use in a surface course to assist in providing adequate friction. Similarly, based on the texture indexes,

using a limestone source in a surface course may not provide suitable pavement friction. Overall, increased Micro-Deval conditioning yielded a decreasing trend in fine aggregate two-dimensional form. This indicated the aggregates became more rounded. The bauxite showed minimal change in its particle shape when subjected to conditioning, validating its capability of resisting the effects from conditioning. No trends were observed for coarse aggregate sphericity as well as F&E values with increased conditioning time. These two parameters do not play a role in pavement friction, so this did not introduce any hindrances when finding correlations between lab data and field friction data.

# CHAPTER 6: COMPARISON OF AIMS-II LAB RESULTS AND FIELD FRICTION

This chapter focuses on comparing the lab results obtained from the AIMS-II device with the results obtained from the NCAT Pavement Test Track field test sections using the locked-wheel skid trailer. For the purpose of this chapter, the AIMS-II lab results for the Opelika limestone were omitted because none of the surface mixtures on the Test Track sections were composed of Opelika limestone as the dominant aggregate in the mix.

## 6.1 Field Results

Friction data were collected from NCAT's 2009 Test Track research cycle using the locked-wheel skid trailer. As mentioned previously, the skid trailer is run at 40 miles per hour with a ribbed tire and produces a skid number, denoted as SN40R. Field friction data from the last few months of testing in the 2009 research cycle was omitted due to irregularities within the data. The irregularities came from testing field friction a couple of months after the traffic cycles had stopped. This caused the field friction to yield measurements inconsistent with the rest of the friction measurements from the same research cycle.

Initially, the field test sections were ranked on an individual basis. However, using individual test sections for the analysis proved to be inconclusive. Therefore, test sections were grouped together according to the surface mix design, resulting in five separate groups of mixtures. As described in Chapter 4, these groups included two sections of the HFST using bauxite, seven sections of fine-dense graded (FDG) mix composed primarily of Columbus granite, one section of the OGFC composed of Columbus granite, three sections of the OGFC composed of LaGrange granite, and one section characterized as an SMA composed primarily of Calera

limestone. These are summarized in Table 4.2 of Chapter 4. Figure 6.1 shows the design gradation of the four asphalt mix types.

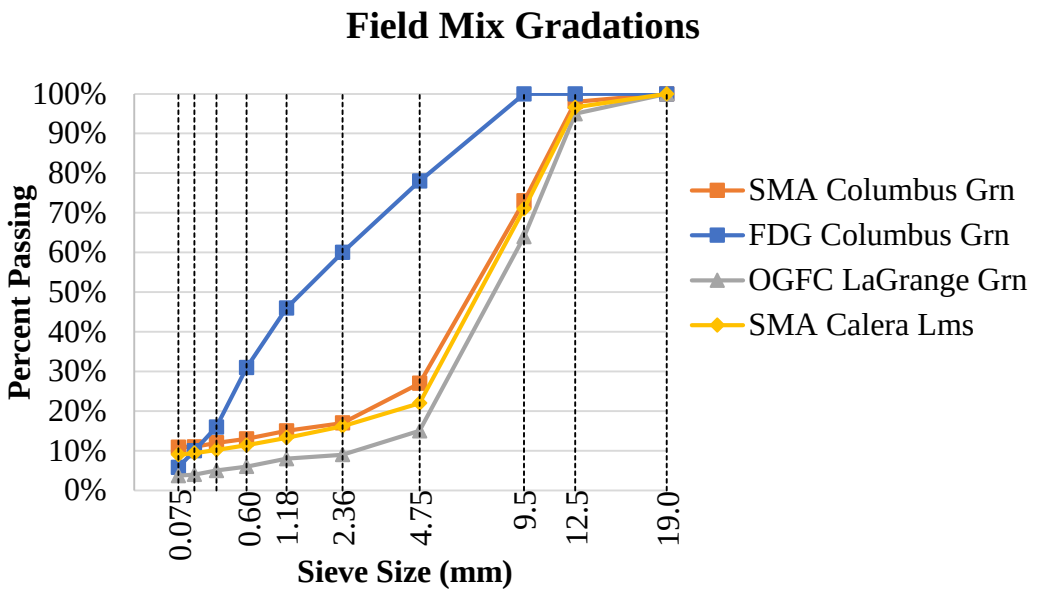


**Figure 6.1: Field mix gradations for each Test Track section**

Based on the mix types, an average of the SN40R for each group was computed to rank the field results (Figure 6.2). The SN40R for bauxite section E3 was unusually high compared to the rest of the data during testing around 5.3 million ESALs. Section E3 was characterized by a SN40R of 68.0 after 5.3 million ESALs of traffic. To justify removing this data point, the difference in SN40R values between section E3 and section E2 were calculated (SN40R of E3 – SN40R of E2). After 5.3 million ESALs, the difference between the measured SN40R values of E3 and E2 was 4.2. This calculated difference was more than two standard deviations away from the average difference between the two test sections, indicating there was some error resulting in the measurement. This was likely attributed to the skid trailer testing outside of the wheel path, which would result in a higher skid number than if the measurement were taken inside the wheel

path. Therefore, the SN40R obtained from the other bauxite section (E2) was used (circled in red in the figure) as opposed to taking an average of the two test sections.

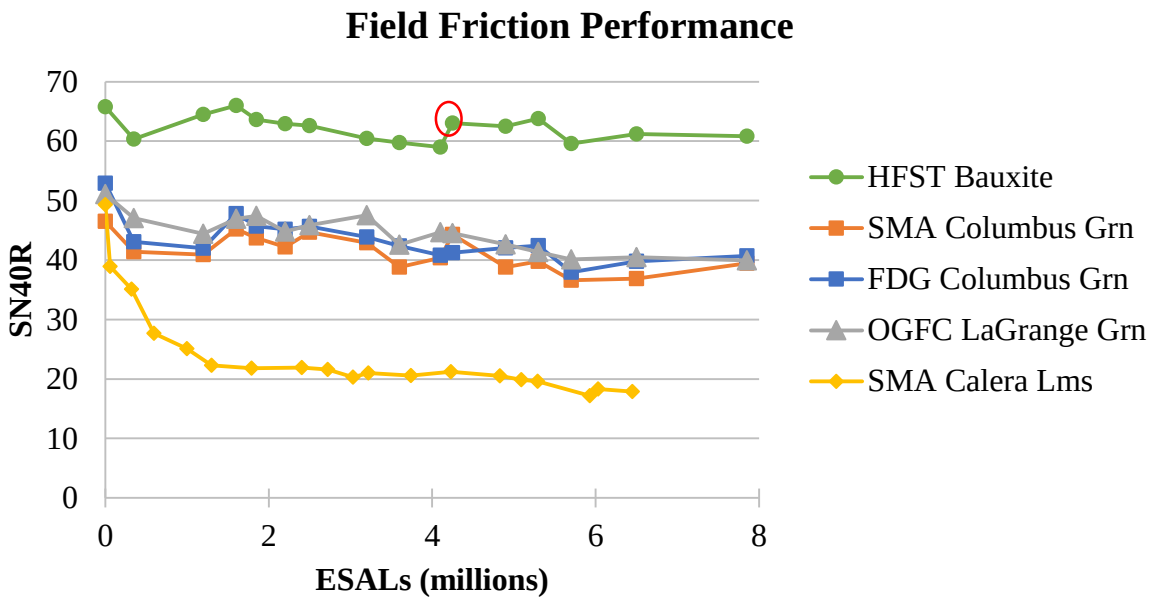


**Figure 6.2: Average of field SN40R data based on mix type**

### *6.1.1 Defining "Terminal Friction"*

Figure 6.2 shows a rapid initial decline in field friction values, primarily with the Calera limestone surface mix. The field friction data showed the rate of friction loss for this mix drastically reduces around 2 million ESALs. Agencies are interested in measuring long-term friction properties, which are commonly called the terminal properties. At 2 million ESALs, all test sections were approaching a point at which the SN40R values were trending to a terminal friction condition (a flat slope), which will be referred to as terminal friction. While friction values tend to continue steadily decreasing, they essentially remain constant at this point with increased polishing from traffic. For this study, it was determined the SN40R at approximately 7 million ESALs was considered the end point of the terminal friction trend for all field test

sections. A linear trend is typically appropriate to portray terminal friction because the change in friction is decreasing at a steady rate. Therefore, a linear trendline was applied to the friction data from 2 to 7 million ESALs (Figure 6.3). The resulting equation from the linear trend was used to calculate average skid numbers from 2 million ESALs to 7 million ESALs to use for comparison with the AIMS-II angularity and AIMS-II texture indexes.

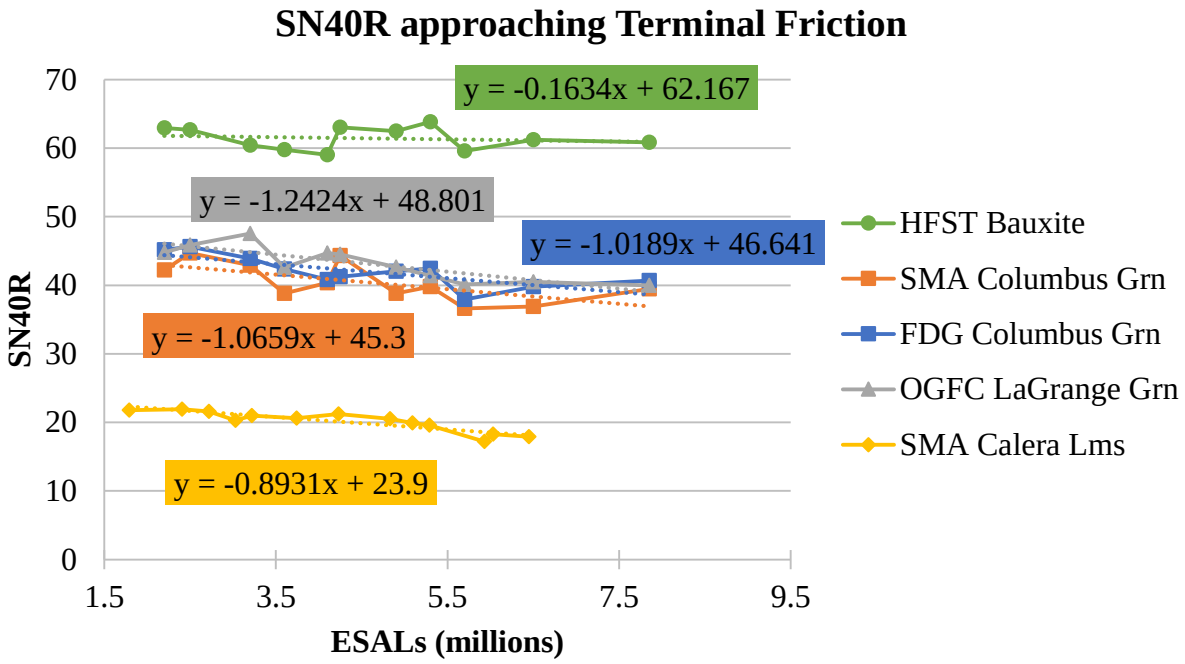


**Figure 6.3: SN40R approaching terminal friction for each Test Track section**

### 6.2 Comparing AIMS-II Aggregate Angularity to Field Friction Performance

A relationship between the AIMS-II angularity and SN40R was assessed as part of the research study. AIMS-II coarse aggregate angularity and AIMS-II fine aggregate angularity were compared separately with the field friction performance. The skid number obtained from the field before the test sections were opened to traffic (0 ESALs) was not altered and was used to compare with preconditioned AIMS-II indexes, which is further discussed within this chapter.

### *6.2.1 AIMS-II Coarse Aggregate Angularity and SN40R*

Four measurement intervals were selected at specific points in time during conditioning to evaluate if a relationship could be established between the AIMS-II results and field friction. The first interval selected compared the field SN40R with the AIMS-II prior to any conditioning from traffic in the field or the Micro-Deval in the lab. Lab results (shown in Chapter 4 of this report) portrayed a linear decline from 20 to 100 minutes for AIMS-II coarse aggregate angularity. A similar trend was seen in the field friction performance data as it was approaching terminal friction from approximately 2 to 7 million ESALs. Therefore, the end of the significant decline was selected as the second interval of comparison, which compared the AIMS-II CA angularity at 20 minutes and the field SN40R at 2 million ESALs. A third interval was selected to compare points in the middle of the linear decline as the values approached terminal values, which included AIMS-II CA angularity at 60 minutes and SN40R at 4 million ESALs. Lab testing was not carried out to a terminal value. It was believed that 100 minutes of conditioning coarse aggregates was reaching near a terminal value based on a study by Moaveni et al. (2008), which found the AIMS-II indexes significantly reduced after 105 minutes of Micro-Deval conditioning. Therefore, AIMS-II CA angularity at 100 minutes was compared with the SN40R at 6 million ESALs, a value approaching close to the end point of the terminal friction trend (7 million ESALs) in the field. The results of the comparison are shown in Figure 6.4. Bauxite is not included in the figure because there were no coarse aggregates to test bauxite. To clarify, the field friction values were acquired from the trendlines shown in Figure 6.3, whereas the AIMS-II indexes are the actual indexes provided by AIMS-II testing. The isolated data points represent the comparison of the AIMS-II results with the field friction data prior to any conditioning. As mentioned previously, these points were not altered for comparison.

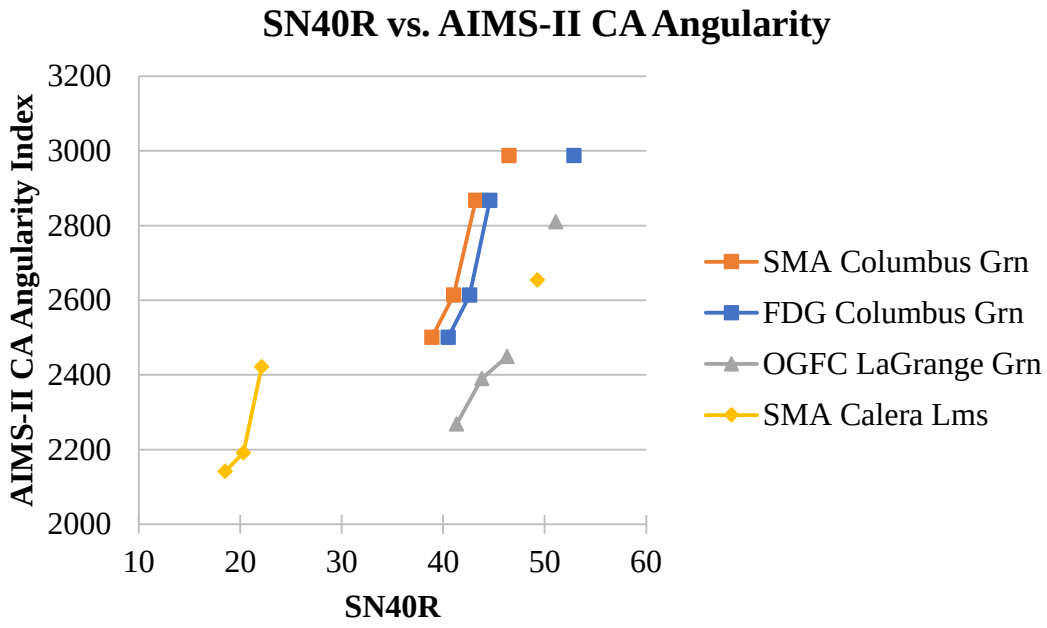


**Figure 6.4: Comparison of AIMS-II coarse aggregate angularity with field friction**

The results showed some inconsistencies among the data. For example, the Calera limestone in the field showed barely any reduction in the SN40R after the initial 2 million ESALs of conditioning. However, in the laboratory after initial conditioning to 20 minutes, the AIMS-II angularity continued to decrease from approximately 2,400 to 2,200. As a result, the steep slope of the Calera limestone reflects the change in laboratory properties while field friction remained reasonably constant. A similar trend was seen when comparing the AIMS-II Columbus granite angularity indexes with the field friction of the two mixes containing Columbus granite. Therefore, it was determined that generating a trendline to the linear portion of the AIMS-II coarse aggregate angularity data may provide more consistent results (Figure 6.5).

The trendline equations were used to calculate the average lab values to be used for comparison after conditioning at 20, 60, and 100 minutes. These values were then used to rank the aggregates and mixtures based on the AIMS-II coarse aggregate angularity indexes and SN40R values, respectively (Table 6.1). To clarify, the aggregates and mixtures are ranked from 1 to 3, where 1 denotes the aggregate or mixture as being characterized as having the highest AIMS-II index or SN40R. The AIMS-II lab values at 20, 60, and 100 minutes were used to compare with the field SN40R at 2, 4, and 6 million ESALs (Figure 6.6).

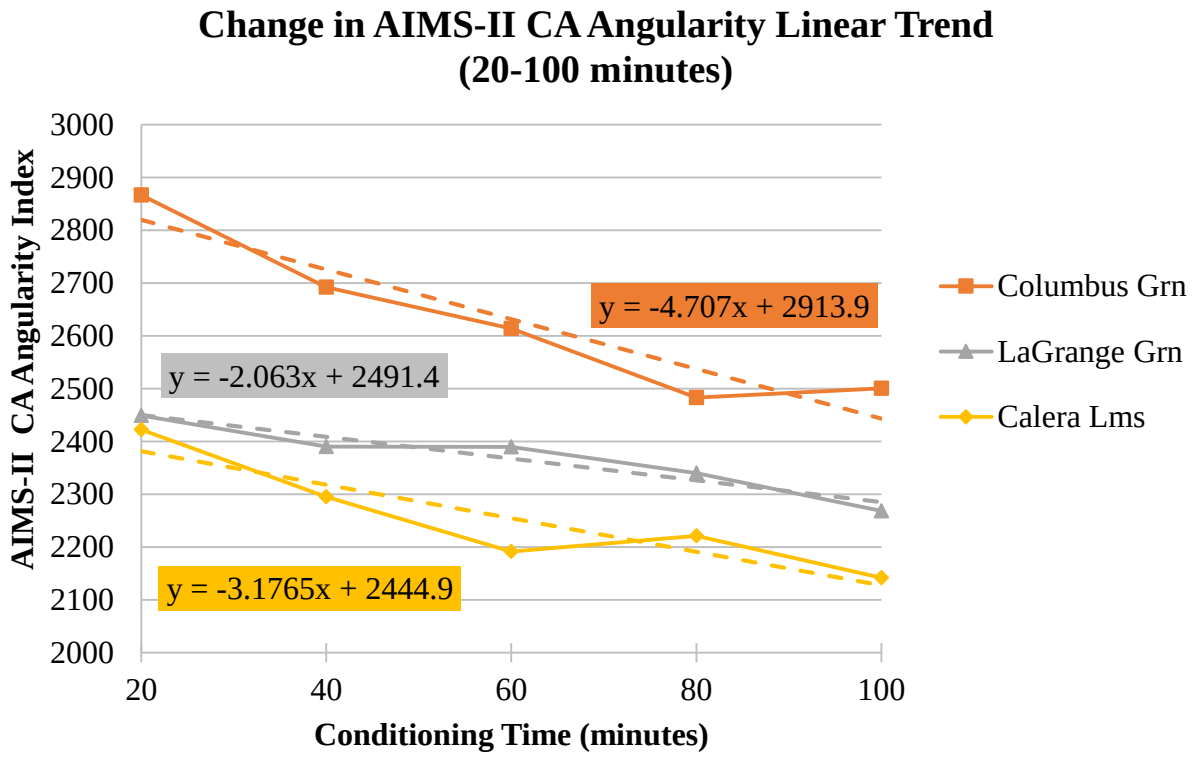


**Figure 6.5: Linear trend in AIMS-II coarse aggregate angularity from 20 to 100 minutes**

**Table 6.1 Comparison of AIMS-II coarse aggregate angularity and field SN40R Rankings**

| Field Mix ID | Pre-conditioned | 2 mESALs | 4 mESALs | 6 mESALs |
|---|---|---|---|---|
| OGFC LaGrange Grn | 1 | 1 | 1 | 1 |
| SMA/FDG Columbus Grn | 3/1 | 2 | 2 | 2 |
| SMA Calera Lms | 2 | 3 | 3 | 3 |
| **#4 Aggregate** | **Pre-conditioned** | **20 minutes** | **60 minutes** | **100 minutes** |
| LaGrange Grn | 2 | 2 | 2 | 2 |
| Columbus Grn | 1 | 1 | 1 | 1 |
| Calera Lms | 3 | 3 | 3 | 3 |

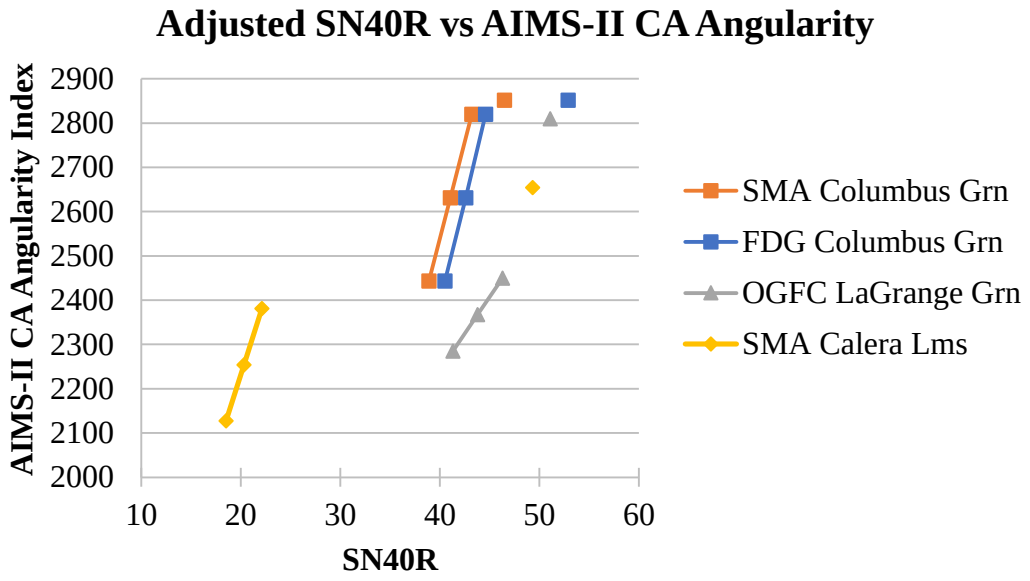


**Figure 6.6: Adjusted trend for field friction and AIMS-II coarse aggregate angularity comparison**

Table 6.1 compares the ranking of the AIMS-II coarse aggregate angularity with that of the field SN40R. To further clarify, the preconditioned ranking follows the order using the SMA Columbus granite ranked third. If the remaining field sections were ranked based on the FDG Columbus granite ranking prior to any conditioning, which was ranked first, the OGFC LaGrange granite section would rank second, and the SMA Calera limestone section would rank

third. With the exception of the pre-conditioned rankings, the rankings of the mix types were identical, regardless of which Columbus granite surface mix was used. This suggests the mix type did not impact the field friction performance. The #4 Calera limestone consistently ranked last after it was subjected to conditioning. Similarly, the field mix composed primarily of Calera limestone consistently ranked last after being subjected to polishing due to traffic.

Figure 6.6 shows that a positive relationship between the AIMS-II coarse aggregate angularity and the field SN40R. In general, a decrease in the AIMS-II coarse aggregate angularity results in a decrease in SN40R of the surface mix in the field. Unfortunately, a good correlation between the AIMS-II coarse aggregate angularity results and the field SN40R could not be established. This can be attributed to discrepancies within the results that question the capability of the AIMS-II/Micro-Deval combination to relate to field friction performance. The AIMS-II lab results show the Columbus granite to be the aggregate characterized by the highest coarse aggregate angularity. However, the field results show the mix containing primarily LaGrange granite as exhibiting the best field friction performance. In the lab, the LaGrange granite exhibited AIMS-II coarse aggregate angularity indexes that were closer to the Calera limestone, an aggregate known to yield poor friction performance in the field.

### *6.2.2 AIMS-II Fine Aggregate Angularity and SN40R*

A similar process was carried out for evaluating the relationship between AIMS-II fine aggregate angularity from the #16 aggregate particles and the SN40R from the surface mixtures in the field. The AIMS-II fine aggregate angularity began exhibiting a linear trend at 10 minutes. Therefore, a linear trendline was applied to the data from 10 to 30 minutes (Figure 6.7). The resulting equations were used to generate average AIMS-II fine aggregate angularity indexes which were

used to rank the aggregate's (Table 6.2) and to compare with the field SN40R values (Figure 6.8).

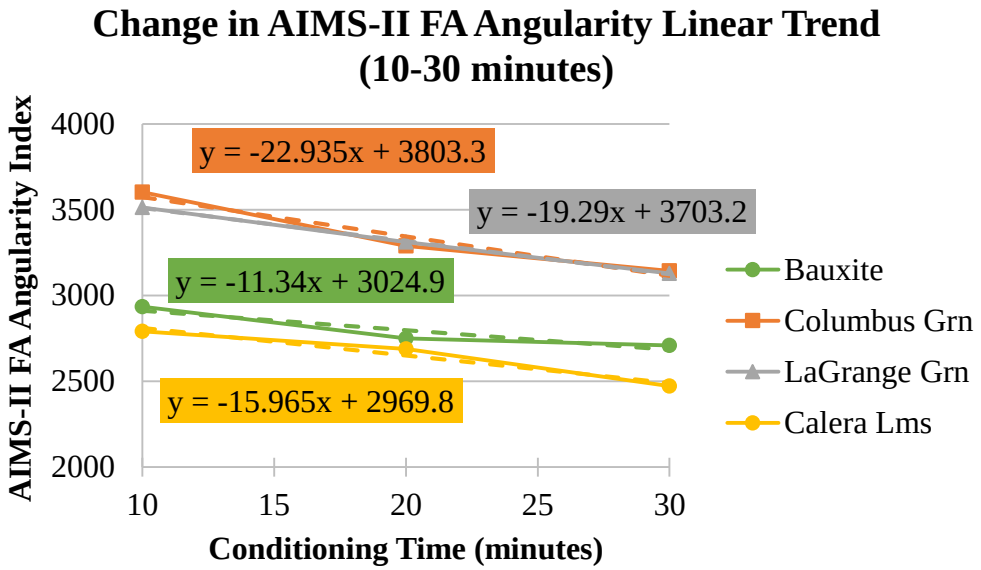


**Figure 6.7: Linear trend in AIMS-II fine aggregate angularity from 10 to 30 minutes**

**Table 6.2: Comparison of AIMS-II fine aggregate angularity and field SN40R Rankings**

| Field Mix ID | Pre-conditioned | 2 mESALs | 4 mESALs | 6 mESALs |
|---|---|---|---|---|
| HFST Bauxite | 1 | 1 | 1 | 1 |
| OGFC LaGrange Grn | 2 | 2 | 2 | 2 |
| SMA/FDG Columbus Grn | 4/2 | 3 | 3 | 3 |
| SMA Calera Lms | 3 | 4 | 4 | 4 |
| **#16 Aggregate** | **Pre-conditioned** | **10 minutes** | **20 minutes** | **30 minutes** |
| Bauxite | 4 | 3 | 3 | 3 |
| LaGrange Grn | 2 | 2 | 2 | 1 |
| Columbus Grn | 1 | 1 | 1 | 2 |
| Calera Lms | 3 | 4 | 4 | 4 |

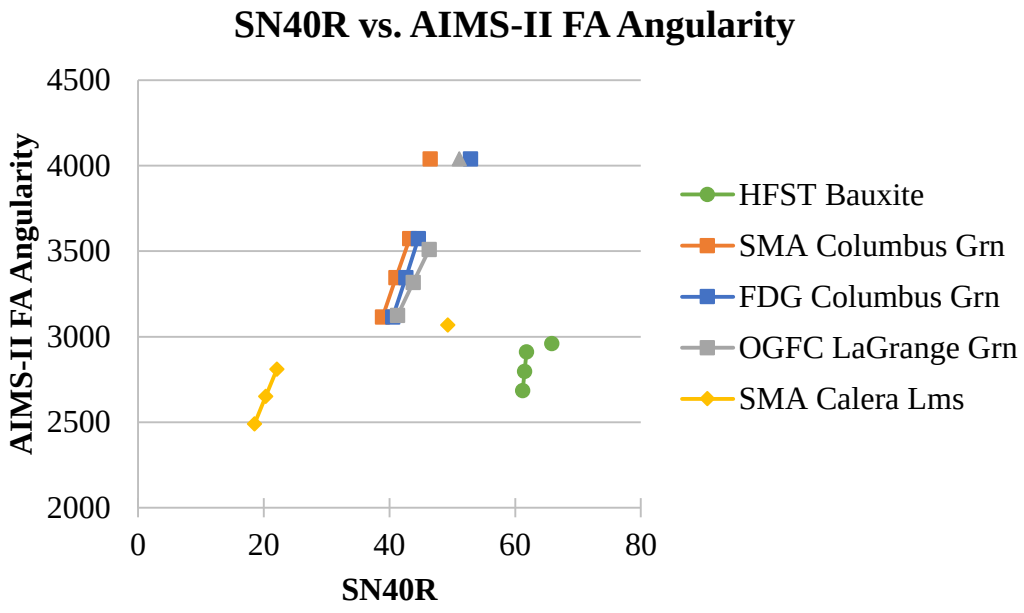


**Figure 6.8: Adjusted trend for field friction and AIMS-II fine aggregate angularity comparison**

After the aggregates were subjected to conditioning in the Micro-Deval, the Calera limestone consistently exhibited the lowest AIMS-II fine aggregate angularity, which agrees with the SN40R results of the Calera limestone mix in the field. However, the results also showed some inconsistencies. The aggregates which portrayed the highest and lowest friction in the field were characterized by the same angularity in the AIMS-II. The bauxite, which excelled in field friction performance, yielded AIMS-II angularity indexes close to the Calera limestone, which exhibited poor friction performance. This may be attributed to the bauxite being used as a high friction surface treatment in the field as opposed to a component in a surface mixture.

Figure 6.8 shows that AIMS-II fine aggregate angularity decreases as friction decreases in the field for each of the surface mixes. The figure also indicates no correlation between the AIMS-II fine aggregate angularity and the field SN40R could be established. If the bauxite were removed,

a possible correlation could be made between AIMS-II fine aggregate angularity and field friction among the granite sources and Calera limestone. This indicates the AIMS-II may not be suitable in evaluating aggregate sources that are used in typical high friction surface treatments, such as the bauxite.

### 6.3 Comparing AIMS-II Texture to Field Friction Performance

Similar to the AIMS-II coarse aggregate angularity, the AIMS-II coarse aggregate texture results exhibited a linear trend from 20 to 100 minutes of conditioning time. Therefore, linear trendlines were applied (Figure 6.9), and the same points for comparison were selected that were used previously when comparing coarse aggregate angularity with field friction. The AIMS-II lab results at 0, 20, 60, and 100 minutes were compared with the field's SN40R at 0, 2, 4, and 6 million ESALs, respectively, using the same ranking system (Table 6.3) and plotting the values on a graph (Figure 6.10).

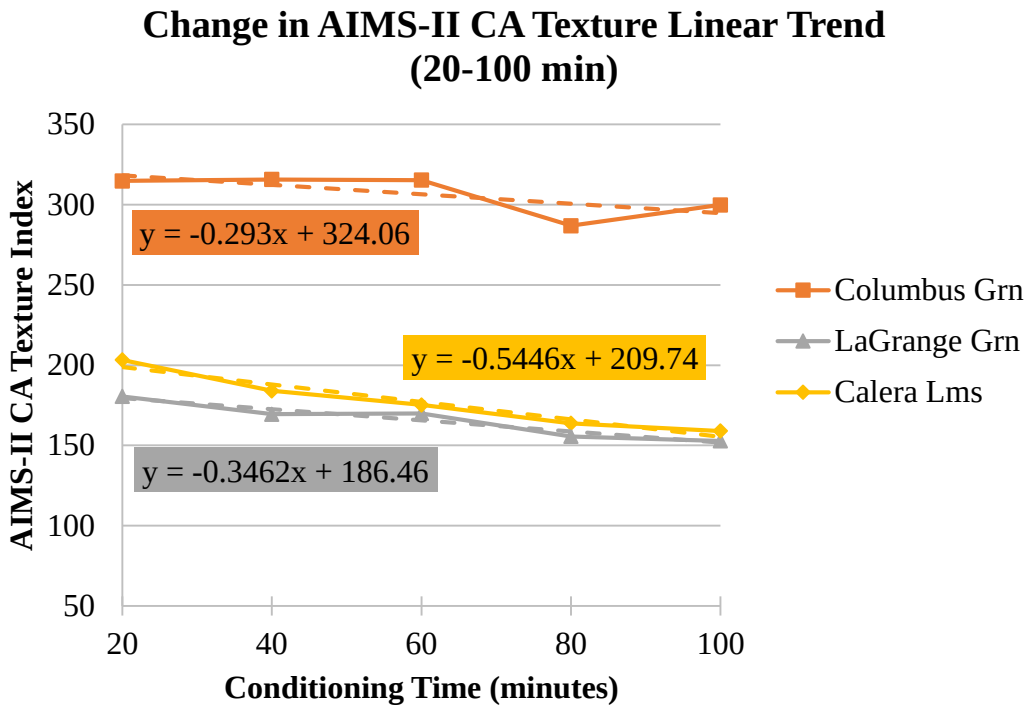


**Figure 6.9: Linear trend for AIMS-II coarse aggregate texture from 20 to 100 minutes**

**Table 6.3: Comparison of AIMS-II coarse aggregate texture and field SN40R rankings**

| Mix ID | Pre-conditioned | 2 mESALs | 4 mESALs | 6 mESALs |
|---|---|---|---|---|
| OGFC LaGrange Grn | 1 | 1 | 1 | 1 |
| SMA/FDG Columbus Grn | 3/1 | 2 | 2 | 2 |
| SMA Calera Lms | 2 | 3 | 3 | 3 |
| **#4 Aggregate** | **Pre-conditioned** | **20 minutes** | **60 minutes** | **100 minutes** |
| LaGrange Grn | 3 | 3 | 3 | 3 |
| Columbus Grn | 1 | 1 | 1 | 1 |
| Calera Lms | 2 | 2 | 2 | 2 |

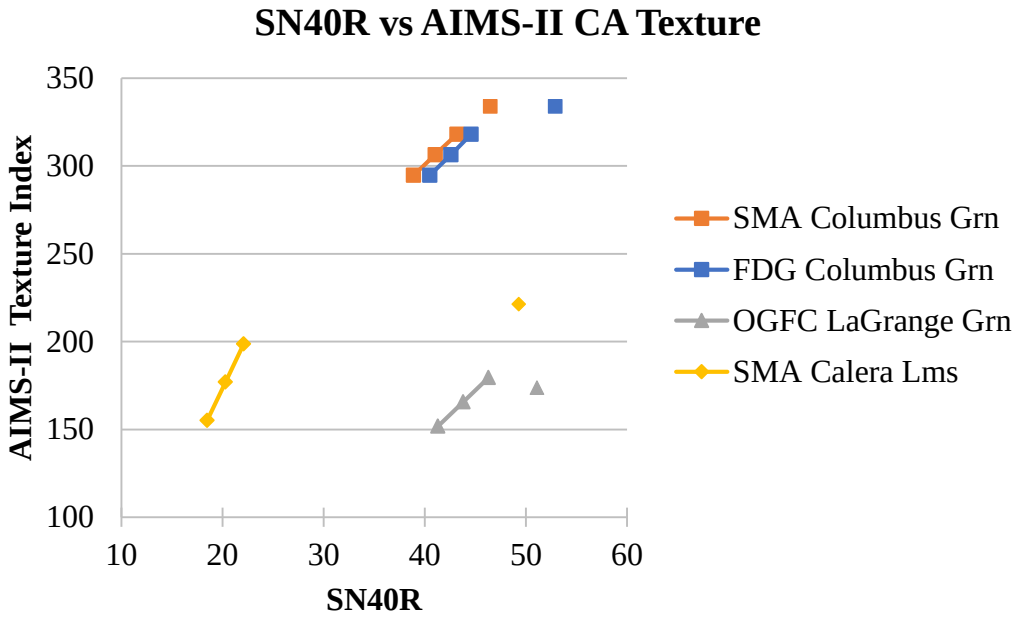


**Figure 6.10: Adjusted trend for AIMS-II coarse aggregate texture and field SN40R comparison**

The results from the AIMS-II coarse aggregate texture measurements did not agree with the friction results obtained from the field SN40R. The AIMS-II texture indexes for the LaGrange granite were consistently ranked the lowest of the aggregates compared. As mentioned previously, the LaGrange granite surface mix exhibited the best field friction performance of the mixes presented in Table 6.3. The results show the #4 LaGrange granite to be exhibiting AIMS-II texture indexes that reflect more closely to the Calera limestone texture indexes, which was not expected. Similar to the AIMS-II coarse aggregate angularity, Figure 6.10 did not show a good correlation between the AIMS-II texture and field SN40R, though it does suggest that a decrease in AIMS-II coarse aggregate texture results in a decrease in SN40R after conditioning, which is what would be expected.

### 6.4 Comparing Micro-Deval Mass Loss to Field Friction Performance

The cumulative percentage of the aggregate mass loss from the Micro-Deval was analyzed to determine if field SN40R data ranking was similar. Table 6.4 shows the ranking of the SN40R in the field and of the cumulative mass loss for the coarse aggregates after 100 minutes of conditioning and fine aggregates after 30 minutes of conditioning. An aggregate ranking of 1 indicates the aggregate yielded the least mass loss at the end of Micro-Deval conditioning, whereas a ranking of 4 is the aggregate with the most mass loss. The ranking system for the coarse aggregate mass loss starts with 2 to be consistent with the ranking of the field and fine aggregate mass loss, as a coarse aggregate bauxite was not tested. As noted earlier, the field mix types containing Columbus granite did not affect the SN40R ranking after conditioning, so for simplicity, they were not separated within the table.

**Table 6.4: Ranking comparison of field friction, coarse aggregate mass loss, and fine aggregate mass loss**

| Aggregate | Field SN40R | CA Mass Loss | FA Mass Loss |
|---|---|---|---|
| Bauxite | 1 | N/A | 1 |
| Columbus Grn | 3 | 4 | 4 |
| LaGrange Grn | 2 | 2 | 3 |
| Calera Lms | 4 | 3 | 2 |

The table shows the performance of the bauxite in the lab, in regards to mass loss, agreed with the HFST bauxite friction from the field, as they both excelled in performance. However, the Columbus granite and LaGrange granite, which performed well in the field, exhibited a significantly higher cumulative mass loss compared to the Calera limestone, which exhibited very poor performance in the field in regards to friction. Unfortunately, a correlation could not be made between cumulative mass loss and the field data, as there was no indication of what the

terminal value would be for mass loss. According to Figure 4.1 and Figure 4.2 from Chapter 4, the cumulative mass loss for both the coarse and fine aggregates, respectively, failed to reach a terminal value.

### 6.5 Statistical Analysis of Comparison Results

A series of statistical analyses were carried out using Excel's data analysis package and DataFit (version 9.1.32) to further analyze the correlations between the AIMS-II indexes and the field friction performance data. The AIMS-II parameters that were used included the coarse aggregate angularity, coarse aggregate texture, coarse aggregate sphericity, fine aggregate angularity, and fine aggregate form2D. Coarse aggregate flat and elongated ratios were excluded from the analysis because they influence the compaction of the mixture and are not tied to friction. Coarse aggregate sphericity and fine aggregate form2D were not previously used to compare with field friction data. However, these two AIMS-II parameters were included in the statistical analysis to evaluate their influence on the correlation.

The first part of the statistical analysis used the average AIMS-II indexes for each aggregate source after final conditioning. These AIMS-II indexes were compared with the average SN40R obtained from the last month of testing that was used for this research study (Figure 6.2). A summary of the data used for comparison is shown in Table 6.5.

**Table 6.5: AIMS-II indexes after final conditioning and average terminal SN40R**

| Aggregate | AIMS-II Indexes | | | | | SN40R |
|---|---|---|---|---|---|---|
| | CA Angularity | CA Texture | CA Sphericity | FA Angularity | FA Form2D | |
| Bauxite | --- | --- | --- | 2708.53 | 6.95 | 60.8 |
| Columbus Grn | 2500.9 | 299.84 | 0.68 | 3143.43 | 6.99 | 40.7 |
| LaGrange Grn | 2268.3 | 152.84 | 0.69 | 3127.73 | 6.84 | 40.0 |
| Calera Lms | 2141.6 | 158.96 | 0.66 | 2472.07 | 6.81 | 17.9 |

The data from Table 6.5 was used to run a Pearson Product-Moment Correlation to detect correlations between the AIMS-II indexes and field friction data (Table 6.6). The Pearson Correlation is used to evaluate the linear relationship between two parameters. It provides a value between -1 and +1, known as the Pearson Correlation coefficient or r-value, which indicates the strength of the correlation between the two sets of data in consideration (Johnson et al. 2000). This r-value should not be confused with the coefficient of determination ($R^2$), which represents how much the variability of the data can be explained by a given model. For the statistical analyses in this research study, variables with an r-value of approximately 0.6 and greater were considered to be an acceptable correlation for further correlation analysis (Pearson's Correlation Coefficient 2009). Table 6.6 shows three of the AIMS-II parameters, coarse aggregate angularity, coarse aggregate sphericity, and fine aggregate form2D, had acceptable correlation coefficients with the field friction data compared to the other parameters.

**Table 6.6: Pearson Correlation Coefficient for AIMS-II indexes and average field friction**

| **Parameter** | CA Angularity | CA Texture | CA Sphericity | FA Angularity | FA Form2D | SN40R |
|---|---|---|---|---|---|---|
| Ca Angularity | 1 | | | | | |
| CA Texture | 0.924 | 1 | | | | |
| CA Sphericity | 0.345 | -0.039 | 1 | | | |
| FA Angularity | 0.783 | 0.486 | 0.854 | 1 | | |
| FA Form2D | 0.977 | 0.984 | 0.139 | 0.417 | 1 | |
| SN40R | **0.787** | 0.491 | **0.851** | 0.325 | **0.683** | 1 |

The correlation between the fine aggregate angularity and field friction was low. This was attributed to the bauxite measuring a low angularity index while performing well in the field from a friction standpoint. To examine the influence of the bauxite, it was omitted from the data, and a second Pearson Correlation was run (Table 6.7).

**Table 6.7: Pearson Correlation Coefficients for AIMS-II indexes and average field friction (excluding bauxite)**

| **Parameter** | CA Angularity | CA Texture | CA Sphericity | FA Angularity | FA Form2D | SN40R |
|---|---|---|---|---|---|---|
| CA Angularity | 1 | | | | | |
| CA Texture | 0.924 | 1 | | | | |
| CA Sphericity | 0.345 | -0.039 | 1 | | | |
| FA Angularity | 0.783 | 0.486 | 0.854 | 1 | | |
| FA Form2D | 0.977 | 0.984 | 0.139 | 0.634 | 1 | |
| SN40R | **0.787** | 0.491 | **0.851** | **1.000** | **0.639** | 1 |

When bauxite was excluded, the correlation between fine aggregate angularity and field friction resulted in an r-value of 1.000, indicating a perfect positive correlation between fine aggregate angularity and field friction (Table 6.7). However, it should be noted that the remaining data

without bauxite represents a linear fit between a single limestone data point and a tight cluster of granite data. Additionally, the correlation between fine aggregate form2D and field friction decreased slightly with the exclusion of bauxite. Graphical representations of the comparisons that resulted in good correlations are shown in the Appendices.

The data set was limited to three data points for coarse aggregates and four data points for fine aggregates when using an average SN40R. In order to expand the amount of data, the SN40R for each individual section was analyzed individually, as opposed to using an average based on surface mix type (Table 6.8). This increased the data for coarse aggregates to 12 data points and for fine aggregates to 14 data points. The AIMS-II indexes remain the same for a specific aggregate type, but the SN40R values are the measured friction for each surface on the Test Track. A Pearson Correlation was run on the data presented in Table 6.8. These results included the bauxite and are summarized in Table 6.9.

**Table 6.8: AIMS-II indexes after final conditioning and terminal SN40R for each section**

| Aggregate | AIMS-II Indexes | | | | | SN40R |
|---|---|---|---|---|---|---|
| | CA Angularity | CA Texture | CA Sphericity | FA Angularity | FA Form2D | |
| Bauxite | --- | --- | --- | 2708.53 | 6.95 | 61.5 |
| | --- | --- | --- | 2708.53 | 6.95 | 60.1 |
| Columbus Grn | 2500.9 | 299.84 | 0.68 | 3143.43 | 6.99 | 42.6 |
| | 2500.9 | 299.84 | 0.68 | 3143.43 | 6.99 | 41 |
| | 2500.9 | 299.84 | 0.68 | 3143.43 | 6.99 | 40.9 |
| | 2500.9 | 299.84 | 0.68 | 3143.43 | 6.99 | 40.7 |
| | 2500.9 | 299.84 | 0.68 | 3143.43 | 6.99 | 40.3 |
| | 2500.9 | 299.84 | 0.68 | 3143.43 | 6.99 | 39.8 |
| | 2500.9 | 299.84 | 0.68 | 3143.43 | 6.99 | 39.5 |
| | 2500.9 | 299.84 | 0.68 | 3143.43 | 6.99 | 39.5 |
| LaGrange Grn | 2268.3 | 152.84 | 0.69 | 3127.73 | 6.84 | 39.4 |
| | 2268.3 | 152.84 | 0.69 | 3127.73 | 6.84 | 38.1 |
| | 2268.3 | 152.84 | 0.69 | 3127.73 | 6.84 | 42.4 |
| Calera Lms | 2141.6 | 158.96 | 0.66 | 2472.07 | 6.81 | 17.9 |

**Table 6.9: Pearson Correlation Coefficients for AIMS-II indexes and field friction (including bauxite)**

| **Parameter** | CA Angularity | CA Texture | CA Sphericity | FA Angularity | FA Form2D | SN40R |
|---|---|---|---|---|---|---|
| CA Angularity | 1 | | | | | |
| CA Texture | 0.963 | 1 | | | | |
| CA Sphericity | 0.093 | -0.177 | 1 | | | |
| FA Angularity | 0.664 | 0.439 | 0.806 | 1 | | |
| FA Form2D | 0.989 | 0.992 | -0.055 | 0.394 | 1 | |
| SN40R | **0.654** | 0.434 | **0.790** | -0.019 | 0.373 | 1 |

The Pearson Correlation showed relatively good correlations for coarse aggregate angularity and coarse aggregate sphericity with field friction. The correlation between fine aggregate angularity and field friction was thought to be lower because of the bauxite. Therefore, bauxite was excluded from the data, and a second Pearson Correlation was run (Table 6.10).

**Table 6.10: Pearson Correlation Coefficients for AIMS-II indexes and field friction (excluding bauxite)**

| **Parameter** | CA Angularity | CA Texture | CA Sphericity | FA Angularity | FA Form2D | SN40R |
|---|---|---|---|---|---|---|
| CA Angularity | 1 | | | | | |
| CA Texture | 0.963 | 1 | | | | |
| CA Sphericity | 0.093 | -0.177 | 1 | | | |
| FA Angularity | 0.664 | 0.439 | 0.806 | 1 | | |
| FA Form2D | 0.989 | 0.992 | -0.055 | 0.546 | 1 | |
| SN40R | **0.654** | 0.434 | **0.790** | **0.982** | 0.538 | 1 |

As expected, the r-value in Table 6.10 increased to 0.982, indicating a near perfect correlation between fine aggregate angularity and field friction. Additionally, after separating out the SN40R from each section, the Pearson Correlation showed lower r-values for the relationship between form2D and field friction. The adjusted r-value indicated a weak correlation between form2D and field friction.

Minitab was used to generate two different general linear models (GLM). Minitab requires a consistent amount of data for all parameters, so the bauxite was excluded in the analyses. The first GLM included all the parameters shown in Table 6.8. The second included just those parameters that exhibited a relatively good r-value with field friction from Table 6.10 (coarse aggregate angularity, coarse aggregate sphericity, and fine aggregate angularity). Minitab removed all the parameters except coarse aggregate angularity from each of the two analyses. These results are shown in the Appendices.

Minitab found there was no reasonable linear correlation for the data in consideration. Therefore, a series of statistical analyses were run through DataFit to determine which model could be fitted to the parameters. All analyses used the data presented in Table 6.8. Bauxite was excluded from the analyses because there were no coarse aggregate sizes of bauxite that were tested, and the

software program requires an even amount of data for each variable. DataFit allows the user to select the type of regression analysis to run. For the purpose of these analyses, all models were selected to assess the best fit model, according to DataFit. The statistical analyses will be summarized in the following tables of this chapter. Detailed result summaries of the DataFit analyses are shown in the Appendices.

Initially, all five parameters were included in the DataFit analysis. Equation 6.1 shows the model that resulted in the highest $R^2$ value. Table 6.11 shows the coefficients that were estimated for each parameter and the corresponding statistics.

$$SN40R = a * CAA + b * CAT + c * CAS + d * FAA + e * FAF2 \quad Equation\ 6.1$$

Where:

*a*, *b*, *c*, *d*, and *e*: Regression coefficients (Table 6.11)

*CAA*: Coarse aggregate angularity

*CAT*: Coarse aggregate texture

*CAS*: Coarse aggregate sphericity

*FAA*: Fine aggregate angularity

*FAF2*: Fine aggregate form2D

**Table 6.11: Summary of DataFit statistics corresponding to Equation 6.1**

| Variable | Value | Standard Error | t-ratio | Prob(t) | $R^2$ | $R_{adj}^2$ |
|---|---|---|---|---|---|---|
| a | 1.04E+12 | 1683.26 | 615403986.30 | 0.0 | 0.964 | 0.944 |
| b | -1.51E+12 | 16914.39 | -88999331.60 | 0.0 | | |
| c | -6.99E+14 | 27986345.74 | -24984423.67 | 0.0 | | |
| d | -1.75E+11 | 2863.03 | -61103630.39 | 0.0 | | |
| e | -1.59E+14 | 4019583.71 | -39644491.47 | 0.0 | | |

The results show estimated coefficients that are very high and indicate all parameters are significant, and the model explains approximately 94% of the variability within the data, as noted by the adjusted $R^2$. Although the model showed a relatively high $R^2$ value (Table 6.11), the model indicates a negative relationship between all AIMS-II indexes and field friction, with the exception of coarse aggregate angularity. This is noted by the negative values that were estimated for each coefficient shown in Equation 6.1, with the exception of coefficient *a*. As mentioned previously, a decrease in texture should result in a decrease in field friction, which is not represented by the model.

A second analysis was carried out in DataFit. This analysis considered only those parameters that showed a relatively good Pearson Correlation with field friction from Table 6.10, including coarse aggregate angularity, coarse aggregate sphericity, and fine aggregate angularity. Additionally, the interactions between those variables that showed strong correlations were considered by multiplying the variables together. This included the interaction between coarse aggregate angularity and fine aggregate angularity as well as coarse aggregate sphericity and fine aggregate angularity. The model resulting in the highest $R^2$ is shown in Equation 6.2 with the estimated parameters and corresponding statistics shown in Table 6.12.

$$SN40R = a * CAA + b * CAS + c * FAA + d * CAAFAA + e * CASFAA \quad Equation\ 6.2$$

Where:

*a*, *b*, *c*, *d*, *e*: Regression coefficients (Table 6.12)

*CAAFAA*: Interaction between coarse aggregate angularity and fine aggregate angularity

*CASFAA*: Interaction between coarse aggregate sphericity and fine aggregate angularity

**Table 6.12: Summary of DataFit statistics corresponding to Equation 6.2**

| Variable | Value | Standard Error | t-ratio | Prob(t) | $R^2$ | $R_{adj}^2$ |
|---|---|---|---|---|---|---|
| a | -9.63E+11 | 12044.64 | -79962762.46 | 0.00 | 0.957 | 0.933 |
| b | -1.11E+12 | 35167769.35 | -31463.04 | 0.00 | | |
| c | 3.88E+12 | 3973.02 | 976137953.60 | 0.00 | | |
| d | 8.17E+07 | 3.56 | 22981404.06 | 0.00 | | |
| e | -4.88E+12 | 15777.62 | -309083062.40 | 0.00 | | |

Similar to the previous model, the estimated coefficients are very large, and the table shows each parameter is statistically significant. When taking the adjusted $R^2$ into consideration, approximately 93% of the variability within the data may be explained by the model. The model shows a negative relationship between coarse aggregate angularity and field friction as well as fine aggregate angularity and field friction, as indicated by the estimated negative coefficients *a* and *e*. Similar to the previous model (Equation 6.1), this demonstrates the model is not reasonable for the parameters in consideration.

A third DataFit analysis only included those variable that indicated strong correlations with the field friction data. The best fit model, according to the software program, is shown in Equation 6.3. The estimated coefficients and corresponding statistics are shown in Table 6.13.

$$SN40R = a * CAA + b * CAS + c * FAA \quad Equation\ 6.3$$

Where:

*a*, *b*, *c*: Regression coefficients (Table 6.13)

**Table 6.13: Summary of DataFit statistics corresponding to Equation 6.3**

| Variable | Value | Standard Error | t-ratio | Prob(t) | $R^2$ | $R_{adj}^2$ |
|---|---|---|---|---|---|---|
| a | -0.005 | 3.87E-03 | -1.22 | 0.25 | 0.964 | 0.957 |
| b | -105.042 | 1.25E+01 | -8.39 | 0.00 | | |
| c | 0.039 | 3.15E-03 | 12.49 | 0.00 | | |

Table 6.13 shows estimated coefficients that are more reasonable than the previous models. The results from Table 6.13 also indicate coarse aggregate angularity is not a statistically significant parameter within the model. Therefore, coarse aggregate angularity was removed from the model, and a fourth analysis was run in DataFit. Equation 6.4 shows the adjusted regression model after removing coarse aggregate angularity. This left the model with two parameters, coarse aggregate sphericity and fine aggregate angularity. The estimated coefficients and corresponding statistics are shown in Table 6.14.

$$SN40R = a + b * CAS + c * FAA \quad Equation\ 6.4$$

Where:

*a*, *b*, *c*: Regression coefficients (Table 6.14)

**Table 6.14: Summary of DataFit statistics corresponding to Equation 6.4**

| Variable | Value | Standard Error | t-ratio | Prob(t) | $R^2$ | $R_{adj}^2$ |
|---|---|---|---|---|---|---|
| a | -63.13 | 51.72 | -1.22 | 0.25 | 0.964 | 0.957 |
| b | -3.96 | 88.65 | -0.04 | 0.97 | | |
| c | 0.03 | 0.00 | 9.28 | 0.00 | | |

Table 6.14 shows the only variable to be significant is *c*, which is tied to fine aggregate angularity. Therefore, coarse aggregate sphericity was removed, and a fifth analysis was run through DataFit to only consider fine aggregate angularity. Bauxite was included for this analysis

because there were no coarse aggregate parameters in consideration. Removing the bauxite would be inappropriate. The analysis resulted in a cubic function shown in Equation 6.5 with the results summarized in Table 6.15. The table shows all variables in the equation to be statistically significant at a 5% level. With this model, approximately all of the variability within the data can be explained, as indicated by the adjusted $R^2$.

$$SN40R = a * FAA^3 + b * FAA^2 + c * FAA + d \quad Equation\ 6.5$$

Where:

*a*, *b*, *c*, and d: Regression coefficients (Table 6.15)

**Table 6.15: Summary of DataFit statistics corresponding to Equation 6.5**

| Variable | Value | Standard Error | t-ratio | Prob(t) | $R^2$ | $R_{adj}^2$ |
|---|---|---|---|---|---|---|
| a | 0.00 | 0.00 | 3.92 | 0.00 | 0.986 | 0.982 |
| b | -0.01 | 0.00 | -4.11 | 0.00 | | |
| c | 20.78 | 4.81 | 4.32 | 0.00 | | |
| d | -19959.38 | 4412.04 | -4.52 | 0.00 | | |

The $R^2$ shown in Table 6.15 indicates the model (Equation 6.5) explained almost 100% of the variability within the data in consideration. However, a high $R^2$ does not indicate the model makes sense from a practical standpoint. Therefore, the logic behind Equation 6.5 was tested by selecting a reasonable range of fine aggregate angularity indexes that were not indexes that resulted from this research study. The AIMS-II fine aggregate angularity index can range from 0 to 10,000. For testing this model, a range similar to the aggregates in this study was used. Therefore, fine aggregate angularity indexes ranging from 2,000 to 3,500 were selected to calculate the predicted SN40R using Equation 6.5 (Figure 6.11). The figure shows that given a fine aggregate particle characterized by an AIMS-II fine aggregate angularity index of 2,000, the

resulting SN40R is predicted to be approximately -500 based on the DataFit model (Equation 6.5). Additionally, the model shows the predicted SN40R would be approximately 200 for a fine aggregate particle characterized by an AIMS-II angularity index of 3,500. It is reasonable for the AIMS-II fine aggregate angularity index to reach a value of 2,000 or 3,500. However, the model results in negative field friction values as well as values in the hundreds, both of which are impossible values for the measured SN40R. This demonstrates using the predictive model would not be logical, despite having a very high $R^2$ value. This was attributed to the small range of AIMS-II data presented in this research study. The AIMS-II indexes that resulted from the particles tested in this research study cover a small percentage of the overall range of AIMS-II indexes aggregate are capable of yielding.

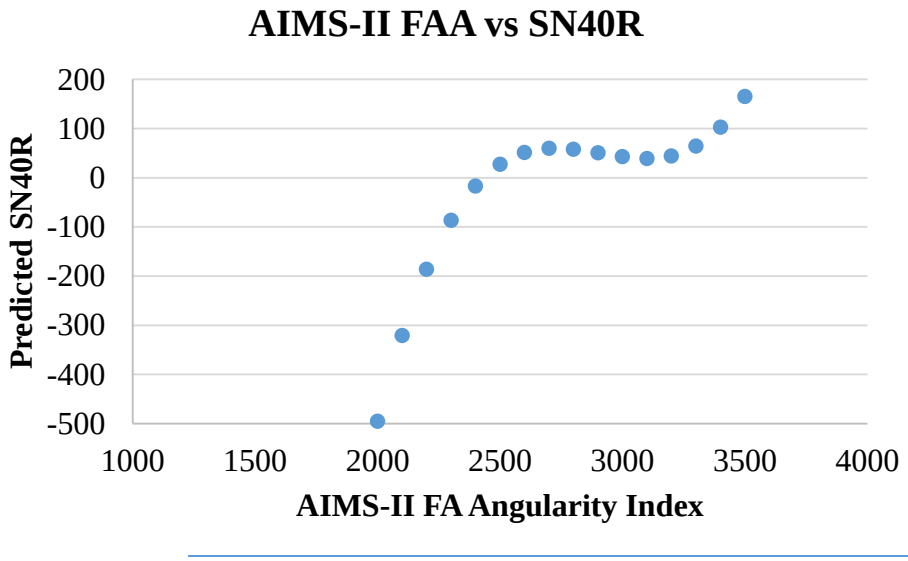


**Figure 6.11: Predicted SN40R (Equation 6.5) from a reasonable range of AIMS-II fine aggregate angularity indexes**

The statistical evaluation of the data was carried out to establish a correlation between the AIMS-II aggregate indexes and field friction. The analysis found no reasonable correlation and supports the findings of the previous evaluation using the rankings.

### 6.6 Summary of Comparison Results

The AIMS-II coarse aggregate angularity and the AIMS-II fine aggregate angularity test methods were capable of recognizing the Calera limestone to be a poor aggregate for use in a surface mix, as it ranked the lowest for both categories. Similarly, the mix made up of primarily Calera limestone ranked last as well and performed very poorly in the field in regards to field friction performance. The results also suggest that a possible correlation could be established between AIMS-II fine aggregate angularity and the SN40R when analyzing it by aggregate type. However, this cannot be confirmed with the results obtained from this research study. Fine aggregate was not the predominant aggregate size in the mix design, and the data was limited to these aggregate sources selected for this study. It could be noted that a comparison cannot be made between the AIMS-II fine aggregate angularity of the #16 bauxite and the SN40R from the HFST bauxite in the field. The lab results revealed bauxite to consistently have the lowest AIMS-II fine aggregate angularity, whereas the surface treatment in the field yielded the best friction performance.

When comparing the AIMS-II coarse aggregate texture results with the friction measurements obtained from the SN40R in the field, the two measurements ranked differently. The AIMS-II revealed the Columbus granite to exhibit significantly higher indexes than the other aggregates. However, the field results showed the LaGrange granite mix measured higher friction performance, whereas in the lab, the #4 LaGrange AIMS-II texture index was more comparable

to the Calera limestone. This was not expected because the Calera limestone was the dominant aggregate used in a poor performing mix from a friction standpoint.

The AIMS-II coarse aggregate angularity, coarse aggregate texture, and fine aggregate angularity indexes could not be correlated with the field SN40R results. These results only reflect the findings of this research study. Additional research is needed to confirm these results and identify another method to establish a relationship between AIMS-II indexes and SN40R.

The ranking between the coarse aggregate mass loss, fine aggregate mass loss, and SN40R were not consistent between all aggregates with the exception of the HFST bauxite SN40R and the fine aggregate bauxite mass loss. A correlation between the Micro-Deval mass loss and field SN40R could not be analyzed. The lab results showed the cumulative mass loss for coarse and fine aggregates did not reach a terminal value and showed no indication of when that value could be reached.

The statistical analysis carried out for this research study included all AIMS-II parameters, with the exception of flat and elongated ratios. Although, all of the models yielded relatively good $R^2$ values, they were not reasonable models for use in predicting the SN40R from AIMS-II parameters. This further supports that there was no reasonable correlation between the AIMS-II indexes and field friction.

# CHAPTER 7: CONCLUSION AND RECOMMENDATIONS

The use of the AIMS-II device in conjunction with the Micro-Deval aggregate conditioning test was evaluated to determine if a correlation with the locked-wheel skid trailer's SN40R could be established. Based on the results, the following conclusions and recommendations were made:

- The AIMS-II coarse aggregate angularity and the AIMS-II fine aggregate angularity decreased with increased conditioning, indicating the AIMS-II device is capable of detecting changes in coarse and fine aggregate angularity when subjected to polishing in the Micro-Deval. The coarse aggregate conditioning time for evaluating friction should be extended beyond 100 minutes to ensure terminal values are reached. Similarly, the AIMS-II fine aggregate angularity failed to reach terminal values after 30 minutes of Micro-Deval conditioning, which is more than twice the amount of conditioning stated in ASTM D7428. Future friction research should consider conditioning fine aggregate particles for more than 30 minutes in the Micro-Deval.
- The AIMS-II device was capable of delineating between aggregate types when analyzing the AIMS-II coarse aggregate angularity indexes after conditioning. As expected, the two granite sources (Columbus and LaGrange granite) retained higher AIMS-II coarse aggregate angularity than the two limestone sources (Opelika and Calera limestone). However, the AIMS-II fine aggregate angularity showed no clear delineation between aggregate types. The Opelika limestone exhibited the highest AIMS-II fine aggregate angularity, whereas the Calera limestone exhibited the lowest. The bauxite, which was used in the field as a high friction surface treatment, yielded the second lowest AIMS-II fine aggregate angularity indexes after conditioning.

- When comparing the AIMS-II coarse aggregate angularity with the field friction data, the results showed similar decreasing trends of the AIMS-II coarse aggregate angularity index with a decrease in the SN40R of the mixture in the field. However, a good correlation between the AIMS-II coarse aggregate angularity and the field SN40R could not be established. Similarly, the results showed an increase in the AIMS-II fine aggregate angularity with an increase in the SN40R, but a good correlation was not established between the two. The high friction surface treatment composed of bauxite in the field yielded good friction performance, whereas in the lab, the #16 bauxite resulted in lower AIMS-II fine aggregate angularity than expected. Therefore, the AIMS-II device is not a good tool for comparing aggregate AIMS-II indexes to high friction surface treatments used in the field due to the nature of the surface in the field.
- The AIMS-II coarse aggregate texture decreased with increased Micro-Deval conditioning, confirming the AIMS-II device was capable of quantifying changes in aggregate texture when subjected to polishing in the Micro-Deval. Micro-Deval conditioning of 100 minutes selected for this research study appeared to be a sufficient amount of time for the AIMS-II coarse aggregate texture to reach a terminal value. However, to achieve terminal texture values, the conditioning time could be extended beyond 100 minutes to confirm terminal conditions are reached.
- The ranking of the aggregates according to the AIMS-II coarse aggregate texture remained consistent throughout each conditioning cycle. The Columbus granite yielded the highest AIMS-II coarse aggregate texture index, whereas the Opelika limestone yielded the lowest. It was expected that the limestone aggregates would yield lower indexes, as they tend to polish faster in the field. However, the Calera limestone ranked

the second highest in the lab but performed poorly in the field in regards to friction performance.

- Although the AIMS-II coarse aggregate texture showed a decreasing trend with decreased field SN40R, there was no correlation between the two. The LaGrange granite measured the best field friction, other than the high friction surface treatment bauxite. However, it exhibited the lowest AIMS-II coarse aggregate texture indexes of the aggregates that were dominant in the field mixes; this excluded the Opelika limestone.
- Micro-Deval mass loss did not reach a terminal value during testing for both coarse and fine aggregates. Therefore, a correlation with the field SN40R could not be assessed. The #16 bauxite yielded the least amount of mass loss compared to the other #16 aggregates, which agreed with the SN40R ranking of the high friction surface treatment bauxite in the field.
- A series of statistical analyses run through DataFit resulted in models that consistently yielded high $R^2$ values. However, the models revealed some discrepancies that proved the regression equation was not a reasonable fit to the data. The statistical analysis suggested fine aggregate angularity to be the primary influence for predicting the SN40R. However, the model was not logical and predicted SN40R values that were outside the possible range of measured values for SN40R. The statistical analysis confirmed that a reasonable correlation between the AIMS-II indexes and field friction could not be established. This was attributed to the data being limited to only three different aggregate sources for comparison. Future friction research should include more than three different aggregate sources to establish a possible correlation between AIMS-II indexes and field friction.

- The AIMS-II in conjunction with the Micro-Deval was unsuccessful in providing a good correlation to field friction results. Only three aggregate sources were available for establishing a correlation between AIMS-II lab results and field friction. Future friction research should consider testing more aggregate sources than three. Additionally, only two sizes of particles were tested in the lab study, and field friction performance is dependent on more than just the contribution of a single sized particle. The AIMS-II device is capable of measuring the surface of a pavement core less than 35 mm thick. It is recommended that a research study evaluate the capability of using the AIMS-II device to measure surface properties of a pavement core and correlating it with the SN40R of the pavement mixture in the field. Using the AIMS-II device to analyze single sized particles was a useful first step toward determining if the AIMS-II and Micro-Deval could be used as a laboratory test method for identifying friction aggregate. Additional research is needed to develop a stronger relationship between the lab aggregate properties and field friction data.

## REFERENCES


Al-Rousan, T., Masad, E., Tutumluer, E., & Pan, T. (2007). Evaluation of Image Analysis Techniques for Quantifying Aggregate Shape Characteristics. Science Direct, 21(Construction and Building Materials), 978-990. Retrieved from http://www.sciencedirect.com

American Association of State Highway Transportation Officials (AASHTO) (2010). AASHTO TP81-10: Standard Method of Test for Determining Aggregate Shape Properties by Means of Digital Analysis. *AASHTO,* Washington, D.C.

American Society for Testing and Materials (ASTM) (2000). ASTM D3319-00: Standard Practice for Accelerated Polishing of Aggregates Using the British Wheel. *ASTM International,* West Conshohocken, PA.

American Society for Testing and Materials (ASTM) (2010). ASTM D6928-10: Standard Test Method for Resistance of Coarse Aggregate to Degradation by Abrasion in the Micro-Deval Apparatus. *ASTM International,* West Conshohocken, PA.

American Society for Testing and Materials (ASTM) (2015). ASTM D7428-15: Standard Test Method for Resistance of Fine Aggregate Degradation by Abrasion in the Micro-Deval Apparatus. *ASTM International,* West Conshohocken, PA.

American Society for Testing and Materials (ASTM) (2013). ASTM E303-13: Standard Test Method for Measuring Surface Frictional Properties Using the British Pendulum Tester. *ASTM International,* West Conshohocken, PA.

American Society for Testing and Materials (ASTM) (2009). ASTM E1911-09: Standard Test Method for Measuring Paved Surface Frictional Properties Using the Dynamic Friction Tester. *ASTM International,* West Conshohocken, PA.

Brown, E., Cooley Jr., L., Hanson, D., Lynn, C., Powell, B., Prowell, B., & Watson, D. (2012). NCAT Test Track Design, Construction, and Performance. NCAT Report 02-12, pg. 43, National Center for Asphalt Technology, Auburn University, AL.

Brzezicki, J. M., & Kasperkiewicz, J. (1999, April). Automatic Image Analysis in Evaluation of Aggregate Shape. Journal of Computing in Civil Engineering, 13(2), 123-128. Retrieved from http://www.ascelibrary.org

Choubane, B., Holzschuber, C., & Gokhale, S. (2006). Precision of Smooth and Ribbed Tire Locked Wheel Testers for Measurement of Roadway Surface Friction Characteristics. Report No. FL/DOT/SMO/06-483. Florida Department of Transportation.

*Circular Texture Meter*. (2015). Retrieved from Applied Pavement Technology: http://www.appliedpavement.com/ct-meter.html

Cooley, L. A., Huner, M. S., & James, R. H. (2002). Micro-Deval Testing of Aggregates in the Southeast. NCAT Report 02-09, National Center for Asphalt Technology, Auburn University, AL.

Devore, J. (2012). *Probability and Statistics for Engineering and the Sciences* (Eighth ed.). Boston, MA: Brooks/Cole Cengage Learning.

*EDC 2012 Initiatives: High Friction Surface Treatment*. (2012). Retrieved from Federal Highway Administration: http://www.fhwa.dot.gov/everydaycounts/edctwo/2012/friction.cfm

Erukulla, S. (2011). Refining Laboratory Procedure to Characterize Change in Hot-Mix Asphalt Surface Friction. Master's Thesis, Auburn University, National Center for Asphalt Technology, Auburn University, AL.

Gates, L., Masad, E., Pyle, R., & Bushee, D. (2011). Aggregate Imaging Measurement System 2 (AIMS2): Final Report. Federal Highway Administration (FHWA), Pine Instrument Company, Washington, D.C.

Gudimettla, J., Myers, L. A., & Paugh, C. (2008). AIMS: The Future in Rapid, Automated Aggregate Shape and Texture Measurement. Federal Highway Administration, Washington, D.C.

Hall, J. W., Smith, K. L., Titus-Glover, L., Wambold, J. C., Yager, T. J., & Rado, Z. (2009). Guide for Pavement Friction. Final Report for Project 01-43, National Cooperative Highway Research Program (NCHRP), Transportation Research Board, Washington, D.C.

Henry, J. J., Abe, H., Kameyama, S., Tamai, A., Kasahara, A., & Saito, K. (2000). Determination of the International Friction Index (IFI) Using the Circular Texture Meter (CTM) and the Dynamic Friction Tester (DFT). Publication No. 109.01.06.B-2000. Permanent International Association of Road Congresses (PIARC). Nantes, France.

Johnson, R. & Kuby, P. (2000). *Elementary Statistics* (Eighth ed.). Pacific Grova, CA: Brooks/Cole Cengage Learning.

Kandhal, P. S., & Parker, F. (1998). Aggregate Tests Related to Asphalt Concrete Performance in Pavements. NCHRP Report 405, National Cooperative Highway Research Program (NCHRP), National Center for Asphalt Technology. Washington, DC: Transportation Research Board.

Kandhal, P. S., Motter, J. B., & Khatri, M. A. (1991). Evaluation of Particle Shape and Texture: Manufactured Versus Natural Sands. NCAT Report 91-03, National Center for Asphalt Technology, Auburn University, AL.

Kowalski, K. J., McDaniel, R. S., & Olek, J. (2010). Identification of Laboratory Techniques to Optimize Superpave HMA Surface Friction Characteristics. Final Report IHRB TR-450, Iowa Highway Research Board. Purdue University, IN.

*Kolmogrov-Smirnov Test*. (2015). Retrieved from Tools for Science: http://www.physics.csbsju.edu/stats/KS-test.html

Little, D., Button, J., Jayawickrama, P., Solaimanian, M., & Hudson, B. (2003). Quantify Shape, Angularity, and Surface Texture of Aggregates using Image Analysis and study their Effect on Performance (FHWA/TX-06/0-1707-4). Technical Report, Federal Highway Administration (FHWA), Texas Transportation Institute (TTI).

*Los Angeles Abrasion*. (2012). Retrieved from Pavement Interactive: http://www.pavementinteractive.org/article/los-angeles-abrasion/

Mahmoud, E., & Ortiz, E. (2014). Implementation of AIMS in Measuring Aggregate Resistance to Polishing, Abrasion, and Breakage (FHWA-ICT-14-014). Federal Highway Administration (FHWA), Illinois Center for Transportation (ICT), University of Illinois at Urbana-Champaign, IL.

Masad, E. (2003). The Development of a Computer Controlled Image Analysis System for Measuring Aggregate Shape Properties. Final Report for Highway-IDEA Project 77, Transportation Research Board, Innovations Deserving Exploratory Analysis Programs (IDEA), Washington, D.C.

Masad, E., Al-Rousan, T., Button, J., Little, D., & Tutumluer, E. (2007). Test Methods for Characterizing Aggregate Shape, Texture, and Angularity. NCHRP Report 555, National Cooperative Highway Research Program (NCHRP), Transportation Research Board, University of Illinois at Urbana-Champaign, IL.

Masad, E., Luce, A., & Mahmoud, E. (2006). Implementation of AIMS in Measuring Aggregate Resistance to Polishing, Abrasion, and Breakage. Texas Transportation Institute. Federal Highway Administration.

Masad, E., Luce, A., Mahmoud, E., & Chowdhury, A. (2007). Relationship of Aggregate Texture to Asphalt Pavement Skid Resistance Using Image Analysis of Aggregate Shape (FHWA/TX-06/5-1707-03-1). Final Report for Highway IDEA Project 114, Transportation Research Board, Innovations Deserving Exploratory Analysis Programs (IDEA), Washington, D.C.

Masad, E., Rezaei, A., Chowdhury, A., & Harris, P. (2009). Predicting Asphalt Mixture Skid Resistance Based on Aggregate Characteristics (FHWA/TX-09/0-5627-1). Texas Transportation Institute (TTI). Federal Highway Administration (FHWA).

McGhee, K. K., & Flintsch, G. W. (2003). High-Speed Texture Measurement of Pavements. Report VTRC 03-R9, Virginia Transportation Research Council, Virginia Department of Transportation, Charlottesville, VA.

Moaveni, M., Mahmoud, E., Ortiz, E., Tutumluer, E., & Beshears, S. (2014). Evaluation of Aggregate Resistance to Breakage, Abrasion, and Polishing Using Advanced Aggregate Imaging Systems. Revised Manuscript 14-4580. University of Illinois at Urbana-Champaign. Washington, D.C: Transportation Research Board (TRB).

Orthmeyer, R., Mikhail, M., Watkins, J., Andrews, J., & Chang, G. (2014). Network Level Pavement Friction Testing: Policy and Promising Practices. Transportation Research Board Webinar.

*Pearson's Correlation Coefficient.* (2009). Retrieved from University of Illinois at Urbana-Champaign: http://www.life.illinois.edu/ib/203/Fall%2009/PEARSONS%20CORRELATION%20COEFFICIENT%20TABLE.pdf

Pine Instrument Company (2011). Aggregate Image Measurement System. Grove City. Retrieved from: http://www.pineinst.com

Prowell, B. D., Brown, E. R., & Zhang, J. (2005). Aggregate Properties and the Performance of Superpave-Designed Hot Mix Asphalt. NCHRP Report 539, National Cooperative Higway Research Program (NCHRP), Transportation Research Board, Washington, D.C.

Rogers, C. A., Lane, B. C., & Senior, S. A. (2003). The Micro-Deval Abrasion Test for Coarse and Fine Aggregate in Asphalt Pavement. Ministry of Transportation (MTO), Ontario.

Serigos, P. A., Smit, A., & Prozzi, J. A. (2014). Incorporating Surface Micro-Texture in the Prediction of Skid Resistance of Flexible Pavements. TRB Paper 14-2278. The University of Texas at Austin. Washington, DC: Transportation Research Board.

Turner, P., & Heitzman, M. (2013). Effect of Friction Aggregate on Hot Mix Asphalt Surface Friction. NCAT Report 13-09, National Center for Asphalt Technology, Auburn University, AL.

Vollor, T. W., & Hanson, D. I. (2006). Development of Laboratory Procedure for Measuring Friction of HMA Mixtures- Phase I. NCAT Report 06-06, National Center for Asphalt Technology, Auburn University, AL.

West, R., Timm, D., Willis, R., Powell, B., Tran, N., Watson, D., Sakhaeifar, M., Brown, R., Robbins, M., Vargas-Nordcbeck, A., Villacorta, F. L., Guo, X., & Nelson, J. (2012). Phase IV NCAT Pavement Test Track Findings. NCAT Report 12-10, National Center for Asphalt Technology, Auburn University, AL.

Willis, R., Timm, D., West, R., Powell, B., Robbins, M., Taylor, A., Smit, A., Tran, N., Heitzman, M., & Bianchini, A. (2009) Phase III NCAT Test Track Findings. NCAT Report 09-08, National Center for Asphalt Technology, Auburn University, AL.

Wu, Y., Parker, F., & Kandhal, K. (1998). Aggregate Toughness/ Abrasion Resistance and Durability/ Soundness Tests Related to Asphalt Concrete Performance in Pavements. NCAT Report 98-04, National Center for Asphalt Technology, Auburn University, AL.

Yut, I., Henault, J. W., & Mahoney, J. (2013). Friction Study on LTPP SPS-9A Sections in Connecticut. TRB Paper 14-1649. University of Connecticut. Washington, D.C: Transportation Research Board (TRB).

# APPENDICES

## Appendix A: Minitab Graphical Summaries of AIMS-II Index Distributions after each Micro-Deval Conditioning Interval

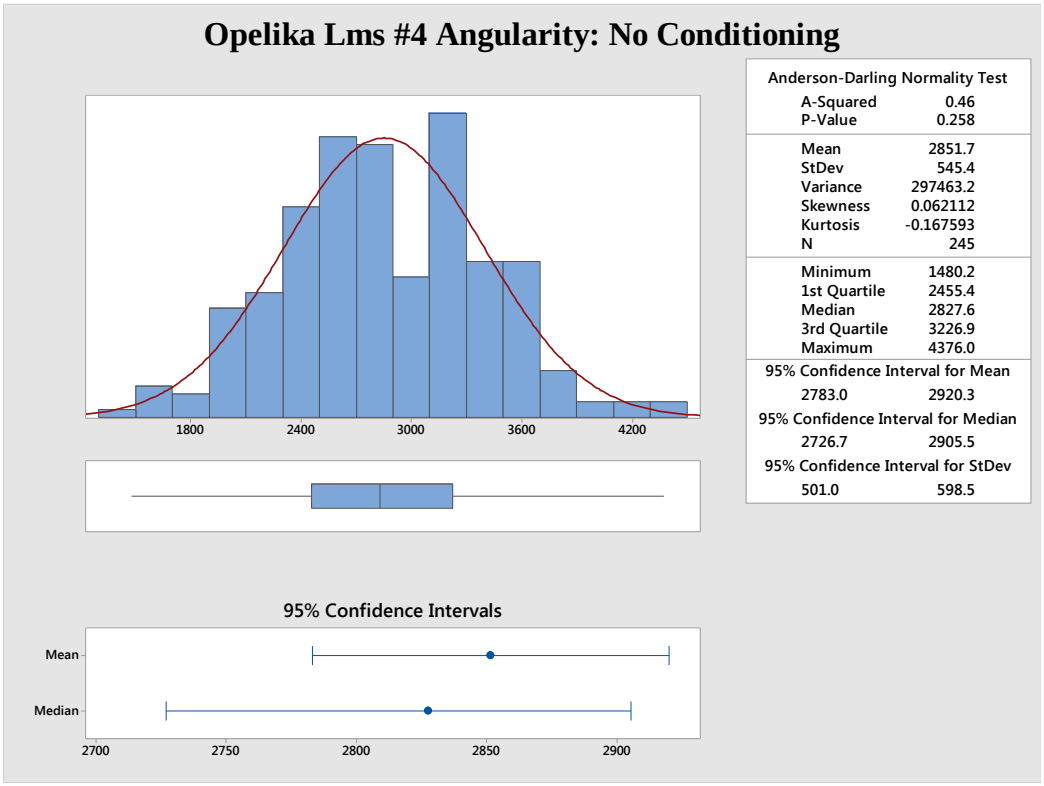


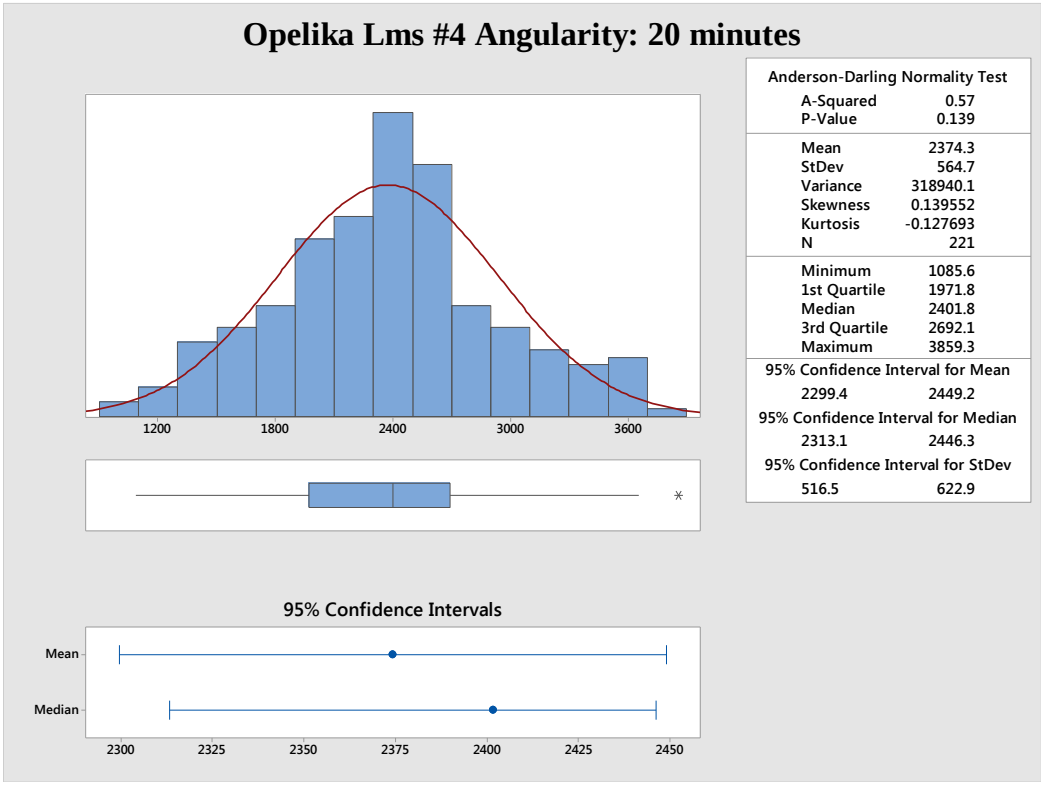

# Opelika Lms #4 Angularity: 40 minutes

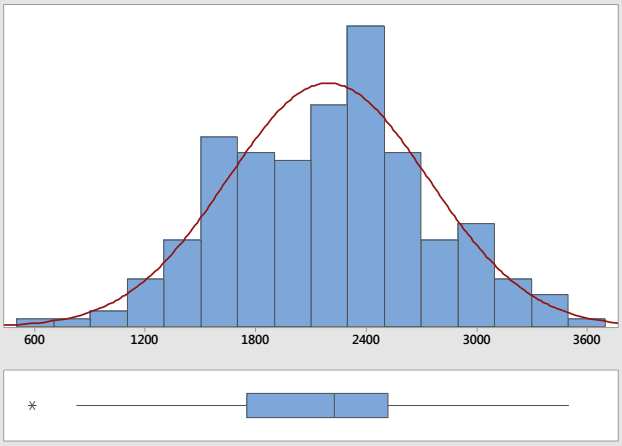




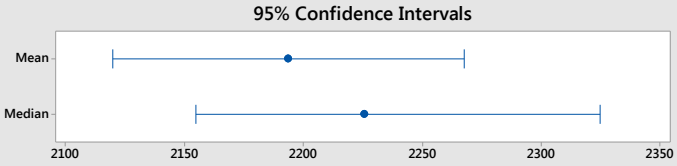


| Anderson-Darling Normality Test | |
|---|---|
| A-Squared | 0.47 |
| P-Value | 0.240 |
| Mean | 2193.6 |
| StDev | 546.4 |
| Variance | 298537.0 |
| Skewness | -0.017524 |
| Kurtosis | -0.218157 |
| N | 211 |
| Minimum | 582.5 |
| 1st Quartile | 1752.6 |
| Median | 2225.7 |
| 3rd Quartile | 2516.9 |
| Maximum | 3502.8 |
| 95% Confidence Interval for Mean | |
| 2119.5 | 2267.8 |
| 95% Confidence Interval for Median | |
| 2154.5 | 2324.8 |
| 95% Confidence Interval for StDev | |
| 498.8 | 604.2 |

# Opelika Lms #4 Angularity: 60 minutes

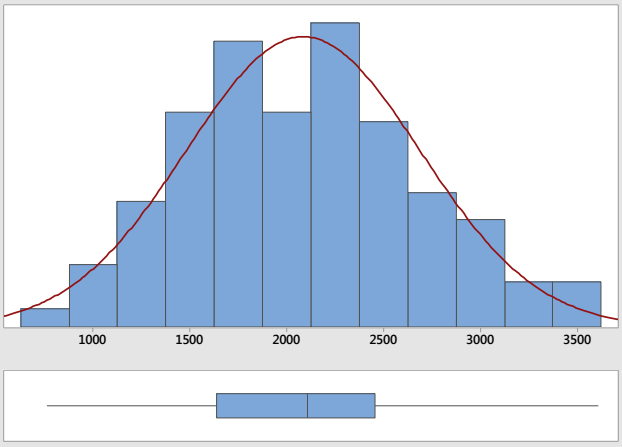




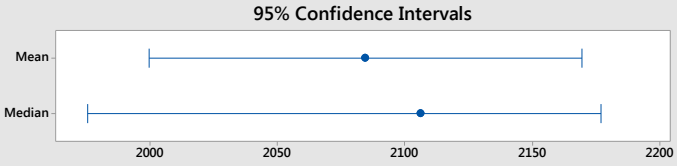


| Anderson-Darling Normality Test | |
|---|---|
| A-Squared | 0.42 |
| P-Value | 0.318 |
| Mean | 2084.5 |
| StDev | 605.2 |
| Variance | 366310.6 |
| Skewness | 0.226150 |
| Kurtosis | -0.305095 |
| N | 197 |
| Minimum | 759.2 |
| 1st Quartile | 1637.0 |
| Median | 2106.5 |
| 3rd Quartile | 2457.9 |
| Maximum | 3611.6 |
| 95% Confidence Interval for Mean | |
| 1999.4 | 2169.5 |
| 95% Confidence Interval for Median | |
| 1975.1 | 2177.0 |
| 95% Confidence Interval for StDev | |
| 550.8 | 671.7 |

## Opelika Lms #4 Angularity: 80 minutes

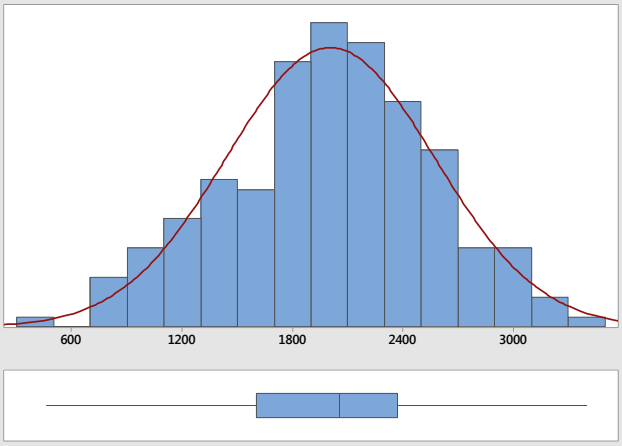




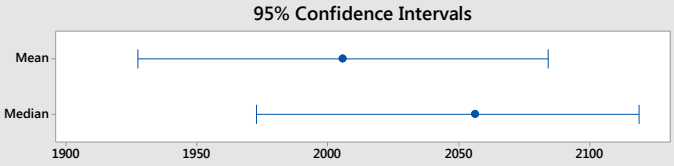


| Anderson-Darling Normality Test | |
|---|---|
| A-Squared | 0.46 |
| P-Value | 0.256 |
| Mean | 2005.8 |
| StDev | 566.6 |
| Variance | 321016.6 |
| Skewness | -0.161542 |
| Kurtosis | -0.276846 |
| N | 202 |
| Minimum | 461.4 |
| 1st Quartile | 1601.6 |
| Median | 2056.5 |
| 3rd Quartile | 2370.6 |
| Maximum | 3399.9 |
| 95% Confidence Interval for Mean | |
| 1927.2 | 2084.4 |
| 95% Confidence Interval for Median | |
| 1972.7 | 2119.2 |
| 95% Confidence Interval for StDev | |
| 516.2 | 628.0 |

## Opelika Lms #4 Angularity: 100 minutes

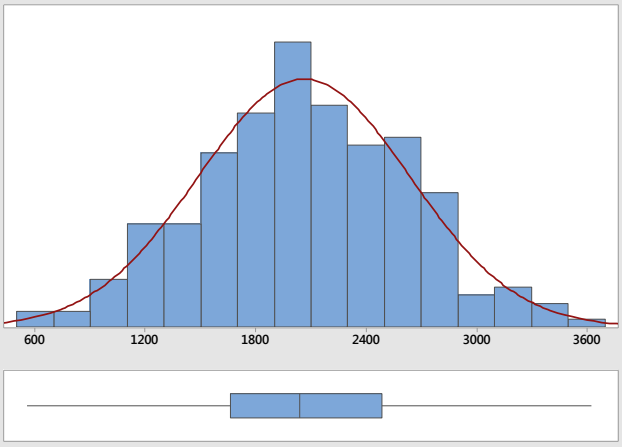




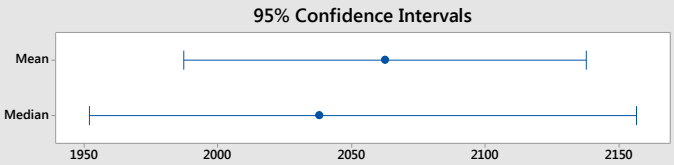


| Anderson-Darling Normality Test | |
|---|---|
| A-Squared | 0.25 |
| P-Value | 0.754 |
| Mean | 2062.6 |
| StDev | 575.5 |
| Variance | 331223.1 |
| Skewness | 0.038925 |
| Kurtosis | -0.225769 |
| N | 226 |
| Minimum | 555.6 |
| 1st Quartile | 1661.3 |
| Median | 2037.9 |
| 3rd Quartile | 2486.1 |
| Maximum | 3623.1 |
| 95% Confidence Interval for Mean | |
| 1987.2 | 2138.0 |
| 95% Confidence Interval for Median | |
| 1951.8 | 2156.7 |
| 95% Confidence Interval for StDev | |
| 526.9 | 634.1 |

## Columbus Grn #4 Angularity: No Conditioning

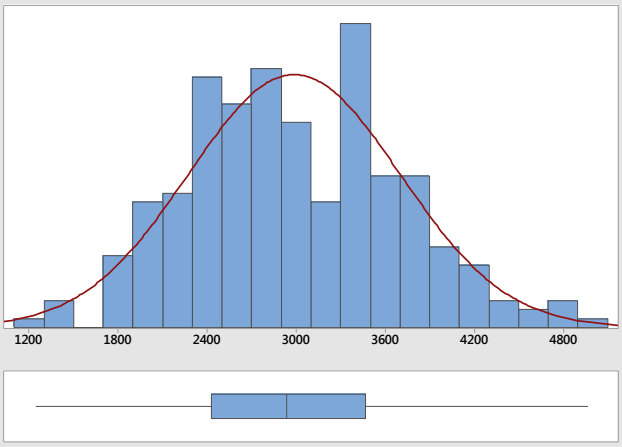




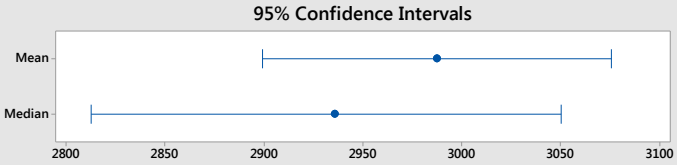


| Anderson-Darling Normality Test | |
|---|---|
| A-Squared | 0.60 |
| P-Value | 0.117 |
| Mean | 2987.6 |
| StDev | 713.3 |
| Variance | 508740.4 |
| Skewness | 0.238898 |
| Kurtosis | -0.211743 |
| N | 253 |
| Minimum | 1245.2 |
| 1st Quartile | 2427.8 |
| Median | 2935.9 |
| 3rd Quartile | 3468.4 |
| Maximum | 4966.1 |
| 95% Confidence Interval for Mean | |
| 2899.2 | 3075.9 |
| 95% Confidence Interval for Median | |
| 2812.3 | 3050.5 |
| 95% Confidence Interval for StDev | |
| 656.1 | 781.5 |

## Columbus Grn #4 Angularity: 20 minutes

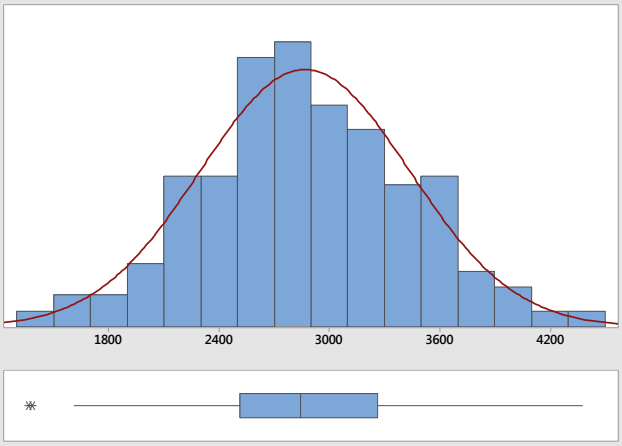




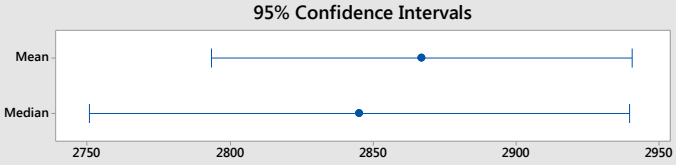


| Anderson-Darling Normality Test | |
|---|---|
| A-Squared | 0.22 |
| P-Value | 0.836 |
| Mean | 2867.0 |
| StDev | 569.5 |
| Variance | 324323.9 |
| Skewness | 0.0316841 |
| Kurtosis | -0.0952321 |
| N | 232 |
| Minimum | 1367.1 |
| 1st Quartile | 2512.2 |
| Median | 2845.3 |
| 3rd Quartile | 3262.6 |
| Maximum | 4380.6 |
| 95% Confidence Interval for Mean | |
| 2793.3 | 2940.7 |
| 95% Confidence Interval for Median | |
| 2750.4 | 2939.7 |
| 95% Confidence Interval for StDev | |
| 522.0 | 626.6 |

# Columbus Grn #4 Angularity: 40 minutes

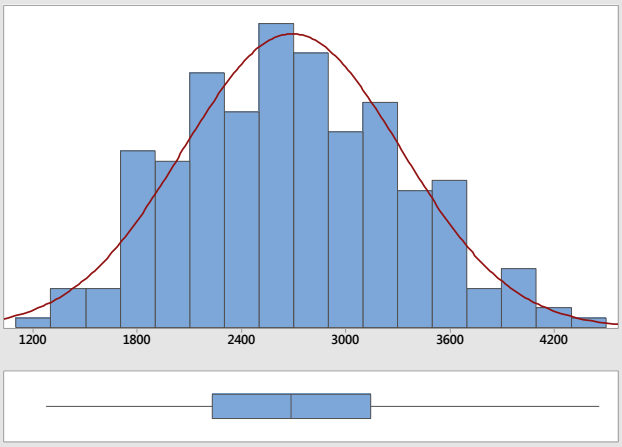




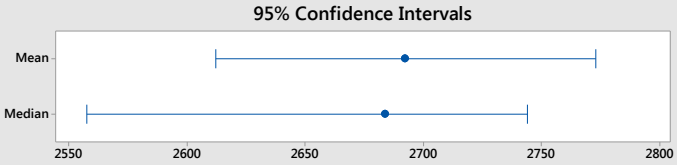


| Anderson-Darling Normality Test | |
|---|---|
| A-Squared | 0.40 |
| P-Value | 0.365 |
| Mean | 2692.4 |
| StDev | 628.7 |
| Variance | 395269.7 |
| Skewness | 0.199795 |
| Kurtosis | -0.436732 |
| N | 236 |
| Minimum | 1272.9 |
| 1st Quartile | 2231.7 |
| Median | 2684.0 |
| 3rd Quartile | 3145.2 |
| Maximum | 4463.7 |
| 95% Confidence Interval for Mean | |
| 2611.8 | 2773.0 |
| 95% Confidence Interval for Median | |
| 2557.4 | 2744.0 |
| 95% Confidence Interval for StDev | |
| 576.6 | 691.2 |

# Columbus Grn #4 Angularity: 60 minutes

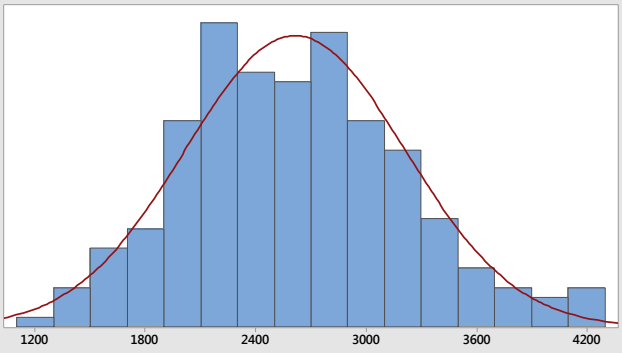


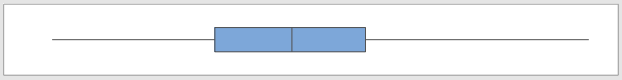

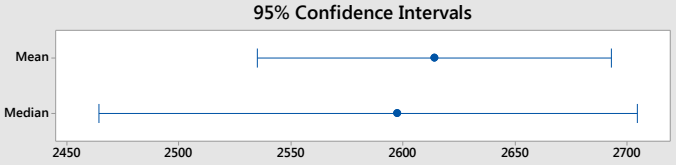


| Anderson-Darling Normality Test | |
|---|---|
| A-Squared | 0.45 |
| P-Value | 0.275 |
| Mean | 2614.1 |
| StDev | 599.0 |
| Variance | 358843.6 |
| Skewness | 0.301977 |
| Kurtosis | -0.142823 |
| N | 223 |
| Minimum | 1294.1 |
| 1st Quartile | 2179.1 |
| Median | 2597.6 |
| 3rd Quartile | 2997.1 |
| Maximum | 4211.5 |
| 95% Confidence Interval for Mean | |
| 2535.1 | 2693.2 |
| 95% Confidence Interval for Median | |
| 2464.3 | 2704.6 |
| 95% Confidence Interval for StDev | |
| 548.1 | 660.5 |

## Columbus Grn #4 Angularity: 80 minutes

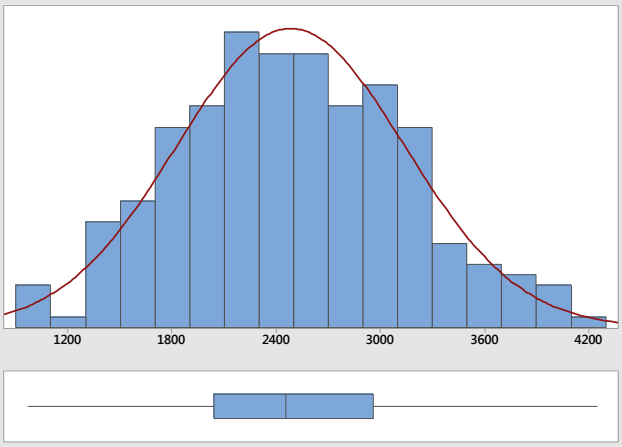




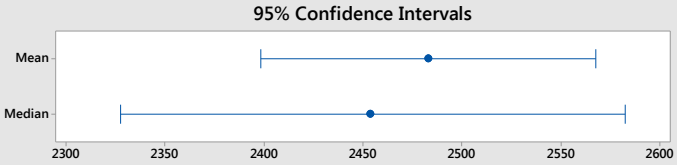


| Anderson-Darling Normality Test | |
|---|---|
| A-Squared | 0.25 |
| P-Value | 0.726 |
| Mean | 2483.2 |
| StDev | 658.5 |
| Variance | 433609.6 |
| Skewness | 0.137821 |
| Kurtosis | -0.303319 |
| N | 234 |
| Minimum | 970.0 |
| 1st Quartile | 2039.9 |
| Median | 2453.8 |
| 3rd Quartile | 2957.9 |
| Maximum | 4252.1 |
| 95% Confidence Interval for Mean | |
| 2398.4 | 2568.0 |
| 95% Confidence Interval for Median | |
| 2327.4 | 2582.9 |
| 95% Confidence Interval for StDev | |
| 603.7 | 724.2 |

## Columbus Grn #4 Angularity: 100 minutes

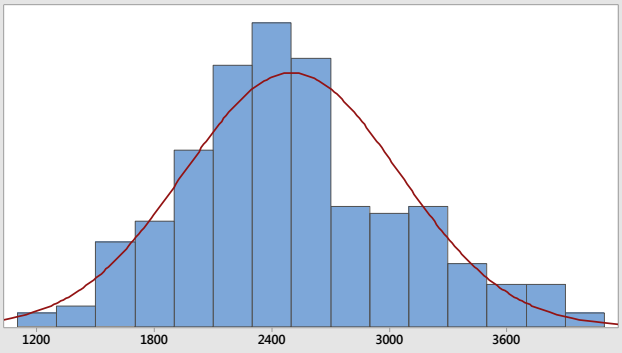


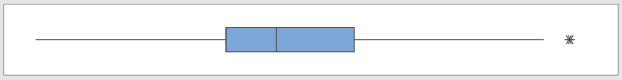

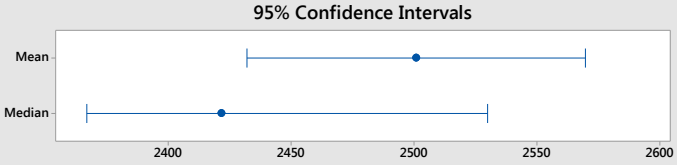


| Anderson-Darling Normality Test | |
|---|---|
| A-Squared | 1.21 |
| P-Value | <0.005 |
| Mean | 2500.9 |
| StDev | 550.7 |
| Variance | 303232.2 |
| Skewness | 0.333047 |
| Kurtosis | -0.138943 |
| N | 248 |
| Minimum | 1191.2 |
| 1st Quartile | 2167.1 |
| Median | 2421.7 |
| 3rd Quartile | 2822.2 |
| Maximum | 3925.6 |
| 95% Confidence Interval for Mean | |
| 2432.1 | 2569.8 |
| 95% Confidence Interval for Median | |
| 2366.5 | 2529.8 |
| 95% Confidence Interval for StDev | |
| 506.1 | 603.9 |

# LaGrange Grn #4 Angularity: No Conditioning

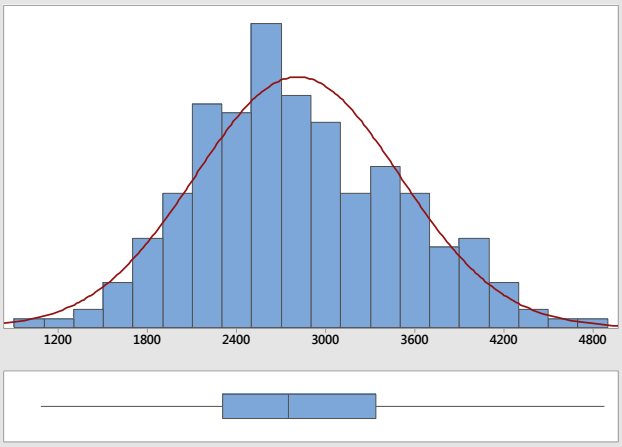




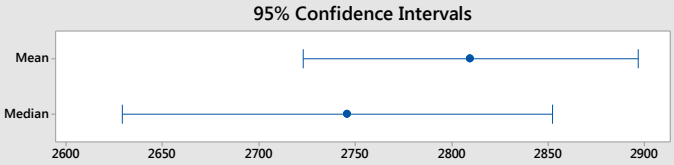


| Anderson-Darling Normality Test | |
|---|---|
| A-Squared | 0.92 |
| P-Value | 0.019 |
| Mean | 2809.9 |
| StDev | 688.6 |
| Variance | 474152.4 |
| Skewness | 0.307875 |
| Kurtosis | -0.202484 |
| N | 242 |
| Minimum | 1080.6 |
| 1st Quartile | 2302.5 |
| Median | 2745.6 |
| 3rd Quartile | 3335.6 |
| Maximum | 4876.6 |
| 95% Confidence Interval for Mean | |
| 2722.7 | 2897.1 |
| 95% Confidence Interval for Median | |
| 2628.7 | 2852.3 |
| 95% Confidence Interval for StDev | |
| 632.2 | 756.1 |

# LaGrange Grn #4 Angularity: 20 minutes

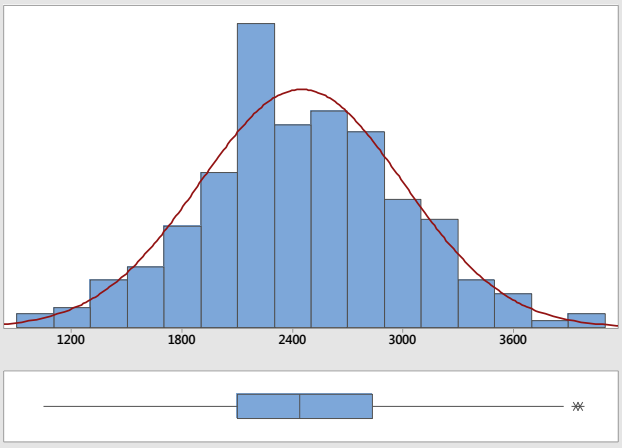




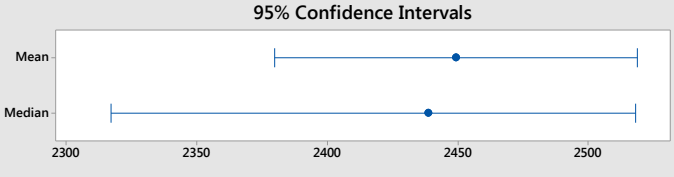


| Anderson-Darling Normality Test | |
|---|---|
| A-Squared | 0.26 |
| P-Value | 0.724 |
| Mean | 2449.4 |
| StDev | 554.3 |
| Variance | 307286.1 |
| Skewness | 0.0722049 |
| Kurtosis | -0.0182018 |
| N | 245 |
| Minimum | 1044.3 |
| 1st Quartile | 2101.9 |
| Median | 2439.0 |
| 3rd Quartile | 2833.8 |
| Maximum | 3964.0 |
| 95% Confidence Interval for Mean | |
| 2379.6 | 2519.1 |
| 95% Confidence Interval for Median | |
| 2316.8 | 2518.3 |
| 95% Confidence Interval for StDev | |
| 509.2 | 608.3 |

# LaGrange Grn #4 Angularity: 40 minutes

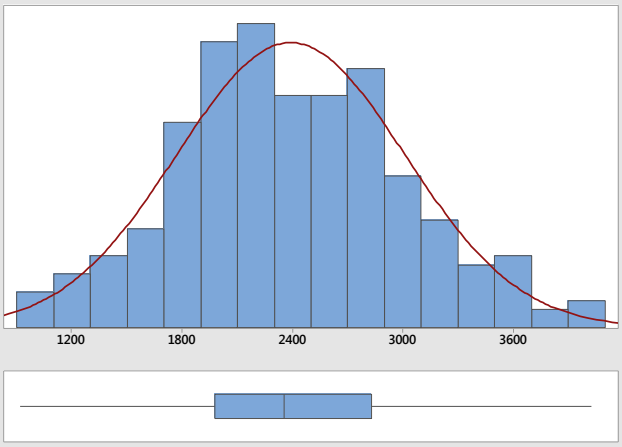




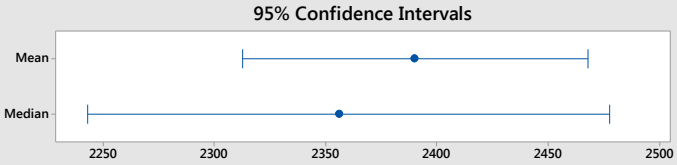


| Anderson-Darling Normality Test | |
|---|---|
| A-Squared | 0.33 |
| P-Value | 0.511 |
| Mean | 2390.3 |
| StDev | 621.1 |
| Variance | 385729.4 |
| Skewness | 0.181293 |
| Kurtosis | -0.187547 |
| N | 248 |
| Minimum | 918.0 |
| 1st Quartile | 1976.9 |
| Median | 2356.1 |
| 3rd Quartile | 2827.6 |
| Maximum | 4027.7 |
| 95% Confidence Interval for Mean | |
| 2312.6 | 2468.0 |
| 95% Confidence Interval for Median | |
| 2242.9 | 2477.7 |
| 95% Confidence Interval for StDev | |
| 570.8 | 681.1 |

# LaGrange Grn #4 Angularity: 60 minutes

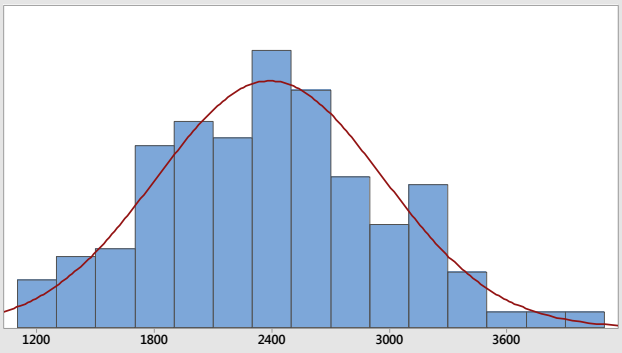


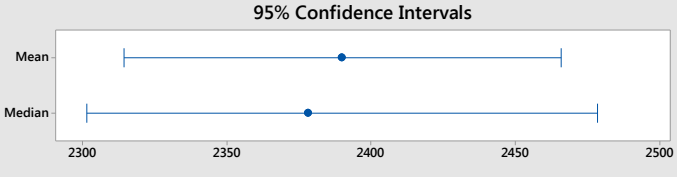


| Anderson-Darling Normality Test | |
|---|---|
| A-Squared | 0.38 |
| P-Value | 0.405 |
| Mean | 2390.0 |
| StDev | 578.8 |
| Variance | 334960.2 |
| Skewness | 0.170939 |
| Kurtosis | -0.334235 |
| N | 226 |
| Minimum | 1138.4 |
| 1st Quartile | 1959.5 |
| Median | 2378.3 |
| 3rd Quartile | 2772.4 |
| Maximum | 3942.6 |
| 95% Confidence Interval for Mean | |
| 2314.1 | 2465.9 |
| 95% Confidence Interval for Median | |
| 2301.5 | 2478.7 |
| 95% Confidence Interval for StDev | |
| 529.9 | 637.7 |

## LaGrange Grn #4 Angularity: 80 minutes

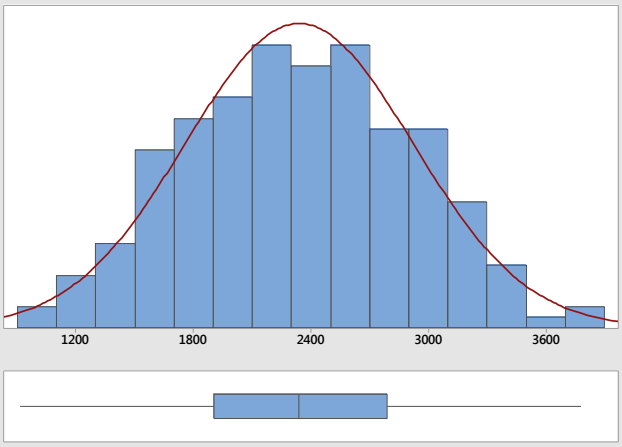




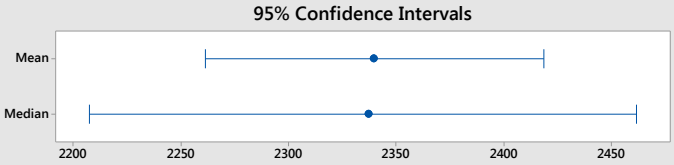


| Anderson-Darling Normality Test | |
|---|---|
| A-Squared | 0.36 |
| P-Value | 0.437 |
| Mean | 2339.9 |
| StDev | 581.7 |
| Variance | 338425.9 |
| Skewness | -0.028416 |
| Kurtosis | -0.531390 |
| N | 212 |
| Minimum | 912.4 |
| 1st Quartile | 1904.4 |
| Median | 2337.4 |
| 3rd Quartile | 2789.1 |
| Maximum | 3780.5 |
| 95% Confidence Interval for Mean | |
| 2261.1 | 2418.6 |
| 95% Confidence Interval for Median | |
| 2207.3 | 2461.8 |
| 95% Confidence Interval for StDev | |
| 531.1 | 643.1 |

## LaGrange Grn #4 Angularity: 100 minutes

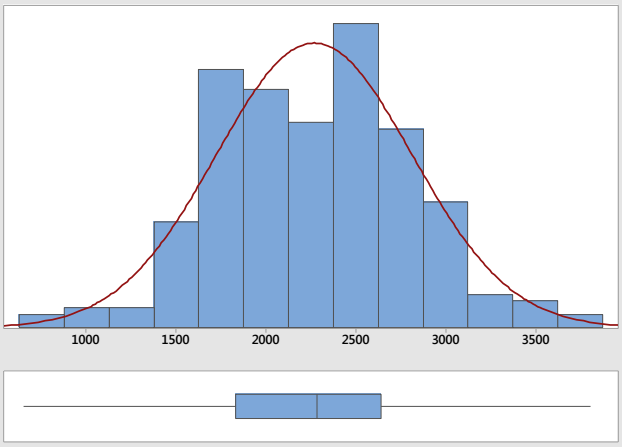




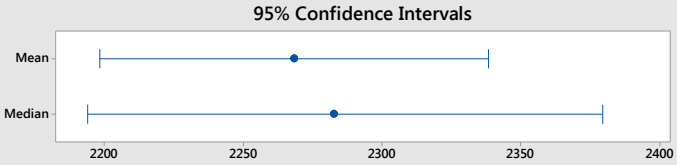


| Anderson-Darling Normality Test | |
|---|---|
| A-Squared | 0.48 |
| P-Value | 0.233 |
| Mean | 2268.3 |
| StDev | 546.6 |
| Variance | 298742.3 |
| Skewness | 0.080489 |
| Kurtosis | 0.101806 |
| N | 236 |
| Minimum | 649.4 |
| 1st Quartile | 1831.9 |
| Median | 2282.7 |
| 3rd Quartile | 2642.7 |
| Maximum | 3807.7 |
| 95% Confidence Interval for Mean | |
| 2198.2 | 2338.4 |
| 95% Confidence Interval for Median | |
| 2193.7 | 2379.8 |
| 95% Confidence Interval for StDev | |
| 501.3 | 600.9 |

## Calera Lms #4 Angularity: No Conditioning

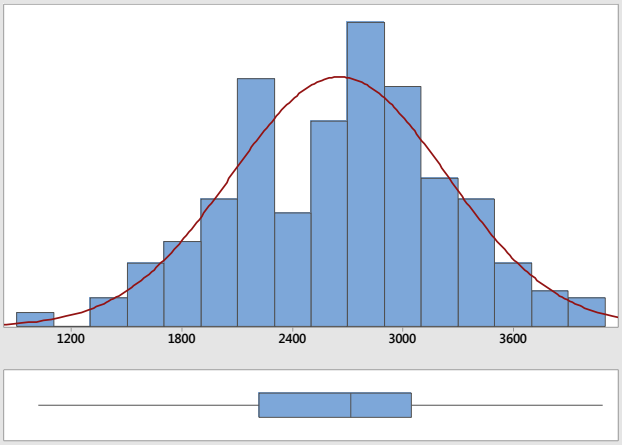




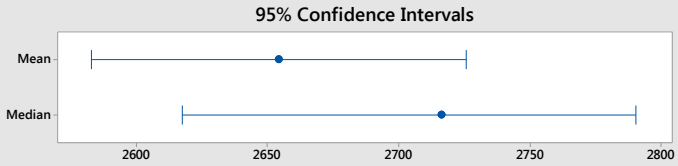


| Anderson-Darling Normality Test | |
|---|---|
| A-Squared | 0.45 |
| P-Value | 0.275 |
| Mean | 2654.2 |
| StDev | 585.7 |
| Variance | 343085.1 |
| Skewness | -0.138179 |
| Kurtosis | -0.252410 |
| N | 259 |
| Minimum | 1017.9 |
| 1st Quartile | 2216.2 |
| Median | 2716.6 |
| 3rd Quartile | 3046.9 |
| Maximum | 4086.6 |
| 95% Confidence Interval for Mean | |
| 2582.6 | 2725.9 |
| 95% Confidence Interval for Median | |
| 2617.4 | 2790.6 |
| 95% Confidence Interval for StDev | |
| 539.3 | 641.0 |

## Calera Lms #4 Angularity: 20 minutes

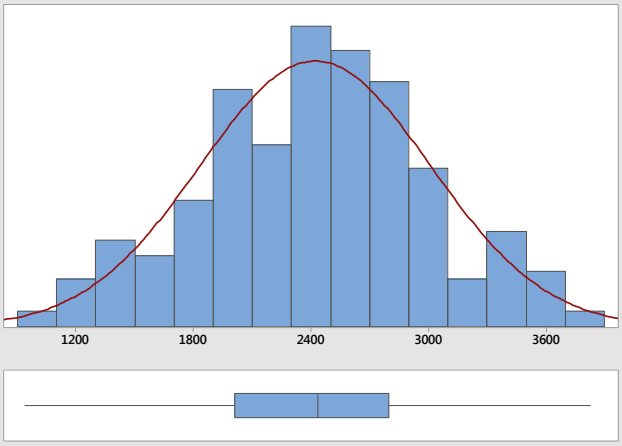




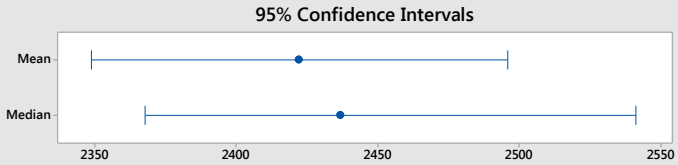


| Anderson-Darling Normality Test | |
|---|---|
| A-Squared | 0.35 |
| P-Value | 0.459 |
| Mean | 2422.2 |
| StDev | 588.7 |
| Variance | 346600.9 |
| Skewness | -0.084265 |
| Kurtosis | -0.263026 |
| N | 248 |
| Minimum | 934.0 |
| 1st Quartile | 2010.7 |
| Median | 2436.8 |
| 3rd Quartile | 2799.6 |
| Maximum | 3828.3 |
| 95% Confidence Interval for Mean | |
| 2348.6 | 2495.9 |
| 95% Confidence Interval for Median | |
| 2367.8 | 2541.2 |
| 95% Confidence Interval for StDev | |
| 541.1 | 645.7 |

## Calera Lms #4 Angularity: 40 minutes

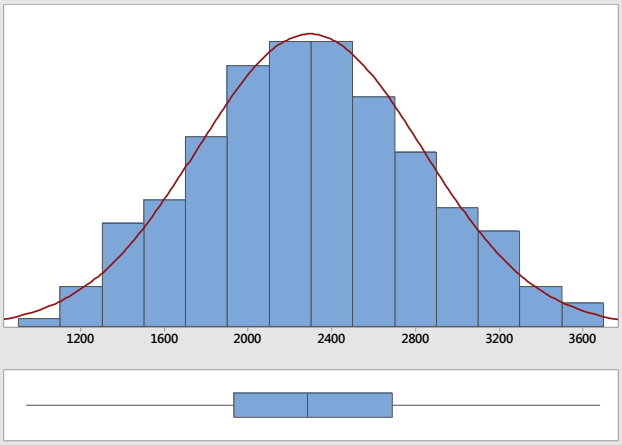




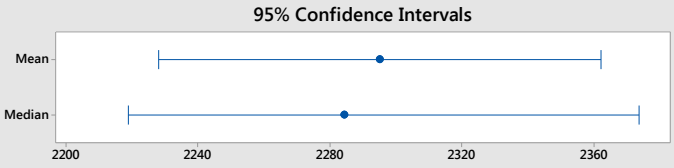


| Anderson-Darling Normality Test | |
|---|---|
| A-Squared | 0.19 |
| P-Value | 0.892 |
| Mean | 2295.1 |
| StDev | 539.4 |
| Variance | 290953.7 |
| Skewness | 0.084294 |
| Kurtosis | -0.351606 |
| N | 250 |
| Minimum | 937.5 |
| 1st Quartile | 1931.6 |
| Median | 2284.4 |
| 3rd Quartile | 2688.2 |
| Maximum | 3684.6 |
| 95% Confidence Interval for Mean | |
| 2228.0 | 2362.3 |
| 95% Confidence Interval for Median | |
| 2218.6 | 2373.7 |
| 95% Confidence Interval for StDev | |
| 495.9 | 591.3 |

## Calera Lms #4 Angularity: 60 minutes

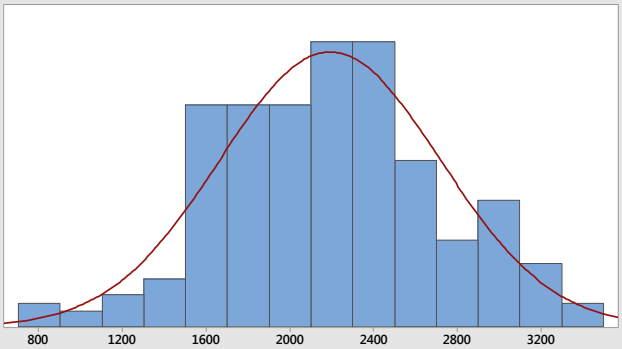


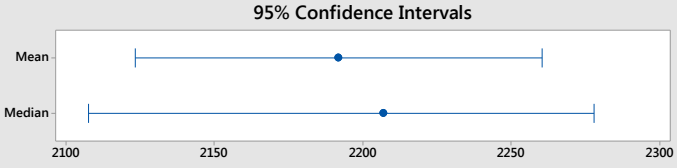


| Anderson-Darling Normality Test | |
|---|---|
| A-Squared | 0.34 |
| P-Value | 0.491 |
| Mean | 2191.7 |
| StDev | 528.4 |
| Variance | 279233.9 |
| Skewness | 0.006984 |
| Kurtosis | -0.160003 |
| N | 230 |
| Minimum | 760.5 |
| 1st Quartile | 1826.1 |
| Median | 2206.9 |
| 3rd Quartile | 2527.1 |
| Maximum | 3493.6 |
| 95% Confidence Interval for Mean | |
| 2123.1 | 2260.4 |
| 95% Confidence Interval for Median | |
| 2107.5 | 2277.9 |
| 95% Confidence Interval for StDev | |
| 484.1 | 581.7 |

## Calera Lms #4 Angularity: 80 minutes

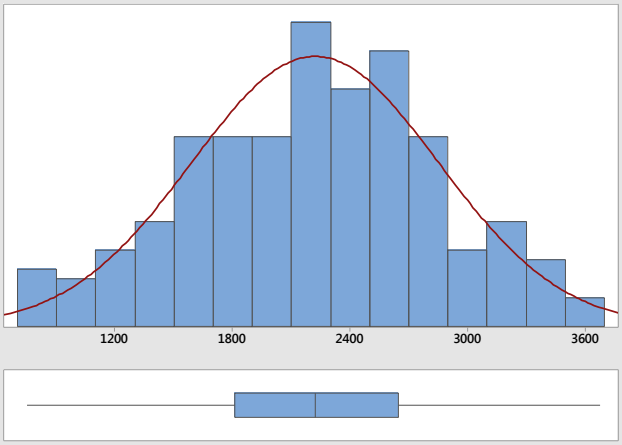


| Anderson-Darling Normality Test | |
|---|---|
| A-Squared | 0.28 |
| P-Value | 0.632 |
| Mean | 2221.0 |
| StDev | 631.6 |
| Variance | 398881.8 |
| Skewness | -0.120400 |
| Kurtosis | -0.367773 |
| N | 225 |
| Minimum | 748.9 |
| 1st Quartile | 1810.8 |
| Median | 2223.6 |
| 3rd Quartile | 2648.5 |
| Maximum | 3680.0 |
| 95% Confidence Interval for Mean | |
| 2138.1 | 2304.0 |
| 95% Confidence Interval for Median | |
| 2153.5 | 2364.0 |
| 95% Confidence Interval for StDev | |
| 578.1 | 696.0 |

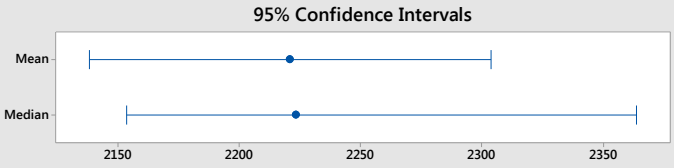


## Calera Lms #4 Angularity: 100 minutes

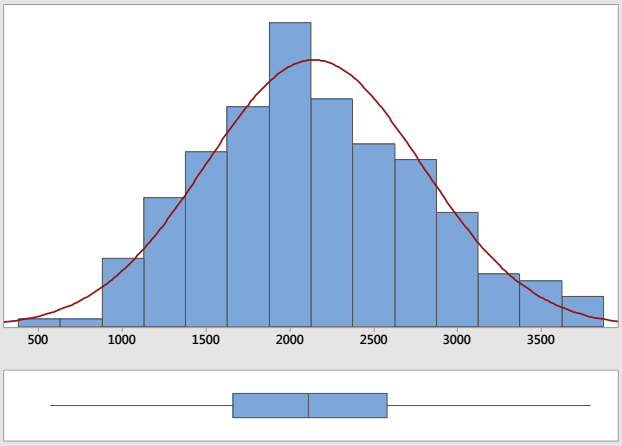


| Anderson-Darling Normality Test | |
|---|---|
| A-Squared | 0.53 |
| P-Value | 0.171 |
| Mean | 2141.6 |
| StDev | 647.9 |
| Variance | 419772.9 |
| Skewness | 0.273391 |
| Kurtosis | -0.274168 |
| N | 228 |
| Minimum | 567.5 |
| 1st Quartile | 1660.4 |
| Median | 2109.2 |
| 3rd Quartile | 2582.2 |
| Maximum | 3799.0 |
| 95% Confidence Interval for Mean | |
| 2057.1 | 2226.2 |
| 95% Confidence Interval for Median | |
| 2059.3 | 2180.4 |
| 95% Confidence Interval for StDev | |
| 593.4 | 713.5 |

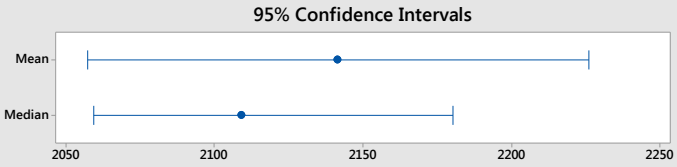

## Bauxite #16 Angularity: No Conditioning

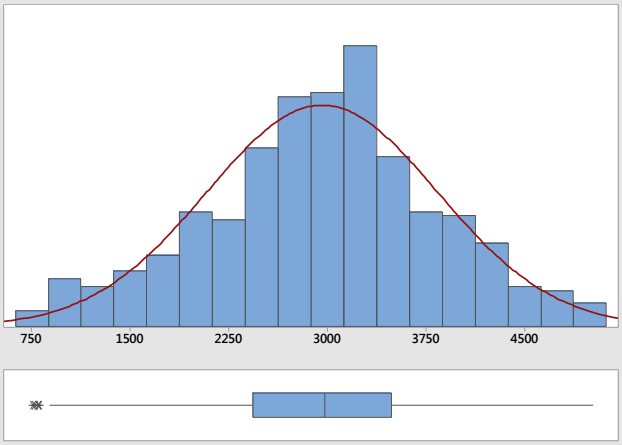




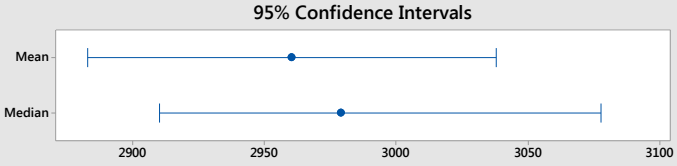


| Anderson-Darling Normality Test | |
|---|---|
| A-Squared | 1.00 |
| P-Value | 0.012 |
| Mean | 2960.4 |
| StDev | 879.8 |
| Variance | 773992.8 |
| Skewness | -0.161065 |
| Kurtosis | -0.123849 |
| N | 493 |
| Minimum | 758.4 |
| 1st Quartile | 2434.9 |
| Median | 2979.2 |
| 3rd Quartile | 3490.7 |
| Maximum | 5024.2 |
| 95% Confidence Interval for Mean | |
| 2882.5 | 3038.2 |
| 95% Confidence Interval for Median | |
| 2909.9 | 3078.0 |
| 95% Confidence Interval for StDev | |
| 828.1 | 938.4 |

## Bauxite #16 Angularity: 10 minutes

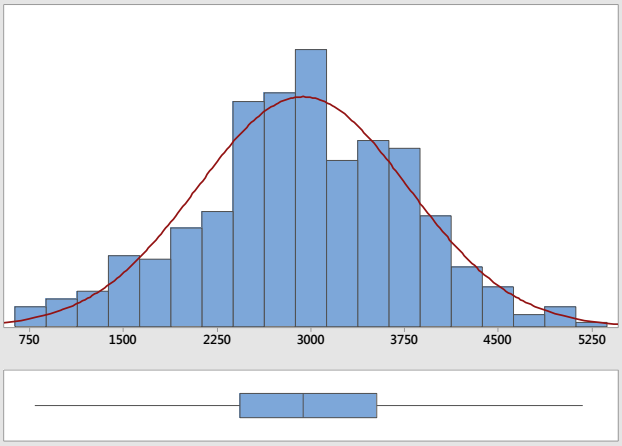




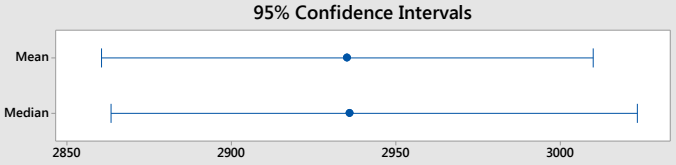


| Anderson-Darling Normality Test | |
|---|---|
| A-Squared | 0.59 |
| P-Value | 0.126 |
| Mean | 2935.3 |
| StDev | 844.5 |
| Variance | 713144.3 |
| Skewness | -0.155664 |
| Kurtosis | -0.129572 |
| N | 492 |
| Minimum | 782.8 |
| 1st Quartile | 2431.2 |
| Median | 2936.0 |
| 3rd Quartile | 3530.8 |
| Maximum | 5178.4 |
| 95% Confidence Interval for Mean | |
| 2860.5 | 3010.1 |
| 95% Confidence Interval for Median | |
| 2863.4 | 3023.5 |
| 95% Confidence Interval for StDev | |
| 794.8 | 900.8 |

## Bauxite #16 Angularity: 20 minutes

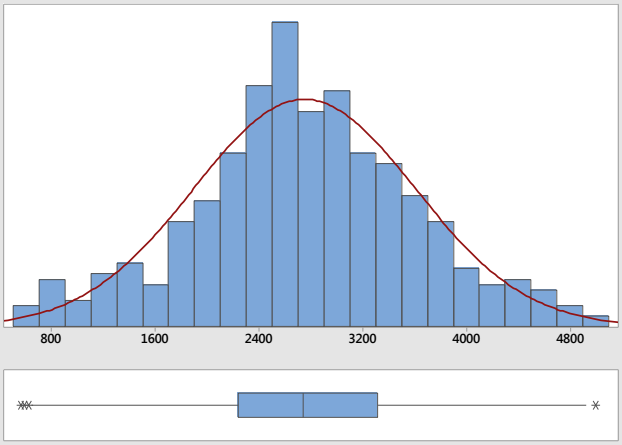


| Anderson-Darling Normality Test | |
|---|---|
| A-Squared | 0.76 |
| P-Value | 0.048 |
| Mean | 2750.5 |
| StDev | 856.2 |
| Variance | 733054.4 |
| Skewness | -0.0391391 |
| Kurtosis | 0.0185226 |
| N | 465 |
| Minimum | 558.5 |
| 1st Quartile | 2239.7 |
| Median | 2738.8 |
| 3rd Quartile | 3315.2 |
| Maximum | 5001.7 |
| 95% Confidence Interval for Mean | |
| 2672.5 | 2828.5 |
| 95% Confidence Interval for Median | |
| 2618.1 | 2814.8 |
| 95% Confidence Interval for StDev | |
| 804.5 | 915.1 |

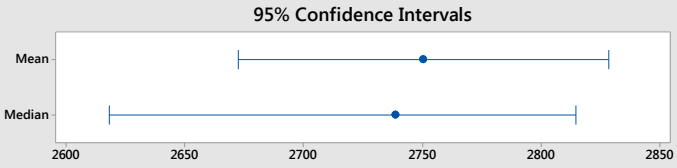


## Bauxite #16 Angularity: 30 minutes

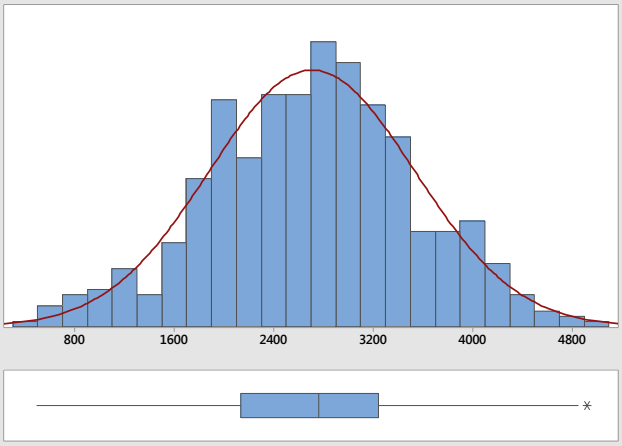


| Anderson-Darling Normality Test | |
|---|---|
| A-Squared | 0.35 |
| P-Value | 0.469 |
| Mean | 2708.5 |
| StDev | 826.4 |
| Variance | 682987.0 |
| Skewness | -0.0949290 |
| Kurtosis | -0.0932686 |
| N | 504 |
| Minimum | 492.4 |
| 1st Quartile | 2133.6 |
| Median | 2760.8 |
| 3rd Quartile | 3243.8 |
| Maximum | 4924.8 |
| 95% Confidence Interval for Mean | |
| 2636.2 | 2780.9 |
| 95% Confidence Interval for Median | |
| 2634.5 | 2841.0 |
| 95% Confidence Interval for StDev | |
| 778.4 | 880.9 |

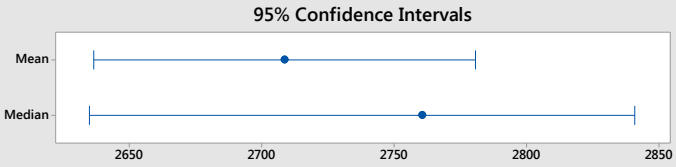

## Opelika Lms #16 Angularity: No Conditioning

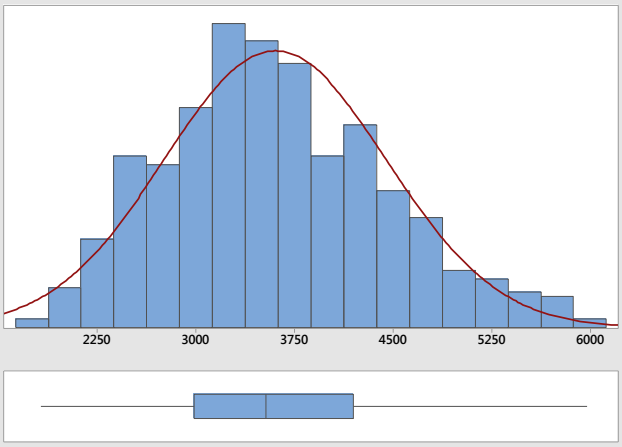




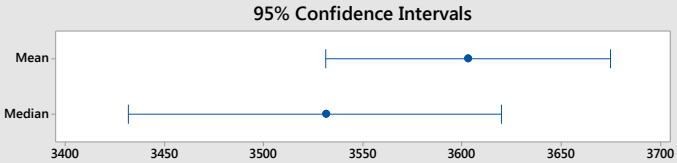


| Anderson-Darling Normality Test | |
|---|---|
| A-Squared | 1.41 |
| P-Value | <0.005 |
| Mean | 3603.3 |
| StDev | 846.1 |
| Variance | 715934.5 |
| Skewness | 0.363262 |
| Kurtosis | -0.229082 |
| N | 533 |
| Minimum | 1815.6 |
| 1st Quartile | 2984.4 |
| Median | 3531.8 |
| 3rd Quartile | 4195.4 |
| Maximum | 5977.3 |
| 95% Confidence Interval for Mean | |
| 3531.3 | 3675.3 |
| 95% Confidence Interval for Median | |
| 3431.3 | 3619.8 |
| 95% Confidence Interval for StDev | |
| 798.2 | 900.2 |

## Opelika Lms #16 Angularity: 10 minutes

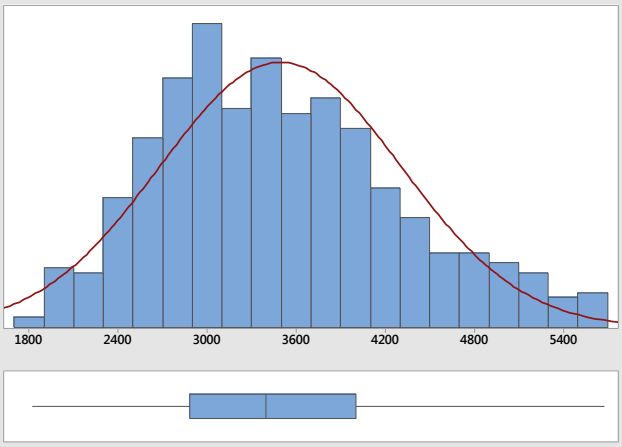




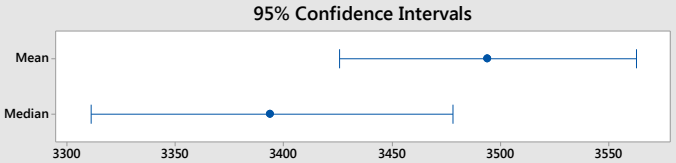


| Anderson-Darling Normality Test | |
|---|---|
| A-Squared | 2.98 |
| P-Value | <0.005 |
| Mean | 3494.2 |
| StDev | 815.2 |
| Variance | 664557.9 |
| Skewness | 0.463836 |
| Kurtosis | -0.247671 |
| N | 544 |
| Minimum | 1821.0 |
| 1st Quartile | 2881.9 |
| Median | 3393.6 |
| 3rd Quartile | 4006.2 |
| Maximum | 5681.4 |
| 95% Confidence Interval for Mean | |
| 3425.6 | 3562.9 |
| 95% Confidence Interval for Median | |
| 3310.8 | 3478.2 |
| 95% Confidence Interval for StDev | |
| 769.5 | 866.8 |

## Opelika Lms #16 Angularity: 20 minutes

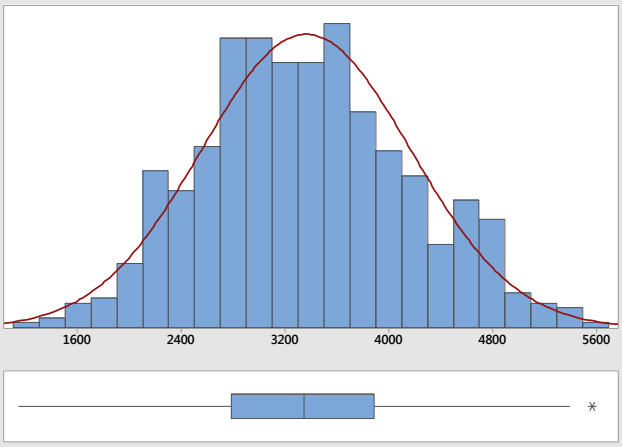




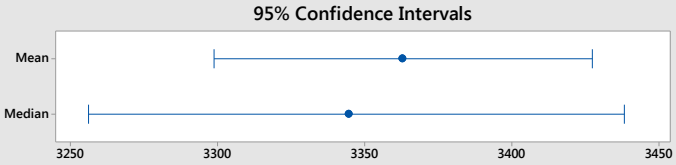


| Anderson-Darling Normality Test | |
|---|---|
| A-Squared | 0.91 |
| P-Value | 0.021 |
| Mean | 3362.9 |
| StDev | 806.8 |
| Variance | 650873.7 |
| Skewness | 0.168697 |
| Kurtosis | -0.347421 |
| N | 605 |
| Minimum | 1142.1 |
| 1st Quartile | 2786.1 |
| Median | 3344.5 |
| 3rd Quartile | 3887.2 |
| Maximum | 5571.3 |
| 95% Confidence Interval for Mean | |
| 3298.5 | 3427.3 |
| 95% Confidence Interval for Median | |
| 3255.9 | 3438.5 |
| 95% Confidence Interval for StDev | |
| 763.7 | 855.0 |

## Opelika Lms #16 Angularity: 30 minutes

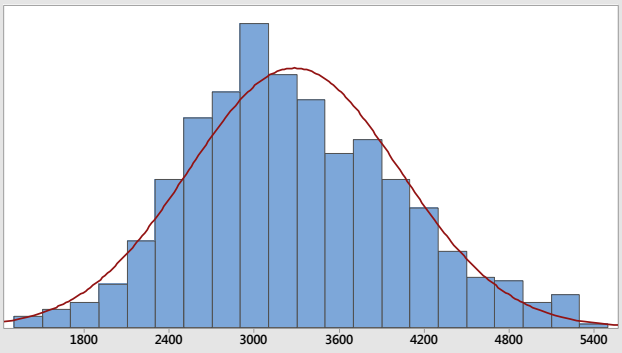


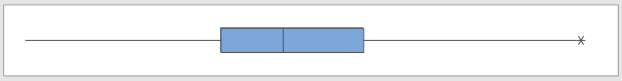

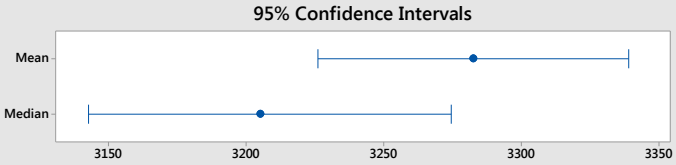


| Anderson-Darling Normality Test | |
|---|---|
| A-Squared | 1.85 |
| P-Value | <0.005 |
| Mean | 3282.6 |
| StDev | 746.6 |
| Variance | 557459.4 |
| Skewness | 0.298641 |
| Kurtosis | -0.139303 |
| N | 671 |
| Minimum | 1377.8 |
| 1st Quartile | 2765.1 |
| Median | 3205.2 |
| 3rd Quartile | 3772.3 |
| Maximum | 5312.6 |
| 95% Confidence Interval for Mean | |
| 3226.0 | 3339.2 |
| 95% Confidence Interval for Median | |
| 3142.6 | 3274.6 |
| 95% Confidence Interval for StDev | |
| 708.7 | 788.9 |

## Columbus Grn #16 Angularity: No Conditioning

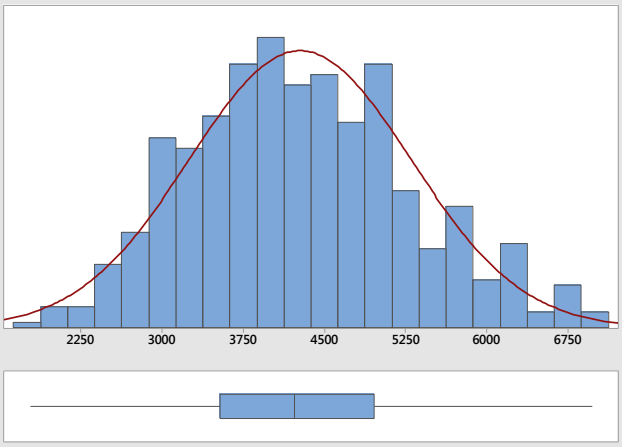




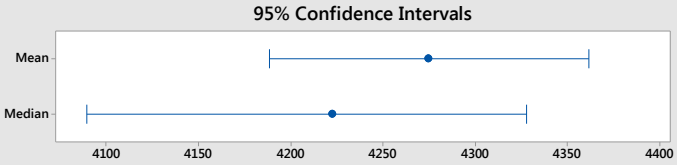


| Anderson-Darling Normality Test | |
|---|---|
| A-Squared | 1.04 |
| P-Value | 0.010 |
| Mean | 4274.9 |
| StDev | 1025.7 |
| Variance | 1051963.6 |
| Skewness | 0.264220 |
| Kurtosis | -0.331420 |
| N | 540 |
| Minimum | 1780.8 |
| 1st Quartile | 3535.0 |
| Median | 4222.8 |
| 3rd Quartile | 4956.0 |
| Maximum | 6977.4 |
| 95% Confidence Interval for Mean | |
| 4188.2 | 4361.6 |
| 95% Confidence Interval for Median | |
| 4089.0 | 4328.0 |
| 95% Confidence Interval for StDev | |
| 967.9 | 1090.8 |

## Columbus Grn #16 Angularity: 10 minutes

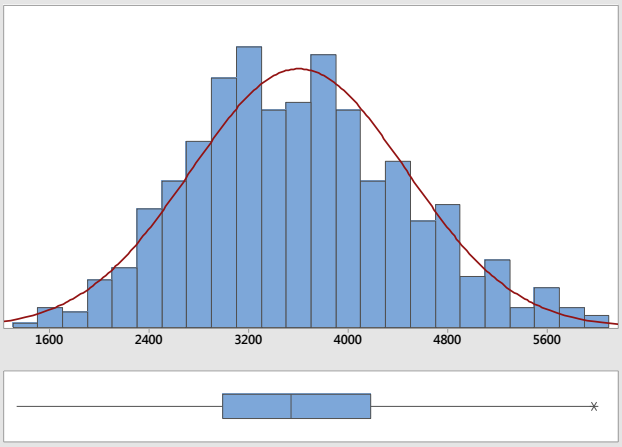




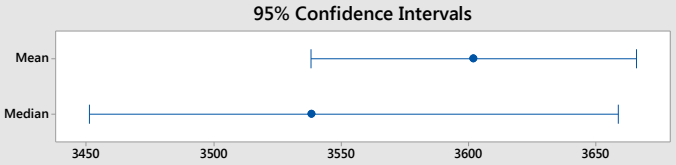


| Anderson-Darling Normality Test | |
|---|---|
| A-Squared | 1.33 |
| P-Value | <0.005 |
| Mean | 3602.1 |
| StDev | 867.8 |
| Variance | 753066.2 |
| Skewness | 0.268810 |
| Kurtosis | -0.230087 |
| N | 711 |
| Minimum | 1333.3 |
| 1st Quartile | 2992.1 |
| Median | 3538.4 |
| 3rd Quartile | 4183.4 |
| Maximum | 5978.7 |
| 95% Confidence Interval for Mean | |
| 3538.2 | 3666.0 |
| 95% Confidence Interval for Median | |
| 3451.0 | 3658.9 |
| 95% Confidence Interval for StDev | |
| 824.9 | 915.4 |

## Columbus Grn #16 Angularity: 20 minutes

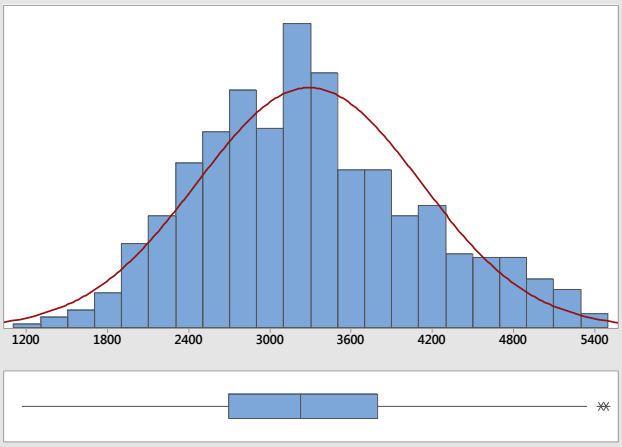




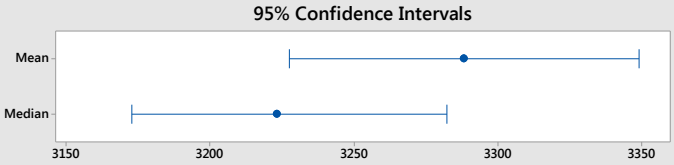


| Anderson-Darling Normality Test | |
|---|---|
| A-Squared | 3.15 |
| P-Value | <0.005 |
| Mean | 3288.3 |
| StDev | 825.0 |
| Variance | 680608.8 |
| Skewness | 0.361818 |
| Kurtosis | -0.291649 |
| N | 710 |
| Minimum | 1162.9 |
| 1st Quartile | 2696.2 |
| Median | 3223.2 |
| 3rd Quartile | 3794.9 |
| Maximum | 5485.0 |
| 95% Confidence Interval for Mean | |
| 3227.5 | 3349.1 |
| 95% Confidence Interval for Median | |
| 3172.6 | 3282.3 |
| 95% Confidence Interval for StDev | |
| 784.2 | 870.3 |

## Columbus Grn #16 Angularity: 30 minutes

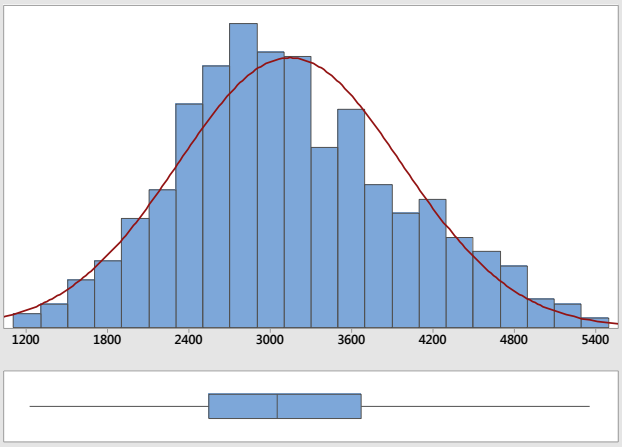




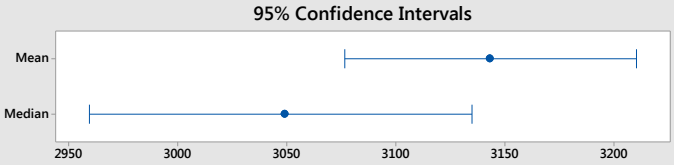


| Anderson-Darling Normality Test | |
|---|---|
| A-Squared | 2.05 |
| P-Value | <0.005 |
| Mean | 3143.4 |
| StDev | 830.0 |
| Variance | 688970.5 |
| Skewness | 0.311021 |
| Kurtosis | -0.311973 |
| N | 591 |
| Minimum | 1220.0 |
| 1st Quartile | 2545.8 |
| Median | 3049.0 |
| 3rd Quartile | 3674.5 |
| Maximum | 5363.6 |
| 95% Confidence Interval for Mean | |
| 3076.4 | 3210.5 |
| 95% Confidence Interval for Median | |
| 2959.1 | 3134.8 |
| 95% Confidence Interval for StDev | |
| 785.3 | 880.3 |

## LaGrange Grn #16 Angularity: No Conditioning

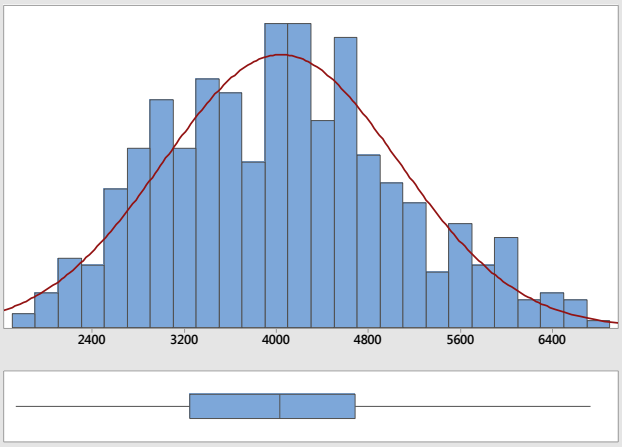




| Anderson-Darling Normality Test | |
|---|---|
| A-Squared | 1.14 |
| P-Value | 0.005 |
| Mean | 4039.6 |
| StDev | 1025.9 |
| Variance | 1052543.7 |
| Skewness | 0.260184 |
| Kurtosis | -0.388086 |
| N | 508 |
| Minimum | 1733.8 |
| 1st Quartile | 3245.8 |
| Median | 4027.0 |
| 3rd Quartile | 4687.4 |
| Maximum | 6735.9 |
| 95% Confidence Interval for Mean | |
| 3950.1 | 4129.0 |
| 95% Confidence Interval for Median | |
| 3951.4 | 4133.1 |
| 95% Confidence Interval for StDev | |
| 966.5 | 1093.2 |

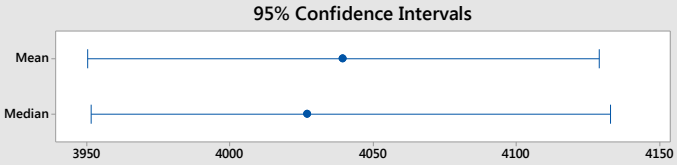


## LaGrange Grn #16 Angularity: 10 minutes

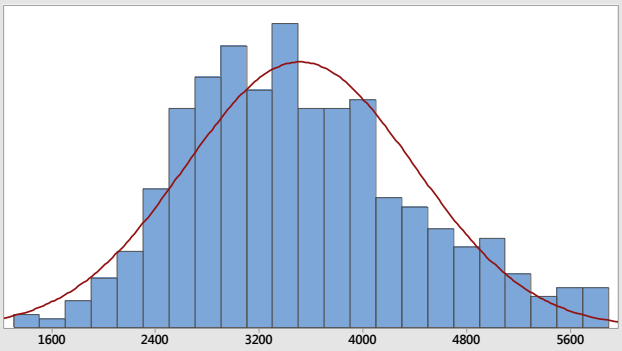


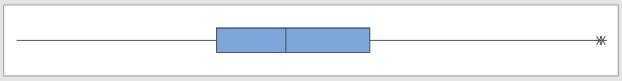

| Anderson-Darling Normality Test | |
|---|---|
| A-Squared | 3.61 |
| P-Value | <0.005 |
| Mean | 3513.5 |
| StDev | 887.4 |
| Variance | 787436.7 |
| Skewness | 0.443870 |
| Kurtosis | -0.164787 |
| N | 661 |
| Minimum | 1320.1 |
| 1st Quartile | 2869.7 |
| Median | 3401.6 |
| 3rd Quartile | 4051.8 |
| Maximum | 5853.1 |
| 95% Confidence Interval for Mean | |
| 3445.8 | 3581.3 |
| 95% Confidence Interval for Median | |
| 3335.4 | 3485.1 |
| 95% Confidence Interval for StDev | |
| 842.0 | 938.0 |

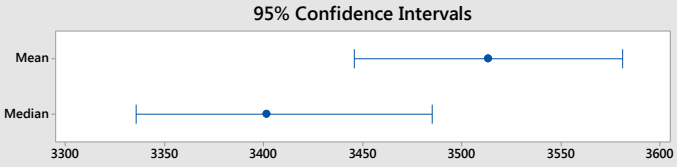

## LaGrange Grn #16 Angularity: 20 minutes

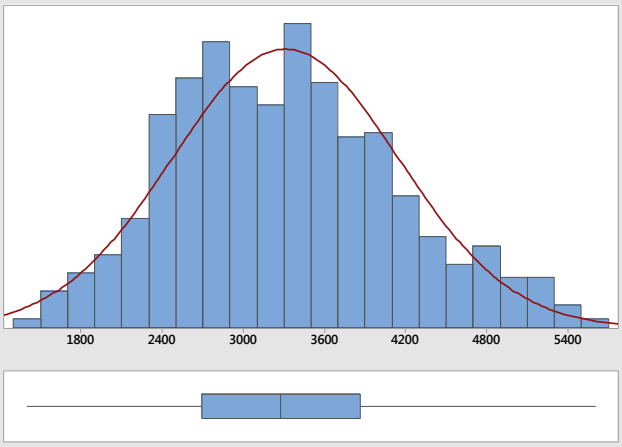




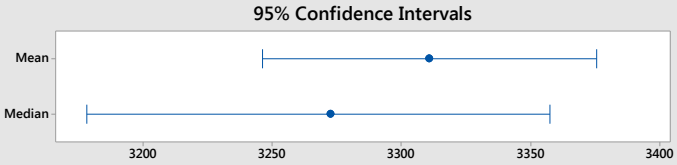


| Anderson-Darling Normality Test | |
|---|---|
| A-Squared | 1.85 |
| P-Value | <0.005 |
| Mean | 3311.0 |
| StDev | 838.3 |
| Variance | 702830.6 |
| Skewness | 0.316470 |
| Kurtosis | -0.314833 |
| N | 645 |
| Minimum | 1397.6 |
| 1st Quartile | 2690.3 |
| Median | 3272.9 |
| 3rd Quartile | 3862.0 |
| Maximum | 5606.9 |
| 95% Confidence Interval for Mean | |
| 3246.2 | 3375.9 |
| 95% Confidence Interval for Median | |
| 3178.2 | 3357.7 |
| 95% Confidence Interval for StDev | |
| 795.0 | 886.8 |

## LaGrange Grn #16 Angularity: 30 minutes

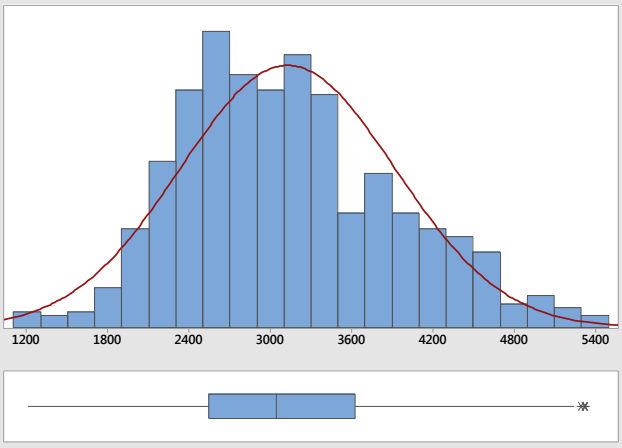




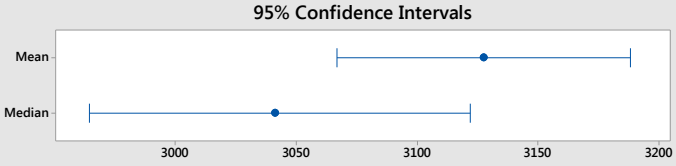


| Anderson-Darling Normality Test | |
|---|---|
| A-Squared | 3.92 |
| P-Value | <0.005 |
| Mean | 3127.7 |
| StDev | 795.5 |
| Variance | 632764.7 |
| Skewness | 0.430235 |
| Kurtosis | -0.180040 |
| N | 661 |
| Minimum | 1207.8 |
| 1st Quartile | 2547.3 |
| Median | 3041.5 |
| 3rd Quartile | 3627.7 |
| Maximum | 5327.8 |
| 95% Confidence Interval for Mean | |
| 3067.0 | 3188.5 |
| 95% Confidence Interval for Median | |
| 2964.2 | 3122.1 |
| 95% Confidence Interval for StDev | |
| 754.8 | 840.8 |

# Calera Lms #16 Angularity: No Conditioning

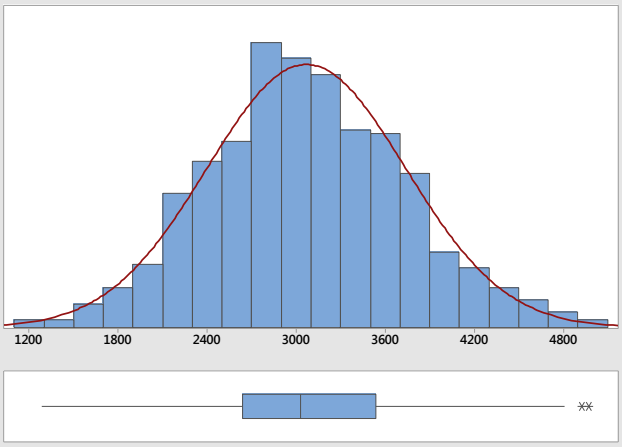




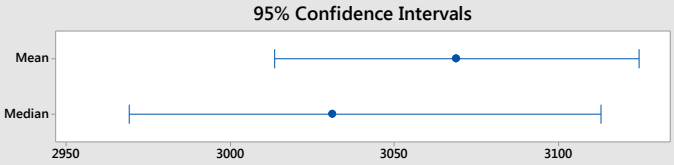


| Anderson-Darling Normality Test | |
|---|---|
| A-Squared | 0.32 |
| P-Value | 0.529 |
| Mean | 3069.1 |
| StDev | 669.6 |
| Variance | 448301.7 |
| Skewness | 0.132559 |
| Kurtosis | -0.088553 |
| N | 558 |
| Minimum | 1285.3 |
| 1st Quartile | 2637.5 |
| Median | 3031.3 |
| 3rd Quartile | 3539.2 |
| Maximum | 4972.9 |
| 95% Confidence Interval for Mean | |
| 3013.4 | 3124.7 |
| 95% Confidence Interval for Median | |
| 2969.0 | 3113.3 |
| 95% Confidence Interval for StDev | |
| 632.4 | 711.3 |

# Calera Lms #16 Angularity: 10 minutes

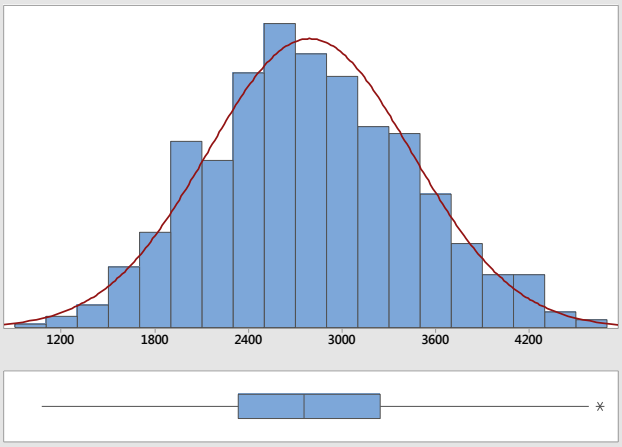




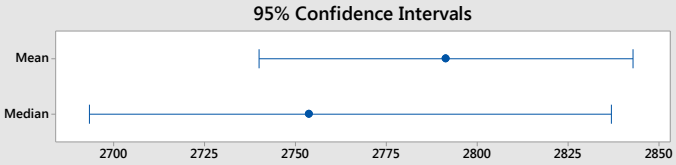


| Anderson-Darling Normality Test | |
|---|---|
| A-Squared | 0.48 |
| P-Value | 0.233 |
| Mean | 2791.4 |
| StDev | 654.9 |
| Variance | 428834.0 |
| Skewness | 0.166814 |
| Kurtosis | -0.258269 |
| N | 624 |
| Minimum | 1071.7 |
| 1st Quartile | 2333.1 |
| Median | 2753.6 |
| 3rd Quartile | 3244.2 |
| Maximum | 4655.9 |
| 95% Confidence Interval for Mean | |
| 2740.0 | 2842.9 |
| 95% Confidence Interval for Median | |
| 2693.0 | 2836.9 |
| 95% Confidence Interval for StDev | |
| 620.4 | 693.4 |

## Calera Lms #16 Angularity: 20 minutes

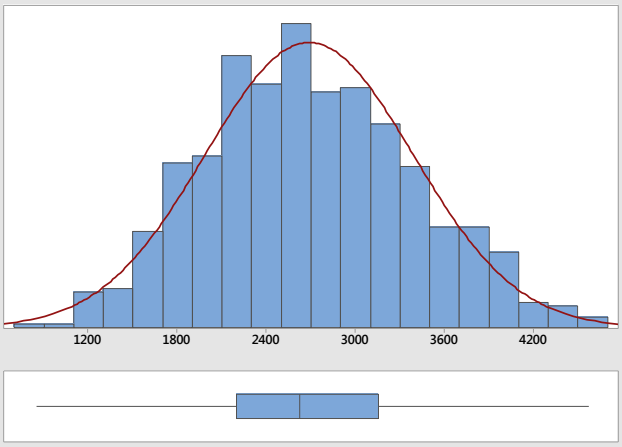




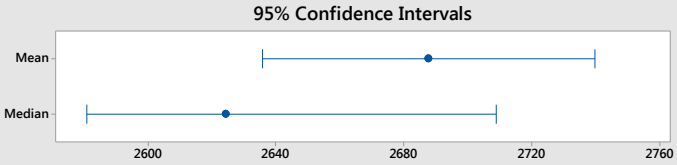


| Anderson-Darling Normality Test | |
|---|---|
| A-Squared | 1.00 |
| P-Value | 0.012 |
| Mean | 2687.9 |
| StDev | 701.6 |
| Variance | 492288.0 |
| Skewness | 0.192361 |
| Kurtosis | -0.356134 |
| N | 701 |
| Minimum | 849.8 |
| 1st Quartile | 2199.8 |
| Median | 2624.4 |
| 3rd Quartile | 3154.4 |
| Maximum | 4572.9 |
| 95% Confidence Interval for Mean | |
| 2635.9 | 2739.9 |
| 95% Confidence Interval for Median | |
| 2580.8 | 2708.9 |
| 95% Confidence Interval for StDev | |
| 666.7 | 740.4 |

## Calera Lms #16 Angularity: 30 minutes

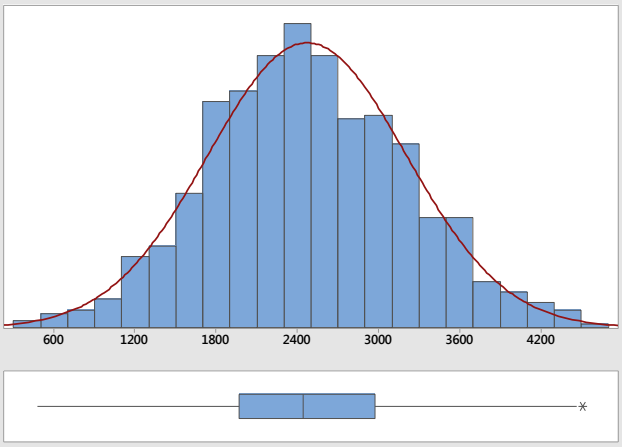




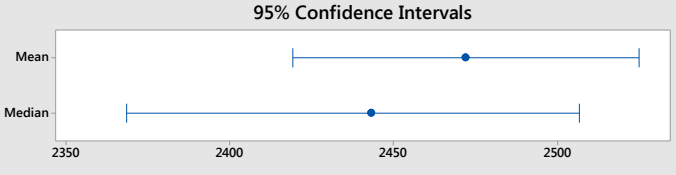


| Anderson-Darling Normality Test | |
|---|---|
| A-Squared | 0.47 |
| P-Value | 0.245 |
| Mean | 2472.1 |
| StDev | 732.8 |
| Variance | 537067.3 |
| Skewness | 0.090629 |
| Kurtosis | -0.128641 |
| N | 740 |
| Minimum | 479.2 |
| 1st Quartile | 1965.4 |
| Median | 2443.2 |
| 3rd Quartile | 2971.3 |
| Maximum | 4510.8 |
| 95% Confidence Interval for Mean | |
| 2419.2 | 2525.0 |
| 95% Confidence Interval for Median | |
| 2368.4 | 2506.8 |
| 95% Confidence Interval for StDev | |
| 697.3 | 772.2 |

## Opelika Lms #4 Texture: No Conditioning

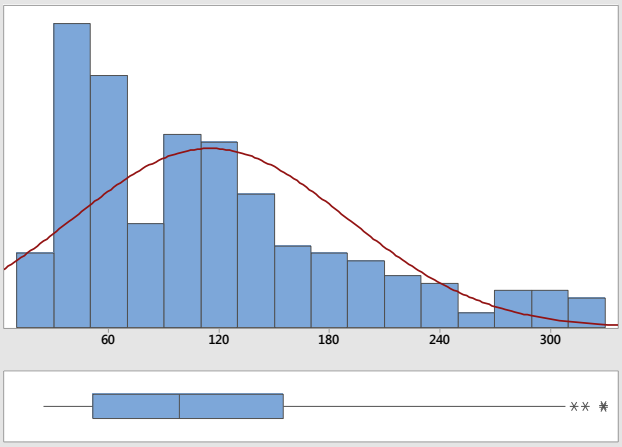


| Anderson-Darling Normality Test | |
|---|---|
| A-Squared | 6.12 |
| P-Value | <0.005 |
| Mean | 115.16 |
| StDev | 74.95 |
| Variance | 5617.20 |
| Skewness | 0.983407 |
| Kurtosis | 0.302052 |
| N | 227 |
| Minimum | 24.56 |
| 1st Quartile | 51.58 |
| Median | 98.25 |
| 3rd Quartile | 154.75 |
| Maximum | 329.14 |
| 95% Confidence Interval for Mean | |
| 105.36 | 124.96 |
| 95% Confidence Interval for Median | |
| 89.97 | 115.13 |
| 95% Confidence Interval for StDev | |
| 68.63 | 82.56 |



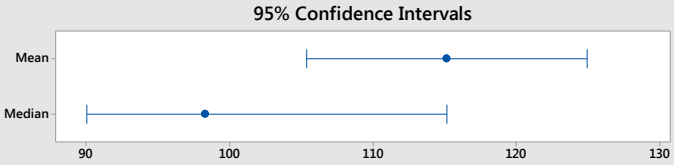


## Opelika Lms #4 Texture: 20 minutes

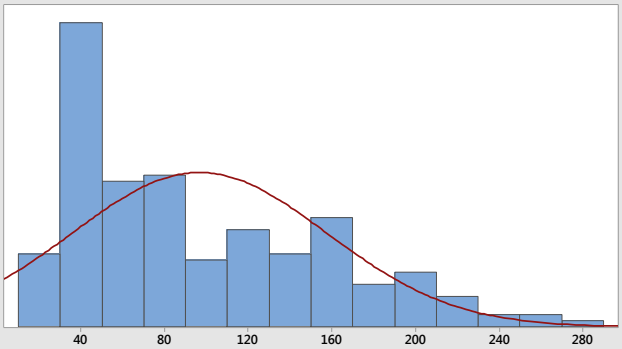


| Anderson-Darling Normality Test | |
|---|---|
| A-Squared | 6.29 |
| P-Value | <0.005 |
| Mean | 96.638 |
| StDev | 61.002 |
| Variance | 3721.294 |
| Skewness | 0.798463 |
| Kurtosis | -0.315596 |
| N | 194 |
| Minimum | 24.563 |
| 1st Quartile | 44.213 |
| Median | 79.830 |
| 3rd Quartile | 142.465 |
| Maximum | 283.703 |
| 95% Confidence Interval for Mean | |
| 87.999 | 105.276 |
| 95% Confidence Interval for Median | |
| 63.864 | 89.816 |
| 95% Confidence Interval for StDev | |
| 55.476 | 67.761 |

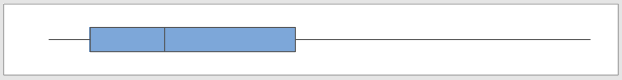

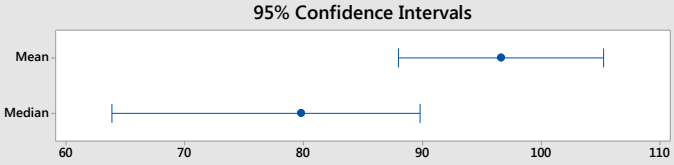

## Opelika Lms #4 Texture: 40 minutes

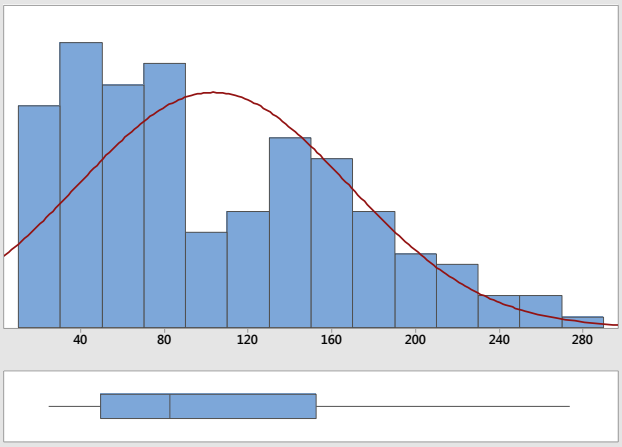




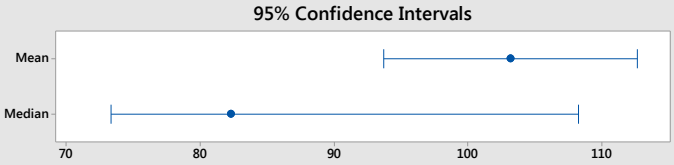


| Anderson-Darling Normality Test | |
|---|---|
| A-Squared | 4.44 |
| P-Value | <0.005 |
| Mean | 103.25 |
| StDev | 64.78 |
| Variance | 4196.62 |
| Skewness | 0.617385 |
| Kurtosis | -0.652955 |
| N | 181 |
| Minimum | 24.56 |
| 1st Quartile | 49.13 |
| Median | 82.29 |
| 3rd Quartile | 152.29 |
| Maximum | 273.88 |
| 95% Confidence Interval for Mean | |
| 93.74 | 112.75 |
| 95% Confidence Interval for Median | |
| 73.29 | 108.28 |
| 95% Confidence Interval for StDev | |
| 58.72 | 72.24 |

## Opelika Lms #4 Texture: 60 minutes

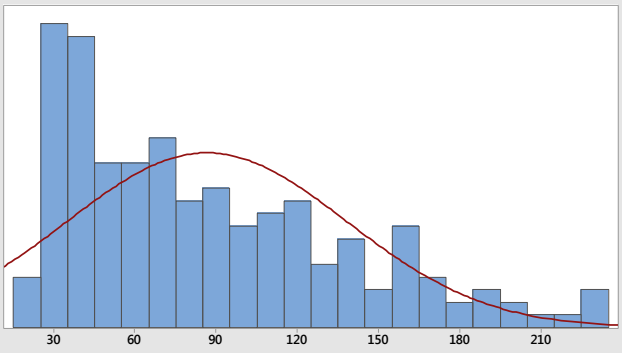


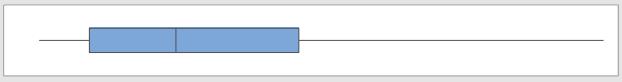

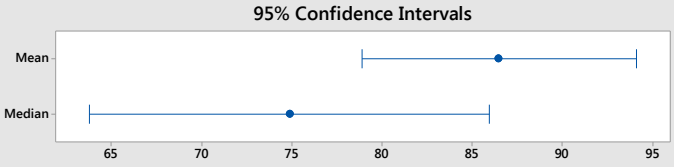


| Anderson-Darling Normality Test | |
|---|---|
| A-Squared | 4.63 |
| P-Value | <0.005 |
| Mean | 86.513 |
| StDev | 51.733 |
| Variance | 2676.329 |
| Skewness | 0.890193 |
| Kurtosis | 0.051238 |
| N | 179 |
| Minimum | 24.563 |
| 1st Quartile | 42.985 |
| Median | 74.917 |
| 3rd Quartile | 120.359 |
| Maximum | 233.348 |
| 95% Confidence Interval for Mean | |
| 78.882 | 94.143 |
| 95% Confidence Interval for Median | |
| 63.745 | 85.970 |
| 95% Confidence Interval for StDev | |
| 46.872 | 57.728 |

## Opelika Lms #4 Texture: 80 minutes

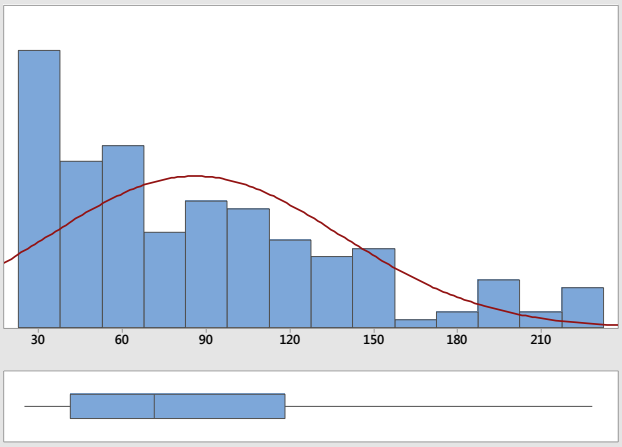




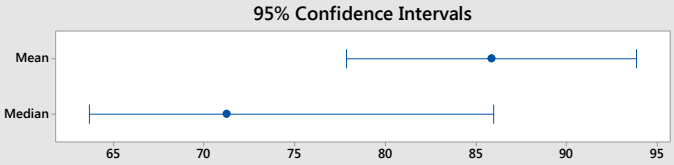


| Anderson-Darling Normality Test | |
|---|---|
| A-Squared | 4.41 |
| P-Value | <0.005 |
| Mean | 85.883 |
| StDev | 52.549 |
| Variance | 2761.362 |
| Skewness | 0.922462 |
| Kurtosis | 0.120141 |
| N | 168 |
| Minimum | 24.563 |
| 1st Quartile | 41.143 |
| Median | 71.233 |
| 3rd Quartile | 118.210 |
| Maximum | 228.436 |
| 95% Confidence Interval for Mean | |
| 77.879 | 93.887 |
| 95% Confidence Interval for Median | |
| 63.646 | 85.970 |
| 95% Confidence Interval for StDev | |
| 47.467 | 58.859 |

## Opelika Lms #4 Texture: 100 minutes

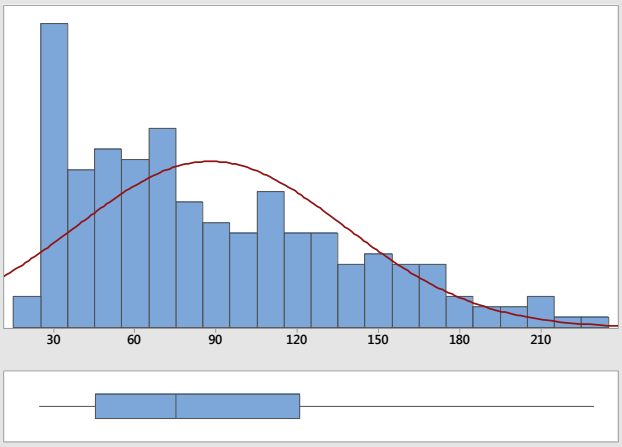




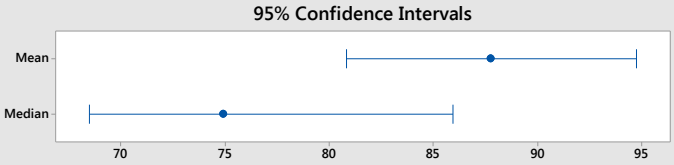


| Anderson-Darling Normality Test | |
|---|---|
| A-Squared | 3.97 |
| P-Value | <0.005 |
| Mean | 87.800 |
| StDev | 49.820 |
| Variance | 2482.081 |
| Skewness | 0.730675 |
| Kurtosis | -0.297458 |
| N | 198 |
| Minimum | 24.563 |
| 1st Quartile | 45.442 |
| Median | 74.917 |
| 3rd Quartile | 120.973 |
| Maximum | 229.664 |
| 95% Confidence Interval for Mean | |
| 80.818 | 94.783 |
| 95% Confidence Interval for Median | |
| 68.456 | 85.970 |
| 95% Confidence Interval for StDev | |
| 45.349 | 55.278 |

## Columbus Grn #4 Texture: No Conditioning

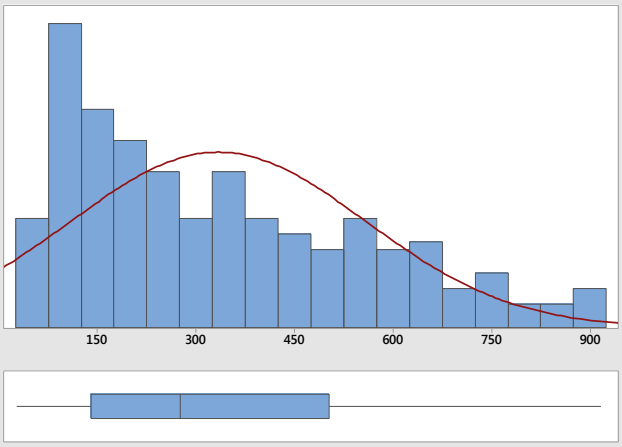


| Anderson-Darling Normality Test | |
|---|---|
| A-Squared | 5.88 |
| P-Value | <0.005 |
| Mean | 333.95 |
| StDev | 224.22 |
| Variance | 50274.66 |
| Skewness | 0.720037 |
| Kurtosis | -0.433237 |
| N | 253 |
| Minimum | 27.02 |
| 1st Quartile | 140.62 |
| Median | 276.33 |
| 3rd Quartile | 502.93 |
| Maximum | 916.20 |
| 95% Confidence Interval for Mean | |
| 306.19 | 361.72 |
| 95% Confidence Interval for Median | |
| 233.21 | 332.29 |
| 95% Confidence Interval for StDev | |
| 206.24 | 245.67 |

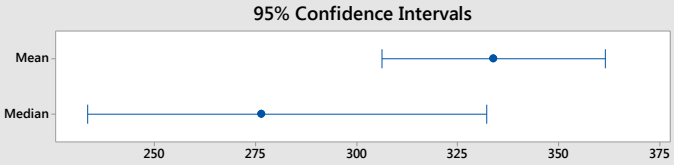




## Columbus Grn #4 Texture: 20 minutes

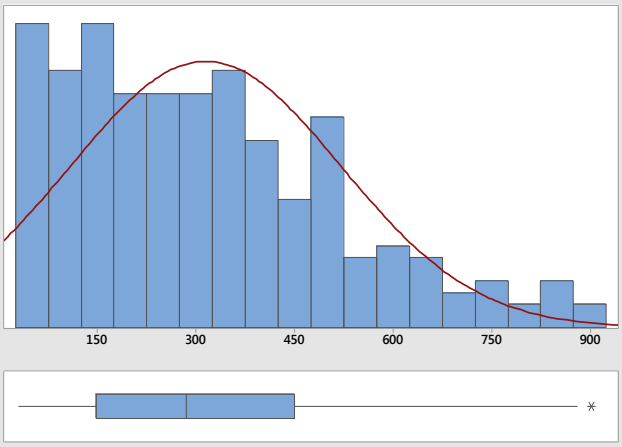


| Anderson-Darling Normality Test | |
|---|---|
| A-Squared | 3.34 |
| P-Value | <0.005 |
| Mean | 314.73 |
| StDev | 205.79 |
| Variance | 42349.33 |
| Skewness | 0.758218 |
| Kurtosis | 0.003196 |
| N | 235 |
| Minimum | 29.48 |
| 1st Quartile | 148.61 |
| Median | 284.93 |
| 3rd Quartile | 449.50 |
| Maximum | 902.69 |
| 95% Confidence Interval for Mean | |
| 288.28 | 341.18 |
| 95% Confidence Interval for Median | |
| 240.72 | 321.77 |
| 95% Confidence Interval for StDev | |
| 188.71 | 226.29 |

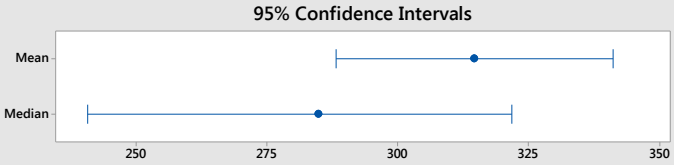

## Columbus Grn #4 Texture: 40 minutes

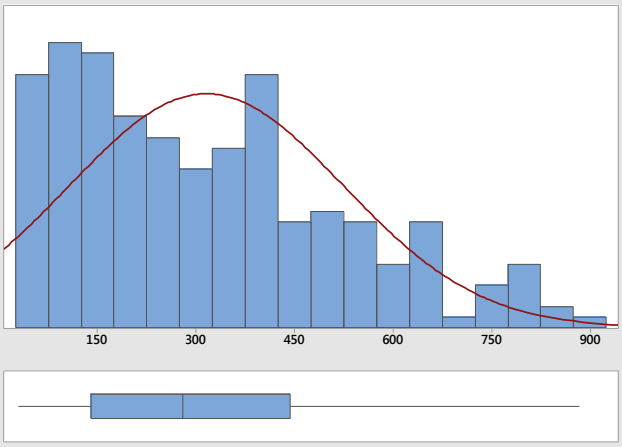




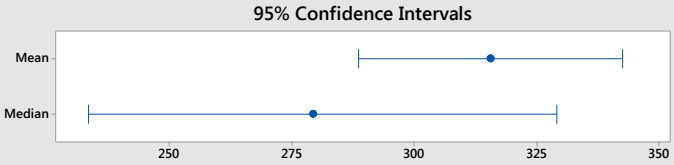


| Anderson-Darling Normality Test | |
|---|---|
| A-Squared | 4.10 |
| P-Value | <0.005 |
| Mean | 315.67 |
| StDev | 208.74 |
| Variance | 43574.43 |
| Skewness | 0.703475 |
| Kurtosis | -0.311263 |
| N | 232 |
| Minimum | 29.48 |
| 1st Quartile | 140.32 |
| Median | 279.40 |
| 3rd Quartile | 443.98 |
| Maximum | 883.04 |
| 95% Confidence Interval for Mean | |
| 288.67 | 342.67 |
| 95% Confidence Interval for Median | |
| 233.35 | 329.11 |
| 95% Confidence Interval for StDev | |
| 191.32 | 229.69 |

## Columbus Grn #4 Texture: 60 minutes

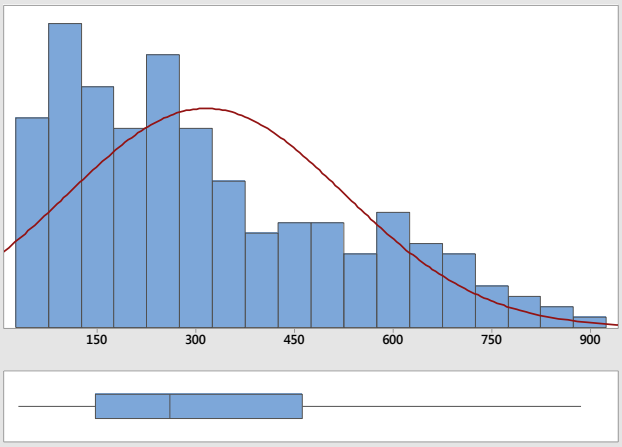




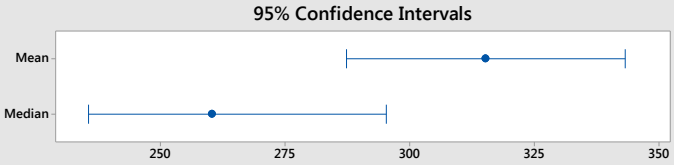


| Anderson-Darling Normality Test | |
|---|---|
| A-Squared | 5.42 |
| P-Value | <0.005 |
| Mean | 315.29 |
| StDev | 211.72 |
| Variance | 44826.84 |
| Skewness | 0.743169 |
| Kurtosis | -0.429769 |
| N | 222 |
| Minimum | 29.48 |
| 1st Quartile | 146.15 |
| Median | 260.37 |
| 3rd Quartile | 461.48 |
| Maximum | 886.72 |
| 95% Confidence Interval for Mean | |
| 287.29 | 343.30 |
| 95% Confidence Interval for Median | |
| 235.48 | 295.30 |
| 95% Confidence Interval for StDev | |
| 193.69 | 233.49 |

## Columbus Grn #4 Texture: 80 minutes

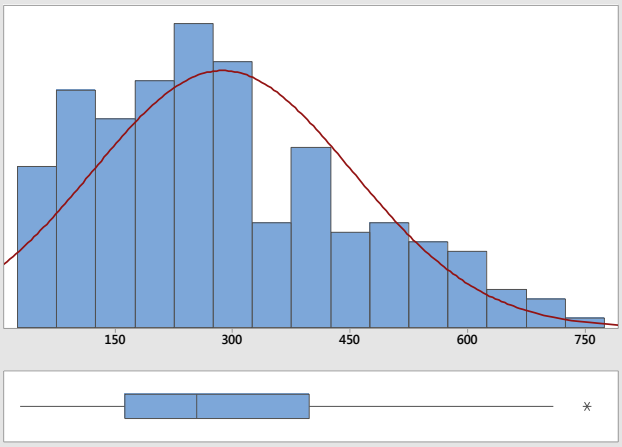




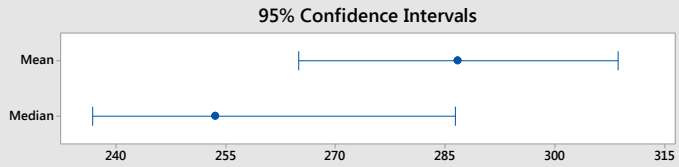


| Anderson-Darling Normality Test | |
|---|---|
| A-Squared | 2.88 |
| P-Value | <0.005 |
| Mean | 286.84 |
| StDev | 166.66 |
| Variance | 27775.24 |
| Skewness | 0.639267 |
| Kurtosis | -0.305214 |
| N | 226 |
| Minimum | 28.25 |
| 1st Quartile | 162.12 |
| Median | 253.61 |
| 3rd Quartile | 397.61 |
| Maximum | 752.86 |
| 95% Confidence Interval for Mean | |
| 264.99 | 308.68 |
| 95% Confidence Interval for Median | |
| 236.78 | 286.42 |
| 95% Confidence Interval for StDev | |
| 152.58 | 183.62 |

## Columbus Grn #4 Texture: 100 minutes

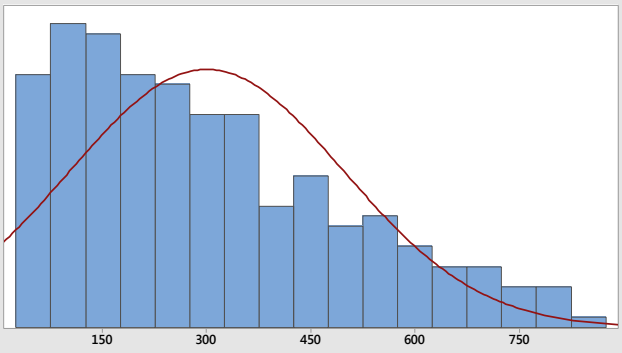


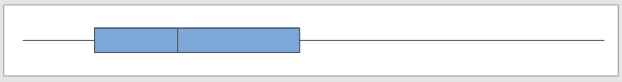

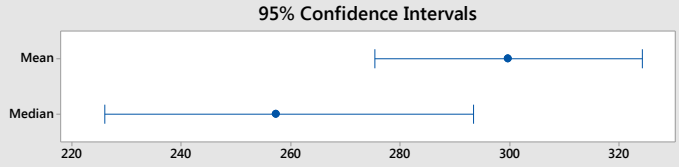


| Anderson-Darling Normality Test | |
|---|---|
| A-Squared | 5.04 |
| P-Value | <0.005 |
| Mean | 299.84 |
| StDev | 197.32 |
| Variance | 38935.87 |
| Skewness | 0.747185 |
| Kurtosis | -0.290202 |
| N | 252 |
| Minimum | 34.39 |
| 1st Quartile | 138.47 |
| Median | 257.30 |
| 3rd Quartile | 434.15 |
| Maximum | 873.22 |
| 95% Confidence Interval for Mean | |
| 275.36 | 324.32 |
| 95% Confidence Interval for Median | |
| 225.98 | 293.53 |
| 95% Confidence Interval for StDev | |
| 181.47 | 216.24 |

## LaGrange Grn #4 Texture: No Conditioning

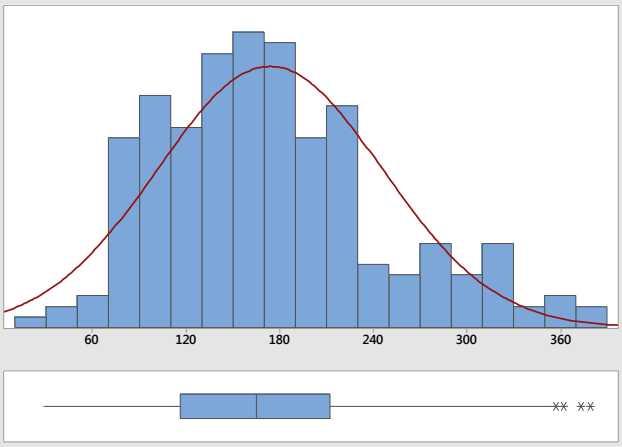




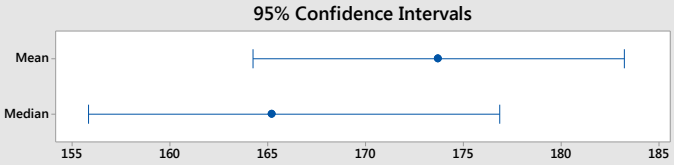


| Anderson-Darling Normality Test | |
|---|---|
| A-Squared | 2.35 |
| P-Value | <0.005 |
| Mean | 173.73 |
| StDev | 72.14 |
| Variance | 5204.88 |
| Skewness | 0.680859 |
| Kurtosis | 0.106469 |
| N | 224 |
| Minimum | 28.25 |
| 1st Quartile | 116.06 |
| Median | 165.19 |
| 3rd Quartile | 212.16 |
| Maximum | 379.50 |
| 95% Confidence Interval for Mean | |
| 164.23 | 183.23 |
| 95% Confidence Interval for Median | |
| 155.79 | 176.85 |
| 95% Confidence Interval for StDev | |
| 66.03 | 79.52 |

## LaGrange Grn #4 Texture: 20 minutes

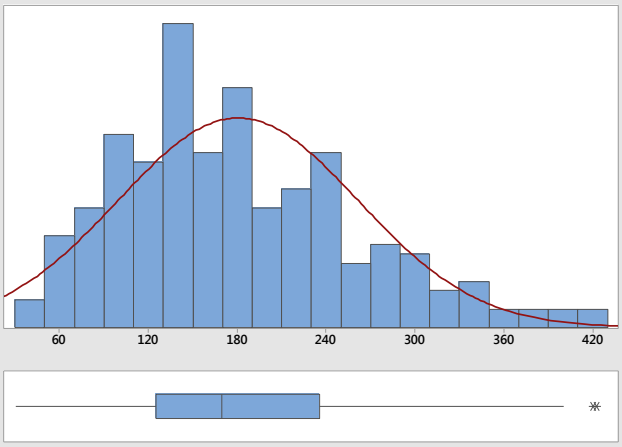




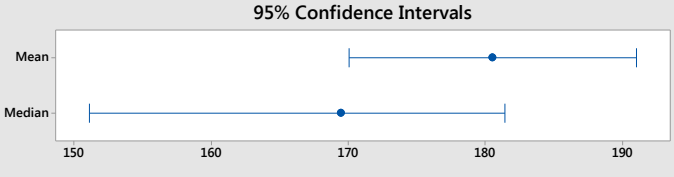


| Anderson-Darling Normality Test | |
|---|---|
| A-Squared | 2.34 |
| P-Value | <0.005 |
| Mean | 180.56 |
| StDev | 81.05 |
| Variance | 6568.46 |
| Skewness | 0.684445 |
| Kurtosis | 0.082141 |
| N | 231 |
| Minimum | 30.70 |
| 1st Quartile | 125.27 |
| Median | 169.49 |
| 3rd Quartile | 235.81 |
| Maximum | 422.48 |
| 95% Confidence Interval for Mean | |
| 170.06 | 191.07 |
| 95% Confidence Interval for Median | |
| 151.06 | 181.48 |
| 95% Confidence Interval for StDev | |
| 74.27 | 89.20 |

# LaGrange Grn #4 Texture: 40 minutes

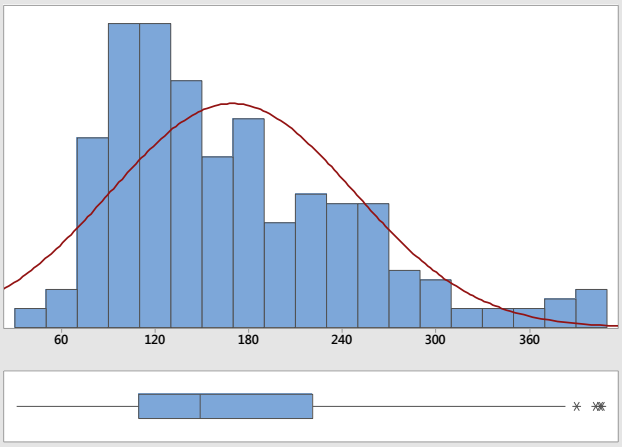




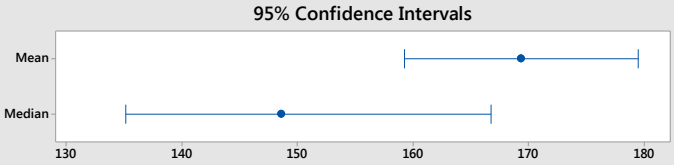


| Anderson-Darling Normality Test | |
|---|---|
| A-Squared | 4.97 |
| P-Value | <0.005 |
| Mean | 169.42 |
| StDev | 78.15 |
| Variance | 6107.65 |
| Skewness | 0.969563 |
| Kurtosis | 0.550153 |
| N | 231 |
| Minimum | 30.70 |
| 1st Quartile | 109.31 |
| Median | 148.61 |
| 3rd Quartile | 221.07 |
| Maximum | 406.52 |
| 95% Confidence Interval for Mean | |
| 159.29 | 179.55 |
| 95% Confidence Interval for Median | |
| 135.10 | 166.74 |
| 95% Confidence Interval for StDev | |
| 71.62 | 86.01 |

# LaGrange Grn #4 Texture: 60 minutes

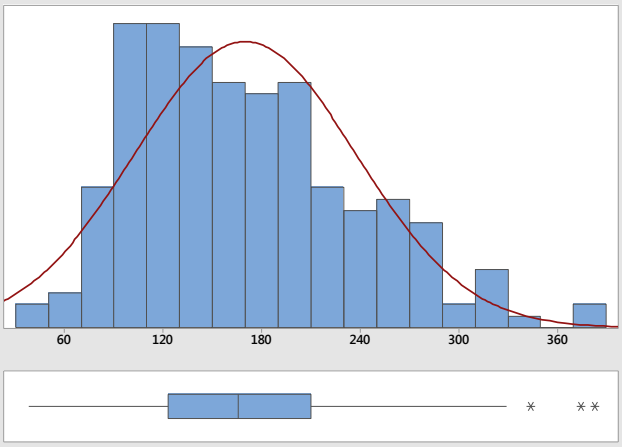




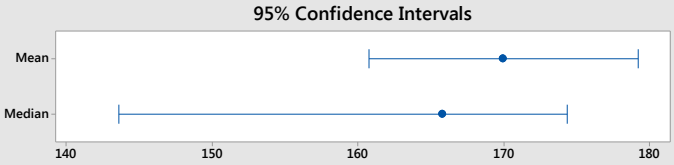


| Anderson-Darling Normality Test | |
|---|---|
| A-Squared | 1.96 |
| P-Value | <0.005 |
| Mean | 170.01 |
| StDev | 67.55 |
| Variance | 4563.04 |
| Skewness | 0.634809 |
| Kurtosis | 0.043058 |
| N | 207 |
| Minimum | 38.07 |
| 1st Quartile | 122.82 |
| Median | 165.80 |
| 3rd Quartile | 210.01 |
| Maximum | 383.18 |
| 95% Confidence Interval for Mean | |
| 160.76 | 179.27 |
| 95% Confidence Interval for Median | |
| 143.59 | 174.40 |
| 95% Confidence Interval for StDev | |
| 61.61 | 74.77 |

# LaGrange Grn #4 Texture: 80 minutes

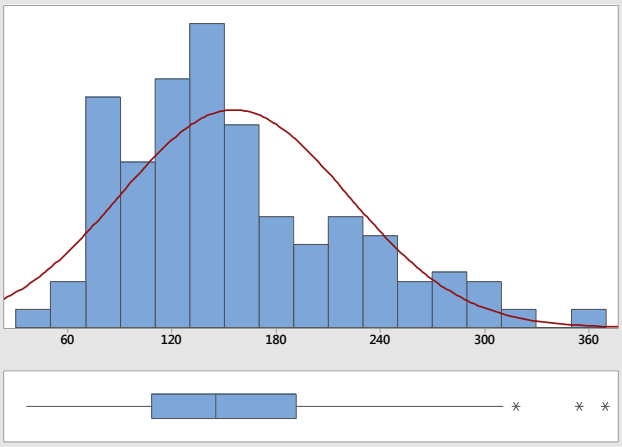




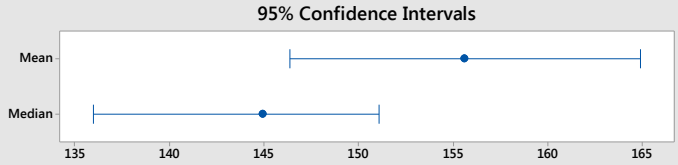


| Anderson-Darling Normality Test | |
|---|---|
| A-Squared | 3.07 |
| P-Value | <0.005 |
| Mean | 155.63 |
| StDev | 65.83 |
| Variance | 4334.11 |
| Skewness | 0.819843 |
| Kurtosis | 0.285430 |
| N | 195 |
| Minimum | 35.62 |
| 1st Quartile | 108.08 |
| Median | 144.92 |
| 3rd Quartile | 191.59 |
| Maximum | 369.67 |
| 95% Confidence Interval for Mean | |
| 146.34 | 164.93 |
| 95% Confidence Interval for Median | |
| 135.95 | 151.06 |
| 95% Confidence Interval for StDev | |
| 59.88 | 73.11 |

# LaGrange Grn #4 Texture: 100 minutes

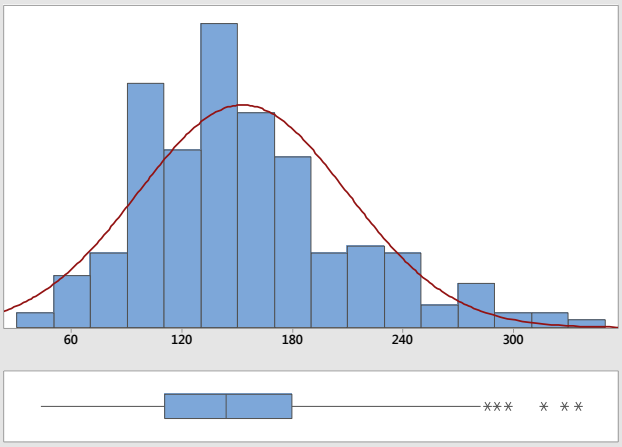




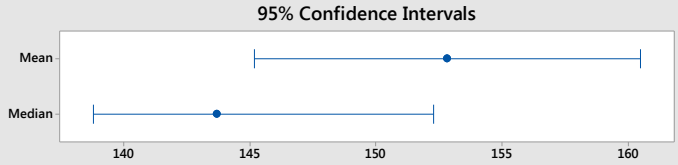


| Anderson-Darling Normality Test | |
|---|---|
| A-Squared | 2.65 |
| P-Value | <0.005 |
| Mean | 152.84 |
| StDev | 56.86 |
| Variance | 3233.13 |
| Skewness | 0.792056 |
| Kurtosis | 0.517640 |
| N | 214 |
| Minimum | 42.98 |
| 1st Quartile | 110.53 |
| Median | 143.69 |
| 3rd Quartile | 179.62 |
| Maximum | 335.29 |
| 95% Confidence Interval for Mean | |
| 145.18 | 160.50 |
| 95% Confidence Interval for Median | |
| 138.78 | 152.29 |
| 95% Confidence Interval for StDev | |
| 51.94 | 62.83 |

## Calera Lms #4 Texture: No Conditioning

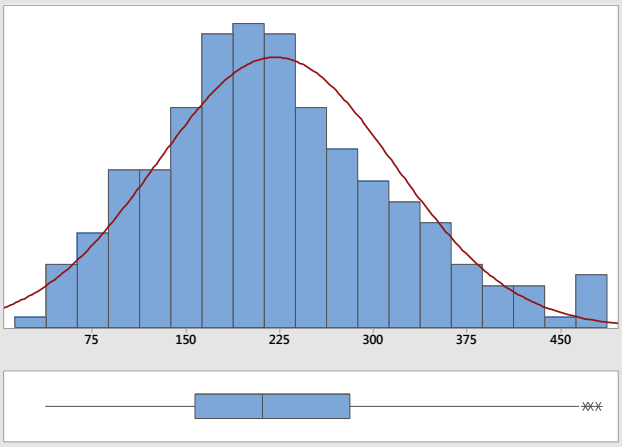




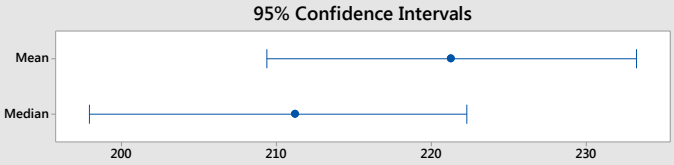


| Anderson-Darling Normality Test | |
|---|---|
| A-Squared | 1.27 |
| P-Value | <0.005 |
| Mean | 221.33 |
| StDev | 95.16 |
| Variance | 9056.00 |
| Skewness | 0.492699 |
| Kurtosis | -0.064465 |
| N | 246 |
| Minimum | 36.84 |
| 1st Quartile | 157.20 |
| Median | 211.24 |
| 3rd Quartile | 281.55 |
| Maximum | 480.21 |
| 95% Confidence Interval for Mean | |
| 209.38 | 233.28 |
| 95% Confidence Interval for Median | |
| 197.91 | 222.29 |
| 95% Confidence Interval for StDev | |
| 87.43 | 104.41 |

## Calera Lms #4 Texture: 20 minutes

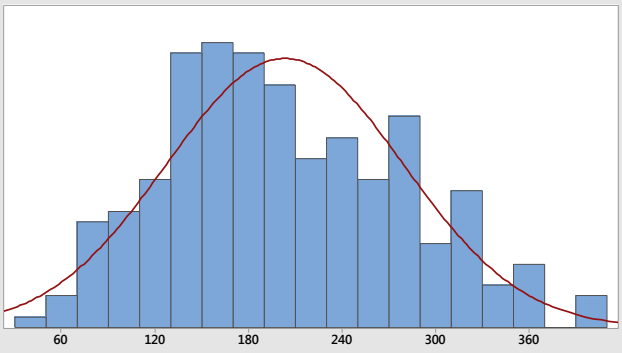


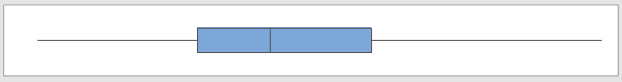

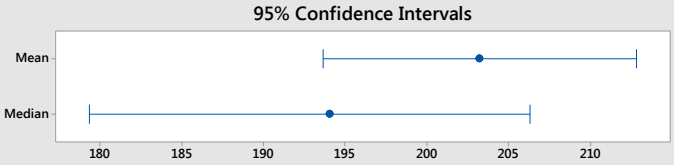


| Anderson-Darling Normality Test | |
|---|---|
| A-Squared | 1.20 |
| P-Value | <0.005 |
| Mean | 203.27 |
| StDev | 76.00 |
| Variance | 5775.74 |
| Skewness | 0.336623 |
| Kurtosis | -0.489565 |
| N | 243 |
| Minimum | 44.21 |
| 1st Quartile | 147.38 |
| Median | 194.05 |
| 3rd Quartile | 259.14 |
| Maximum | 406.52 |
| 95% Confidence Interval for Mean | |
| 193.66 | 212.87 |
| 95% Confidence Interval for Median | |
| 179.31 | 206.33 |
| 95% Confidence Interval for StDev | |
| 69.79 | 83.43 |

## Calera Lms #4 Texture: 40 minutes

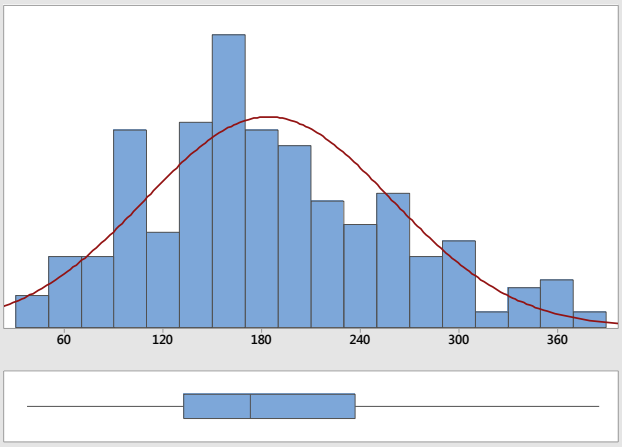




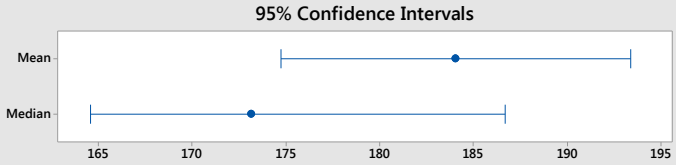


| Anderson-Darling Normality Test | |
|---|---|
| A-Squared | 1.35 |
| P-Value | <0.005 |
| Mean | 184.06 |
| StDev | 75.19 |
| Variance | 5652.87 |
| Skewness | 0.436187 |
| Kurtosis | -0.249122 |
| N | 251 |
| Minimum | 36.84 |
| 1st Quartile | 132.64 |
| Median | 173.17 |
| 3rd Quartile | 237.03 |
| Maximum | 385.64 |
| 95% Confidence Interval for Mean | |
| 174.71 | 193.40 |
| 95% Confidence Interval for Median | |
| 164.57 | 186.68 |
| 95% Confidence Interval for StDev | |
| 69.13 | 82.41 |

## Calera Lms #4 Texture: 60 minutes

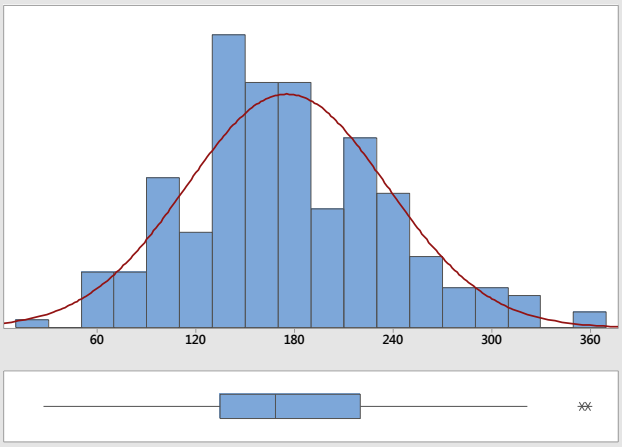




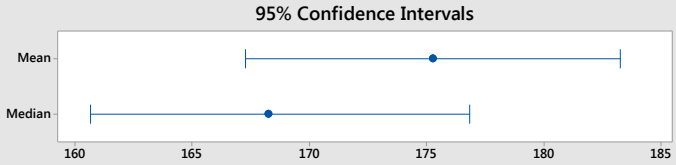


| Anderson-Darling Normality Test | |
|---|---|
| A-Squared | 0.81 |
| P-Value | 0.036 |
| Mean | 175.28 |
| StDev | 61.08 |
| Variance | 3731.03 |
| Skewness | 0.355831 |
| Kurtosis | 0.018202 |
| N | 226 |
| Minimum | 27.02 |
| 1st Quartile | 134.79 |
| Median | 168.26 |
| 3rd Quartile | 220.15 |
| Maximum | 358.62 |
| 95% Confidence Interval for Mean | |
| 167.27 | 183.28 |
| 95% Confidence Interval for Median | |
| 160.63 | 176.85 |
| 95% Confidence Interval for StDev | |
| 55.92 | 67.30 |

# Calera Lms #4 Texture: 80 minutes

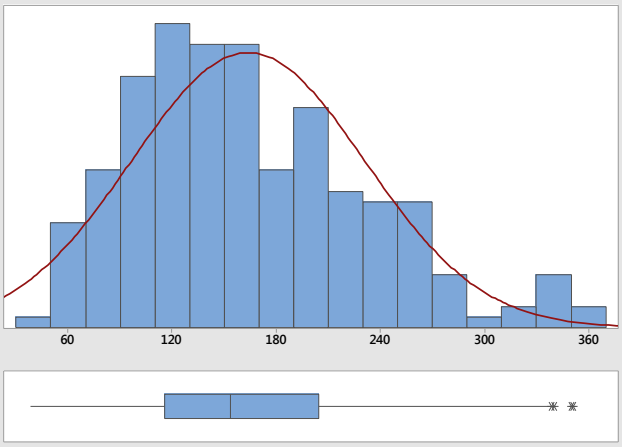




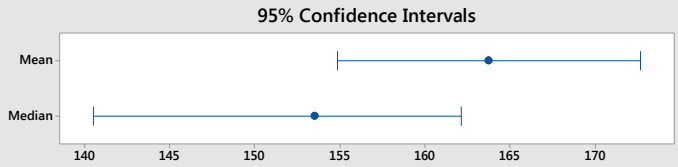


| Anderson-Darling Normality Test | |
|---|---|
| A-Squared | 2.20 |
| P-Value | <0.005 |
| Mean | 163.77 |
| StDev | 67.23 |
| Variance | 4519.84 |
| Skewness | 0.679216 |
| Kurtosis | 0.074712 |
| N | 221 |
| Minimum | 38.07 |
| 1st Quartile | 115.45 |
| Median | 153.52 |
| 3rd Quartile | 204.49 |
| Maximum | 351.25 |
| 95% Confidence Interval for Mean | |
| 154.86 | 172.68 |
| 95% Confidence Interval for Median | |
| 140.49 | 162.12 |
| 95% Confidence Interval for StDev | |
| 61.49 | 74.16 |

# Calera Lms #4 Texture: 100 minutes

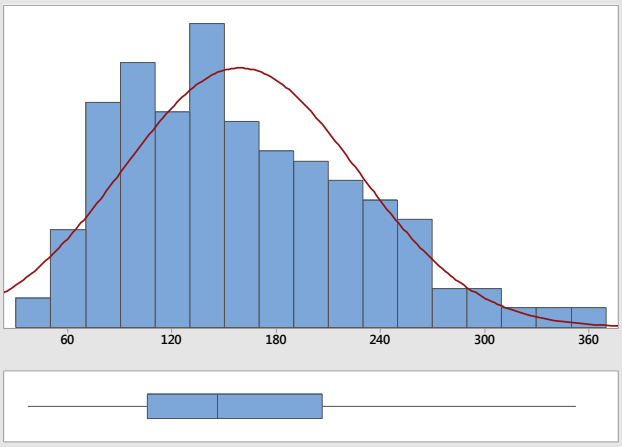




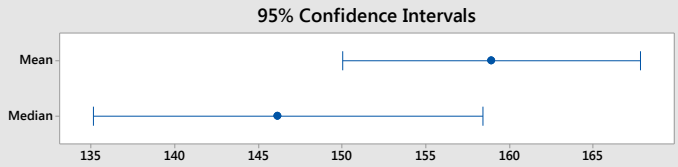


| Anderson-Darling Normality Test | |
|---|---|
| A-Squared | 2.09 |
| P-Value | <0.005 |
| Mean | 158.96 |
| StDev | 67.80 |
| Variance | 4597.19 |
| Skewness | 0.601943 |
| Kurtosis | -0.175702 |
| N | 225 |
| Minimum | 36.84 |
| 1st Quartile | 105.62 |
| Median | 146.15 |
| 3rd Quartile | 206.33 |
| Maximum | 352.48 |
| 95% Confidence Interval for Mean | |
| 150.05 | 167.87 |
| 95% Confidence Interval for Median | |
| 135.10 | 158.43 |
| 95% Confidence Interval for StDev | |
| 62.06 | 74.72 |

## Appendix B: AIMS-II Test Repeatability for Angularity, Texture, and Two-Dimensional Form Results

| Opelika Lms #4: Angularity | | | | | | |
|---|---|---|---|---|---|---|
| Conditioning Time (min) | Overall Average | Lower Limit | Upper Limit | Replicate 1 Average | Replicate 2 Average | Replicate 3 Average |
| 0 | 2851.70 | 2769.00 | 2934.40 | 2847.91 | 2852.37 | 2854.43 |
| 20 | 2345.80 | 2277.77 | 2413.83 | 2405.99 | 22879.90 | 2351.05 |
| 40 | 2193.60 | 2130.00 | 2257.20 | 2218.10 | 2152.63 | 2210.70 |
| 60 | 2084.50 | 2024.05 | 2144.95 | 2082.62 | 2085.30 | 2085.68 |
| 80 | 2005.80 | 1947.63 | 2063.97 | 2007.56 | 2062.05 | 1947.88 |
| 100 | 2062.60 | 2002.80 | 2122.40 | 2103.40 | 2041.80 | 2042.02 |

| Columbus Grn #4: Angularity | | | | | | |
|---|---|---|---|---|---|---|
| Conditioning Time (min) | Overall Average | Lower Limit | Upper Limit | Replicate 1 Average | Replicate 2 Average | Replicate 3 Average |
| 0 | 2987.60 | 2900.96 | 3074.24 | 2923.36 | 2999.09 | 3038.28 |
| 20 | 2867.00 | 2783.86 | 2950.14 | 2847.15 | 2826.94 | 2930.19 |
| 40 | 2692.40 | 2614.32 | 2770.48 | 2700.67 | 2665.14 | 2712.72 |
| 60 | 2614.10 | 2538.29 | 2689.91 | 2581.98 | 2632.64 | 2626.54 |
| 80 | 2483.20 | 2411.19 | 2555.21 | 2462.28 | 2489.00 | 2495.99 |
| 100 | 2500.90 | 2428.40 | 2573.40 | 2468.80 | 2485.40 | 2548.30 |

| LaGrange Grn #4: Angularity | | | | | | |
|---|---|---|---|---|---|---|
| Conditioning Time (min) | Overall Average | Lower Limit | Upper Limit | Replicate 1 Average | Replicate 2 Average | Replicate 3 Average |
| 0 | 2809.90 | 2728.41 | 2891.39 | 2821.35 | 2783.50 | 2823.56 |
| 20 | 2449.40 | 2378.37 | 2520.43 | 2407.12 | 2454.96 | 2484.04 |
| 40 | 2390.30 | 2320.98 | 2459.62 | 2433.57 | 2376.25 | 2362.95 |
| 60 | 2390.00 | 2320.69 | 2459.31 | 2387.12 | 2335.57 | 2454.11 |
| 80 | 2339.90 | 2272.04 | 2407.76 | 2373.09 | 2297.67 | 2348.94 |
| 100 | 2268.30 | 2202.50 | 2334.10 | 2341.90 | 2246.40 | 2216.70 |

| Calera Lms #4: Angularity | | | | | | |
|---|---|---|---|---|---|---|
| Conditioning Time (min) | Overall Average | Lower Limit | Upper Limit | Replicate 1 Average | Replicate 2 Average | Replicate 3 Average |
| 0 | 2654.20 | 2577.23 | 2731.17 | 2699.72 | 2615.61 | 2642.64 |
| 20 | 2422.20 | 2351.96 | 2492.44 | 2382.17 | 2492.48 | 2392.04 |
| 40 | 2295.10 | 2228.54 | 2361.66 | 2272.87 | 2312.71 | 2302.87 |
| 60 | 2191.70 | 2128.14 | 2255.26 | 2177.20 | 2237.57 | 2160.31 |
| 80 | 2221.00 | 2156.60 | 2285.40 | 2265.70 | 2220.97 | 2182.59 |
| 100 | 2141.60 | 2079.50 | 2203.70 | 2100.18 | 2181.60 | 2146.96 |

| Bauxite #16: Angularity | | | | | | |
|---|---|---|---|---|---|---|
| Conditioning Time (min) | Overall Average | Lower Limit | Upper Limit | Replicate 1 Average | Replicate 2 Average | Replicate 3 Average |
| 0 | 2960.40 | 2874.55 | 3046.25 | 2963.66 | 2957.89 | 2959.94 |
| 10 | 2935.30 | 2850.18 | 3020.42 | 2986.51 | 2912.45 | 2909.92 |
| 20 | 2750.50 | 2670.70 | 2830.30 | 2739.10 | 2742.90 | 2769.70 |
| 30 | 2708.50 | 2629.95 | 2787.05 | 2689.30 | 2737.40 | 2698.30 |

| Opelika Lms #16: Angularity | | | | | | |
|---|---|---|---|---|---|---|
| Conditioning Time (min) | Overall Average | Lower Limit | Upper Limit | Replicate 1 Average | Replicate 2 Average | Replicate 3 Average |
| 0 | 3603.30 | 3498.80 | 3707.80 | 3652.10 | 3578.34 | 3568.74 |
| 10 | 3494.20 | 3392.87 | 3595.53 | 3467.47 | 3471.37 | 3550.30 |
| 20 | 3362.90 | 3265.38 | 3460.42 | 3345.54 | 3415.44 | 3318.33 |
| 30 | 3282.60 | 3187.40 | 3377.80 | 3286.31 | 3316.85 | 3249.45 |

| Columbus Grn #16: Angularity | | | | | | |
|---|---|---|---|---|---|---|
| Conditioning Time (min) | Overall Average | Lower Limit | Upper Limit | Replicate 1 Average | Replicate 2 Average | Replicate 3 Average |
| 0 | 4274.90 | 4150.93 | 4398.87 | 4305.83 | 4287.96 | 4233.23 |
| 10 | 3602.10 | 3497.64 | 3706.56 | 3670.75 | 3549.57 | 3594.72 |
| 20 | 3288.30 | 3192.94 | 3383.66 | 3277.12 | 3261.07 | 3321.33 |
| 30 | 3143.40 | 3052.24 | 3234.56 | 3136.86 | 3172.82 | 3126.67 |

| LaGrange Grn #16: Angularity | | | | | | |
|---|---|---|---|---|---|---|
| Conditioning Time (min) | Overall Average | Lower Limit | Upper Limit | Replicate 1 Average | Replicate 2 Average | Replicate 3 Average |
| 0 | 4039.60 | 3922.45 | 4156.75 | 4016.65 | 4075.12 | 4026.50 |
| 10 | 3513.50 | 3411.61 | 3615.39 | 3422.21 | 3622.14 | 3500.21 |
| 20 | 3311.00 | 3214.98 | 3407.02 | 3345.32 | 3316.00 | 3273.89 |
| 30 | 3127.70 | 3037.00 | 3218.40 | 3082.39 | 3133.97 | 3162.62 |

| Calera Lms #16: Angularity | | | | | | |
|---|---|---|---|---|---|---|
| Conditioning Time (min) | Overall Average | Lower Limit | Upper Limit | Replicate 1 Average | Replicate 2 Average | Replicate 3 Average |
| 0 | 30.69.10 | 2980.1 | 3158.1 | 3080.62 | 3083.61 | 3039.25 |
| 10 | 2791.40 | 2710.45 | 2872.35 | 2823.65 | 2750.7 | 2796.37 |
| 20 | 2687.90 | 2611.95 | 2765.85 | 2705.36 | 2685.99 | 2674.91 |
| 30 | 2472.10 | 2400.4 | 2543.8 | 2475.68 | 2516.11 | 2413.33 |

| Opelika Lms #4: Texture | | | | | | |
|---|---|---|---|---|---|---|
| Conditioning Time (min) | Overall Average | Lower Limit | Upper Limit | Replicate 1 Average | Replicate 2 Average | Replicate 3 Average |
| 0 | 115.16 | 109.98 | 120.34 | 103.37 | 127.15 | 116.01 |
| 20 | 96.64 | 92.29 | 100.99 | 90.22 | 98.00 | 101.96 |
| 40 | 103.25 | 98.60 | 107.90 | 106.93 | 102.17 | 100.52 |
| 60 | 86.51 | 82.62 | 90.41 | 84.96 | 93.23 | 81.68 |
| 80 | 85.88 | 82.02 | 89.75 | 89.01 | 92.36 | 76.17 |
| 100 | 87.80 | 83.85 | 91.75 | 87.09 | 84.31 | 92.23 |

| Columbus Grn #4: Texture | | | | | | |
|---|---|---|---|---|---|---|
| Conditioning Time (min) | Overall Average | Lower Limit | Upper Limit | Replicate 1 Average | Replicate 2 Average | Replicate 3 Average |
| 0 | 333.95 | 318.92 | 348.98 | 344.87 | 322.10 | 335.74 |
| 20 | 314.73 | 300.57 | 328.89 | 328.08 | 294.69 | 319.96 |
| 40 | 315.67 | 301.46 | 329.88 | 330.51 | 299.82 | 318.25 |
| 60 | 315.29 | 301.10 | 329.48 | 301.33 | 320.62 | 323.55 |
| 80 | 286.84 | 273.93 | 299.75 | 278.63 | 285.20 | 295.40 |
| 100 | 299.84 | 286.35 | 313.33 | 321.40 | 292.93 | 285.42 |

| LaGrange Grn #4: Texture | | | | | | |
|---|---|---|---|---|---|---|
| Conditioning Time (min) | Overall Average | Lower Limit | Upper Limit | Replicate 1 Average | Replicate 2 Average | Replicate 3 Average |
| 0 | 173.73 | 165.91 | 181.55 | 159.75 | 184.28 | 178.43 |
| 20 | 180.56 | 172.43 | 188.68 | 172.39 | 180.65 | 188.24 |
| 40 | 169.42 | 161.80 | 177.04 | 176.44 | 166.28 | 165.83 |
| 60 | 170.01 | 162.36 | 177.66 | 166.76 | 166.44 | 177.98 |
| 80 | 155.63 | 148.63 | 162.63 | 150.83 | 173.48 | 138.37 |
| 100 | 152.84 | 146.00 | 159.72 | 148.50 | 152.30 | 158.14 |

| Calera Lms #4: Texture | | | | | | |
|---|---|---|---|---|---|---|
| Conditioning Time (min) | Overall Average | Lower Limit | Upper Limit | Replicate 1 Average | Replicate 2 Average | Replicate 3 Average |
| 0 | 221.33 | 211.37 | 231.29 | 213.35 | 206.36 | 244.60 |
| 20 | 203.27 | 194.12 | 212.42 | 215.43 | 198.17 | 194.75 |
| 40 | 184.06 | 175.78 | 192.34 | 185.57 | 182.64 | 183.70 |
| 60 | 175.28 | 167.39 | 183.17 | 173.81 | 169.94 | 182.04 |
| 80 | 163.77 | 156.40 | 171.14 | 159.81 | 162.48 | 168.29 |
| 100 | 158.96 | 151.80 | 166.10 | 155.68 | 157.47 | 163.44 |

| Bauxite #16: Form 2D | | | | | | |
|---|---|---|---|---|---|---|
| Conditioning Time (min) | Overall Average | Lower Limit | Upper Limit | Replicate 1 Average | Replicate 2 Average | Replicate 3 Average |
| 0 | 7.19 | 6.99 | 7.39 | 7.28 | 7.13 | 7.19 |
| 10 | 7.12 | 6.91 | 7.33 | 7.28 | 7.01 | 7.10 |
| 20 | 6.93 | 6.74 | 7.12 | 6.97 | 6.77 | 7.04 |
| 30 | 6.95 | 6.76 | 7.14 | 6.98 | 6.94 | 6.93 |

| Opelika Lms #16: Form 2D | | | | | | |
|---|---|---|---|---|---|---|
| Conditioning Time (min) | Overall Average | Lower Limit | Upper Limit | Replicate 1 Average | Replicate 2 Average | Replicate 3 Average |
| 0 | 8.79 | 8.55 | 9.03 | 8.66 | 8.97 | 8.77 |
| 10 | 8.31 | 8.08 | 8.53 | 8.05 | 8.37 | 8.56 |
| 20 | 8.15 | 7.93 | 8.37 | 7.92 | 8.25 | 8.28 |
| 30 | 7.90 | 7.69 | 8.11 | 7.88 | 7.91 | 7.90 |

| Columbus Grn #16: Form 2D | | | | | | |
|---|---|---|---|---|---|---|
| Conditioning Time (min) | Overall Average | Lower Limit | Upper Limit | Replicate 1 Average | Replicate 2 Average | Replicate 3 Average |
| 0 | 8.72 | 8.47 | 8.94 | 8.59 | 8.93 | 8.64 |
| 10 | 7.49 | 7.29 | 7.69 | 7.55 | 7.45 | 7.47 |
| 20 | 7.26 | 7.06 | 7.45 | 7.24 | 7.32 | 7.21 |
| 30 | 6.99 | 6.80 | 7.18 | 7.04 | 7.08 | 6.88 |

| LaGrange Grn #16: Form 2D | | | | | | |
|---|---|---|---|---|---|---|
| Conditioning Time (min) | Overall Average | Lower Limit | Upper Limit | Replicate 1 Average | Replicate 2 Average | Replicate 3 Average |
| 0 | 8.25 | 8.03 | 8.47 | 8.20 | 8.46 | 8.09 |
| 10 | 7.56 | 7.36 | 7.77 | 7.58 | 7.52 | 7.59 |
| 20 | 7.06 | 6.87 | 7.25 | 6.98 | 7.06 | 7.13 |
| 30 | 6.84 | 6.66 | 7.02 | 6.89 | 6.73 | 6.90 |

| Calera Lms #16: Form 2D | | | | | | |
|---|---|---|---|---|---|---|
| Conditioning Time (min) | Overall Average | Lower Limit | Upper Limit | Replicate 1 Average | Replicate 2 Average | Replicate 3 Average |
| 0 | 7.83 | 7.62 | 8.04 | 7.72 | 7.94 | 7.83 |
| 10 | 7.43 | 7.23 | 7.63 | 7.50 | 7.31 | 7.46 |
| 20 | 7.26 | 7.07 | 7.46 | 7.07 | 7.24 | 7.45 |
| 30 | 6.81 | 6.63 | 6.99 | 6.75 | 6.80 | 6.89 |

## Appendix C: Cumulative Distribution Trends of AIMS-II Results

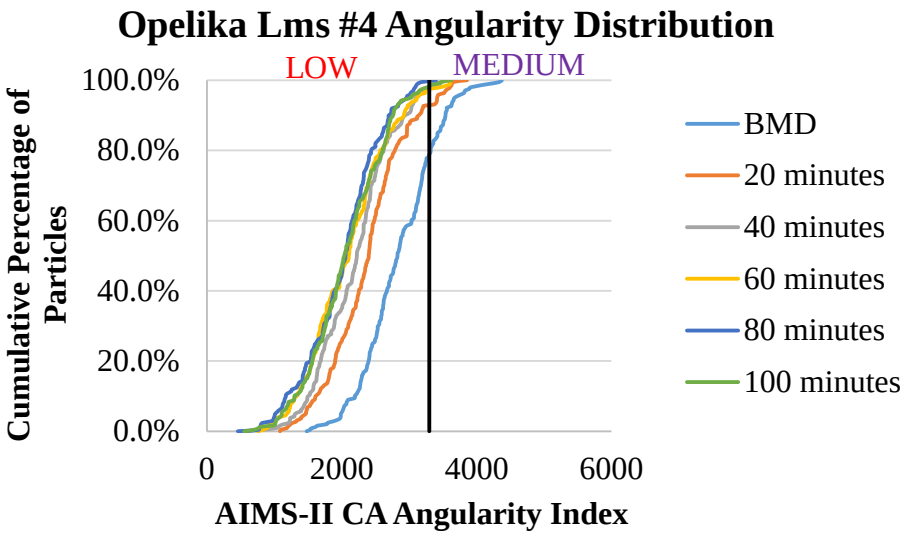


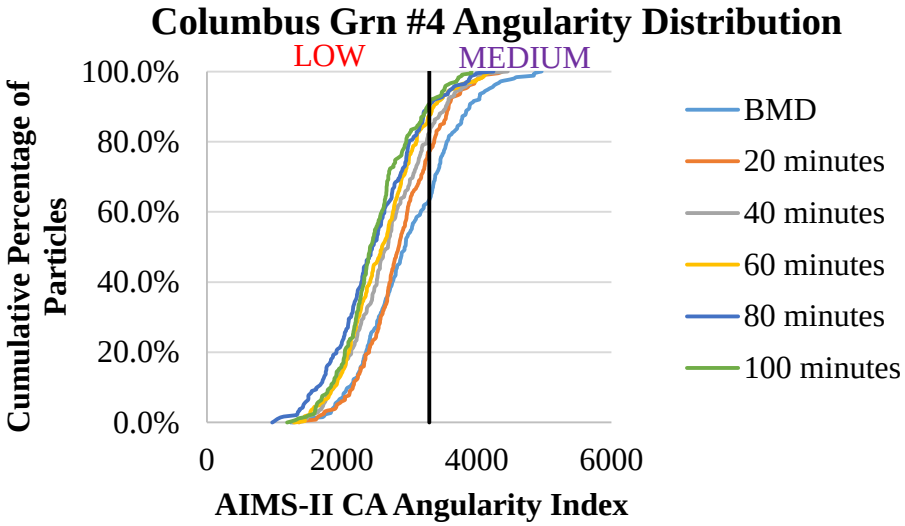

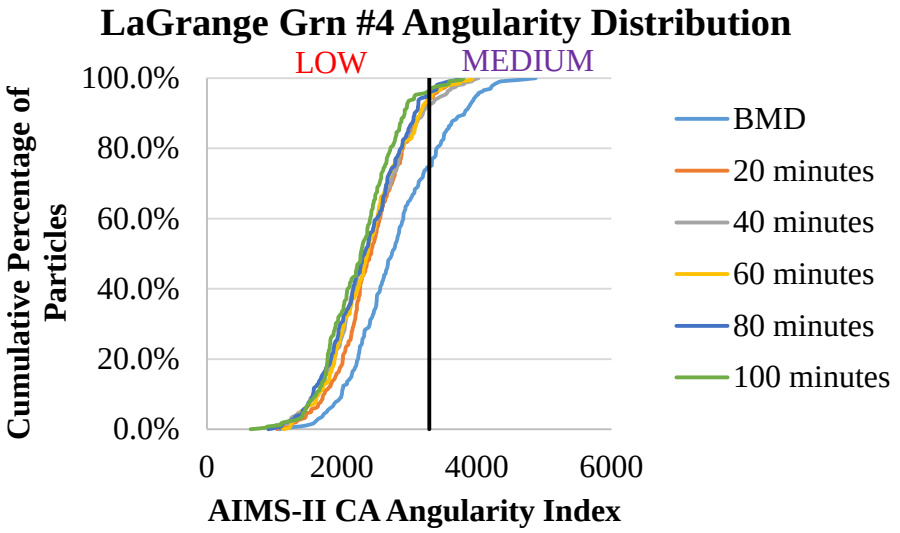
LaGrange Grn #4 Angularity Distribution
LOW
MEDIUM
Cumulative Percentage of Particles
100.0%
80.0%
60.0%
40.0%
20.0%
0.0%
0
2000
4000
6000
AIMS-II CA Angularity Index
BMD
20 minutes
40 minutes
60 minutes
80 minutes
100 minutes

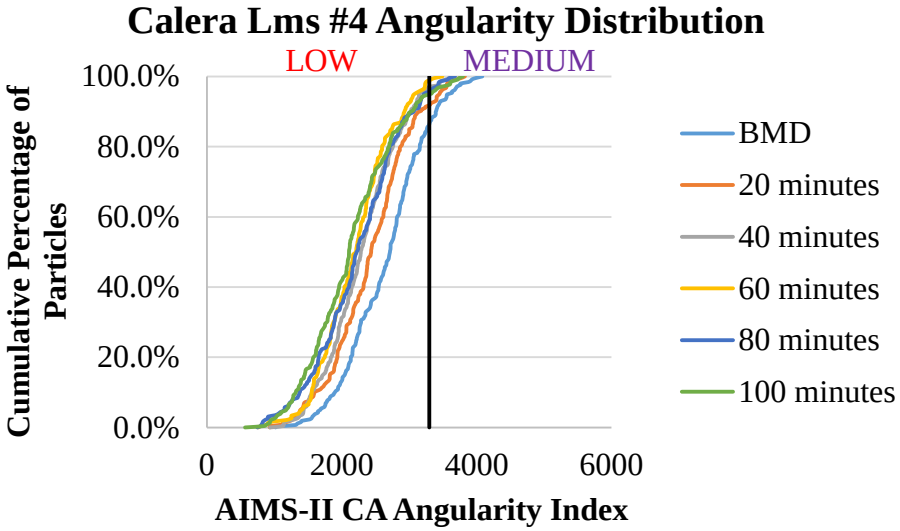
Calera Lms #4 Angularity Distribution
LOW
MEDIUM
Cumulative Percentage of Particles
100.0%
80.0%
60.0%
40.0%
20.0%
0.0%
0
2000
4000
6000
AIMS-II CA Angularity Index
BMD
20 minutes
40 minutes
60 minutes
80 minutes
100 minutes

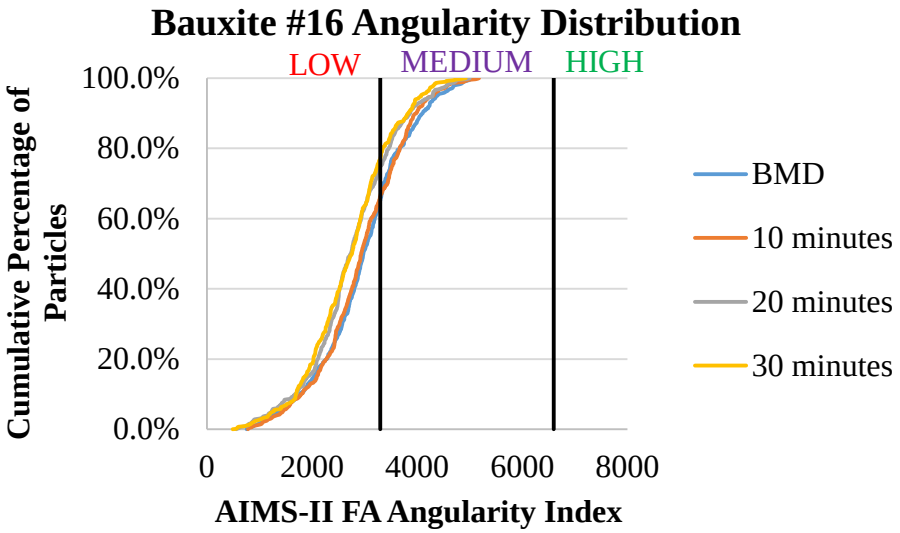
Bauxite #16 Angularity Distribution
LOW
MEDIUM
HIGH
100.0%
80.0%
60.0%
40.0%
20.0%
0.0%
Cumulative Percentage of Particles
0
2000
4000
6000
8000
AIMS-II FA Angularity Index
BMD
10 minutes
20 minutes
30 minutes

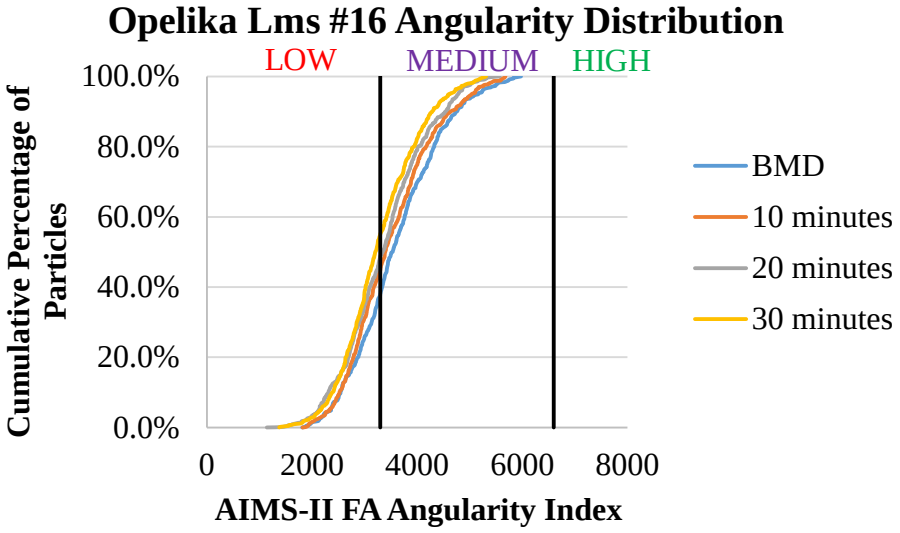
Opelika Lms #16 Angularity Distribution
LOW
MEDIUM
HIGH
100.0%
80.0%
60.0%
40.0%
20.0%
0.0%
Cumulative Percentage of Particles
0
2000
4000
6000
8000
AIMS-II FA Angularity Index
BMD
10 minutes
20 minutes
30 minutes

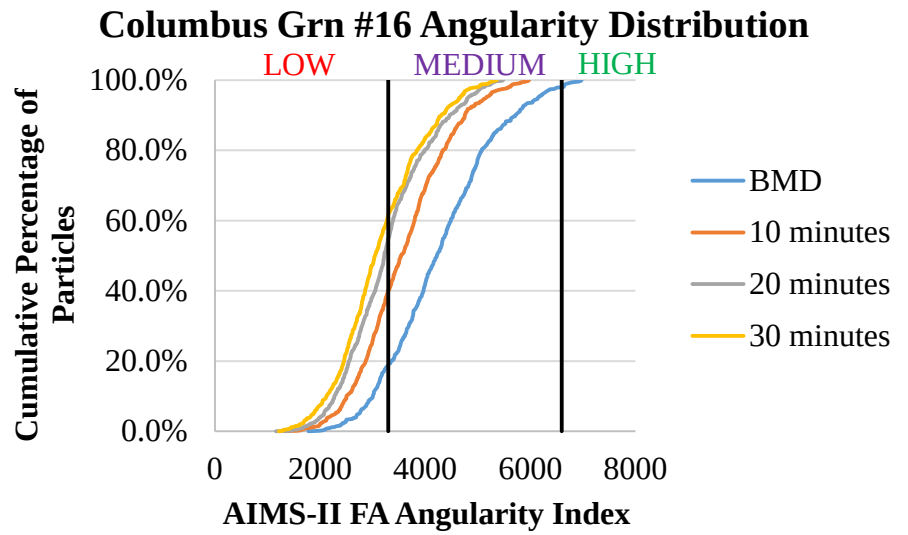
Columbus Grn #16 Angularity Distribution
LOW
MEDIUM
HIGH
100.0%
80.0%
60.0%
40.0%
20.0%
0.0%
Cumulative Percentage of Particles
0
2000
4000
6000
8000
AIMS-II FA Angularity Index
BMD
10 minutes
20 minutes
30 minutes

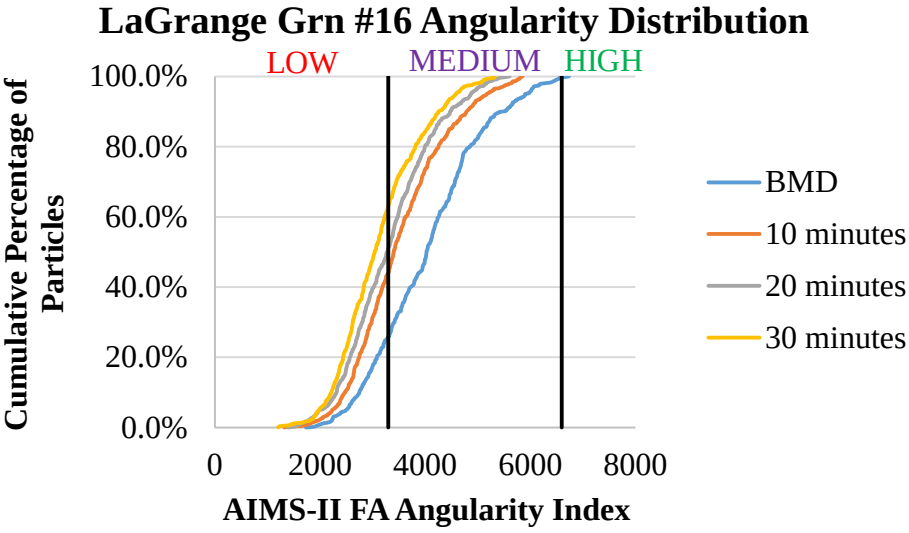
LaGrange Grn #16 Angularity Distribution
LOW
MEDIUM
HIGH
100.0%
80.0%
60.0%
40.0%
20.0%
0.0%
Cumulative Percentage of Particles
0
2000
4000
6000
8000
AIMS-II FA Angularity Index
BMD
10 minutes
20 minutes
30 minutes

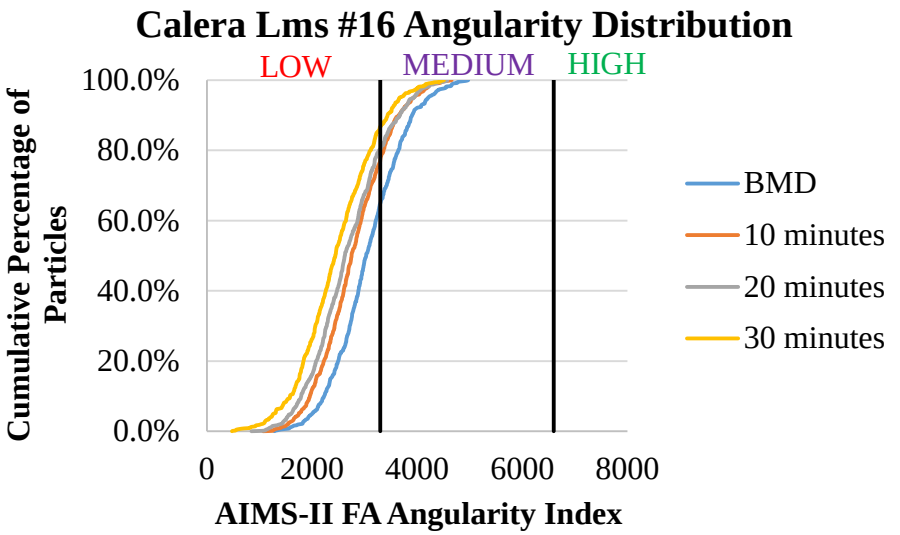
Calera Lms #16 Angularity Distribution
LOW
MEDIUM
HIGH
100.0%
80.0%
60.0%
40.0%
20.0%
0.0%
Cumulative Percentage of Particles
0
2000
4000
6000
8000
AIMS-II FA Angularity Index
BMD
10 minutes
20 minutes
30 minutes

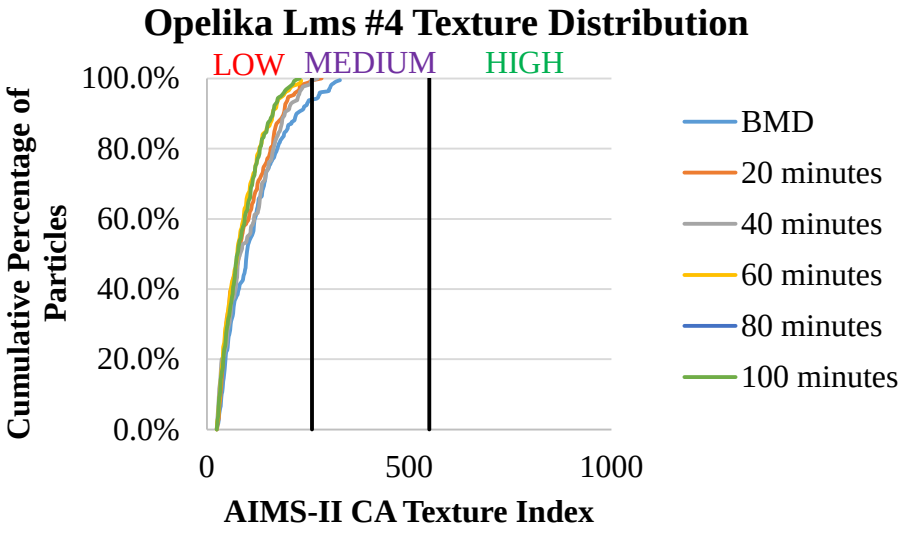
Opelika Lms #4 Texture Distribution
LOW
MEDIUM
HIGH
100.0%
80.0%
60.0%
40.0%
20.0%
0.0%
Cumulative Percentage of Particles
0
500
1000
AIMS-II CA Texture Index
BMD
20 minutes
40 minutes
60 minutes
80 minutes
100 minutes

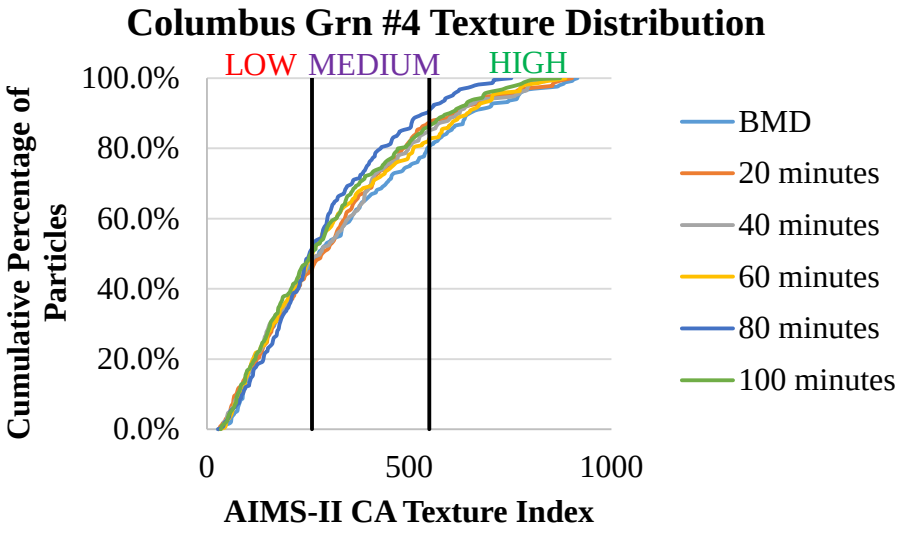
Columbus Grn #4 Texture Distribution
LOW
MEDIUM
HIGH
100.0%
80.0%
60.0%
40.0%
20.0%
0.0%
Cumulative Percentage of Particles
0
500
1000
AIMS-II CA Texture Index
BMD
20 minutes
40 minutes
60 minutes
80 minutes
100 minutes

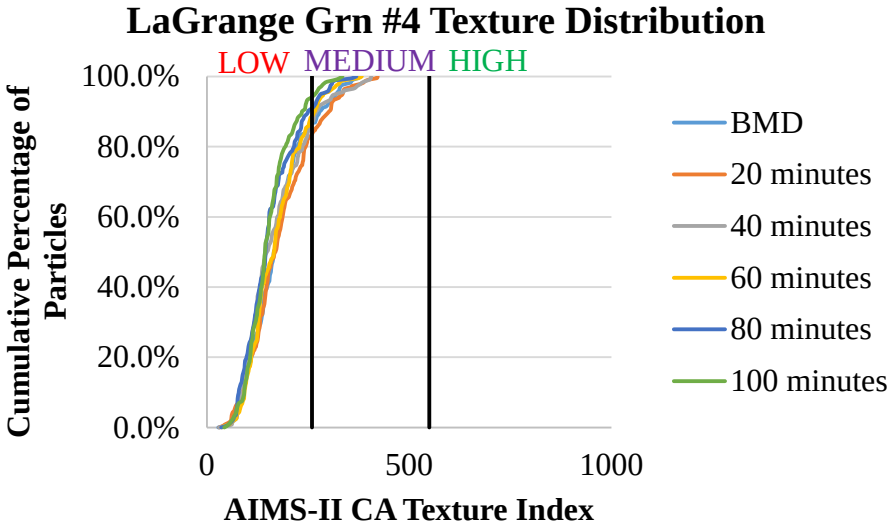
LaGrange Grn #4 Texture Distribution
LOW
MEDIUM
HIGH
100.0%
80.0%
60.0%
40.0%
20.0%
0.0%
Cumulative Percentage of Particles
0
500
1000
AIMS-II CA Texture Index
BMD
20 minutes
40 minutes
60 minutes
80 minutes
100 minutes

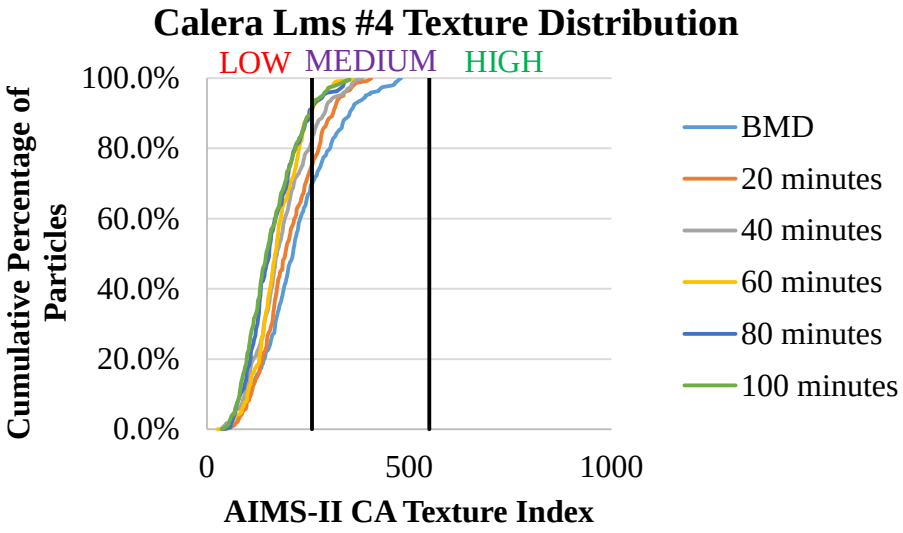
Calera Lms #4 Texture Distribution
LOW
MEDIUM
HIGH
100.0%
80.0%
60.0%
40.0%
20.0%
0.0%
Cumulative Percentage of Particles
0
500
1000
AIMS-II CA Texture Index
BMD
20 minutes
40 minutes
60 minutes
80 minutes
100 minutes

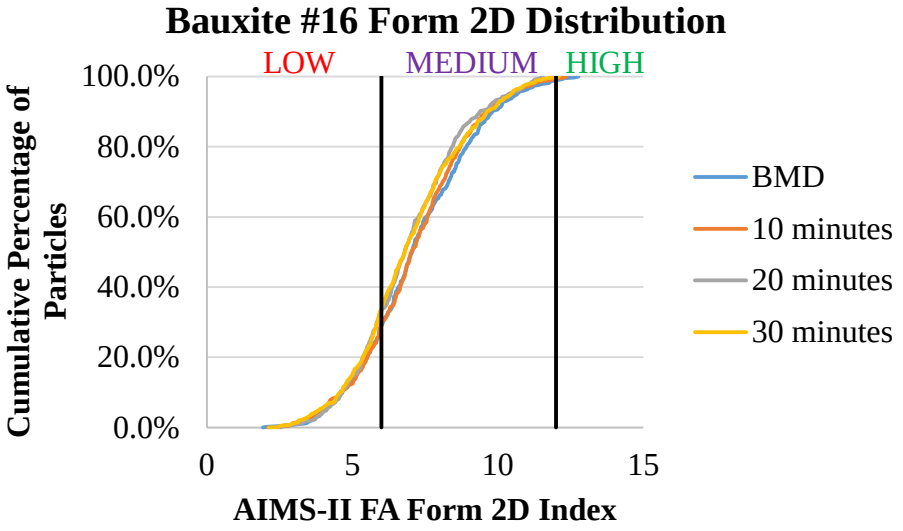
Bauxite #16 Form 2D Distribution
LOW
MEDIUM
HIGH
100.0%
80.0%
60.0%
40.0%
20.0%
0.0%
Cumulative Percentage of Particles
0
5
10
15
AIMS-II FA Form 2D Index
BMD
10 minutes
20 minutes
30 minutes

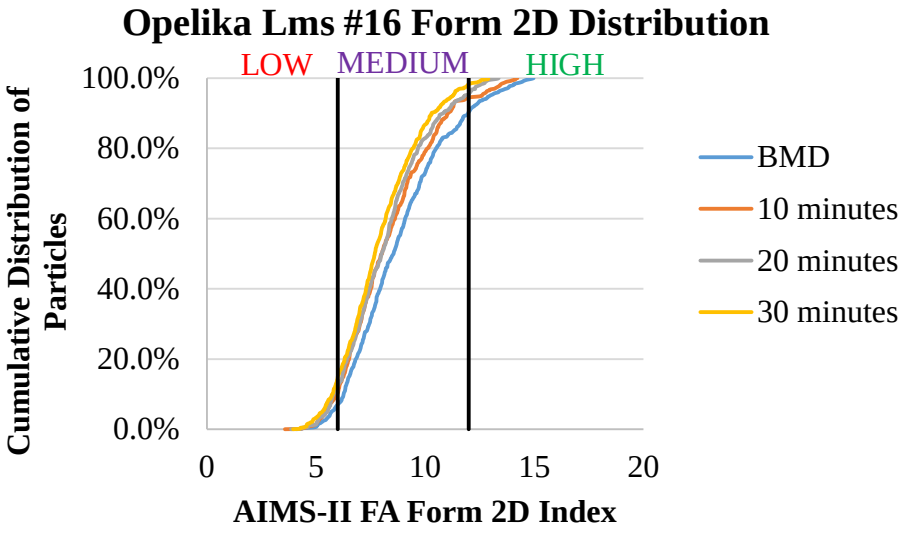
Opelika Lms #16 Form 2D Distribution
LOW
MEDIUM
HIGH
100.0%
80.0%
60.0%
40.0%
20.0%
0.0%
Cumulative Distribution of Particles
0
5
10
15
20
AIMS-II FA Form 2D Index
BMD
10 minutes
20 minutes
30 minutes

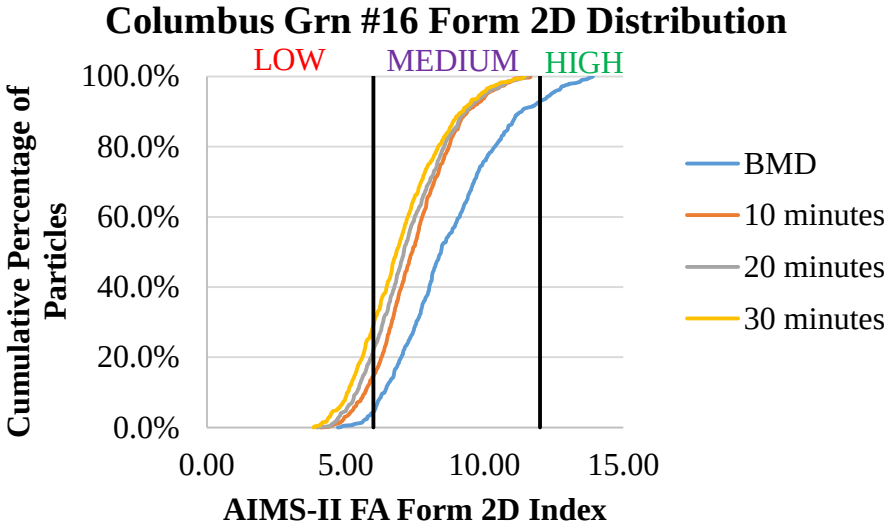
Columbus Grn #16 Form 2D Distribution
LOW
MEDIUM
HIGH
100.0%
80.0%
60.0%
40.0%
20.0%
0.0%
Cumulative Percentage of Particles
0.00
5.00
10.00
15.00
AIMS-II FA Form 2D Index
BMD
10 minutes
20 minutes
30 minutes

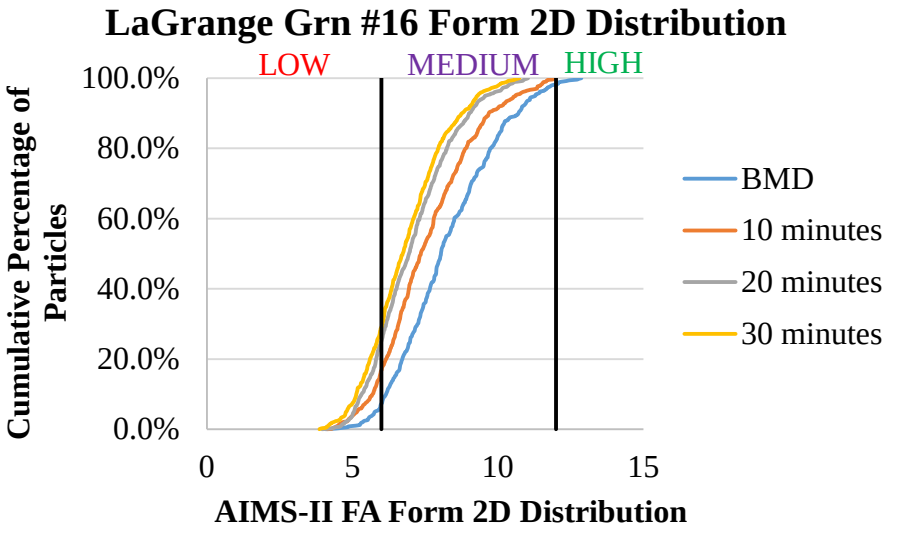
LaGrange Grn #16 Form 2D Distribution
LOW
MEDIUM
HIGH
100.0%
80.0%
60.0%
40.0%
20.0%
0.0%
Cumulative Percentage of Particles
0
5
10
15
AIMS-II FA Form 2D Distribution
BMD
10 minutes
20 minutes
30 minutes

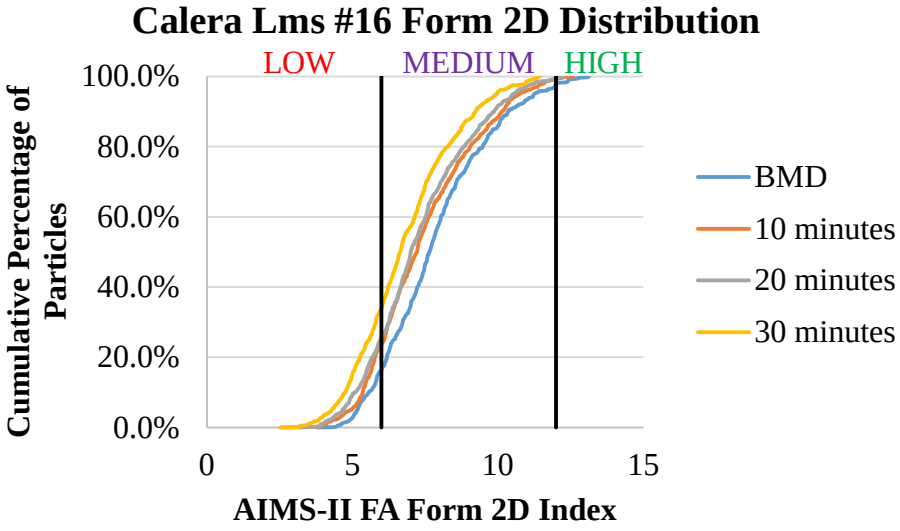
Calera Lms #16 Form 2D Distribution
LOW
MEDIUM
HIGH
100.0%
80.0%
60.0%
40.0%
20.0%
0.0%
Cumulative Percentage of Particles
0
5
10
15
AIMS-II FA Form 2D Index
BMD
10 minutes
20 minutes
30 minutes

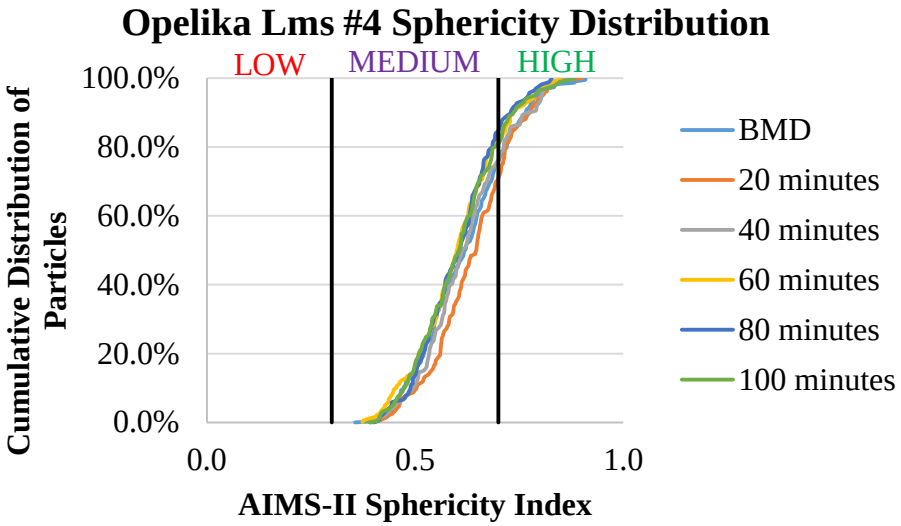
Opelika Lms #4 Sphericity Distribution
LOW
MEDIUM
HIGH
Cumulative Distribution of Particles
100.0%
80.0%
60.0%
40.0%
20.0%
0.0%
0.0
0.5
1.0
AIMS-II Sphericity Index
BMD
20 minutes
40 minutes
60 minutes
80 minutes
100 minutes

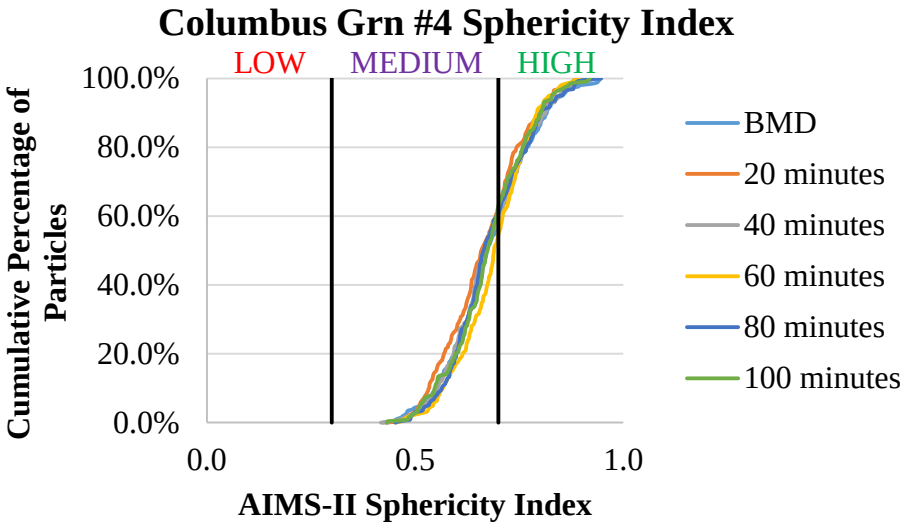
Columbus Grn #4 Sphericity Index
LOW
MEDIUM
HIGH
Cumulative Percentage of Particles
100.0%
80.0%
60.0%
40.0%
20.0%
0.0%
0.0
0.5
1.0
AIMS-II Sphericity Index
BMD
20 minutes
40 minutes
60 minutes
80 minutes
100 minutes

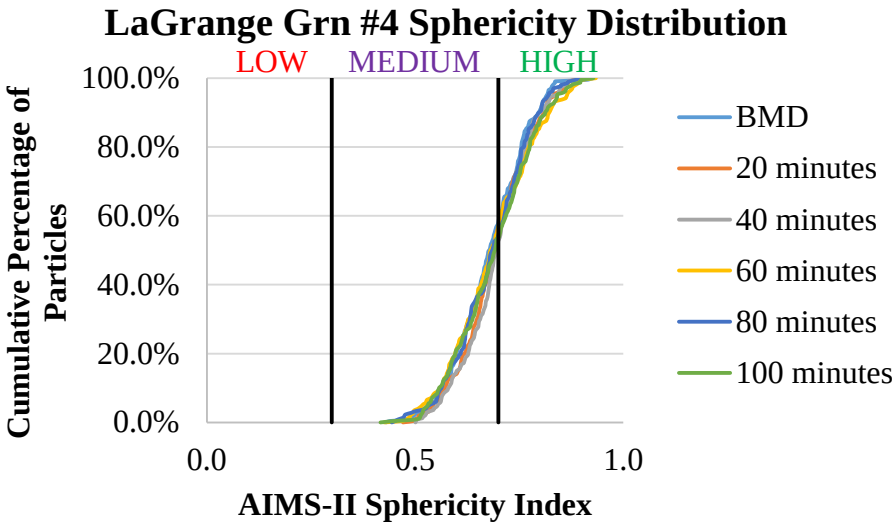
LaGrange Grn #4 Sphericity Distribution
LOW
MEDIUM
HIGH
100.0%
80.0%
60.0%
40.0%
20.0%
0.0%
Cumulative Percentage of Particles
0.0
0.5
1.0
AIMS-II Sphericity Index
BMD
20 minutes
40 minutes
60 minutes
80 minutes
100 minutes

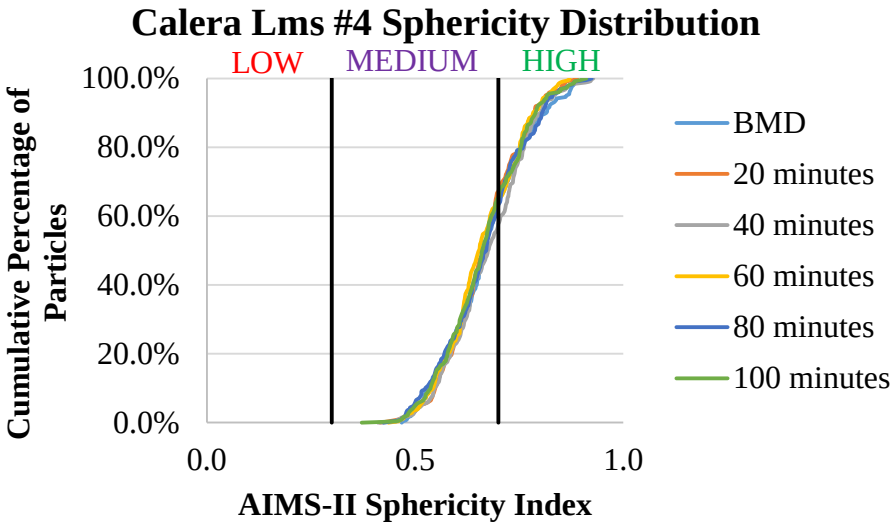
Calera Lms #4 Sphericity Distribution
LOW
MEDIUM
HIGH
100.0%
80.0%
60.0%
40.0%
20.0%
0.0%
Cumulative Percentage of Particles
0.0
0.5
1.0
AIMS-II Sphericity Index
BMD
20 minutes
40 minutes
60 minutes
80 minutes
100 minutes

## Appendix D: Kolmogorov-Smirnov Test Results for AIMS-II Cumulative Distributions

| Opelika LMS #4 KS Test | | | | |
|---|---|---|---|---|
| Comparisons | Angularity | | Texture | |
| | Max Difference | P-value | Max Difference | P-value |
| BMD vs 20 | 0.38 | 0.00 | 0.14 | 0.03 |
| 20 vs 40 | 0.16 | 0.01 | 0.09 | 0.45 |
| 40 vs 60 | 0.13 | 0.06 | 0.17 | 0.01 |
| 60 vs 80 | 0.09 | 0.34 | 0.05 | 0.99 |
| 80 vs 100 | 0.07 | 0.65 | 0.06 | 0.92 |
| BMD vs 100 | 0.53 | 0.00 | 0.16 | 0.01 |

| Columbus Grn #4 KS Test | | | | |
|---|---|---|---|---|
| Comparisons | Angularity | | Texture | |
| | Max Difference | P-value | Max Difference | P-value |
| BMD vs 20 | 0.14 | 0.01 | 0.09 | 0.24 |
| 20 vs 40 | 0.17 | 0.00 | 0.04 | 0.99 |
| 40 vs 60 | 0.09 | 0.27 | 0.66 | 0.69 |
| 60 vs 80 | 0.10 | 0.18 | 0.10 | 0.24 |
| 80 vs 100 | 0.09 | 0.23 | 0.07 | 0.51 |
| BMD vs 100 | 0.35 | 0.00 | 0.08 | 0.40 |

| LaGrange Grn #4 KS Test | | | | |
|---|---|---|---|---|
| Comparisons | Angularity | | Texture | |
| | Max Difference | P-value | Max Difference | P-value |
| BMD vs 20 | 0.22 | 0.00 | 0.09 | 0.30 |
| 20 vs 40 | 0.12 | 0.06 | 0.13 | 0.04 |
| 40 vs 60 | 0.05 | 0.96 | 0.10 | 0.20 |
| 60 vs 80 | 0.06 | 0.86 | 0.15 | 0.02 |
| 80 vs 100 | 0.11 | 0.15 | 0.08 | 0.59 |
| BMD vs 100 | 0.36 | 0.00 | 0.18 | 0.00 |

| Calera LMS #4 KS Test | | | | |
|---|---|---|---|---|
| Comparisons | Angularity | | Texture | |
| | Max Difference | P-value | Max Difference | P-value |
| BMD vs 20 | 0.21 | 0.00 | 0.10 | 0.16 |
| 20 vs 40 | 0.14 | 0.01 | 0.11 | 0.08 |
| 40 vs 60 | 0.09 | 0.25 | 0.10 | 0.16 |
| 60 vs 80 | 0.10 | 0.17 | 0.17 | 0.00 |
| 80 vs 100 | 0.12 | 0.07 | 0.07 | 0.67 |
| BMD vs 100 | 0.37 | 0.00 | 0.31 | 0.00 |

| Bauxite #16 KS Test | | | | |
|---|---|---|---|---|
| Comparisons | Angularity | | Form 2D | |
| | Max Difference | P-value | Max Difference | P-value |
| BMD vs 10 | 0.04 | 0.72 | 0.04 | 0.78 |
| 10 vs 20 | 0.13 | 0.00 | 0.08 | 0.12 |
| 20 vs 30 | 0.05 | 0.59 | 0.04 | 0.76 |
| BMD vs 30 | 0.15 | 0.00 | 0.07 | 0.15 |

| Opelika LMS #16 KS Test | | | | |
|---|---|---|---|---|
| Comparisons | Angularity | | Form 2D | |
| | Max Difference | P-value | Max Difference | P-value |
| BMD vs 10 | 0.09 | 0.03 | 0.10 | 0.01 |
| 10 vs 20 | 0.07 | 0.14 | 0.05 | 0.47 |
| 20 vs 30 | 0.08 | 0.04 | 0.07 | 0.06 |
| BMD vs 30 | 0.17 | 0.00 | 0.17 | 0.00 |

| Columbus Grn #16 KS Test | | | | |
|---|---|---|---|---|
| Comparisons | Angularity | | Form 2D | |
| | Max Difference | P-value | Max Difference | P-value |
| BMD vs 10 | 0.29 | 0.00 | 0.28 | 0.00 |
| 10 vs 20 | 0.18 | 0.00 | 0.10 | 0.00 |
| 20 vs 30 | 0.10 | 0.00 | 0.09 | 0.02 |
| BMD vs 30 | 0.46 | 0.00 | 0.37 | 0.00 |

| LaGrange Grn #16 KS Test | | | | |
|---|---|---|---|---|
| Comparisons | Angularity | | Form 2D | |
| | Max Difference | P-value | Max Difference | P-value |
| BMD vs 10 | 0.27 | 0.00 | 0.18 | 0.00 |
| 10 vs 20 | 0.09 | 0.01 | 0.13 | 0.00 |
| 20 vs 30 | 0.13 | 0.00 | 0.07 | 0.12 |
| BMD vs 30 | 0.40 | 0.00 | 0.35 | 0.00 |

| Calera LMS #16 KS Test | | | | |
|---|---|---|---|---|
| Comparisons | Angularity | | Form 2D | |
| | Max Difference | P-value | Max Difference | P-value |
| BMD vs 10 | 0.19 | 0.00 | 0.13 | 0.00 |
| 10 vs 20 | 0.10 | 0.00 | 0.04 | 0.58 |
| 20 vs 30 | 0.13 | 0.00 | 0.11 | 0.00 |
| BMD vs 30 | 0.36 | 0.00 | 0.24 | 0.00 |

## Appendix E: Detailed Statistical Output

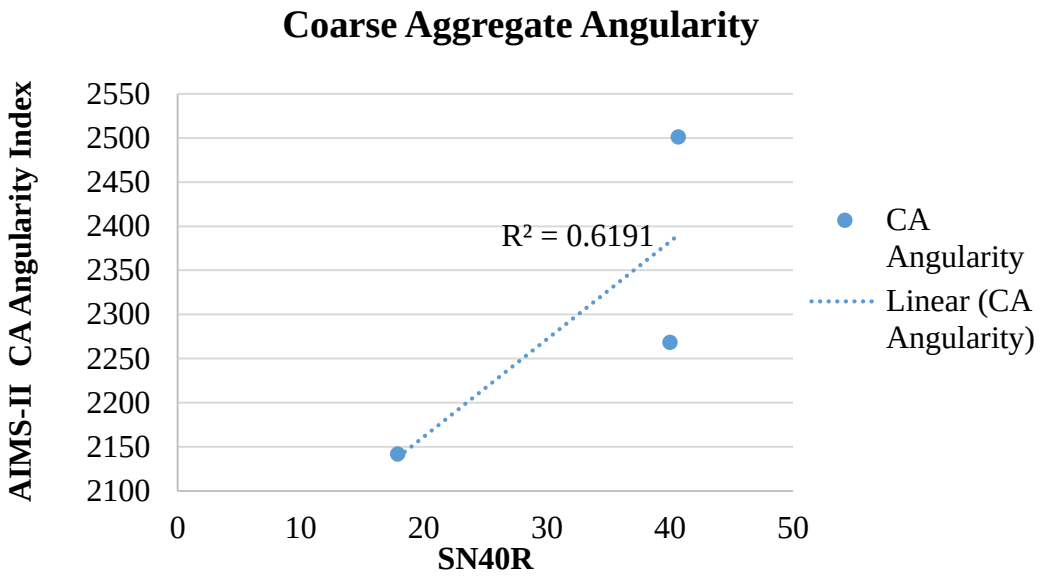


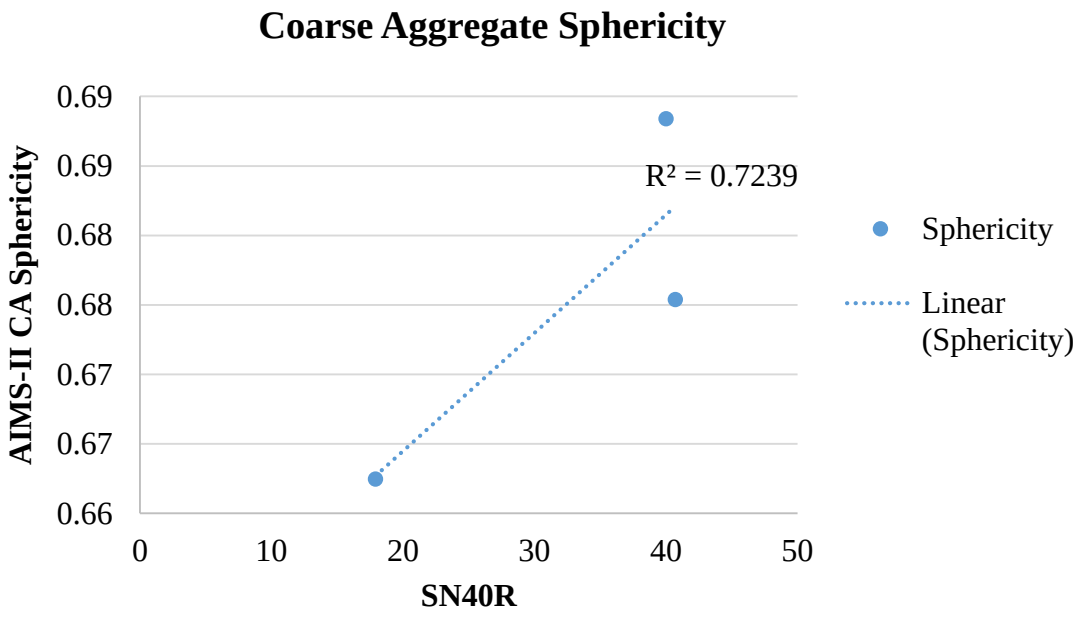

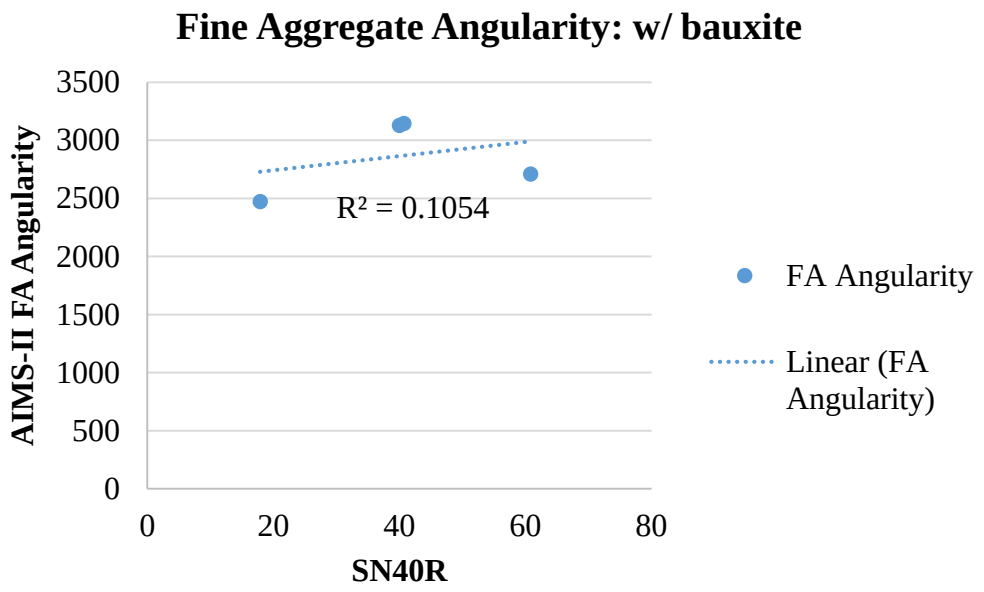
Fine Aggregate Angularity: w/ bauxite
AIMS-II FA Angularity
3500
3000
2500
2000
1500
1000
500
0
0
20
40
60
80
SN40R
R² = 0.1054
FA Angularity
Linear (FA Angularity)

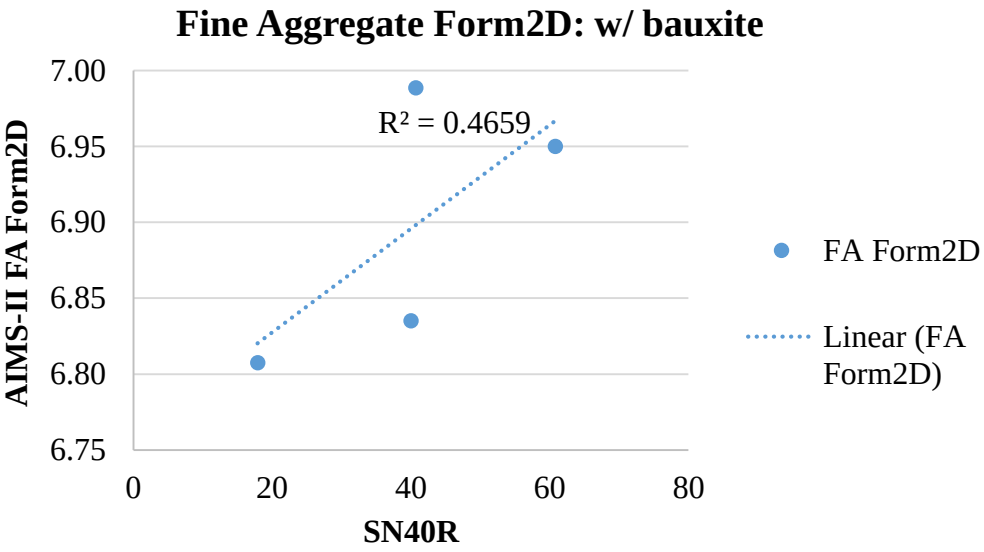
Fine Aggregate Form2D: w/ bauxite
AIMS-II FA Form2D
7.00
6.95
6.90
6.85
6.80
6.75
0
20
40
60
80
SN40R
R² = 0.4659
FA Form2D
Linear (FA Form2D)

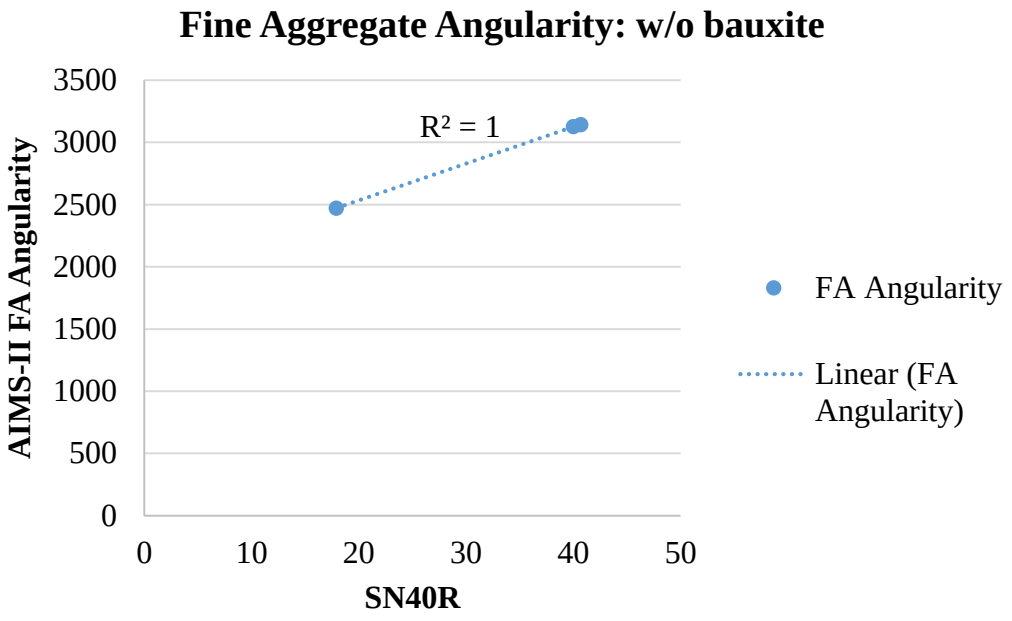
Fine Aggregate Angularity: w/o bauxite
AIMS-II FA Angularity
3500
3000
2500
2000
1500
1000
500
0
R² = 1
0
10
20
30
40
50
SN40R
FA Angularity
Linear (FA Angularity)

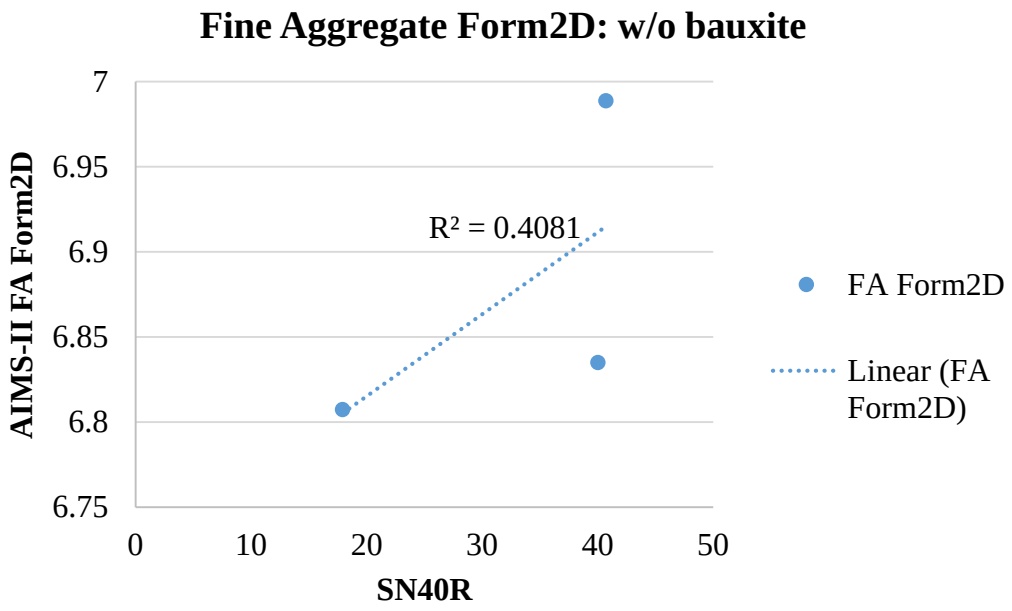
Fine Aggregate Form2D: w/o bauxite
AIMS-II FA Form2D
7
6.95
6.9
6.85
6.8
6.75
R² = 0.4081
0
10
20
30
40
50
SN40R
FA Form2D
Linear (FA Form2D)

## Minitab: General Linear Model: SN40R versus CA Angularity, CA Texture, CA Sphericity, FA Angularity, FA Form2D

```
The following terms cannot be estimated and were removed:
   CA Texture, CA Sphericity, FA Angularity, FA Formd2D


Method

Factor coding  (-1, 0, +1)


Factor Information

Factor         Type   Levels  Values
CA Angularity  Fixed       3  2141.6, 2268.3, 2500.9


Analysis of Variance

Source           DF  Adj SS   Adj MS  F-Value  P-Value
  CA Angularity   2  464.02  232.012   122.07    0.000
Error             9   17.11    1.901
Total            11  481.13


Model Summary

      S    R-sq  R-sq(adj)  R-sq(pred)
1.37862  96.44%     95.65%           *


Coefficients

Term              Coef  SE Coef  T-Value  P-Value   VIF
Constant        32.801    0.555    59.11    0.000
CA Angularity
  2141.6       -14.901    0.970   -15.36    0.000  2.44
  2268.3         7.165    0.721     9.94    0.000  2.44


Regression Equation

SN40R = 32.801 - 14.901 CA Angularity_2141.6 + 7.165 CA Angularity_2268.3
        + 7.736 CA Angularity_2500.9


Fits and Diagnostics for Unusual Observations

                              Std
Obs   SN40R     Fit  Resid  Resid
 11  42.400  39.967  2.433   2.16  R
 12  17.900  17.900  0.000      *     X

R  Large residual
X  Unusual X
```

## Minitab: General Linear Model: SN40R versus CA Angularity, CA Sphericity, FA Angularity

```
The following terms cannot be estimated and were removed:
   CA Sphericity, FA Angularity


Method

Factor coding  (-1, 0, +1)


Factor Information

Factor         Type   Levels  Values
CA Angularity  Fixed       3  2141.6, 2268.3, 2500.9


Analysis of Variance

Source           DF  Adj SS   Adj MS  F-Value  P-Value
  CA Angularity   2  464.02  232.012   122.07    0.000
Error             9   17.11    1.901
Total            11  481.13


Model Summary

      S    R-sq  R-sq(adj)  R-sq(pred)
1.37862  96.44%     95.65%           *


Coefficients

Term              Coef  SE Coef  T-Value  P-Value   VIF
Constant        32.801    0.555    59.11    0.000
CA Angularity
  2141.6       -14.901    0.970   -15.36    0.000  2.44
  2268.3         7.165    0.721     9.94    0.000  2.44


Regression Equation

SN40R = 32.801 - 14.901 CA Angularity_2141.6 + 7.165 CA Angularity_2268.3
        + 7.736 CA Angularity_2500.9


Fits and Diagnostics for Unusual Observations

                              Std
Obs   SN40R     Fit  Resid  Resid
 11  42.400  39.967  2.433   2.16  R
 12  17.900  17.900  0.000      *     X

R  Large residual
X  Unusual X
```

## DataFit Summary: Equation 6.1, Table 6.11

Equation ID: a*x1+b*x2+c*x3+d*x4+e*x5
Model Definition:
Y = a*x1+b*x2+c*x3+d*x4+e*x5

Number of observations = 12
Number of missing observations = 0
Solver type: Nonlinear
Nonlinear iteration limit = 250
Diverging nonlinear iteration limit =10
Number of nonlinear iterations performed = 26
Residual tolerance = 0.0000000001
Sum of Residuals = -0.775000000000006
Average Residual = -6.45833333333338E-02
Residual Sum of Squares (Absolute) = 17.170625
Residual Sum of Squares (Relative) = 17.170625
Standard Error of the Estimate = 1.56618850352422
Coefficient of Multiple Determination (R^2) = 0.9643118186
Proportion of Variance Explained = 96.43118186%
Adjusted coefficient of multiple determination (Ra^2) = 0.943918572
Durbin-Watson statistic = 1.70094274378481

**Regression Variable Results**

| Variable | Value | Standard Error | t-ratio | Prob(t) |
|---|---|---|---|---|
| **a** | 1035885108114.53 | 1683.26031538751 | 615403986.3 | 0.0 |
| **b** | -1505369848829.76 | 16914.3949934118 | -88999331.6 | 0.0 |
| **c** | -699222718978454 | 27986345.7422513 | -24984423.67 | 0.0 |
| **d** | -174941577256.979 | 2863.03082386847 | -61103630.39 | 0.0 |
| **e** | -159354351975424 | 4019583.70681438 | -39644491.47 | 0.0 |

**68% Confidence Intervals**

| Variable | Value | 68% (+/-) | Lower Limit | Upper Limit |
|---|---|---|---|---|
| **a** | 1035885108114.53 | 1801.59351555925 | 1035885106312.94 | 1035885109916.12 |
| **b** | -1505369848829.76 | 18103.4769614486 | -1505369866933.24 | -1505369830726.28 |
| **c** | -699222718978454 | 29953785.8479316 | -699222748932240 | -699222689024668 |
| **d** | -174941577256.979 | 3064.30189078642 | -174941580321.281 | -174941574192.677 |
| **e** | -159354351975424 | 4302160.44140343 | -159354356277584 | -159354347673264 |

**90% Confidence Intervals**

| Variable | Value | 90% (+/-) | Lower Limit | Upper Limit |
|---|---|---|---|---|
| **a** | 1035885108114.53 | 3189.10499353317 | 1035885104925.43 | 1035885111303.64 |
| **b** | -1505369848829.76 | 32046.0127545179 | -1505369880875.77 | -1505369816783.75 |
| **c** | -699222718978454 | 53022930.6432693 | -699222772001385 | -699222665955523 |
| **d** | -174941577256.979 | 5424.2981989012 | -174941582681.277 | -174941571832.681 |
| **e** | -159354351975424 | 7615503.29093052 | -159354359590927 | -159354344359921 |

**95% Confidence Intervals**

| Variable | Value | 95% (+/-) | Lower Limit | Upper Limit |
|---|---|---|---|---|
| **a** | 1035885108114.53 | 3980.2373417653 | 1035885104134.29 | 1035885112094.77 |
| **b** | -1505369848829.76 | 39995.7784014215 | -1505369888825.54 | -1505369808833.98 |

| | | | | |
|---|---|---|---|---|
| **c** | -699222718978454 | 66176513.1421274 | -699222785154967 | -699222652801941 |
| **d** | -174941577256.979 | 6769.92268611937 | -174941584026.902 | -174941570487.056 |
| **e** | -159354351975424 | 9504707.63313328 | -159354361480132 | -159354342470716 |

**99% Confidence Intervals**

| Variable | Value | 99% (+/-) | Lower Limit | Upper Limit |
|---|---|---|---|---|
| **a** | 1035885108114.53 | 5890.56947369859 | 1035885102223.96 | 1035885114005.1 |
| **b** | -1505369848829.76 | 59191.9252794445 | -1505369908021.69 | -1505369789637.83 |
| **c** | -699222718978454 | 97938216.9250085 | -699222816916671 | -699222621040237 |
| **d** | -174941577256.979 | 10019.1763681277 | -174941587276.155 | -174941567237.803 |
| **e** | -159354351975424 | 14066533.1819969 | -159354366041957 | -159354337908891 |

**Variance Analysis**

| Source | DF | Sum of Squares | Mean Square | F Ratio | Prob(F) |
|---|---|---|---|---|---|
| Regression | 4 | 463.958541666667 | 115.989635416667 | 47.28584125 | 0.00004 |
| Error | 7 | 17.170625 | 2.45294642857143 | | |
| Total | 11 | 481.129166666667 | | | |

## DataFit Summary: Equation 6.2, Table 6.12

Equation ID: a*x1+b*x2+c*x3+d*x4+e*x5
Model Definition:
Y = a*x1+b*x2+c*x3+d*x4+e*x5

Number of observations = 12
Number of missing observations = 0
Solver type: Nonlinear
Nonlinear iteration limit = 250
Diverging nonlinear iteration limit =10
Number of nonlinear iterations performed = 13
Residual tolerance = 0.0000000001
Sum of Residuals = 3.09999999999999
Average Residual = 0.258333333333333
Residual Sum of Squares (Absolute) = 20.63
Residual Sum of Squares (Relative) = 20.63
Standard Error of the Estimate = 1.71672445580031
Coefficient of Multiple Determination (R^2) = 0.9571217016
Proportion of Variance Explained = 95.71217016%
Adjusted coefficient of multiple determination (Ra^2) = 0.9326198167
Durbin-Watson statistic = 1.72321861366941

**Regression Variable Results**

| Variable | Value | Standard Error | t-ratio | Prob(t) |
|---|---|---|---|---|
| **a** | -963122784867.742 | 12044.641220282 | -79962762.46 | 0.0 |
| **b** | -1106484994878.07 | 35167769.3538509 | -31463.04173 | 0.0 |
| **c** | 3878211226936.09 | 3973.01550717438 | 976137953.6 | 0.0 |
| **d** | 81717947.3821655 | 3.55582919004318 | 22981404.06 | 0.0 |
| **e** | -4876593749010.23 | 15777.6156077052 | -309083062.4 | 0.0 |

**68% Confidence Intervals**

| Variable | Value | 68% (+/-) | Lower Limit | Upper Limit |
|---|---|---|---|---|
| **a** | -963122784867.742 | 12891.3794980679 | -963122797759.121 | -963122771976.362 |
| **b** | -1106484994878.07 | 37640063.5394266 | -1106522634941.61 | -1106447354814.53 |
| **c** | 3878211226936.09 | 4252.31849732874 | 3878211222683.77 | 3878211231188.41 |
| **d** | 81717947.3821655 | 3.80580398210321 | 81717943.5763615 | 81717951.1879695 |
| **e** | -4876593749010.23 | 16886.7819849269 | -4876593765897.01 | -4876593732123.45 |

**90% Confidence Intervals**

| Variable | Value | 90% (+/-) | Lower Limit | Upper Limit |
|---|---|---|---|---|
| **a** | -963122784867.742 | 22819.7772559463 | -963122807687.519 | -963122762047.965 |
| **b** | -1106484994878.07 | 66628855.8178059 | -1106551623733.89 | -1106418366022.25 |
| **c** | 3878211226936.09 | 7527.27517989258 | 3878211219408.81 | 3878211234463.37 |
| **d** | 81717947.3821655 | 6.7368739834558 | 81717940.6452915 | 81717954.1190395 |
| **e** | -4876593749010.23 | 29892.2705303582 | -4876593778902.5 | -4876593719117.96 |

**95% Confidence Intervals**

| Variable | Value | 95% (+/-) | Lower Limit | Upper Limit |
|---|---|---|---|---|
| **a** | -963122784867.742 | 28480.7586294789 | -963122813348.501 | -963122756386.983 |
| **b** | -1106484994878.07 | 83157707.4141158 | -1106568152585.48 | -1106401837170.66 |

| | | | | |
|---|---|---|---|---|
| **c** | 3878211226936.09 | 9394.59246826454 | 3878211217541.5 | 3878211236330.68 |
| **d** | 81717947.3821655 | 8.40811370277609 | 81717938.9740518 | 81717955.7902792 |
| **e** | -4876593749010.23 | 37307.7498659797 | -4876593786317.98 | -4876593711702.48 |

**99% Confidence Intervals**

| **Variable** | **Value** | **99% (+/-)** | **Lower Limit** | **Upper Limit** |
|---|---|---|---|---|
| **a** | -963122784867.742 | 42150.221950377 | -963122827017.964 | -963122742717.52 |
| **b** | -1106484994878.07 | 123069608.853801 | -1106608064486.92 | -1106361925269.22 |
| **c** | 3878211226936.09 | 13903.5677673567 | 3878211213032.52 | 3878211240839.66 |
| **d** | 81717947.3821655 | 12.4436242505561 | 81717934.9385413 | 81717959.8257898 |
| **e** | -4876593749010.23 | 55213.7658191643 | -4876593804224 | -4876593693796.46 |

**Variance Analysis**

| **Source** | **DF** | **Sum of Squares** | **Mean Square** | **F Ratio** | **Prob(F)** |
|---|---|---|---|---|---|
| Regression | 4 | 460.499166666667 | 115.124791666667 | 39.0631867 | 0.00007 |
| Error | 7 | 20.63 | 2.94714285714286 | | |
| Total | 11 | 481.129166666667 | | | |

## DataFit Summary: Equation 6.3, Table 6.13

Equation ID: a*x1+b*x2+c*x3
Model Definition:
Y = a*x1+b*x2+c*x3

Number of observations = 12
Number of missing observations = 0
Solver type: Nonlinear
Nonlinear iteration limit = 250
Diverging nonlinear iteration limit =10
Number of nonlinear iterations performed = 11
Residual tolerance = 0.0000000001
Sum of Residuals = 4.95106178277638E-10
Average Residual = 4.12588481898032E-11
Residual Sum of Squares (Absolute) = 17.1054166666667
Residual Sum of Squares (Relative) = 17.1054166666667
Standard Error of the Estimate = 1.3786231725355
Coefficient of Multiple Determination (R^2) = 0.9644473504
Proportion of Variance Explained = 96.44473504%
Adjusted coefficient of multiple determination (Ra^2) = 0.9565467616
Durbin-Watson statistic = 1.72067104312488

**Regression Variable Results**

| Variable | Value | Standard Error | t-ratio | Prob(t) |
|---|---|---|---|---|
| **a** | -4.71950576173437E-03 | 3.86604391808778E-03 | -1.220758445 | 0.25319 |
| **b** | -105.042020599295 | 12.5138223781086 | -8.394079557 | 0.00002 |
| **c** | 3.93738960202708E-02 | 3.15157283068247E-03 | 12.49341143 | 0.0 |

**68% Confidence Intervals**

| Variable | Value | 68% (+/-) | Lower Limit | Upper Limit |
|---|---|---|---|---|
| **a** | -4.71950576173437E-03 | 4.06901122378739E-03 | -8.78851698552176E-03 | -6.50494537946978E-04 |
| **b** | -105.042020599295 | 13.1707980529593 | -118.212818652254 | -91.8712225463357 |
| **c** | 3.93738960202708E-02 | 3.3170304042933E-03 | 3.60568656159775E-02 | 4.26909264245641E-02 |

**90% Confidence Intervals**

| Variable | Value | 90% (+/-) | Lower Limit | Upper Limit |
|---|---|---|---|---|
| **a** | -4.71950576173437E-03 | 7.08684510624671E-03 | -1.18063508679811E-02 | 2.36733934451234E-03 |
| **b** | -105.042020599295 | 22.9390878013109 | -127.981108400606 | -82.1029327979841 |
| **c** | 3.93738960202708E-02 | 5.77714815592404E-03 | 3.35967478643468E-02 | 4.51510441761948E-02 |

**95% Confidence Intervals**

| Variable | Value | 95% (+/-) | Lower Limit | Upper Limit |
|---|---|---|---|---|
| **a** | -4.71950576173437E-03 | 8.74576455149818E-03 | -1.34652703132326E-02 | 4.02625878976381E-03 |
| **b** | -105.042020599295 | 28.3087689837573 | -133.350789583052 | -76.7332516155377 |
| **c** | 3.93738960202708E-02 | 7.12948805756989E-03 | 3.22444079627009E-02 | 4.65033840778407E-02 |

**99% Confidence Intervals**

| Variable | Value | 99% (+/-) | Lower Limit | Upper Limit |
|---|---|---|---|---|
| **a** | -4.71950576173437E-03 | 1.25638695250017E-02 | -0.017283375286736 | 7.84436376326731E-03 |
| **b** | -105.042020599295 | 40.6674199643774 | -145.709440563672 | -64.3746006349176 |
| **c** | 3.93738960202708E-02 | 1.02419813851519E-02 | 2.91319146351189E-02 | 4.96158774054227E-02 |

**Variance Analysis**

| Source | DF | Sum of Squares | Mean Square | F Ratio | Prob(F) |
|---|---|---|---|---|---|
| Regression | 2 | 464.02375 | 232.011875 | 122.0728449 | 0 |
| Error | 9 | 17.1054166666667 | 1.90060185185186 | | |
| Total | 11 | 481.129166666667 | | | |

## DataFit Summary: Equation 6.4, Table 6.14

Equation ID: a+b*x1+c*x2
Model Definition:
Y = a+b*x1+c*x2

Number of observations = 12
Number of missing observations = 0
Solver type: Nonlinear
Nonlinear iteration limit = 250
Diverging nonlinear iteration limit =10
Number of nonlinear iterations performed = 11
Residual tolerance = 0.0000000001
Sum of Residuals = -6.4090954765561E-12
Average Residual = -5.34091289713009E-13
Residual Sum of Squares (Absolute) = 17.1054166666667
Residual Sum of Squares (Relative) = 17.1054166666667
Standard Error of the Estimate = 1.3786231725355
Coefficient of Multiple Determination (R^2) = 0.9644473504
Proportion of Variance Explained = 96.44473504%
Adjusted coefficient of multiple determination (Ra^2) = 0.9565467616
Durbin-Watson statistic = 1.72067104312281

**Regression Variable Results**

| Variable | Value | Standard Error | t-ratio | Prob(t) |
|---|---|---|---|---|
| **a** | -63.1337156948226 | 51.7167961878667 | -1.220758445 | 0.25319 |
| **b** | -3.95951913401735 | 88.6527271811408 | -0.044663252 | 0.96535 |
| **c** | 3.38368243307326E-02 | 3.64814393857193E-03 | 9.275079301 | 0.00001 |

**68% Confidence Intervals**

| Variable | Value | 68% (+/-) | Lower Limit | Upper Limit |
|---|---|---|---|---|
| **a** | -63.1337156948226 | 54.4319279877297 | -117.565643682552 | -8.70178770709288 |
| **b** | -3.95951913401735 | 93.3069953581507 | -97.266514492168 | 89.3474762241333 |
| **c** | 3.38368243307326E-02 | 3.83967149534696E-03 | 2.99971528353856E-02 | 3.76764958260796E-02 |

**90% Confidence Intervals**

| Variable | Value | 90% (+/-) | Lower Limit | Upper Limit |
|---|---|---|---|---|
| **a** | -63.1337156948226 | 94.8020590919785 | -157.935774786801 | 31.6683433971559 |
| **b** | -3.95951913401735 | 162.509314195749 | -166.468833329766 | 158.549795061732 |
| **c** | 3.38368243307326E-02 | 6.68741265379621E-03 | 2.71494116769364E-02 | 4.05242369845288E-02 |

**95% Confidence Intervals**

| Variable | Value | 95% (+/-) | Lower Limit | Upper Limit |
|---|---|---|---|---|
| **a** | -63.1337156948226 | 116.993736336192 | -180.127452031015 | 53.8600206413695 |
| **b** | -3.95951913401735 | 200.550199429177 | -204.509718563194 | 196.590680295159 |
| **c** | 3.38368243307326E-02 | 8.25283121783742E-03 | 2.55839931128952E-02 | 0.04208965554857 |

**99% Confidence Intervals**

| Variable | Value | 99% (+/-) | Lower Limit | Upper Limit |
|---|---|---|---|---|
| **a** | -63.1337156948226 | 168.069244251329 | -231.202959946152 | 104.935528556507 |
| **b** | -3.95951913401735 | 288.103632793271 | -292.063151927289 | 284.144113659254 |

| | | | | |
|---|---|---|---|---|
| **c** | 3.38368243307326E-02 | 1.18557381715711E-02 | 2.19810861591615E-02 | 4.56925625023037E-02 |

**Variance Analysis**

| **Source** | **DF** | **Sum of Squares** | **Mean Square** | **F Ratio** | **Prob(F)** |
|---|---|---|---|---|---|
| Regression | 2 | 464.02375 | 232.011875 | 122.0728449 | 0 |
| Error | 9 | 17.1054166666667 | 1.90060185185186 | | |
| Total | 11 | 481.129166666667 | | | |

## DataFit Summary: Equation 6.5, Table 6.15

Equation ID: a*x^3+b*x^2+c*x+d
Model Definition:
Y = a*x^3+b*x^2+c*x+d

Number of observations = 14
Number of missing observations = 0
Solver type: Nonlinear
Nonlinear iteration limit = 250
Diverging nonlinear iteration limit =10
Number of nonlinear iterations performed = 11
Residual tolerance = 0.0000000001
Sum of Residuals = 4.65618654743594E-11
Average Residual = 3.32584753388281E-12
Residual Sum of Squares (Absolute) = 18.0854166666667
Residual Sum of Squares (Relative) = 18.0854166666667
Standard Error of the Estimate = 1.34482031017778
Coefficient of Multiple Determination (R^2) = 0.986442404
Proportion of Variance Explained = 98.6442404%
Adjusted coefficient of multiple determination (Ra^2) = 0.9823751252
Durbin-Watson statistic = 2.15777176198056

**Regression Variable Results**

| Variable | Value | Standard Error | t-ratio | Prob(t) |
|---|---|---|---|---|
| **a** | 8.19802400372808E-07 | 2.09253048712928E-07 | 3.917756063 | 0.00288 |
| **b** | -7.16369455251768E-03 | 1.74256506380859E-03 | -4.111005495 | 0.00211 |
| **c** | 20.7804309759503 | 4.81363972239797 | 4.316989259 | 0.00152 |
| **d** | -19959.3814444567 | 4412.03700852675 | -4.52384724 | 0.0011 |

**68% Confidence Intervals**

| Variable | Value | 68% (+/-) | Lower Limit | Upper Limit |
|---|---|---|---|---|
| **a** | 8.19802400372808E-07 | 2.18962390173208E-07 | 6.008400101996E-07 | 1.03876479054602E-06 |
| **b** | -7.16369455251768E-03 | 1.82342008276931E-03 | -8.98711463528699E-03 | -5.34027446974837E-03 |
| **c** | 20.7804309759503 | 5.03699260551724 | 15.7434383704331 | 25.8174235814675 |
| **d** | -19959.3814444567 | 4616.75552572239 | -24576.1369701791 | -15342.6259187343 |

**90% Confidence Intervals**

| Variable | Value | 90% (+/-) | Lower Limit | Upper Limit |
|---|---|---|---|---|
| **a** | 8.19802400372808E-07 | 3.79271150792182E-07 | 4.40531249580626E-07 | 1.19907355116499E-06 |
| **b** | -7.16369455251768E-03 | 3.15839917815307E-03 | -1.03220937306707E-02 | -4.00529537436461E-03 |
| **c** | 20.7804309759503 | 8.72472199684633 | 12.055708979104 | 29.5051529727966 |
| **d** | -19959.3814444567 | 7996.81707795473 | -27956.1985224114 | -11962.564366502 |

**95% Confidence Intervals**

| Variable | Value | 95% (+/-) | Lower Limit | Upper Limit |
|---|---|---|---|---|
| **a** | 8.19802400372808E-07 | 4.66236717837274E-07 | 3.53565682535534E-07 | 1.28603911821008E-06 |
| **b** | -7.16369455251768E-03 | 3.88260921867192E-03 | -1.10463037711896E-02 | -3.28108533384576E-03 |
| **c** | 20.7804309759503 | 10.7252706654749 | 10.0551603104754 | 31.5057016414252 |
| **d** | -19959.3814444567 | 9830.45965869845 | -29789.8411031552 | -10128.9217857582 |

**99% Confidence Intervals**

| Variable | Value | 99% (+/-) | Lower Limit | Upper Limit |
|---|---|---|---|---|
| **a** | 8.19802400372808E-07 | 6.63185687285882E-07 | 1.56616713086926E-07 | 1.48298808765869E-06 |

| | | | | |
|---|---|---|---|---|
| **b** | -7.16369455251768E-03 | 5.52271145672856E-03 | -1.26864060092462E-02 | -1.64098309578912E-03 |
| **c** | 20.7804309759503 | 15.2558683721959 | 5.5245626037544 | 36.0362993481462 |
| **d** | -19959.3814444567 | 13983.0688911238 | -33942.4503355805 | -5976.31255333287 |

**Variance Analysis**

| **Source** | **DF** | **Sum of Squares** | **Mean Square** | **F Ratio** | **Prob(F)** |
|---|---|---|---|---|---|
| Regression | 3 | 1315.88386904762 | 438.627956349208 | 242.5312971 | 0 |
| Error | 10 | 18.0854166666667 | 1.80854166666667 | | |
| Total | 13 | 1333.96928571429 | | | |